

CAMBRIDGE UNIVERSITY

DOCTORAL THESIS

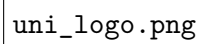
---

# On the Simulation of Boson Stars in General Relativity

---

Author: Robin Croft

Supervisor: Dr. Ulrich Sperhake

A square box containing the text 'uni\_logo.png', which serves as a placeholder for the university's logo.

uni\_logo.png

# Contents

<b>1</b>	<b>Introduction to Differential Geometry and General Relativity</b>	<b>1</b>
1.1	Introduction . . . . .	2
1.1.1	Introduction to General Relativity . . . . .	2
1.1.2	Introduction to Compact Objects and Boson Stars . . . . .	2
1.1.3	Conventions . . . . .	2
1.2	Differential Geometry . . . . .	3
1.2.1	Introduction to Geometry and Manifolds . . . . .	3
1.2.2	Functions, Curves and Tensors on Manifolds . . . . .	4
1.2.3	The Inner Product and the Metric . . . . .	6
1.2.4	Maps Between Manifolds . . . . .	7
1.2.5	Lie Derivatives . . . . .	8
1.2.6	Lengths on Manifolds . . . . .	9
1.2.7	Volumes on Manifolds . . . . .	9
1.2.8	Geodesics . . . . .	10
1.3	Tensor Calculus and Curvature . . . . .	11
1.3.1	General Covariance and Coordinate transformations . . . . .	11
1.3.2	The Covariant Derivative . . . . .	14
1.3.3	The Connection . . . . .	16
1.3.4	Curvature Tensors . . . . .	19
1.3.5	The Divergence Theorem . . . . .	21
1.4	Relativity . . . . .	23
1.4.1	Special Relativity . . . . .	23
1.4.2	Physics in Special Relativity . . . . .	24
1.4.3	Physics in Curved Space . . . . .	26
1.4.4	The Stress-Energy-Momentum Tensor . . . . .	27
1.4.5	The Einstein Equation . . . . .	27
1.4.6	Black Holes . . . . .	28
1.4.7	The Cosmological Constant . . . . .	32
1.4.8	The Lagrangean Formulation of General Relativity . . . . .	33
1.5	Stuff . . . . .	35
1.5.1	notes . . . . .	35
1.5.2	Differential Forms . . . . .	35
1.5.3	Parallel Transport . . . . .	36
1.5.4	Low Curvature Limit of General Relativity . . . . .	37
<b>2</b>	<b>Numerical Relativity, Numerical Methods and Boson Stars</b>	<b>39</b>
2.1	Numerical Relativity . . . . .	40
2.1.1	Spacetime Foliation . . . . .	40
2.1.2	The 3+1 Decomposition . . . . .	40
2.1.3	Gauss, Codazzi and Ricci Equations . . . . .	42

2.1.4	Decomposition of Einstein's Equation . . . . .	43
2.1.5	Foliation Adapted Coordinates . . . . .	45
2.1.6	ADM Equations . . . . .	46
2.1.7	BSSN . . . . .	46
2.1.8	Z4 Formalism . . . . .	47
2.1.9	CCZ4 . . . . .	47
2.1.10	Gauge Conditions . . . . .	49
2.1.11	stuff . . . . .	51
2.2	Mathematical Modelling of Boson Stars . . . . .	52
2.2.1	Action . . . . .	52
2.2.2	Solitons . . . . .	53
2.2.3	3+1 Klein Gordon System . . . . .	54
2.2.4	Klein Gordon's Noether Charge . . . . .	55
2.2.5	Boosted Boson Stars and Black Holes . . . . .	56
2.2.6	Spherical Harmonics in Curved Space DO I KEEP THIS SECTION? MAYBE JUST FOR INTERPITING SOME SIMS . . . . .	58
2.3	GRChombo . . . . .	60
2.3.1	Numerical Discretisation of Spacetime . . . . .	60
2.3.2	Boundary Conditions . . . . .	60
2.3.3	Overview of GRChombo . . . . .	60
2.3.4	Simulation Units . . . . .	60
2.3.5	Boson Star Initial Data . . . . .	60
2.3.6	Single Star Evolutions . . . . .	62
2.3.7	Superposition of Initial Data . . . . .	66
2.3.8	Head-on Collisions . . . . .	66
2.3.9	Binary Inspiral . . . . .	66
2.3.10	STUFF . . . . .	70

### 3 MALAISE PAPER 73

3.1	Introduction . . . . .	74
3.2	Formalism . . . . .	76
3.2.1	Action and covariant field equations . . . . .	76
3.2.2	3+1 formulation . . . . .	76
3.2.3	Stationary boson stars and initial data . . . . .	78
3.2.4	Boosted boson stars . . . . .	81
3.3	Boson-star binary initial data . . . . .	82
3.3.1	Simple superposition of boson stars . . . . .	82
3.3.2	Improved superposition . . . . .	83
3.4	Models and results . . . . .	83
3.4.1	Initial constraint violations . . . . .	84
3.4.2	Convergence and numerical uncertainties . . . . .	84
3.4.3	Radiated gravitational-wave energy . . . . .	85
3.4.4	Evolution of the scalar amplitude and gravitational collapse . . . . .	86
3.5	Conclusions . . . . .	87
3.6	Analytic treatment of the Hamiltonian constraint . . . . .	88

### 4 Local Continuity of Angular Momentum and Noether Charge for Matter in General Relativity 95

4.1	Local Continuity of Angular Momentum and Noether Charge for Matter in General Relativity . . . . .	96
4.1.1	Introduction . . . . .	96
4.1.2	Derivation of the QFS System . . . . .	98

4.1.3	Application to Spherical extraction . . . . .	101
4.1.4	Noether Currents . . . . .	102
4.1.5	Energy-Momentum Currents . . . . .	104
4.1.6	Numerical Application . . . . .	106
4.1.7	Conclusion . . . . .	112
4.1.8	Source Term Calculation . . . . .	113
4.1.9	Generality of Result . . . . .	114
4.2	STUFF . . . . .	116

<b>5</b>	<b>STUFF TO DO</b>	<b>117</b>
----------	--------------------	------------

## Chapter 1

# Introduction to Differential Geometry and General Relativity

## 1.1 Introduction

### 1.1.1 Introduction to General Relativity

general gr shit? mention einstein derivation (hilbert derivation a potentially earlier but vacuum), karl schwarzschild (ironically meaning black shield), then low mass limit, photon deflection and mercury perihelion around sun. mention cosmology, gravitational waves, more black holes, minkowski. more compact objects.

### 1.1.2 Introduction to Compact Objects and Boson Stars

The first non-trivial solution to Einstein's equation found was that of the spherically symmetric, static and asymptotically flat vacuum spacetime by Karl Schwarzschild in 1915. The solution was designed to be used outside a spherically symmetric, non-spinning, body of mass; however it turned out to provide use in describing black holes. This metric was then modified by Tolman, Oppenheimer and Volkov in 1939 to describe the non-vacuum case of a constant density neutron star. This turned out to give an unphysical estimate of  $0.7M_{\odot}$  for the upper limit of neutron star mass due to the equation of state.

The study of compact exotic objects can be traced back to John Wheeler who investigated Geons in 1955 for their potential similarity to elementary particles. Geons are gravito-electromagnetic objects with the name arising from "gravitational electromagnetic entity". In 1968 David Kaup published [1] describing what he called "Klein-Gordon Geons", nowadays referred to as boson stars. Importantly, boson stars are a localised complex Klein-Gordon configuration, with the real counterparts being unstable. Many variants such as (Spin 1) proca stars [2], electromagnetically charged boson stars and many others have been studied.

Interest in boson stars remains for many reasons. Given the recent discovery of the higgs boson, we know that scalar fields exist in nature and any gravitational wave signals created by compact objects could theoretically be detected with modern gravitational wave interferometers. Secondly, boson stars are a good candidate for dark matter haloes. Boson stars are also useful as a proxy to other compact objects in general relativity; there is a lot of freedom in the construction of different types of boson star and they can be fine tuned to model dense neutron stars for one example. The advantage this would have over simulating a real fluid is that the Klein Gordon equation is linear in the principal part meaning smooth data must always remain smooth; thus avoiding shocks and conserving particle numbers relatively well with less sophisticated numerical schemes.

On a slightly different topic, collisions of boson stars could be a natural method to produce scalar hair around black holes which will be discussed later in more detail.

### 1.1.3 Conventions

Throughout this thesis physical quantities will be expressed as a dimensionless ratio of the Planck length, time and mass  $L_{pl}$ ,  $T_{pl}$  and  $M_{pl}$  respectively; consequently the constants  $c$ ,  $G$  and  $\hbar$  evaluate numerically to 1. As an example, Newtons equation of gravity would be recast like

$$F = \frac{GMm}{r^2} \rightarrow \left( \frac{F}{F_{pl}} \right) = \frac{\left( \frac{M}{M_{pl}} \right) \left( \frac{m}{M_{pl}} \right)}{\left( \frac{r}{L_{pl}} \right)^2} \quad (1.1.1)$$

where  $F_{pl} = M_{pl}L_{pl}T_{pl}^{-2}$  is the Planck force.  $c = G = \hbar = 1$ , unless stated otherwise. The metric signature will always be  $(-, +, +, +)$ .

Tensors and tensor fields will be denoted using bold font for index free notation and normal font for the components. The dot product between two vectors or vector fields will be written interchangeably as  $\mathbf{A} \cdot \mathbf{B} \leftrightarrow A_{\mu}B^{\mu}$  for readability. Additionally,  $\nabla_{\mu}$  denotes the covariant derivative and  $\partial_{\mu}$  is the partial derivative, both with respect to coordinate  $x^{\mu}$ .

When considering the ADM decomposition, as in [REF SECT], objects can be associated with both the 3+1 dimensional manifold  $\mathcal{M}$  or the 3 dimensional hypersurface  $\Sigma$ . To differentiate here, standard Roman letters such as  $R$  represent the object belonging to  $\mathcal{M}$  and calligraphic letters such as  $\mathcal{R}$  correspond to the projected object belonging to  $\Sigma$ . [MAYBE JUST REMOVE THIS BIT AND MAKE IT OBVIOUS IN THE ACTUAL 3+1 SECTION].

Finally, unless stated otherwise, Greek indices such as  $\{\alpha, \beta, \dots, \mu, \nu, \dots\}$  label four dimensional tensor components whereas late Latin indices such as  $\{i, j, k, \dots\}$  label three dimensional tensor components and early Latin indices such as  $\{a, b, \dots\}$  label two dimensional ones. When the index range is unspecified and unimportant Greek letters will also be used.

## EINSTEIN SUMMATION CONV

make explicit th inner product, dot product, outer product (otimes) and wedge product (for forms, antisymm)

## Conventions (from q)

Throughout this work the metric has sign  $\{-, +, +, +\}$  and physical quantities will be expressed as a dimensionless ratio of the Planck length  $L_{pl}$ , time  $T_{pl}$  and mass  $M_{pl}$  unless stated otherwise; for example Newtons equation of gravity would be written as

$$F = \frac{GMm}{r^2} \rightarrow \left( \frac{F}{F_{pl}} \right) = \frac{\left( \frac{M}{M_{pl}} \right) \left( \frac{m}{M_{pl}} \right)}{\left( \frac{r}{L_{pl}} \right)^2}, \quad (1.1.2)$$

where  $F_{pl} = M_{pl}L_{pl}T_{pl}^{-2}$  is the Planck force. Consequently  $c$ ,  $G$  and  $\hbar$  take the numerical value of 1. Additionally, tensor fields will be denoted using bold font for index free notation and normal font for the components. The dot product between two vector fields will be written interchangeably as  $\mathbf{A} \cdot \mathbf{B} \leftrightarrow A^\mu B_\mu$  for readability. Additionally,  $\nabla_\mu$  denotes the covariant derivative and  $\partial_\mu$  is the partial derivative, both with respect to coordinate  $x^\mu$ . Finally, unless stated otherwise, Greek indices such as  $\{\alpha, \beta, \dots, \mu, \nu, \dots\}$  label four dimensional tensor components whereas late Latin indices such as  $\{i, j, k, \dots\}$  label three dimensional tensor components and early Latin indices such as  $\{a, b, \dots\}$  label two dimensional ones.

PROBABLY DELETE THIS

## 1.2 Differential Geometry

### 1.2.1 Introduction to Geometry and Manifolds

Everyones first encounter with geometry will cover Pythagoras' theorem; arguably the most famous and useful equation in existence. Pythagoras' equation relates the sidelengths of a right angled triangle, it says that  $s^2 = x^2 + y^2$  for a triangle with height  $y$ , width  $x$  and hypotenuse length  $s$ . This can be shown very simply by looking at Fig. 1.1. The area of the partially rotated square is  $s^2$ , but we can also calculate it from the the area of the larger square  $A_{sq}$  and subtracting four times the area of one of the triangles  $A_{tr}$ . Given that  $A_{sq} = (x + y)^2$  and  $A_{tr} = \frac{1}{2}xy$ , then

$$s^2 = (x + y)^2 - 2xy = x^2 + y^2, \quad (1.2.1)$$

and we have proved Pythagoras' theorem. Using an infinitessimally small triangle, we can write  $ds^2 = dx^2 + dy^2$  and this can be trivially extended to arbitrary dimensions like

$$ds^2 = dx^2 + dy^2 + dz^2 + \dots \quad (1.2.2)$$

The infinitesimal form of Pythagoras' theorem is very powerful as it can be used to calculate the length of a generic curve by approximating the curve as a collection of infinitesimally small straight lines with length  $ds$ . So far we have assumed that space is flat meaning Eq. (1.2.2) is true for all points in space, this is an assumption we will have to drop if we want to study the curved spaces arising in strong gravity. In the next sections we will explore the generalisation of Pythagoras' equation to curved spaces and use it to measure curve lengths as well as volumes and areas.

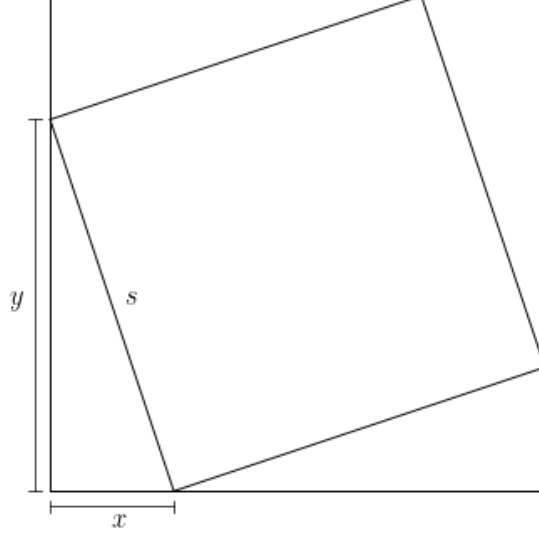


Figure 1.1: Diagram for proof of Pythagoras' theorem.

Differential Geometry (DG) is the extension of calculus, linear algebra and multilinear algebra to general geometries. Einstein's Theory of Relativity is written using the language of DG as it is the natural way to deal with curves, tensor calculus and differential tensor equations in curved spaces. For a basic introduction to DG, we should start with a manifold  $\mathcal{M}$  which is an  $N$  dimensional space that locally looks like  $\mathbb{R}^N$ ,  $N$  dimensional Euclidean space. This is important as at a point  $p \in \mathcal{M}$  we can find infinitesimally close neighbouring points  $p + \delta p \in \mathcal{M}$ . In the following sections we will explore curves, functions, tensors and calculus on manifolds using DG.

### 1.2.2 Functions, Curves and Tensors on Manifolds

A real scalar function  $f$  over  $\mathcal{M}$  maps any point  $p \in \mathcal{M}$  to a real number, this is denoted as  $f : p \rightarrow \mathbb{R}$ . An important example of a set of scalar functions is the coordinate system  $\phi$ ,  $\phi : p \rightarrow \mathbb{R}^N$ , this is normally written  $x^\mu$  where  $\mu \in \{0, 1, \dots, N - 1\}$  is an index labelling the coordinate. The map  $\phi$  is called a chart, and unlike Euclidean space one chart may not be enough to cover the entire manifold; in this case a set of compatible charts should be smoothly joined, collectively known as an atlas.

Now that functions have been discussed, the next simplest object we can discuss is a curve, or path, through  $\mathcal{M}$ . A curve  $\Gamma$  is a set of smoothly connected points  $p(\lambda) \in \mathcal{M}$  that smoothly depend on an input parameter  $\lambda \in [\lambda_0, \lambda_1]$ . This can be expressed in terms of coordinates as  $x^\mu(\lambda)$  where  $\phi : p(\lambda) \rightarrow x^\mu(\lambda)$ . Differentiating a function  $f$  along  $\Gamma$  with respect to  $\lambda$  gives

$$\frac{d}{d\lambda} f(x^\mu(\lambda)) = \frac{dx^\nu}{d\lambda} \frac{\partial f(x^\mu)}{\partial x^\nu} = \frac{dx^\nu}{d\lambda} \partial_\nu f, \quad (1.2.3)$$

where the Einstein summation convention was invoked, summing over all values of  $\nu$ , and  $\partial_\nu = \partial/\partial x^\nu$ . Equation (1.2.3) was derived independantly of the choice of  $f$ , therefore we can generally write

$$\frac{d}{d\lambda} = \frac{dx^\nu}{d\lambda} \partial_\nu. \quad (1.2.4)$$



The operator  $d/d\lambda$  can act on any function  $f$  and return a new function  $\tilde{f}$  over  $\mathcal{M}$ , this is written as  $d/d\lambda(f) = \tilde{f}$  where  $\tilde{f} : p \rightarrow \mathbb{R}$  for  $p \in \mathcal{M}$ . We can also think of  $d/d\lambda$  as a vector  $\mathbf{X}$  with components  $X^\mu = dx^\mu/d\lambda$  and basis vectors  $\mathbf{e}_\mu := \partial_\mu$  taken from Eq. (1.2.4). The vector  $\mathbf{X}$  can be written as  $\mathbf{X} = X^\mu \mathbf{e}_\mu$  and can act on a general function  $f$  over  $\mathcal{M}$  as  $\mathbf{X}(f) = X^\mu \mathbf{e}_\mu(f) = X^\mu \partial_\mu f$ . Considering the set of all possible curves through a points  $p \in \mathcal{M}$ , the tangent vector components  $dx^\mu/d\lambda$  span an  $N$  dimensional space with basis  $\mathbf{e}_\mu = \partial_\mu$ ; this space is called the tangent space and is denoted as  $\mathcal{T}_p(\mathcal{M})$  at a point  $p \in \mathcal{M}$ .

The next object to discuss is the co-vector which is defined as a map from vectors to real numbers; not to be confused with the dot product in section 1.2.3. Similarly to vectors, a co-vector  $\omega$  can be expressed as a sum of components  $\omega_\mu$  and basis co-vectors  $\theta^\mu$  like  $\omega = \omega_\mu \theta^\mu$ . Contrary to vectors, co-vector components have downstairs indeces and the basis has upstairs indeces; this choice improves the readability of tensor equations when working with components. A co-vector can map a vector to a real number like  $\omega : \mathbf{X} \rightarrow \mathbb{R}$  or  $\omega(\mathbf{X}) \rightarrow \mathbb{R}$ . Vectors are equally able to map co-vectors to real numbers, denoted as  $\mathbf{X} : \omega \rightarrow \mathbb{R}$ . Co-vectors are defined such that  $\theta^\mu : \mathbf{e}_\nu = \delta_\nu^\mu$  where  $\delta_\nu^\mu$  are the components of the Kroneka delta equating to zero unless  $\mu = \nu$  in which case they equal unity. The operation of a generic co-vector  $\omega$  on a generic vector  $\mathbf{X}$  is

$$\omega : \mathbf{X} = \omega_\mu X^\nu \theta^\mu : \mathbf{e}_\nu = \omega_\mu X^\nu \delta_\nu^\mu = \omega_\mu X^\mu \in \mathbb{R}. \quad (1.2.5)$$

This map is linear and identical under reversing the order of operation;  $\omega : \mathbf{X} = \mathbf{X} : \omega$ . Similarly to vectors, the set of all possible co-vectors at a point  $p \in \mathcal{M}$  span an  $N$ -dimensional space called the co-tangent space, written as  $\mathcal{T}_p^*(\mathcal{M})$ .

## Multilinear Maps and Tensors

Generalising the previous linear maps between vectors and co-vectors gives the multilinear map. Consider a tensor  $\mathbf{T}$ , this can be expressed in component form like

$$\mathbf{T} = T_{\mu\nu,\dots}^{\alpha\beta,\dots} \mathbf{e}_\alpha \otimes \mathbf{e}_\beta \otimes \dots \otimes \theta^\mu \otimes \theta^\nu \otimes \dots \quad (1.2.6)$$

for an arbitrary number of outer products of vector and co-vector bases. A tensor with  $m$  co-vector bases and  $n$  vector bases is called an  $(m, n)$  tensor and has a rank of  $m + n$ . Vectors, co-vectors and scalars are  $(1, 0)$ ,  $(0, 1)$  and  $(0, 0)$  tensors respectively. Tensors can act as multilinear maps between tensors. We have already seen how a vector and co-vector can map each other to a scalar, let's extend this with an example. An  $(0, 2)$  tensor,  $\mathbf{T} = T_{\mu\nu} \theta^\mu \otimes \theta^\nu$  at  $p \in \mathcal{M}$ , can map two vectors  $\mathbf{X}$  and  $\mathbf{Y}$  to a scalar as shown,

$$\mathbf{T}(\mathbf{X}, \mathbf{Y}) = T_{\mu\nu} X^\alpha Y^\beta \theta^\mu \otimes \theta^\nu (\mathbf{e}_\alpha, \mathbf{e}_\beta), \quad (1.2.7)$$

$$= T_{\mu\nu} X^\alpha Y^\beta (\theta^\mu : \mathbf{e}_\alpha) (\theta^\nu : \mathbf{e}_\beta), \quad (1.2.8)$$

$$= T_{\mu\nu} X^\alpha Y^\beta \delta_\alpha^\mu \delta_\beta^\nu, \quad (1.2.9)$$

$$= T_{\mu\nu} X^\mu Y^\nu. \quad (1.2.10)$$

The multilinear map can also output generic tensors, for example consider

$$\mathbf{T}(\mathbf{X}, \star) = T_{\mu\nu} X^\alpha (\theta^\mu : \mathbf{e}_\alpha) \theta^\nu = T_{\mu\nu} X^\mu \theta^\nu, \quad (1.2.11)$$

which uses the  $(0, 2)$  tensor  $\mathbf{T}$  to map the vector  $\mathbf{X}$  to a co-vector  $\mathbf{W}$  with components  $W_\mu = T_{\mu\nu} X^\nu$ .

One final example of a mapping is from a single tensor to a lower rank tensor, this is called contraction. To illustrate this, let's take a  $(1, 3)$  tensor  $\mathbf{Z} = Z_{\mu\nu\rho}^\alpha \mathbf{e}_\alpha \otimes \theta^\mu \otimes \theta^\nu \otimes \theta^\rho$ . We can choose to use the basis vector  $\mathbf{e}_\alpha$  to act on any of the three co-vector bases, choosing  $\theta^\mu$  this is

$$Z_{\mu\nu\rho}^\alpha (\mathbf{e}_\alpha : \theta^\mu) \theta^\nu \otimes \theta^\rho = Z_{\mu\nu\rho}^\mu \theta^\nu \otimes \theta^\rho = \tilde{Z}_{\nu\rho} \theta^\nu \otimes \theta^\rho \quad (1.2.12)$$

where  $\tilde{Z}_{\nu\rho} = Z_{\mu\nu\rho}^\mu$ .

### 1.2.3 The Inner Product and the Metric

To introduce the notion of length on a tangent plane  $\mathcal{T}_p(\mathcal{M})$  at a point  $p \in \mathcal{M}$  the metric tensor  $\mathbf{g}$  is introduced. The metric tensor is

$$g_{\mu\nu} = \mathbf{e}_\mu \cdot \mathbf{e}_\nu \quad (1.2.13)$$

where  $\mathbf{e}_\mu \cdot \mathbf{e}_\nu$  represents the inner product (or dot product) on  $\mathcal{T}_p(\mathcal{M})$ ; clearly the metric is symmetric by construction as  $\mathbf{e}_\mu \cdot \mathbf{e}_\nu = \mathbf{e}_\nu \cdot \mathbf{e}_\mu$ . The inner product can be thought of as a multilinear map,

$$\mathbf{g} : (\mathbf{X}, \mathbf{Y}) \rightarrow \mathbb{R}, \quad (1.2.14)$$

$$\mathbf{g}(\mathbf{X}, \mathbf{Y}) = g_{\mu\nu} X^\mu Y^\nu, \quad (1.2.15)$$

where  $\mathbf{X} \in \mathcal{T}_p(\mathcal{M})$ ,  $\mathbf{Y} \in \mathcal{T}_p(\mathcal{M})$  and  $\mathbf{g} \in \mathcal{T}_p^*(\mathcal{M}) \otimes \mathcal{T}_p^*(\mathcal{M})$ . The inner product can also be represented by a second map

$$\mathbf{X} : \mathbf{Y} \rightarrow \mathbb{R}, \quad (1.2.16)$$

$$\mathbf{X} \cdot \mathbf{Y} = X^\mu Y^\nu \mathbf{e}_\mu \cdot \mathbf{e}_\nu = X^\mu Y^\nu g_{\mu\nu}, \quad (1.2.17)$$

which is a new mapping. The inner product also gives the length  $|\mathbf{X}|$  or magnitude of any vector  $\mathbf{X} \in \mathcal{T}_p(\mathcal{M})$  as,

$$|\mathbf{X}|^2 = \mathbf{X} \cdot \mathbf{X} = g_{\mu\nu} X^\mu X^\nu. \quad (1.2.18)$$

Another way to think of the inner product is that the metric maps a vector  $\mathbf{X}$  to an "equivalent" or "dual" co-vector  $\Xi$  such that  $\mathbf{X} : \Xi = X^\mu \Xi_\mu = g_{\mu\nu} X^\mu X^\nu$ . In component form  $\Xi$  is

$$\Xi_\mu = g_{\mu\nu} X^\nu; \quad (1.2.19)$$

this use of the metric to map a vector to its corresponding co-vector (and vice versa) is extremely useful. Without loss of information we can write  $\Xi_\nu = X_\nu$  to make it obvious that  $X_\nu = X^\mu g_{\mu\nu}$  and this convention will be used from now on.

The metric also assigns an inner product and a length measure on the co-tangent plane  $\mathcal{T}_p^*(\mathcal{M})$  but instead using the inverse components  $g^{\mu\nu} = (g^{-1})_{\mu\nu}$ ,

$$g^{\mu\nu} = \boldsymbol{\theta}^\mu \cdot \boldsymbol{\theta}^\nu. \quad (1.2.20)$$

Similarly to before the inner product of two co-vectors  $\boldsymbol{\omega}$  and  $\boldsymbol{\sigma}$  is

$$\boldsymbol{\omega} \cdot \boldsymbol{\sigma} = \omega_\mu \sigma_\nu \boldsymbol{\theta}^\mu \cdot \boldsymbol{\theta}^\nu = \omega_\mu \sigma_\nu g^{\mu\nu} = \omega_\mu \sigma^\mu. \quad (1.2.21)$$

The reason that  $g^{\mu\nu}$  must be the inverse matrix to  $g_{\mu\nu}$  is as follows. For a vector  $x^\mu \mathbf{e}_\mu$  and a co-vector  $\omega_\mu \boldsymbol{\theta}^\mu$  we would like,

$$\mathbf{X} : \boldsymbol{\omega} = \mathbf{g}(\mathbf{X}, \star) : \mathbf{g}^{-1}(\boldsymbol{\omega}, \star), \quad (1.2.22)$$

$$X^\mu \omega_\mu = X_\mu \omega^\mu, \quad (1.2.23)$$

$$= X^\rho g_{\rho\mu} g^{\mu\sigma} \omega_\sigma \quad (1.2.24)$$

which is only true if  $g_{\rho\mu} g^{\mu\sigma} = \delta_\rho^\sigma$  which is true by definition if  $(g^{-1})_{\mu\nu} = g^{\mu\nu}$ .

Not only has the metric provided us with an inner product and a length on tangent planes and cotangent planes, but it has also given a mapping between the two. The metric can raise and lower indices on general tensors such as

$$T^{\mu\nu\dots}_{\alpha\beta} = g^{\mu\rho} g_{\beta\sigma} T_\rho{}^\nu{}_\sigma{}^{\dots}. \quad (1.2.25)$$

### 1.2.4 Maps Between Manifolds

In section we will be interested in the maps between two manifolds  $M$  and  $N$ . This has many uses such as pushing and pulling tensors between manifolds, allowing us to calculate a Lie derivative of tensor fields and finding the metric (or any tensor field) on an embedded surface; this very importantly allowed us to perform the 3+1 decomposition [REF] on a spacetime.

Defining a smooth map  $\Phi : M \rightarrow N$  between manifolds on some coordinate patch and labelling coordinates  $x^\mu \in M$  and  $y^\mu \in N$ . The map  $\Phi : x^\mu \rightarrow y^\mu$  gives  $y^\mu = \Phi^\mu(x^\nu)$ , or equivalently  $y^\mu(x^\nu)$ . Scalar functions must also map trivially  $f_N(y^\mu(x^\nu)) = f_M(x^\mu)$  where  $f_N \in N$  and  $f_M \in M$ , thus we will no longer identify which manifold a function is on. The map  $\Phi$  allows us to push the vector  $\mathbf{X} \in \mathcal{T}_p(M)$  to  $\Phi_*\mathbf{X} \in \mathcal{T}_q(N)$ , where  $q = \Phi(p)$ , in a way such that it's action on a function  $f$  is the same in either manifold.

$$\mathbf{X}(f)\big|_p = \Phi_*\mathbf{X}(f)\big|_q, \quad (1.2.26)$$

$$X^\mu \frac{\partial f}{\partial x^\mu} = (\Phi_*X)^\nu \frac{\partial f}{\partial y^\nu}, \quad (1.2.27)$$

$$\left(X^\mu \frac{\partial y^\nu}{\partial x^\mu}\right) \frac{\partial f}{\partial y^\nu} = (\Phi_*X)^\nu \frac{\partial f}{\partial y^\nu} \quad (1.2.28)$$

and hence the components of the push-forward  $\Phi_*\mathbf{X}$  can be read off,

$$(\Phi_*X)^\mu = \frac{\partial y^\mu}{\partial x^\nu} X^\nu. \quad (1.2.29)$$

Given a co-vector field  $\omega \in \mathcal{T}_p^*(N)$  we can pull the field back from  $\mathcal{T}_p^*(M) \leftarrow \mathcal{T}_q^*(N)$ , denoted  $\Phi^*\omega$ , by demanding that  $\Phi^*\omega(\mathbf{X})\big|_p = \omega(\Phi_*\mathbf{X})\big|_q$ . Evaluating this gives

$$\Phi^*\omega(\mathbf{X})\big|_p = \omega(\Phi_*\mathbf{X})\big|_q, \quad (1.2.30)$$

$$(\Phi^*\omega)_\mu X^\mu = \omega_\nu (\Phi_*X)^\nu, \quad (1.2.31)$$

$$(\Phi^*\omega)_\mu X^\mu = \omega_\nu \frac{\partial y^\nu}{\partial x^\mu} X^\mu, \quad (1.2.32)$$

and the components of pull-back  $\Phi^*\omega$  can be read off,

$$(\Phi^*\omega)_\mu = \omega_\nu \frac{\partial y^\nu}{\partial x^\mu}. \quad (1.2.33)$$

Considering an  $(0,2)$  tensor  $\mathbf{T} \in N$ , the pullback  $\Phi^*\mathbf{T} \in M$  follows simply from demanding that  $\mathbf{T}(\Phi_*\mathbf{X}, \Phi_*\mathbf{Y}) = \Phi^*\mathbf{T}(\mathbf{X}, \mathbf{Y})$  where  $\mathbf{X}$  and  $\mathbf{Y}$  are vector fields on  $M$ . The components of the pull-back of  $\mathbf{T}$  are therefore

$$(\Phi^*T)_{\mu\nu} = \frac{\partial y^\rho}{\partial x^\mu} \frac{\partial y^\sigma}{\partial x^\nu} T_{\rho\sigma}, \quad (1.2.34)$$

and the pull-back of a generic  $(0,q)$  tensor and the push-forward of a generic  $(p,0)$  tensor can be found similarly.

### Diffeomorphisms

So far we have only discussed the mapping  $\Phi : M \rightarrow N$  which requires a well behaved  $\partial y^\nu / \partial x^\mu$ . A diffeomorphism is an isomorphism<sup>1</sup> between smooth manifolds  $\Phi : M \rightarrow N$ , meaning  $M$  and  $N$  have the same number of dimensions. Two infinitesimally close points  $\{p, p+\delta p\} \in \mathcal{M}$  map to two infinitesimally close points  $\{q, q+\delta q\} \in \mathcal{N}$  meaning that open sets are preserved. Given that a diffeomorphism is smooth bijective map then it must be invertible with inverse map  $\Phi^{-1} : N \rightarrow M$ , and  $y^\nu(x^\mu)$  has a smooth inverse

<sup>1</sup>An isomorphism is a structure preserving bijective map between sets.

$x^\nu(y^\mu)$ . When an inverse map  $\Phi^{-1}$  is defined then the pull-back of  $(p, 0)$  tensors from  $N$  to  $M$  along with the push-forward of  $(0, q)$  tensors from  $M$  to  $N$  is possible. This means it is possible to push or pull generic tensors between  $M$  and  $N$  in any direction. The tangent spaces associated with  $p \in \mathcal{M}$  or  $q \in \mathcal{N}$  are therefore also preserved under mapping (aswell as open sets) meaning that local structure on the manifold is preserved under the mapping. Two common examples of diffeomorphisms are coordinate changes and translations.

## Projection Mappings

As mentioned, maps between manifolds can be used to determine the metric on an embedded surface. This requires us to consider an  $m$  dimensional manifold  $M$  with metric  $g_{\mu\nu}$  and coordinates  $x^\mu$  aswell as an embedded  $n$  dimensional surface  $N$  where  $n < m$ . We can treat  $N$  as a separate  $n$  dimensional manifold with metric  $h_{\mu\nu}$ . As before, we can define a map  $\Phi : x^\mu \rightarrow y^\mu$

PROJECTIONS HERE I THINK THEN USE IT IN VOLUMES ON MANIFOLDS TO PROJECT THE METRIC.

### 1.2.5 Lie Derivatives

We have now discussed the necessary formalism to define the Lie derivative. The Lie derivative at a point is the rate of change of a tensor field with respect to a pull-back from a diffeomorphism  $\Phi$  mapping infinitessimally close points  $p, q \in \mathcal{M}$  like  $\Phi : p = x^\mu \rightarrow q = x^\mu + \epsilon \xi^\mu$  for some vector field  $\xi$ . Like any good differential operator, the Lie derivative  $\mathcal{L}_\xi$  along  $\xi$  (and  $\mathcal{L}_\zeta$  along  $\zeta$ ) should obey,

$$\mathcal{L}_{a\xi+b\zeta}\mathbf{T} = a\mathcal{L}_\xi\mathbf{T} + b\mathcal{L}_\zeta\mathbf{T}, \quad (1.2.35)$$

$$\mathcal{L}_\xi(a\mathbf{T} + b\mathbf{W}) = a\mathcal{L}_\xi\mathbf{T} + b\mathcal{L}_\xi\mathbf{W}, \quad (1.2.36)$$

$$\mathcal{L}_\xi(f\mathbf{T}) = \mathbf{T}\mathcal{L}_\xi f + f\mathcal{L}_\xi\mathbf{T}, \quad (1.2.37)$$

for constant  $\{a, b\}$ , function  $f$  and generic tensorial objects of same type  $\mathbf{T}$  and  $\mathbf{W}$ .

The simplest example is the Lie derivative of a scalar field  $\phi$ , denoted  $\mathcal{L}_\xi\phi$  with respect to vector field  $\xi$ , is

$$\mathcal{L}_\xi\phi = \lim_{\epsilon \rightarrow 0} \left[ \frac{\Phi^*\phi|_q - \phi|_p}{\epsilon} \right], \quad (1.2.38)$$

$$= \lim_{\epsilon \rightarrow 0} \left[ \frac{\phi(x^\mu + \epsilon \xi^\mu) - \phi(x^\mu)}{\epsilon} \right], \quad (1.2.39)$$

$$= \xi^\mu \partial_\mu \phi, \quad (1.2.40)$$

which reduces to the directional derivative of  $\phi$  with respect to  $\xi$ . Next let's calculate the Lie derivative of a vector field  $\mathbf{X}$  with respect to vector field  $\xi$ . Starting with the same definition as Eq. (1.2.38), and using  $y^\mu = x^\mu + \epsilon \xi^\mu$ , the Lie derivative of  $\mathbf{X}$  is

$$(\mathcal{L}_\xi X)^\mu = \lim_{\epsilon \rightarrow 0} \left[ \frac{(\Phi^* X|_q)^\mu - X|_p^\mu}{\epsilon} \right], \quad (1.2.41)$$

$$= \lim_{\epsilon \rightarrow 0} \left[ \frac{\frac{\partial x^\mu}{\partial y^\nu} X^\nu(x^\rho + \epsilon \xi^\rho) - X^\mu(x^\rho)}{\epsilon} \right], \quad (1.2.42)$$

$$= \lim_{\epsilon \rightarrow 0} \left[ \frac{(\delta_\nu^\mu - \epsilon \partial_\nu \xi^\mu) X^\nu(x^\rho + \epsilon \xi^\rho) - X^\mu(x^\rho)}{\epsilon} \right], \quad (1.2.43)$$

$$= \lim_{\epsilon \rightarrow 0} \left[ \frac{-\epsilon \partial_\nu \xi^\mu X^\nu(x^\rho + \epsilon \xi^\rho) + X^\mu(x^\rho + \epsilon \xi^\rho) - X^\mu(x^\rho)}{\epsilon} \right], \quad (1.2.44)$$

$$= \lim_{\epsilon \rightarrow 0} \left[ \frac{-\epsilon \partial_\nu \xi^\mu X^\nu(x^\rho) + X^\mu(x^\rho + \epsilon \xi^\rho) - X^\mu(x^\rho) + \mathcal{O}(\epsilon^2)}{\epsilon} \right], \quad (1.2.45)$$

$$= \xi^\nu \partial_\nu X^\mu - X^\nu \partial_\nu \xi^\mu. \quad (1.2.46)$$

The Lie derivative for co-vectors and tensors can be derived in the same way, but can be quickly derived from the Liebnitz rule as follows. Define a scalar field  $\psi$ , vector field  $\mathbf{X}$  and co-vector field  $\omega$ , where  $\psi = X^\mu \omega_\mu$ , then it follows that

$$\mathcal{L}_\xi \psi = \xi^\mu \partial_\mu \psi = X^\nu \xi^\mu \partial_\mu \omega_\nu + \omega_\nu \xi^\mu \partial_\mu X^\nu, \quad (1.2.47)$$

$$= \mathcal{L}_\xi (X^\mu \omega_\mu), \quad (1.2.48)$$

$$= \omega_\mu (\mathcal{L}_\xi X)^\mu + X^\mu (\mathcal{L}_\xi \omega)_\mu, \quad (1.2.49)$$

$$X^\mu (\mathcal{L}_\xi \omega)_\mu = X^\nu \xi^\mu \partial_\mu \omega_\nu + \omega_\nu \xi^\mu \partial_\mu X^\nu - \omega_\mu (\mathcal{L}_\xi X)^\mu, \quad (1.2.50)$$

$$(\mathcal{L}_\xi \omega)_\mu = \xi^\nu \partial_\nu \omega_\mu + \omega_\nu \partial_\mu \xi^\nu. \quad (1.2.51)$$

Derivatives of a generic tensor  $\mathbf{T}$  follows simply, for example

$$(\mathcal{L}_\xi T)^{\alpha\beta\cdots}_{\mu\nu\cdots} = \xi^\sigma \partial_\sigma T^{\alpha\beta\cdots}_{\mu\nu\cdots} + T^{\alpha\beta\cdots}_{\sigma\nu\cdots} \partial_\mu \xi^\sigma + T^{\alpha\beta\cdots}_{\mu\sigma\cdots} \partial_\nu \xi^\sigma + \dots - T^{\sigma\beta\cdots}_{\mu\nu\cdots} \partial_\sigma \xi^\alpha - T^{\alpha\sigma\cdots}_{\mu\nu\cdots} \partial_\sigma \xi^\beta - \dots \quad (1.2.52)$$

### 1.2.6 Lengths on Manifolds

The natural entry point for studying curved geometry is to revisit Pythagoras' theorem. For this we need a manifold  $\mathcal{M}$  equipped with a metric  $g$ , written as  $(\mathcal{M}, g)$  for short. The distance  $ds$  between two infinitessimally close points  $p \in \mathcal{M}$  and  $p + \delta p \in \mathcal{M}$ , with coordinates  $x^\mu$  and  $x^\mu + dx^\mu$ , is given by

$$ds^2 = \mathbf{g}(\mathbf{dx}, \mathbf{dx}) = g_{\mu\nu} dx^\mu dx^\nu, \quad (1.2.53)$$

where  $g_{\mu\nu}$  are the components of the metric tensor. This is the generalisation of Eq. (1.2.2) to curved space; notably the line element can now have varying coefficients from  $g_{\mu\nu}$  and cross terms such as  $dx^\mu dx^\nu$ . The special choice of  $g_{\mu\nu} = \delta_{\mu\nu}$  gives us flat space, also called Euclidean space, where  $\delta_{\mu\nu} = 1$  if  $\mu = \nu$  and vanishes otherwise. With the line element defined, we can immediately apply it to calculating the length of a general curve in curved space. Consider the curve  $\Gamma$  consisting of a set of smoothly connected points  $p(\lambda) \in \mathcal{M}$  smoothly parameterised by  $\lambda$ . We can calculate the length  $\Delta s$  of the curve between  $\lambda_1 \geq \lambda \geq \lambda_0$  by

$$ds^2 = \frac{\partial x^\mu}{\partial \lambda} \frac{\partial x^\nu}{\partial \lambda} g_{\mu\nu} d\lambda^2, \quad (1.2.54)$$

$$\Delta s = \int_{\lambda_0}^{\lambda_1} \sqrt{\left( \frac{\partial x^\mu}{\partial \lambda} \frac{\partial x^\nu}{\partial \lambda} g_{\mu\nu} \right)} d\lambda. \quad (1.2.55)$$

In the simplified case where  $\lambda$  is one of the coordinates, say  $\xi$ , the length  $\Delta s$  becomes,

$$\Delta s = \int_{\xi_0}^{\xi_1} \sqrt{g_{\xi\xi}} d\xi. \quad (1.2.56)$$

### 1.2.7 Volumes on Manifolds

The natural extension to measuring the length of a curve is the measurement of volumes; of course we still require a metric  $\mathbf{g}$  over the manifold  $\mathcal{M}$ . Let's say that in a coordinate system  $x^\mu$  we can define the volume  $V$  of some subregion  $M$  of  $\mathcal{M}$  by integrating some weight function  $w(x^\mu)$ ,

$$V = \int_M w(x^\mu) dx^1 dx^2 \dots dx^n, \quad (1.2.57)$$

over  $M$ . To find  $w(\mu)$ , start by defining an orthogonal coordinate transformation  $x^\mu \rightarrow \tilde{x}^\mu$  such that  $\tilde{\mathbf{g}}$  is diagonal and  $\det(\mathbf{g}) = \det(\tilde{\mathbf{g}})$ ; this is always possible as  $\mathbf{g}$  is real and symmetric. In this coordinate system, the volume  $\delta V$  in an infinitesimal cuboid, with  $i$ 'th sidelength  $\delta \tilde{x}^i$ , is

$$\delta V = \left( \sqrt{\tilde{g}_{11}} \delta \tilde{x}^1 \right) \left( \sqrt{\tilde{g}_{22}} \delta \tilde{x}^2 \right) \dots \left( \sqrt{\tilde{g}_{nn}} \delta \tilde{x}^n \right), \quad (1.2.58)$$

where Eq. (1.2.56) was used to get the length between each  $\tilde{x}^i$  and  $\tilde{x}^i + \delta\tilde{x}^i$ . Given that  $\tilde{\mathbf{g}}$  is diagonal we know the  $i$ 'th eigenvalue  $\tilde{\lambda}_i = \tilde{g}_{ii}$  and therefore  $\det(\tilde{\mathbf{g}}) = \prod_i \tilde{g}_{ii}$ . Thus the volume  $\delta V$  can be rewritten

$$\delta V = \sqrt{|\det(\tilde{\mathbf{g}})|} \delta\tilde{x}^1 \delta\tilde{x}^2 \dots \delta\tilde{x}^n, \quad (1.2.59)$$

and the formula for the finite volume  $M$  is

$$V = \int_M \sqrt{|\det\{\tilde{\mathbf{g}}\}|} d\tilde{x}^1 d\tilde{x}^2 \dots d\tilde{x}^n, \quad (1.2.60)$$

and the form of the weight function in  $\tilde{x}^\mu$  coordinates is  $w(\tilde{x}^\mu) = \sqrt{|\det(\tilde{\mathbf{g}})|}$ . We are now free to transform back from  $\tilde{x}^\mu \rightarrow x^\mu$ , and given that the transformation is orthogonal we know that  $\det(\mathbf{g}) = \det(\tilde{\mathbf{g}})$  and the Jacobian matrix  $\mathbf{J}$  of the coordinate transformation has  $\det(\mathbf{J}) = 1$ , therefore

$$V = \int_M \sqrt{|\det\{\mathbf{g}\}|} dx^1 dx^2 \dots dx^n, \quad (1.2.61)$$

which holds for any non-diagonal, real and symmetric metric  $\mathbf{g}$ . In general we will now denote the determinant of a metric  $\det(\mathbf{g})$  with the lower case letter  $g$ . When dealing with a pseudo-Riemannian manifold with a negative determinant, such as spacetime, it is more common to see  $\sqrt{-g}$  written rather than  $\sqrt{|g|}$  giving

$$V = \int_M \sqrt{-g} dx^1 dx^2 \dots dx^n. \quad (1.2.62)$$

Equation (1.2.60) can also be used to find the volume (or area) of a lower dimensional sub-volume. First cover the new sub-volume  $A$  with coordinates  $y^\mu$ , where  $\mu \in \{1, 2, \dots, m\}$  for  $m < n$ , and then calculate the metric  $\mathbf{h}$  which can be done using the pullback of  $\mathbf{g}$

$$h_{\sigma\rho} = (\Phi^* g)_{\sigma\rho} = \frac{\partial x^\mu}{\partial y^\sigma} \frac{\partial x^\nu}{\partial y^\rho} g_{\mu\nu} \quad (1.2.63)$$

as shown in Section 1.2.4. Using  $y^\mu$  and  $h$ , the volume  $V_A$  of  $A$  as

$$V_A = \int_A \sqrt{|h|} dy^1 dy^2 \dots dy^m. \quad (1.2.64)$$

NEED TO RE-WRITE THE MAPS SECTION TO HAVE PROJECTIONS AT THE END THEN QUOTE IT FOR THE PROJECTED METRIC HERE INSTEAD OF DERIVING THE PROJECTED METRIC HERE

### 1.2.8 Geodesics

For a manifold equipped with metric  $(\mathcal{M}, g)$  the curve with shortest distance between two points  $p, q \in \mathcal{M}$  is called a geodesic. To find the geodesic joining  $p$  and  $q$  we need to use calculus of variation on the total length  $\Delta s$  from Eq. (1.2.55) of a general curve between two points. Given that the integrand  $\mathcal{L}$  of Eq. (1.2.55) is a function like  $\mathcal{L}(x^\mu, \dot{x}^\mu)$ , where the dot means differentiation by  $\lambda$ , we can use the Euler-Lagrange equation,

$$\frac{\partial \mathcal{L}}{\partial x^\mu} - \frac{d}{d\lambda} \frac{\partial \mathcal{L}}{\partial \dot{x}^\mu} = 0 \quad (1.2.65)$$

to give a differential equation with solution being a geodesic. Applyin the EL equation to the integrand of Eq. (1.2.55) is algebraically messy, it is easier to square the integrand and start from  $\mathcal{L}^2$  giving the

same solution if  $d\mathcal{L}/d\lambda = 0^2$ ,

$$\frac{\partial \mathcal{L}^2}{\partial x^\alpha} - \frac{d}{d\lambda} \frac{\partial \mathcal{L}^2}{\partial \dot{x}^\alpha} = 0, \quad (1.2.66)$$

$$\frac{\partial}{\partial x^\alpha} (g_{\mu\nu} \dot{x}^\mu \dot{x}^\nu) - \frac{d}{d\lambda} \frac{\partial}{\partial \dot{x}^\alpha} (g_{\mu\nu} \dot{x}^\mu \dot{x}^\nu) = 0, \quad (1.2.67)$$

$$(\partial_\alpha g_{\mu\nu}) \dot{x}^\mu \dot{x}^\nu - 2 \frac{d}{d\lambda} (g_{\alpha\nu} \dot{x}^\nu) = 0, \quad (1.2.68)$$

$$(\partial_\alpha g_{\mu\nu}) \dot{x}^\mu \dot{x}^\nu - 2 (\dot{x}^\rho \partial_\rho (g_{\alpha\nu}) \dot{x}^\nu) - 2 \ddot{x}^\nu g_{\alpha\nu} = 0. \quad (1.2.69)$$

Rearranging and multiplying by  $g^{\alpha\beta}$  gives

$$\ddot{x}^\beta + \frac{1}{2} g^{\alpha\beta} (\partial_\mu g_{\alpha\nu} + \partial_\nu g_{\alpha\mu} - \partial_\alpha g_{\mu\nu}) \dot{x}^\mu \dot{x}^\nu = 0, \quad (1.2.70)$$

$$\ddot{x}^\beta + \Gamma^\beta_{\mu\nu} \dot{x}^\mu \dot{x}^\nu = 0, \quad (1.2.71)$$

where  $\Gamma^\beta_{\mu\nu}$  is the components of the connection-symbol from Eq. (1.3.77). A trivial solution to Eq. (1.2.71) is in flat space using cartesian coordinates where  $\Gamma^\beta_{\mu\nu} = 0$  and therefore  $\ddot{x}^\beta = 0$  so  $\dot{x}^\beta$  is a constant; this tells us the shortest distance between two points in flat space is a straight line. In other words, geodesics are straight lines in flat space.

## Non-affine Geodesics

The equation of a geodesic given above is true for an affinely parameterised curve. An affine parameter  $\lambda$  is defined so that the length of a curve  $\Delta s$  between two parameter values  $\lambda_0$  and  $\lambda_1$  is given by  $\Delta s = k(\lambda_1 - \lambda_0)$  for constant  $k$ ; the arclength along a curve is linearly proportional to the value of the  $\lambda$ . The reason this happened with the calculation above is that  $d\mathcal{L}/d\lambda = 0$  was assumed.

A non-affine parameter  $\mu$  could equally be used to describe the curve. Writing  $\mu(\lambda)$  the geodesic equation is transformed as shown,

$$\frac{d^2 x^\beta}{d\lambda^2} + \Gamma^\beta_{\mu\nu} \frac{dx^\mu}{d\lambda} \frac{dx^\nu}{d\lambda} = 0, \quad (1.2.72)$$

$$\left( \frac{d^2 \mu}{d\lambda^2} \frac{d}{d\mu} + \left( \frac{d\mu}{d\lambda} \right)^2 \frac{d^2}{d\mu^2} \right) x^\beta + \Gamma^\beta_{\mu\nu} \frac{dx^\mu}{d\mu} \frac{dx^\nu}{d\mu} \left( \frac{d\mu}{d\lambda} \right)^2 = 0, \quad (1.2.73)$$

$$\frac{d^2 x^\beta}{d\mu^2} + \Gamma^\beta_{\mu\nu} \frac{dx^\mu}{d\mu} \frac{dx^\nu}{d\mu} = - \left( \frac{d\mu}{d\lambda} \right)^{-2} \frac{d^2 \mu}{d\lambda^2} \frac{dx^\beta}{d\mu}, \quad (1.2.74)$$

$$\frac{d^2 x^\beta}{d\mu^2} + \Gamma^\beta_{\mu\nu} \frac{dx^\mu}{d\mu} \frac{dx^\nu}{d\mu} = -f(\mu) \frac{dx^\beta}{d\mu}, \quad (1.2.75)$$

$$(1.2.76)$$

which is the same as the affine geodesic equation except with an extra non-zero right hand side proportional to  $dx^\beta/d\mu$  and some function  $f(\mu)$ .

IS THIS WELL ENOUGH EXPLAINED, ESPECIALLY THE DLDLAMBDA=0 Bit?

## 1.3 Tensor Calculus and Curvature

### 1.3.1 General Covariance and Coordinate transformations

Many laws of physics can be expressed as tensor field equations where a tensor field is the assignment of a tensor to each point in space. This assignment must be smooth as it is to describe physical quantities.

---

<sup>2</sup>Given that  $\mathcal{L}$  is homogenous to degree  $k$ ,  $\dot{x}^i \partial \mathcal{L} / \partial \dot{x}^i = k\mathcal{L}$  for constant  $k$ , one can show that  $d\mathcal{L}/d\lambda = 0$  if the Euler-Lagrange equation is assumed.

The power of tensor algebra and tensor calculus is that if a tensor field equation can be written in one coordinate system then must hold (in index form) in all sensible coordinate system. This is a consequence of the tensor transformation law. Looking back, we can write a generic vector  $\mathbf{X}$  as  $X^\mu \mathbf{e}_\mu = X^\mu \partial_\mu$  and if we choose a coordinate transformation  $x^\mu \rightarrow \tilde{x}^\mu$  then we see that in the transformed coordinate system the vector field  $\mathbf{X}$ , written  $\tilde{\mathbf{X}}$ , becomes

$$\tilde{\mathbf{X}} = \tilde{X}^\mu \frac{\partial}{\partial \tilde{x}^\mu}, \quad (1.3.1)$$

$$= \tilde{X}^\mu \frac{\partial x^\nu}{\partial \tilde{x}^\mu} \frac{\partial}{\partial x^\nu}, \quad (1.3.2)$$

$$= X^\nu \frac{\partial}{\partial x^\nu}, \quad (1.3.3)$$

$$= \mathbf{X}, \quad (1.3.4)$$

where the components  $X^\nu = \tilde{X}^\mu \frac{\partial x^\nu}{\partial \tilde{x}^\mu}$  are required to transform in order to ensure  $\mathbf{X} = \tilde{\mathbf{X}}$ . This says that the underlying geometric object (a vector in this case) is independent of the coordinates used to describe them; the tradeoff for this useful property is that the vectors components  $X^\mu$  have to transform under the tensor transformation law, effectively opposing the transformation of the basis vectors. Working from a co-vector  $\omega$  we can write it as  $\omega_\mu \theta^\mu = \omega_\mu dx^\mu$  in component-basis form [REF THIS?] and the same coordinate transform gives

$$\tilde{\omega} = \tilde{\omega}_\mu d\tilde{x}^\mu, \quad (1.3.5)$$

$$= \tilde{\omega}_\mu \frac{\partial \tilde{x}^\mu}{\partial x^\nu} dx^\nu, \quad (1.3.6)$$

$$= \omega_\nu dx^\nu, \quad (1.3.7)$$

where the co-vector components transform like  $\omega_\nu = \tilde{\omega}_\mu \frac{\partial \tilde{x}^\mu}{\partial x^\nu}$ , the opposite way to the vector components. These transformation laws ensure that a scalar field created from the product of a vector field and a co-vector field, like  $\omega : \mathbf{X}$ , is a Lorentz scalar not transforming under coordinate transformations. This can be seen from

$$\tilde{\omega} : \tilde{\mathbf{X}} = \tilde{X}^\mu \tilde{\omega}_\mu, \quad (1.3.8)$$

$$= X^\nu \frac{\partial \tilde{x}^\mu}{\partial x^\nu} \frac{\partial x^\rho}{\partial \tilde{x}^\mu} \omega_\rho, \quad (1.3.9)$$

$$= X^\nu \frac{\partial x^\rho}{\partial x^\nu} \omega_\rho, \quad (1.3.10)$$

$$= X^\nu \delta_\nu^\rho \omega_\rho, \quad (1.3.11)$$

$$= X^\nu \omega_\nu, \quad (1.3.12)$$

$$= \omega : \mathbf{X}. \quad (1.3.13)$$

The general tensor transformation law can be derived easily from chaining multiple of the previous examples together, for example

$$\tilde{T}^{\mu\nu\dots}_{\rho\sigma\dots} = T^{\alpha\beta\dots}_{\gamma\delta\dots} \left( \frac{\partial \tilde{x}^\mu}{\partial x^\alpha} \frac{\partial \tilde{x}^\nu}{\partial x^\beta}, \dots \times \frac{\partial x^\gamma}{\partial \tilde{x}^\rho} \frac{\partial x^\delta}{\partial \tilde{x}^\sigma}, \dots \right). \quad (1.3.14)$$

## Tensor Densities

A tensor density is the generalisation of a tensor field obeying the tensor transformation law in Eq. (1.3.14) to a tensor field multiplied by a power of the determinant of the Jacobian matrix of a coordinate transformation. One important example of a tensor density is the volume element  $\sqrt{-g}$ , this is a scalar density. This object does not have any indices so at first glance may pass for a true scalar field. However,



when a coordinate transformation  $x^\mu \rightarrow \tilde{x}^\mu$  is applied we find that  $\sqrt{-g} \rightarrow \sqrt{-\tilde{g}} \neq \sqrt{-g}$  but for a general scalar field  $\phi$  we find  $\phi \rightarrow \tilde{\phi} = \phi$ ; therefore  $\sqrt{-g}$  cannot be a scalar field. This can be shown explicitly by look at the the determinant of the metric,

$$\sqrt{-\tilde{g}} = \sqrt{\det(-\tilde{g}_{\mu\nu})}, \quad (1.3.15)$$

$$= \sqrt{\det \left( -g_{\alpha\beta} \frac{\partial x^\alpha}{\partial \tilde{x}^\mu} \frac{\partial x^\beta}{\partial \tilde{x}^\nu} \right)}, \quad (1.3.16)$$

$$= \sqrt{-g} \det \left( \frac{\partial x^\alpha}{\partial \tilde{x}^\mu} \right), \quad (1.3.17)$$

and as can be seen, the volume element picks up a factor of the determinant of the Jacobean. This property shows up in multidimensional intergrals, for instance when taking a three-dimensional integral over cartesian coordinates we must replace the  $dx dy dz \rightarrow dr d\theta d\phi r^2 \sin(\theta)$  [MAYBE DO THIS LATER AFTER INTEGRATION ON MANIFODS?]

A tensor density  $\mathcal{T}$  of weight  $w$  can be written in the form,

$$\mathcal{T} = \sqrt{-g}^w T, \quad (1.3.18)$$

where  $T$  is a tensor obeying the tensor transformation law. It should be noted that a tensor density of weight zero is a regular tensors and the weight of a tensor has nothing to do with the rank of the tensor.

### Lie Derivatives of Tensor Densities

To calculate the Lie derivative of a tensor density, first the Lie derivative of  $\sqrt{-g}$  should be calculated, and in order to calculate the Lie derivative of the volume element a preliminary result is needed. Following the definition of a Lie derivative in section 1.2.5 and setting  $y^\mu = x^\mu + \epsilon \xi^\mu$ , the determinant of the Jacobean matrix is,

$$\det \left( \frac{\partial y^\mu}{\partial x^\rho} \right) = \det \left( \delta_\rho^\mu + \epsilon \frac{\partial \xi^\mu}{\partial x^\rho} \right), \quad (1.3.19)$$

$$= \det \begin{pmatrix} 1 + \epsilon \frac{\partial \xi^1}{\partial x^1} & \epsilon \frac{\partial \xi^1}{\partial x^2} & \epsilon \frac{\partial \xi^1}{\partial x^3} & \epsilon \frac{\partial \xi^1}{\partial x^4} \\ \epsilon \frac{\partial \xi^2}{\partial x^1} & 1 + \epsilon \frac{\partial \xi^2}{\partial x^2} & \epsilon \frac{\partial \xi^2}{\partial x^3} & \epsilon \frac{\partial \xi^2}{\partial x^4} \\ \epsilon \frac{\partial \xi^3}{\partial x^1} & \epsilon \frac{\partial \xi^3}{\partial x^2} & 1 + \epsilon \frac{\partial \xi^3}{\partial x^3} & \epsilon \frac{\partial \xi^3}{\partial x^4} \\ \epsilon \frac{\partial \xi^4}{\partial x^1} & \epsilon \frac{\partial \xi^4}{\partial x^2} & \epsilon \frac{\partial \xi^4}{\partial x^3} & 1 + \epsilon \frac{\partial \xi^4}{\partial x^4} \end{pmatrix}, \quad (1.3.20)$$

$$= \left( 1 + \epsilon \sum_i \frac{\partial \xi^i}{\partial x^i} + \mathcal{O}(\epsilon^2) \right), \quad (1.3.21)$$

$$= 1 + \epsilon \partial_\mu \xi^\mu + \mathcal{O}(\epsilon^2), \quad (1.3.22)$$

where four dimensions was used for clarity, but the calculation works exactly the same in any number of dimensions. Using this result and the definition of a Lie derivative,  $\mathcal{L}_\xi \sqrt{-g}$  evaluates to

$$\mathcal{L}_\xi \sqrt{-g} = \lim_{\epsilon \rightarrow 0} \left( \frac{\Phi^* \sqrt{-g}|_q - \sqrt{-g}|_p}{\epsilon} \right), \quad (1.3.23)$$

$$= \lim_{\epsilon \rightarrow 0} \left( \frac{\sqrt{-\det \left( g_{\mu\nu}(y^\alpha) \frac{\partial y^\mu}{\partial x^\rho} \frac{\partial y^\nu}{\partial x^\sigma} \right)} - \sqrt{-g}(x^\alpha)}{\epsilon} \right), \quad (1.3.24)$$

$$= \lim_{\epsilon \rightarrow 0} \left( \frac{\sqrt{-g}(y^\alpha) \det \left( \frac{\partial y^\mu}{\partial x^\rho} \right) - \sqrt{-g}(x^\alpha)}{\epsilon} \right), \quad (1.3.25)$$

$$= \lim_{\epsilon \rightarrow 0} \left( \frac{\sqrt{-g}(y^\alpha) (1 + \epsilon \partial_\mu \xi^\mu + \mathcal{O}(\epsilon^2)) - \sqrt{-g}(x^\alpha)}{\epsilon} \right), \quad (1.3.26)$$

$$= \lim_{\epsilon \rightarrow 0} \left( \frac{[\sqrt{-g}(x^\alpha) + \epsilon \xi^\mu \partial_\mu \sqrt{-g}(x^\alpha)] (1 + \epsilon \partial_\mu \xi^\mu + \mathcal{O}(\epsilon^2)) - \sqrt{-g}(x^\alpha)}{\epsilon} \right), \quad (1.3.27)$$

$$= \lim_{\epsilon \rightarrow 0} \left( \frac{\epsilon \xi^\mu \partial_\mu \sqrt{-g}(x^\alpha) + \epsilon \sqrt{-g}(x^\alpha) \partial_\mu \xi^\mu + \mathcal{O}(\epsilon^2)}{\epsilon} \right), \quad (1.3.28)$$

$$\mathcal{L}_\xi \sqrt{-g} = \xi^\mu \partial_\mu \sqrt{-g} + \sqrt{-g} \partial_\mu \xi^\mu. \quad (1.3.29)$$

Given that  $\mathcal{L}_\xi \sqrt{-g}$  has been calculated, it is straightforward to calculate the Lie derivative of a tensor density  $\mathcal{T} = \sqrt{-g}^w \mathbf{T}$  of weight  $w$ , where  $\mathbf{T}$  is a regular tensor, using the Liebnitz rule in Eq. (1.2.37). The Lie derivative is,

$$\mathcal{L}_\xi \mathcal{T} = \sqrt{-g}^w \left( \mathcal{L}_\xi \mathbf{T} + w \mathbf{T} \left( \frac{1}{\sqrt{-g}} \xi^\mu \partial_\mu \sqrt{-g} + \partial_\mu \xi^\mu \right) \right), \quad (1.3.30)$$

where the Leibnitz rule of differentiation has been used. As would be expected, setting  $w = 0$  returns the regular Lie derivative of a tensor. This can also be written as,

$$\mathcal{L}_\xi \mathcal{T} = \tilde{\mathcal{L}}_\xi \mathcal{T} + w \mathcal{T} \partial_\mu \xi^\mu, \quad (1.3.31)$$

where  $\tilde{\mathcal{L}}_\xi$  is the differential operator equivalent to the Lie derivate of the same tensor but with weight zero.

CHECK THIS IS CORRECT AND USED CORRECTLY LATER IN THE CCZ4 EQUATIONS SECTION

### 1.3.2 The Covariant Derivative

There are many types of derivative on a manifold, all related to each other, that we care about in the context of General Relativity. The simplest is the partial derivative, denoted

$$\partial_\mu = \frac{\partial}{\partial x^\mu}, \quad (1.3.32)$$

which works much the same as always. Two other derivatives are the exterior derivative [MAYBE REF THIS] and the Lie derivative which are discussed in [REF] and section 1.2.5 respectively.

The purpose of the covariant derivative, denoted  $\nabla_\mu$ , is to generalise the partial derivative to curved spaces (or curvilinear coordinates). The covariant derivative exactly reduces to the partial derivative ( $\partial_\mu$ ) in flat space with cartesian coordinates. As suggested by the name, the covariant derivative of an

object is covariant; it obeys the tensor transformation law in section 1.3.1. The covariant derivative uses a vector field  $\mathbf{X}$  to map a  $(p, q)$  tensor field  $\mathbf{T}$  to a  $(p, q)$  tensor field  $\nabla_{\mathbf{X}}\mathbf{T}$ . Requiring the covariant derivative of a tensor to return another tensor may sound pedantic but it allows the writing of physical differential equations that are covariant, i.e. that hold in all coordinate systems. Encoding the laws of physics with tensor differential equations is explored in more detail in Section [REF!].

To be the analogue of the partial derivative, three properties of the covariant derivative are required,

$$\nabla_{f\mathbf{X}+g\mathbf{Y}}\mathbf{T} = f\nabla_{\mathbf{X}}\mathbf{T} + g\nabla_{\mathbf{Y}}\mathbf{T}, \quad (1.3.33)$$

$$\nabla_{\mathbf{X}}(a\mathbf{T} + b\mathbf{W}) = a\nabla_{\mathbf{X}}\mathbf{T} + b\nabla_{\mathbf{X}}\mathbf{W}, \quad (1.3.34)$$

$$\nabla_{\mathbf{X}}(f\mathbf{T}) = f\nabla_{\mathbf{X}}\mathbf{T} + \mathbf{T}\nabla_{\mathbf{X}}f, \quad (1.3.35)$$

where  $a$  and  $b$  are constants,  $f$  and  $g$  are functions and  $\mathbf{T}$  and  $\mathbf{W}$  are tensors of equal type. These are exactly the same as the conditions imposed on Lie derivatives in section 1.2.5. From now on the covariant derivative  $\nabla_{\mathbf{e}_\mu}$  with respect to a basis vector  $\mathbf{e}_\mu$  will be written as  $\nabla_\mu$ .

Lets start by finding the covariant derivative of a scalar field  $\varphi$ . The partial derivative  $\partial_\mu\varphi$  obeys the tensor transformation law for a co-vector,

$$\frac{\partial}{\partial \tilde{x}^\mu} \tilde{\varphi} = \frac{\partial}{\partial \tilde{x}^\mu} \varphi, \quad (1.3.36)$$

$$= \frac{\partial x^\nu}{\partial \tilde{x}^\mu} \frac{\partial}{\partial x^\nu} \varphi, \quad (1.3.37)$$

and therefore the  $\nabla_\mu\varphi = \partial_\mu\varphi$ . Note that  $\varphi = \tilde{\varphi}$  for any point  $p$  as a scalar remains unchanged in a coordinate transformation. Complications arise when taking the partial derivative of any other higher rank tensor; let's demonstrate this with a vector  $\mathbf{X}$ .

$$\frac{\partial}{\partial \tilde{x}^\mu} \tilde{X}^\alpha = \frac{\partial}{\partial \tilde{x}^\mu} \left( \frac{\partial \tilde{x}^\alpha}{\partial x^\beta} X^\beta \right), \quad (1.3.38)$$

$$= \frac{\partial x^\nu}{\partial \tilde{x}^\mu} \frac{\partial}{\partial x^\nu} \left( \frac{\partial \tilde{x}^\alpha}{\partial x^\beta} X^\beta \right), \quad (1.3.39)$$

$$= \underbrace{\frac{\partial \tilde{x}^\alpha}{\partial x^\beta} \frac{\partial x^\nu}{\partial \tilde{x}^\mu}}_{\text{Tensor transformation law}} \frac{\partial}{\partial x^\nu} X^\beta + X^\beta \frac{\partial x^\nu}{\partial \tilde{x}^\mu} \frac{\partial}{\partial x^\nu} \left( \frac{\partial \tilde{x}^\alpha}{\partial x^\beta} \right), \quad (1.3.40)$$

and as can be seen, only the first term on the right hand side should exist if the components  $\partial_\mu X^\alpha$  were to obey the tensor transformation law.

The problem with performing differentiation on tensors is that it requires the comparison of tensors at two different (infinitesimally close) tangent spaces. Lie derivatives circumvented this problem by comparing two tangent planes with a pullback defined by a diffeomorphism. Another way of overcoming this problem is to consider how the coordinate basis vectors change over the manifold, not just the components. Defining the covariant derivative of the basis vector as

$$\nabla_{\mathbf{e}_\rho} \mathbf{e}_\nu = \nabla_\rho \mathbf{e}_\nu := \Gamma_{\nu\rho}^\mu \mathbf{e}_\mu \quad (1.3.41)$$

where  $\Gamma_{\nu\rho}^\mu$  is called the connection due to it defining a connection between neighbouring tangent space. The connection can be used to get the covariant derivative of the vector field  $\mathbf{X} = X^\rho \mathbf{e}_\rho$ ,

$$\nabla_\rho (X^\nu \mathbf{e}_\nu) = (\partial_\rho X^\nu) \mathbf{e}_\nu + X^\nu (\nabla_\rho \mathbf{e}_\nu), \quad (1.3.42)$$

$$= (\partial_\rho X^\nu) \mathbf{e}_\nu + X^\nu \Gamma_{\nu\rho}^\mu \mathbf{e}_\mu, \quad (1.3.43)$$

$$= (\partial_\rho X^\mu + \Gamma_{\nu\rho}^\mu X^\nu) \mathbf{e}_\mu. \quad (1.3.44)$$

Note that on the first line above we used  $\nabla_\rho X^\nu = \partial_\rho X^\nu$  as the  $X^\nu$  are being treated as a set of scalar function coefficients multiplying the basis vectors  $e_\mu$ . Strictly we should write the covariant derivative of  $\mathbf{X}$  as

$$\nabla \mathbf{X} = (\nabla X)_\sigma^\mu e_\mu \otimes \theta^\sigma \quad (1.3.45)$$

but for convenience the coefficients  $(\nabla X)_\sigma^\mu$  are usually denoted as,

$$\nabla_\sigma X^\mu = \partial_\sigma X^\mu + \Gamma_{\nu\sigma}^\mu X^\nu. \quad (1.3.46)$$

This is a slight abuse of notation as  $\nabla_\sigma X^\mu$  might be understood as the covariant derivative of the components  $X^\mu$ , but really it denotes the component  $\theta^\sigma \cdot (\nabla \mathbf{X}) \cdot e_\mu$  where  $\nabla \mathbf{X}$  is given in Eq. (1.3.45).

Given that the covariant derivative of a scalar reduces to the partial derivative we can see that

$$\nabla_\rho(e_\mu : \theta^\nu) = 0, \quad (1.3.47)$$

and using the Liebnitz rule we see that

$$\nabla_\rho(e_\nu : \theta^\mu) = (\nabla_\rho e_\nu) : \theta^\mu + e_\nu : (\nabla_\rho \theta^\mu), \quad (1.3.48)$$

$$= (\Gamma_{\nu\rho}^\sigma e_\sigma) : \theta^\mu + e_\nu : (\nabla_\rho \theta^\mu), \quad (1.3.49)$$

$$= \Gamma_{\nu\rho}^\mu + e_\nu : (\nabla_\rho \theta^\mu), \quad (1.3.50)$$

$$e_\nu : (\nabla_\rho \theta^\mu) = -\Gamma_{\nu\rho}^\mu \quad (1.3.51)$$

therefore we must have

$$\nabla_\rho \theta^\mu = -\Gamma_{\nu\rho}^\mu \theta^\nu. \quad (1.3.52)$$

In an identical way to before, we might ask what is the covariant derivative of a co-vector  $\omega = \omega_\alpha \theta^\alpha$ . The covariant derivative  $\nabla \omega$  can be found like

$$\nabla_\sigma \omega = \nabla_\sigma(\omega_\alpha \theta^\alpha), \quad (1.3.53)$$

$$= \partial_\sigma(\omega_\alpha) \theta^\alpha + \omega_\alpha \nabla_\sigma \theta^\alpha, \quad (1.3.54)$$

$$= \partial_\sigma(\omega_\alpha) \theta^\alpha - \omega_\alpha \Gamma_{\nu\sigma}^\alpha \theta^\nu, \quad (1.3.55)$$

$$= (\partial_\sigma \omega_\alpha - \omega_\nu \Gamma_{\alpha\sigma}^\nu) \theta^\alpha. \quad (1.3.56)$$

Again, we used  $\nabla_\sigma \omega_\alpha = \partial_\sigma \omega_\alpha$  as the components  $\omega_\alpha$  are scalar coefficients of the basis co-vectors  $\theta^\alpha$ . Similarly to earlier, from now on the components  $(\nabla \omega)_{\sigma\alpha}$  are written as  $\nabla_\sigma \omega_\alpha$  even though this is a mild abuse of notation.

The covariant derivative of a general tensor can be found by following the simple rule of adding a connection symbol term for each index, for example

$$\nabla_\mu T_{\lambda\nu\dots}^{\alpha\beta\dots} = \partial_\mu T_{\lambda\nu\dots}^{\alpha\beta\dots} + \Gamma_{\sigma\mu}^\alpha T_{\lambda\nu\dots}^{\sigma\beta\dots} + \Gamma_{\sigma\mu}^\beta T_{\lambda\nu\dots}^{\alpha\sigma\dots} + \dots - \Gamma_{\lambda\mu}^\sigma T_{\sigma\nu\dots}^{\alpha\beta\dots} - \Gamma_{\nu\mu}^\sigma T_{\lambda\sigma\dots}^{\alpha\beta\dots} - \dots \quad (1.3.57)$$

COV DERIV OF TENSOR DENSITIES - MAYBE TENSOR DENSITIES ARE THEIR OWN SECTION. COULD BE QUICK, I ASSUME NABLA MU ROOTG =0

### 1.3.3 The Connection

In flat space we are used to the idea that the partial derivative commutes, i.e.  $\partial_\mu \partial_\nu = \partial_\nu \partial_\mu$ , and this is trivially true in curved space too. However, the covariant derivative does not generally commute,  $\nabla_\mu \nabla_\nu \neq \nabla_\nu \nabla_\mu$ . Applying  $\nabla_\mu \nabla_\nu - \nabla_\nu \nabla_\mu$  to a scalar field  $\varphi$  gives,

$$(\nabla_\mu \nabla_\nu - \nabla_\nu \nabla_\mu) \varphi = \nabla_\mu \nabla_\nu \varphi - \nabla_\nu \nabla_\mu \varphi, \quad (1.3.58)$$

$$= \nabla_\mu \partial_\nu \varphi - \nabla_\nu \partial_\mu \varphi, \quad (1.3.59)$$

$$= (\partial_\mu \partial_\nu - \partial_\nu \partial_\mu) \varphi - \Gamma_{\nu\mu}^\sigma \partial_\sigma \varphi + \Gamma_{\mu\nu}^\sigma \partial_\sigma \varphi, \quad (1.3.60)$$

$$= (\Gamma_{\mu\nu}^\sigma - \Gamma_{\nu\mu}^\sigma) \partial_\sigma \varphi, \quad (1.3.61)$$

where we used the fact that  $\nabla_\mu \varphi = \partial_\mu \varphi$  for a scalar field. This non-commutativity of derivatives on a scalar field is known as torsion.

### Torsion

If a connection is torsion free then  $(\nabla_\mu \nabla_\nu - \nabla_\nu \nabla_\mu) \varphi = 0$  which implies  $\Gamma^\sigma_{\nu\mu} = \Gamma^\sigma_{\mu\nu}$ . This leads to two important tensor identities; first the antisymmetric derivative of a co-vector,

$$\nabla_\mu A_\nu - \nabla_\nu A_\mu = \partial_\mu A_\nu - \partial_\nu A_\mu - \underbrace{(\Gamma^\sigma_{\nu\mu} - \Gamma^\sigma_{\mu\nu})}_{=0} A_\sigma, \quad (1.3.62)$$

$$\nabla_\mu A_\nu - \nabla_\nu A_\mu = \partial_\mu A_\nu - \partial_\nu A_\mu, \quad (1.3.63)$$

and the second identity,

$$\nabla_X Y - \nabla_Y X = (X^\mu \nabla_\mu Y^\nu - Y^\mu \nabla_\mu X^\nu) e_\nu, \quad (1.3.64)$$

$$= (X^\mu \partial_\mu Y^\nu - Y^\mu \partial_\mu X^\nu + \Gamma^\nu_{\sigma\mu} X^\mu Y^\sigma - \Gamma^\nu_{\sigma\mu} Y^\mu X^\sigma) e_\nu, \quad (1.3.65)$$

$$= (X^\mu \partial_\mu Y^\nu - Y^\mu \partial_\mu X^\nu + (\Gamma^\nu_{\sigma\mu} - \Gamma^\nu_{\mu\sigma}) X^\mu Y^\sigma) e_\nu, \quad (1.3.66)$$

$$= (X^\mu \partial_\mu Y^\nu - Y^\mu \partial_\mu X^\nu) e_\nu, \quad (1.3.67)$$

$$\nabla_X Y - \nabla_Y X = [X, Y]. \quad (1.3.68)$$

The commutator bracket  $[X, Y]$  of two vectors  $X$  and  $Y$  is defined by

$$[X^\mu \partial_\mu, Y^\nu \partial_\nu] = X^\mu \partial_\mu (Y^\nu \partial_\nu) - Y^\nu \partial_\nu (X^\mu \partial_\mu), \quad (1.3.69)$$

$$= X^\mu \partial_\mu Y^\nu - Y^\nu \partial_\nu (X^\mu) \partial_\mu + X^\mu Y^\nu \partial_\mu \partial_\nu - Y^\nu X^\mu \partial_\nu \partial_\mu, \quad (1.3.70)$$

$$= (X^\mu \partial_\mu Y^\nu - Y^\mu \partial_\mu X^\nu) \partial_\nu, \quad (1.3.71)$$

where the basis vector  $e_\mu$  has been written as  $\partial_\mu$  with the intention of acting on a function  $f$  over the manifold  $\mathcal{M}$ .

### Metric Compatibility

Another useful property that can be imposed on the connection is metric compatibility; this is  $\nabla_\mu g_{\rho\sigma} = 0$ , where  $g$  is the metric tensor, which immediately tells us  $\nabla_\mu g^{\alpha\beta} = 0$  as

$$\nabla_\mu \delta^\alpha_\rho = 0 \quad (1.3.72)$$

$$= \nabla_\mu (g^{\alpha\nu} g_{\nu\rho}), \quad (1.3.73)$$

$$= g_{\nu\rho} \nabla_\mu g^{\alpha\nu} + g^{\alpha\nu} \underbrace{\nabla_\mu g_{\nu\rho}}_{=0}, \quad (1.3.74)$$

which implies that  $\nabla_\mu g^{\alpha\nu} = 0$ . Demanding metric compatibility may seem a little arbitrary but turns out to have many nice algebraic properties such as the raising and lowering of indices with the metric commuting with the covariant derivatives,

$$\nabla_\mu T^{\alpha\beta\cdots} = \nabla_\mu g^{\alpha\rho} T_\rho^{\beta\cdots} = g^{\alpha\rho} \nabla_\mu T_\rho^{\beta\cdots} \quad (1.3.75)$$

and the derivative of a vector's length,

$$\nabla_\alpha (X^\mu X_\mu) = \nabla_\alpha (g_{\mu\nu} X^\mu X^\nu) = 2X^\mu \nabla_\alpha X_\mu = 2X_\mu \nabla_\alpha X^\mu. \quad (1.3.76)$$

## The Levi Civita-Connection

A connection that obeys Eqs. (1.3.33, 1.3.34 & 1.3.35), is both torsion-free and metric-compatible, can be demanded; this connection is called the Levi-Civita connection. The Levi-Civita connection will always be assumed from now and leads to a unique choice of connection coefficients,

$$\Gamma^\rho_{\mu\nu} = \frac{1}{2}g^{\rho\sigma}(\partial_\mu g_{\sigma\nu} + \partial_\nu g_{\mu\sigma} - \partial_\sigma g_{\nu\mu}), \quad (1.3.77)$$

which are also called Christoffel symbols of the second kind. It is also common to see the connection coefficients with the lowered index

$$\Gamma_{\sigma\mu\nu} = \frac{1}{2}(\partial_\mu g_{\sigma\nu} + \partial_\nu g_{\mu\sigma} - \partial_\sigma g_{\nu\mu}), \quad (1.3.78)$$

this is also called a Christoffel symbol of the first kind. It is very important to note that even though the connection symbols may look like a tensor they are not a tensor. This can easily be seen from applying the tensor transformation law to the Christoffel symbol of the first kind,

$$2\tilde{\Gamma}_{\sigma\mu\nu} = \tilde{\partial}_\mu \tilde{g}_{\sigma\nu} + \tilde{\partial}_\nu \tilde{g}_{\mu\sigma} - \tilde{\partial}_\sigma \tilde{g}_{\nu\mu}, \quad (1.3.79)$$

$$= \frac{\partial x^\alpha}{\partial \tilde{x}^\mu} \partial_\alpha \left( \frac{\partial x^\beta}{\partial \tilde{x}^\sigma} \frac{\partial x^\gamma}{\partial \tilde{x}^\nu} g_{\beta\gamma} \right) + \frac{\partial x^\gamma}{\partial \tilde{x}^\nu} \partial_\gamma \left( \frac{\partial x^\beta}{\partial \tilde{x}^\sigma} \frac{\partial x^\alpha}{\partial \tilde{x}^\mu} g_{\alpha\beta} \right) - \frac{\partial x^\beta}{\partial \tilde{x}^\sigma} \partial_\beta \left( \frac{\partial x^\alpha}{\partial \tilde{x}^\mu} \frac{\partial x^\gamma}{\partial \tilde{x}^\nu} g_{\gamma\alpha} \right), \quad (1.3.80)$$

$$= \frac{\partial x^\alpha}{\partial \tilde{x}^\mu} \frac{\partial x^\beta}{\partial \tilde{x}^\sigma} \frac{\partial x^\gamma}{\partial \tilde{x}^\nu} (\partial_\alpha g_{\beta\gamma} + \partial_\gamma g_{\alpha\beta} - \partial_\beta g_{\gamma\alpha}) \\ + \frac{\partial x^\alpha}{\partial \tilde{x}^\mu} g_{\beta\gamma} \partial_\alpha \left( \frac{\partial x^\beta}{\partial \tilde{x}^\sigma} \frac{\partial x^\gamma}{\partial \tilde{x}^\nu} \right) + \frac{\partial x^\gamma}{\partial \tilde{x}^\nu} g_{\alpha\beta} \partial_\gamma \left( \frac{\partial x^\beta}{\partial \tilde{x}^\sigma} \frac{\partial x^\alpha}{\partial \tilde{x}^\mu} \right) - \frac{\partial x^\beta}{\partial \tilde{x}^\sigma} g_{\gamma\alpha} \partial_\beta \left( \frac{\partial x^\alpha}{\partial \tilde{x}^\mu} \frac{\partial x^\gamma}{\partial \tilde{x}^\nu} \right), \quad (1.3.81)$$

$$= 2 \frac{\partial x^\alpha}{\partial \tilde{x}^\mu} \frac{\partial x^\beta}{\partial \tilde{x}^\sigma} \frac{\partial x^\gamma}{\partial \tilde{x}^\nu} \Gamma_{\beta\alpha\gamma} \\ + \frac{\partial x^\alpha}{\partial \tilde{x}^\mu} g_{\beta\gamma} \partial_\alpha \left( \frac{\partial x^\beta}{\partial \tilde{x}^\sigma} \frac{\partial x^\gamma}{\partial \tilde{x}^\nu} \right) + \frac{\partial x^\gamma}{\partial \tilde{x}^\nu} g_{\alpha\beta} \partial_\gamma \left( \frac{\partial x^\beta}{\partial \tilde{x}^\sigma} \frac{\partial x^\alpha}{\partial \tilde{x}^\mu} \right) - \frac{\partial x^\beta}{\partial \tilde{x}^\sigma} g_{\gamma\alpha} \partial_\beta \left( \frac{\partial x^\alpha}{\partial \tilde{x}^\mu} \frac{\partial x^\gamma}{\partial \tilde{x}^\nu} \right), \quad (1.3.82)$$

$$= 2 \frac{\partial x^\alpha}{\partial \tilde{x}^\mu} \frac{\partial x^\beta}{\partial \tilde{x}^\sigma} \frac{\partial x^\gamma}{\partial \tilde{x}^\nu} \Gamma_{\beta\alpha\gamma} + \Xi_{\sigma\mu\nu}. \quad (1.3.83)$$

$$(1.3.84)$$

As can be seen above, if  $\Xi_{\sigma\mu\nu} = 0$  then the  $\Gamma_{\sigma\mu\nu}$  would transform as an  $(0,3)$  tensor, however this is not the case and the existence of nonzero  $\Xi_{\sigma\mu\nu}$  means the Christoffel symbol of first kind is not a tensor but instead a symbol. The non-tensor nature of the Christoffel symbol of first kind is sufficient to prove that the Christoffel symbol of second kind is also not a tensor.

## Lie Derivatives in the Levi Civita Connection

The covariant derivative  $\nabla$ , described in section 1.3.2 can replace all partial derivatives in a Lie derivative due to the connection symbols  $(\Gamma^\mu_{\rho\sigma})$  cancelling out.

A special example of a Lie derivative is of the metric tensor,  $\mathbf{g}$ , giving

$$(\mathcal{L}_\xi g)_{\mu\nu} = \xi^\rho \partial_\rho g_{\mu\nu} + g_{\rho\nu} \partial_\mu \xi^\rho + g_{\mu\rho} \partial_\nu \xi^\rho, \quad (1.3.85)$$

$$= \xi^\rho \nabla_\rho g_{\mu\nu} + g_{\rho\nu} \nabla_\mu \xi^\rho + g_{\mu\rho} \nabla_\nu \xi^\rho, \quad (1.3.86)$$

$$(1.3.87)$$

where  $\nabla_\rho g_{\mu\nu} = 0$  is assumed from metric compatibility, described in section 1.3.3. In the case the Lie derivative vanishes we get Killing's equation

$$\nabla_\mu \xi_\nu + \nabla_\nu \xi_\mu = 0 \quad (1.3.88)$$

and a vector field  $\xi$  satisfying Killing's equation is called a Killing vector.

MAYBE DERIVE THE FORM OF BIG GAMMA?

### Normal Coordinates

Consider the set of all affinely parameterised geodesics, parameterised with  $\lambda$ , passing through the point  $p$  on a manifold  $\mathcal{M}$ . At  $p$ , each geodesic has a tangent vector  $X^\mu|_p$ . For all geodesics, define  $p$  to be the origin with  $\lambda = 0$  and  $x^\mu = 0$ . Following a geodesic associated with  $X^\mu|_p$  to a parameter value of  $\lambda$  will map to a new point  $q$  close to  $p$  for small enough  $\lambda$ . Normal coordinates  $x^\mu(\lambda)$  at  $q(\lambda)$  are defined such that  $x^\mu(\lambda) = \lambda X^\mu|_p$ . Given that  $X^\mu|_p$  is constant, the geodesic equation, from Eq. (1.2.71), becomes

$$\frac{d^2 x^\mu(\lambda)}{d\lambda^2} + \Gamma^\alpha_{\mu\nu} \frac{dx^\mu(\lambda)}{d\lambda} \frac{dx^\nu(\lambda)}{d\lambda} = \Gamma^\alpha_{\mu\nu} X^\mu|_p X^\nu|_p = 0. \quad (1.3.89)$$

Using the Levi-civita connection, the connection symbol must be symmetric in lower two indices and this implies  $\Gamma^\alpha_{\mu\nu} = 0$  as the geodesic equation must hold for generic  $X^\mu|_p$ . From the definition of the covariant derivative,

$$\partial_\alpha g_{\mu\nu} = \nabla_\alpha g_{\mu\nu} + \Gamma^\beta_{\alpha\nu} g_{\mu\beta} + \Gamma^\beta_{\alpha\mu} g_{\beta\nu}, \quad (1.3.90)$$

which must vanish in normal coordinates as  $\Gamma^\alpha_{\mu\nu} = 0$  and the Levi-Civita connection demands  $\nabla_\alpha g_{\mu\nu} = 0$ . Therefore, it is possible to construct a coordinate system that at one point  $p$  both  $\partial_\alpha g_{\mu\nu} = 0$  and  $\Gamma^\alpha_{\mu\nu} = 0$ ; importantly  $\partial_\alpha \partial_\beta g_{\mu\nu} \neq 0$ . As well as the metric's first derivative vanishing at  $p$ , it is also possible to demand that  $g_{\mu\nu}|_p = \eta_{\mu\nu}$ , the Minkowski metric. This can be done with a set of  $^{(j)}X^\mu|_p$ , one for each normal coordinate  $x^j$ , that satisfy

$$g(^{(j)}\mathbf{X}|_p, ^{(k)}\mathbf{X}|_p) = \eta_{jk}. \quad (1.3.91)$$

#### 1.3.4 Curvature Tensors

We have already seen that with the Levi-Civita connection, the commuted derivative of a scalar field vanishes. But taking the commuted derivative of a vector field  $\mathbf{X}$  gives,

$$(\nabla_\mu \nabla_\nu - \nabla_\nu \nabla_\mu) X^\sigma = (\partial_\mu \nabla_\nu - \partial_\nu \nabla_\mu) X^\sigma + (\Gamma^\sigma_{\mu\rho} \nabla_\nu - \Gamma^\sigma_{\nu\rho} \nabla_\mu) X^\rho - \underbrace{(\Gamma^\rho_{\nu\mu} - \Gamma^\rho_{\mu\nu})}_{=0} \nabla_\rho X^\sigma, \quad (1.3.92)$$

$$= \underbrace{(\partial_\mu \partial_\nu - \partial_\nu \partial_\mu)}_{=0} X^\sigma + (\partial_\mu \Gamma^\sigma_{\nu\rho} - \partial_\nu \Gamma^\sigma_{\mu\rho}) X^\rho + (\Gamma^\sigma_{\mu\rho} \nabla_\nu - \Gamma^\sigma_{\nu\rho} \nabla_\mu) X^\rho, \quad (1.3.93)$$

$$= (\partial_\mu \Gamma^\sigma_{\nu\rho} - \partial_\nu \Gamma^\sigma_{\mu\rho}) X^\rho + (\Gamma^\sigma_{\mu\rho} \partial_\nu - \Gamma^\sigma_{\nu\rho} \partial_\mu) X^\rho + (\Gamma^\sigma_{\mu\rho} \Gamma^\rho_{\nu\lambda} - \Gamma^\sigma_{\nu\rho} \Gamma^\rho_{\mu\lambda}) X^\lambda, \quad (1.3.94)$$

$$= X^\rho (\partial_\mu \Gamma^\sigma_{\nu\rho} - \partial_\nu \Gamma^\sigma_{\mu\rho}) + (\Gamma^\sigma_{\mu\rho} \Gamma^\rho_{\nu\lambda} - \Gamma^\sigma_{\nu\rho} \Gamma^\rho_{\mu\lambda}) X^\lambda, \quad (1.3.95)$$

where one should note that whenever a term appears after a derivative here it is to be differentiated, even if it is outside a bracket. We can introduce the Riemann tensor here from

$$(\nabla_\mu \nabla_\nu - \nabla_\nu \nabla_\mu) X^\sigma = R^\sigma_{\rho\mu\nu} X^\rho, \quad (1.3.96)$$

and setting  $\mathbf{X} = \mathbf{e}_\rho$ , the coordinate basis vector associated with the  $x^\rho$  coordinate, the Riemann tensor can be written as

$$R^\sigma_{\rho\mu\nu} = \partial_\mu \Gamma^\sigma_{\nu\rho} - \partial_\nu \Gamma^\sigma_{\mu\rho} + \Gamma^\sigma_{\mu\lambda} \Gamma^\lambda_{\nu\rho} - \Gamma^\sigma_{\nu\lambda} \Gamma^\lambda_{\mu\rho}. \quad (1.3.97)$$

#### Symmetries of the Riemann Tensor

Now we will discuss the symmetries of the Riemann tensor. Firstly, from the definition of the Riemann tensor, it follows that  $R^\sigma_{\rho\mu\nu} = -R^\sigma_{\rho\nu\mu}$ ; this can be written succinctly as  $R^\sigma_{\rho[\mu\nu]} = 0$ . The next symmetry of the Riemann tensor will prove easy to derive using normal coordinates (described in [REF]) at a point  $p$  where  $\Gamma = 0$  (but  $\partial\Gamma \neq 0$ ) to get

$$R^\sigma_{\rho\mu\nu}|_p = \partial_\mu \Gamma^\sigma_{\nu\rho} - \partial_\nu \Gamma^\sigma_{\mu\rho}, \quad (1.3.98)$$

and it is simple to show that  $R_{[\rho\mu\nu]}^\sigma = 0$  as

$$R_{[\rho\mu\nu]}^\sigma|_p = \partial_{[\mu}\Gamma_{\nu\rho]}^\sigma - \partial_{[\nu}\Gamma_{\mu\rho]}^\sigma = 0, \quad (1.3.99)$$

as the antisymmetrisation of any connection symbol like  $\Gamma_{[\nu\rho]}^\sigma = 0$ . Given that the tensor equation  $R_{[\rho\mu\nu]}^\sigma = 0$  is true at  $p$  in normal coordinates then it is true in any coordinate system; on top of this the point  $p$  was arbitrary so therefore  $R_{[\rho\mu\nu]}^\sigma = 0$  holds globally.

The next symmetry of the Riemann tensor is  $R_{\sigma\rho\mu\nu} = R_{\mu\nu\sigma\rho}$ . We can prove this again using normal coordinates at a point  $p$ ; here derivatives of the metric and it's inverse vanish, but second derivatives do not. The proof of the symmetry is as follows,

$$R_{\sigma\rho\mu\nu}|_p = g_{\lambda\sigma}\partial_\mu\Gamma_{\nu\rho}^\lambda - g_{\lambda\sigma}\partial_\nu\Gamma_{\mu\rho}^\lambda, \quad (1.3.100)$$

$$= \partial_\mu g_{\lambda\sigma}\Gamma_{\nu\rho}^\lambda - \partial_\nu g_{\lambda\sigma}\Gamma_{\mu\rho}^\lambda, \quad (1.3.101)$$

$$= \partial_\mu\Gamma_{\sigma\nu\rho} - \partial_\nu\Gamma_{\sigma\mu\rho}, \quad (1.3.102)$$

$$= \frac{1}{2}(\partial_\mu\partial_\rho g_{\sigma\nu} - \partial_\mu\partial_\sigma g_{\rho\nu} + \partial_\nu\partial_\sigma g_{\rho\mu} - \partial_\nu\partial_\rho g_{\sigma\mu}), \quad (1.3.103)$$

and it is a simple to show that this final expression doesn't change under swapping indices  $\sigma \leftrightarrow \mu$  and  $\rho \leftrightarrow \nu$ .

The final symmetry of the Riemann tensor is the Bianchi identity,  $\nabla_{[\lambda}R_{\sigma\rho]\mu\nu}=0$ . Using normal coordinates at a point  $p$ , we can write

$$\nabla_\lambda R_{\sigma\rho\mu\nu}|_p = \partial_\lambda R_{\sigma\rho\mu\nu}|_p \quad (1.3.104)$$

as all the christoffel symbols generated by the covariant derivative cancel and therefore

$$2\nabla_\lambda R_{\sigma\rho\mu\nu}|_p = \partial_\lambda\partial_\mu\partial_\rho g_{\sigma\nu} - \partial_\lambda\partial_\mu\partial_\sigma g_{\rho\nu} + \partial_\lambda\partial_\nu\partial_\sigma g_{\rho\mu} - \partial_\lambda\partial_\nu\partial_\rho g_{\sigma\mu}. \quad (1.3.105)$$

Antisymmetrising over  $\lambda, \rho$  and  $\sigma$  makes each term vanish as the triple partial derivatives always contain two of the antisymmetrised indices and must vanish.

To summarise, we have the following symmetries of the Riemann tensor;

$$R_{\sigma\rho[\mu\nu]} = 0, \quad (1.3.106)$$

$$R_{\sigma\rho\mu\nu} = R_{\mu\nu\sigma\rho}, \quad (1.3.107)$$

$$\nabla_{[\lambda}R_{\sigma\rho]\mu\nu} = 0. \quad (1.3.108)$$

The first two of these can be used together to give another useful relation  $R_{[\sigma\rho]\mu\nu} = 0$ .

## Contractions of the Riemann Tensor

Now that we have explored the Riemann tensor, it is time to introduce the Ricci tensor and Ricci scalar. The Ricci tensor  $R_{\mu\nu}$  is simply defined by the unique, non-zero self contraction (or trace) of the Riemann tensor,

$$R_{\rho\mu} := R^\mu_{\rho\mu\nu} = R_{\sigma\rho\mu\nu}g^{\sigma\mu}. \quad (1.3.109)$$

Contracting the the Riemann tensor with  $g^{\mu\nu}$  or  $g^{\sigma\rho}$  would give zero due to the antisymmetries of those indices in the tensor. Any other contractions, such as with  $g^{\rho\mu}$  can be shown to be exactly the same (upto a minus sign) as contracting with  $g^{\sigma\mu}$  using the symmetries of the Riemann tensor. The symmetries of the Riemann tensor guarantee that the Ricci tensor itself is symmetric. We can contract the Ricci tensor with itself (the same as taking the trace with the metric) to give us the Ricci scalar  $R$ ,

$$R = g^{\rho\nu}R_{\rho\nu}. \quad (1.3.110)$$



We can also take the trace of the Bianchi identity in Eq. (1.3.108) which gives us

$$g^{\lambda\mu}g^{\rho\nu}(\nabla_\lambda R_{\sigma\rho\mu\nu} + \nabla_\rho R_{\lambda\sigma\mu\nu} + \nabla_\sigma R_{\rho\lambda\mu\nu}) = 0, \quad (1.3.111)$$

$$\nabla^\mu R_{\sigma\mu} + \nabla^\nu R_{\sigma\nu} - \nabla_\sigma R = 0, \quad (1.3.112)$$

$$\nabla^\mu R_{\mu\sigma} - \frac{1}{2}\nabla_\sigma R = 0. \quad (1.3.113)$$

Using the contracted Bianchi identity and  $\nabla\mathbf{g} = 0$  from metric compatibility, we can define the (symmetric) Einstein tensor  $G_{\mu\nu}$ ,

$$G_{\mu\nu} := R_{\mu\nu} - \frac{1}{2}g_{\mu\nu}R, \quad (1.3.114)$$

$$\nabla^\mu G_{\mu\nu} = \nabla^\mu R_{\mu\nu} - \frac{1}{2}(g_{\mu\nu}\nabla^\mu R + \nabla^\mu(g_{\mu\nu})R), \quad (1.3.115)$$

$$= \nabla^\mu R_{\mu\nu} - \frac{1}{2}\nabla_\nu R, \quad (1.3.116)$$

$$= 0. \quad (1.3.117)$$

The Einstein tensor  $G_{\mu\nu}$  therefore has a vanishing divergence  $\nabla_\mu G^{\mu\nu} = 0$ .

One more useful contraction of the Riemann tensor is with a second Riemann tensor which gives the Kretschmann scalar  $k$ ,

$$k := R_{\mu\nu\rho\sigma}R^{\mu\nu\rho\sigma}. \quad (1.3.118)$$

Both  $k$  and  $R$  are scalar fields so they are a coordinate invariant curvature measure; however section 1.4.6 will have more use of the Kretschmann scalar.

NORMAL COORDS SOMEWHERE, MAKES EXPANSIONS AND SOME DERIVATIONS EASIER,  
USE NORMAL COORDS FOR SYMMETRIES OF RIEMANN

MAYBE ADD THE  $\square$  AND  $()$  SYMMETRY DEFINITION IN PRE-DEFINITIONS? ALSO CHECK THIS WITH THE DIFF FORMS SECTION

DEGREES OF FREEDOM

### 1.3.5 The Divergence Theorem

There is a generalisation of the divergence theorem to non-flat spaces, using differential geometry, which will be extremely useful in section [REF]. First, we will have to find a convenient form of the divergence  $\nabla_\mu X^\mu$  of a vector  $\mathbf{X}$ . Expanding the covariant derivative gives

$$\nabla_\mu X^\mu = \partial_\mu X^\mu + \Gamma^\mu_{\mu\nu} X^\nu, \quad (1.3.119)$$

$$= \partial_\mu X^\mu + \frac{1}{2}g^{\mu\rho}(\partial_\mu g_{\rho\nu} + \partial_\nu g_{\mu\rho} - \partial_\rho g_{\mu\nu})X^\nu, \quad (1.3.120)$$

$$= \partial_\mu X^\mu + \frac{1}{2}g^{\mu\rho}\partial_\nu g_{\mu\rho}X^\nu. \quad (1.3.121)$$

To simplify any further, we need to prove a matrix identity for a symmetric real matrix  $\mathbf{M}$  with determinant  $M$ ,

$$M^{-1}\partial_\mu M = M_{ij}^{-1}\partial_\mu M_{ij} = \text{Tr}(\mathbf{M}^{-1}\partial_\mu \mathbf{M}). \quad (1.3.122)$$

Simplifying the left hand side in terms of the eigenvalues  $\lambda_i$  of  $\mathbf{M}$ . Given that  $M = \det\{\mathbf{M}\} = \prod_i \lambda_i$  we can easily write

$$M^{-1} \partial_\mu M = \partial_\mu \ln(|M|), \quad (1.3.123)$$

$$= \partial_\mu \ln \left( \left| \prod_i \lambda_i \right| \right), \quad (1.3.124)$$

$$= \partial_\mu \sum_i \ln(|\lambda_i|), \quad (1.3.125)$$

$$= \sum_i \lambda_i^{-1} \partial_\mu \lambda_i. \quad (1.3.126)$$

Now we will show that the right hand side of Eq. (1.3.122) also equals this. To do this we start by decomposing  $\mathbf{M}$  into a diagonal matrix  $\mathbf{D}$  like

$$\mathbf{M} = \mathbf{O}^{-1} \mathbf{D} \mathbf{O}, \quad (1.3.127)$$

$$\mathbf{M}^{-1} = \mathbf{O}^{-1} \mathbf{D}^{-1} \mathbf{O}, \quad (1.3.128)$$

then using the fact that  $\text{Tr}(\mathbf{A}\mathbf{B}...\mathbf{C}\mathbf{D}) = \text{Tr}(\mathbf{D}\mathbf{A}\mathbf{B}...\mathbf{C})$  for matrices  $\mathbf{A}$ ,  $\mathbf{B}$ ,  $\mathbf{C}$ , ... and  $\mathbf{D}$ ,

$$\text{Tr}(\mathbf{M}^{-1} \partial_\mu \mathbf{M}) = \text{Tr}(\mathbf{O}^{-1} \mathbf{D}^{-1} \mathbf{O} \partial_\mu (\mathbf{O}^{-1} \mathbf{D} \mathbf{O})), \quad (1.3.129)$$

$$= \text{Tr}(\mathbf{D}^{-1} \partial_\mu \mathbf{D}) + \text{Tr}(\mathbf{O}^{-1} \partial_\mu \mathbf{O}) + \text{Tr}(\mathbf{O} \partial_\mu \mathbf{O}^{-1}), \quad (1.3.130)$$

$$= \text{Tr}(\mathbf{D}^{-1} \partial_\mu \mathbf{D}) + \underbrace{\text{Tr}(\partial_\mu (\mathbf{O}^{-1} \mathbf{O}))}_{=0}, \quad (1.3.131)$$

$$= \text{Tr}(\mathbf{D}^{-1} \partial_\mu \mathbf{D}). \quad (1.3.132)$$

Given that  $\mathbf{D}$  is the diagonal matrix composed of the eigenvalues  $\lambda_i$  then it follow that,

$$\mathbf{D} = \text{Diag}\{\lambda_1, \lambda_2, \dots, \lambda_n\}, \quad (1.3.133)$$

$$\partial_\mu \mathbf{D} = \text{Diag}\{\partial_\mu \lambda_1, \partial_\mu \lambda_2, \dots, \partial_\mu \lambda_n\}, \quad (1.3.134)$$

$$\mathbf{D}^{-1} = \text{Diag}\{\lambda_1^{-1}, \lambda_2^{-1}, \dots, \lambda_n^{-1}\}, \quad (1.3.135)$$

then finally  $\text{Tr}(\mathbf{D}^{-1} \partial_\mu \mathbf{D})$  can be evaluated in terms of the  $\lambda_i$  as follows,

$$\text{Tr}(\mathbf{D}^{-1} \partial_\mu \mathbf{D}) = \sum_{ij} D_{ij}^{-1} \partial_\mu D_{ij}, \quad (1.3.136)$$

$$= \sum_i D_{ii}^{-1} \partial_\mu D_{ii}, \quad (1.3.137)$$

$$= \sum_i \lambda_i^{-1} \partial_\mu \lambda_i, \quad (1.3.138)$$

which proves that Eq. (1.3.122) is true. Applying Eq. (1.3.122) to the metric  $\mathbf{g}$  gives,

$$g^{\mu\rho} \partial_\nu g_{\mu\rho} = g^{-1} \partial_\nu g, \quad (1.3.139)$$

and the covariant divergence  $\nabla_\mu X^\mu$  of a vector  $\mathbf{X}$  simplifies to

$$\nabla_\mu X^\mu = \partial_\mu X^\mu + \frac{1}{2g} \partial_\mu g, \quad (1.3.140)$$

$$= \frac{1}{\sqrt{|g|}} \partial_\mu \left( \sqrt{|g|} X^\mu \right), \quad (1.3.141)$$

which in the standard pseudo-Riemannian spacetime is often written

$$\nabla \cdot \mathbf{X} = \nabla_\mu X^\mu = \frac{1}{\sqrt{-g}} \partial_\mu (\sqrt{-g} X^\mu). \quad (1.3.142)$$

This equation will have much use later in section [REF] where the divergence of a vector will be integrated over a finite  $n$ -dimensional volume  $M$  in  $\mathcal{M}$ . In order to do this, the divergence theorem of curved space is used, this is

$$\int_M \nabla \cdot \mathbf{X} \sqrt{|^{(n)}g|} \, d^n x = \sum_i \int_{\partial M_i} \mathbf{s}^{(i)} \cdot \mathbf{X} \sqrt{|^{(n-1)}g^{(i)}|} \, d^{n-1} x, \quad (1.3.143)$$

where the surface of  $M$  is divided into a set of  $(n-1)$ -dimensional surfaces  $\partial M_i$ ; for each of these surfaces there is an  $(n-1)$ -dimensional metric  $^{(n-1)}g^{(i)}$  with determinant  $^{(n-1)}g^{(i)}$  and unit normal vector  $\mathbf{s}^{(i)}$  with  $^{(n-1)}g^{(i)}(\mathbf{s}^{(i)}, \mathbf{s}^{(i)}) = \pm 1$ . When dealing with a pseudo-Riemannian manifold, we need to take care of the direction of  $\mathbf{s}^{(i)}$ ; in the case that  $\mathbf{s}^{(i)}$  is timelike it should be in-directed, and if it's spacelike then it should be out-directed.

CHECK THE LAST STATEMENT

MAYBE DERIVE DIV THEOREM, OTHERWISE REFERENCE IT

## 1.4 Relativity

### 1.4.1 Special Relativity

In the nineteenth century, it was widely beleived that the universe was permeated by an invisible luminous aether. It was thought that light travels at a fixed speed through this aether; the aether could be thought of as a universal rest frame. A consequence of this is that moving towards/away from a light source would cause the wavelength of light to get shorter/longer in a similar fashion to the doppler effect. With that line of thought one could measure the earths speed through this rest frame by setting up an interferometer experiment. An interferometer sends a light beam through a splitter, dividing the beam into two perpendicular paths. The two beams then reach a seperate mirror and are reflected to a half-mirror that recombines the two beams after they have travelled identical distance. If the time taken for the two beams to complete their identical length journeys differs then an interference pattern will be seen at a detector placed after the half-mirror due to the phase change between the two beams. In 1887 Michelson and Morley conducted their famous interferometer experiment to measure the earth's velocity through the aether. They expected to see interferece when the different beams made differnet angles with the velocity through the aether. However, no matter which orientation they put their experiment there was no interference pattern. This implied that light moved at exactly the same speed in any direction; this is only possible if earth is in the rest frame of the aether, but this cannot possibly be true as the planet accelerates round a circular path around a sun that is following a bigger circular path and so on. This famous result demonstrated that the speed of light was constant in all inertial frames - a result that defied newtonian mechanics. This was the first and biggest hint that a new theory of dynamics was needed.

In 1905, Einstein published "On the Electrodynamics of Moving Bodies" which contained a description of Special Relativity (SR) [CHECK THIS]. SR is essentially the idea that the laws (excluding gravity) of physics are the same in any inertial (non-accelerating) rest frame - the consequence of this is that you cannot measure the velocity of your own rest frame as no frame is special. One big problem with SR is that it does not properly describe gravity and thus describes an infinite vaccum universe; this is a problem that will be adressed in the next sections. SR alone contains many interesting results such as time dilation, length contraction and the inclusion of time into the metric.

### Minkowski Space

In Newtonian physics the metric of flat space, using cartesian coordiantes, is

$$g_{ij} = \delta_{ij} = \begin{pmatrix} 1 & 0 & 0 \\ 0 & 1 & 0 \\ 0 & 0 & 1 \end{pmatrix}, \quad (1.4.1)$$

with the line element

$$ds^2 = \delta_{ij} dx^i dx^j = dx^2 + dy^2 + dz^2. \quad (1.4.2)$$

In SR time is promoted to a dimension and the metric is over space and time (spacetime). The spacetime metric has a single negative eigenvalue and hence negative determinant. In cartesian coordinates, the flat spacetime metric is,

$$g_{\mu\nu} = \eta_{\mu\nu} = \begin{pmatrix} -c^2 & 0 & 0 & 0 \\ 0 & 1 & 0 & 0 \\ 0 & 0 & 1 & 0 \\ 0 & 0 & 0 & 1 \end{pmatrix}, \quad (1.4.3)$$

and line element

$$ds^2 = \eta_{\mu\nu} dx^\mu dx^\nu = -c^2 dt^2 + dx^2 + dy^2 + dz^2. \quad (1.4.4)$$

where  $c$  is the speed of light which will be set to unity again. The line element is often written  $ds^2 = -d\tau^2$  where  $\tau$  is the *proper time* experienced by an observer. Having a metric over spacetime is a non-intuitive concept step where time is included into geometry and paths through space and time (spacetime) can have negative length. This flat spacetime is very important and is called the Minkowski spacetime.

### Worldlines and Causality

Consider a particle moving through the rest frame with some world-line (path through spacetime) described by  $x^\mu(\tau)$ . Without loss of generality the motion can be restricted to the  $x$  axis. The world-line of this particle is given by  $x^\mu = \{t, \int_{t_0}^t v(t') dt' + v(t_0), 0, 0\}$ . The infinitesimal form of this description is  $dx^\mu = \{dt, v dt, 0, 0\}$  and the proper time associated with the interval is

$$d\tau^2 = -\eta_{\mu\nu} dx^\mu dx^\nu = (1 - v^2) dt^2. \quad (1.4.5)$$

This equation says that if  $v < 1$ , where it should be remembered that the speed of light here is  $c = 1$ , then proper time  $\tau$  and coordinate time  $t$  both flow in the same direction. Curves like this have  $\eta_{\mu\nu} \dot{x}^\mu \dot{x}^\nu < 0$  and are called *time-like*. If  $v = 1$ , which is only possible for a massless particle, then the path is called *light-like*. For  $v > 1$ , the path is unphysical as nothing can travel faster than the speed of light, it would correspond to an observer travelling backwards in time. A curve  $x^\mu$  with  $\eta_{\mu\nu} \dot{x}^\mu \dot{x}^\nu > 0$  is instead called a *space-like* curve and cannot be traversed by matter or information.

MAYBEW REWRITE THIS JUST FROM A DELTA T DELTA X PERSPECTIVE AND THEN USE IT TO DESCRIBE WORLDLINES AFTER?? MAYBE JUST DO THIS IN THE gr SECTION AS THERES NO REASON NOT TO

MAYBE DO NOW THAT WORLDLINES ARE GEODESICS?

### 1.4.2 Physics in Special Relativity

BOOSTS?

Many physical theories can be written using tensor calculus on this flat spacetime; the correct description of electromagnetism was itself a large reason for the development of special relativity.

### The Wave Equation

One very simple example is the wave equation governing the dynamics of a scalar field  $\phi$ ,

$$\frac{1}{c^2} \frac{\partial^2}{\partial t^2} \phi(x^i, t) - \left( \frac{\partial^2}{\partial x^2} + \frac{\partial^2}{\partial y^2} + \frac{\partial^2}{\partial z^2} \right) \phi(x^i, t) = 0, \quad (1.4.6)$$

using cartesian coordinates and  $c$  as the speed of light which we will set to one. It should be noted that this equation only holds in one coordinate system, changing coordinate system would change the equation of motion. In SR, using the language of tensor calculus, we can write this as

$$\eta^{\mu\nu}\partial_\mu\partial_\nu\phi = 0, \quad (1.4.7)$$

which is not only much simpler but is also true in any inertial frame (using Cartesian coordinates) as is one of the postulates of special relativity.

## Electromagnetism

Electromagnetism can also be cast in a very succinct form using this field theory notation. Traditionally Maxwell's equations of electromagnetism are written as

$$\nabla \cdot \mathbf{E} = \frac{\rho}{\epsilon_0}, \quad (1.4.8)$$

$$\nabla \cdot \mathbf{B} = 0, \quad (1.4.9)$$

$$\nabla \times \mathbf{E} + \frac{d\mathbf{B}}{dt} = 0, \quad (1.4.10)$$

$$\nabla \times \mathbf{B} - \frac{d\mathbf{E}}{dt} = \mu_0 \mathbf{J} \quad (1.4.11)$$

for charge density  $\rho$ , current density  $\mathbf{J}$ . Note these differential equations are not written using the language of differential geometry and tensor calculus. In SR, the current density and charge is promoted to a single 4-vector  $j^\mu = \{\rho, j^i\}$  and the 6 degrees of freedom of the electromagnetic field are encoded in the components  $F_{\mu\nu}$  of an antisymmetric tensor  $\mathbf{F}$ . The four electromagnetic potentials  $\phi$  and  $A_i$ , defined by  $E_i = -\partial_i\phi - \partial_t A_i$  and  $\mathbf{B} = \nabla \times \mathbf{A}$ , are also combined into one 4-vector  $A_\mu = \{-\phi, A_i\}$ . In cartesian coordinates, the Electromagnetic tensor  $\mathbf{F}$  is,

$$F_{\mu\nu} = \partial_\mu A_\nu - \partial_\nu A_\mu = \begin{pmatrix} 0 & E_x & E_y & E_z \\ -E_x & 0 & B_z & -B_y \\ -E_y & -B_z & 0 & B_x \\ -E_z & B_y & -B_x & 0 \end{pmatrix}, \quad (1.4.12)$$

Transforming  $A_\mu$  with the electromagnetic gauge transformation like  $A_\mu \rightarrow A_\mu + \partial_\mu f$ , for some scalar field  $f$ , leaves the physically measureable field  $F_{\mu\nu}$  unchanged,

$$F_{\mu\nu} \rightarrow \partial_\mu(A_\nu + \partial_\nu f) - \partial_\nu(A_\mu + \partial_\mu f), \quad (1.4.13)$$

$$= \partial_\mu A_\nu - \partial_\nu A_\mu + \underbrace{\partial_\mu \partial_\nu f - \partial_\nu \partial_\mu f}_{=0}, \quad (1.4.14)$$

$$= F_{\mu\nu}. \quad (1.4.15)$$

In SR the Maxwell Eqs. (1.4.8) and (1.4.11) can be identically represented as

$$\partial_\mu F^{\mu\nu} = \mu_0 j^\nu, \quad (1.4.16)$$

and the other two Maxwell Eqs. (1.4.9) and (1.4.10) are identically true from computing  $\partial_{[\mu} F_{\alpha\beta]}$ ,

$$\partial_{[\mu} F_{\alpha\beta]} = \partial_\mu \partial_\alpha A_\beta - \partial_\mu \partial_\beta A_\alpha + \partial_\alpha \partial_\beta A_\mu - \partial_\alpha \partial_\mu A_\beta - \partial_\beta \partial_\mu A_\alpha - \partial_\beta \partial_\alpha A_\mu, \quad (1.4.17)$$

$$\partial_{[\mu} F_{\alpha\beta]} = 0. \quad (1.4.18)$$

talk about postulates of SR.

Boosts

stress tensors?

quick conservation law

### 1.4.3 Physics in Curved Space

It is a commonly known result of newtonian physics that in a rotating reference frame, with angular velocity  $\omega$ , a test particle will experience three fictitious forces; the centrifugal force that grows with distance from the origin, the coriolis force that depends on the velocity of the test particle, and the Euler force depending on  $\partial_t \omega$ . From the point of view of an observer in the rotating frame a test particle would appear to accelerate which is a violation of Newton's first law if there is no external force. The curved path followed by the particle in the rotating reference frame is of course a constant speed straight line in the non-rotating frame, and therefore the particle follows a geodesic in the inertial frame. It is possible (but very involved) to do a coordinate transformation from the rest frame to the inertial frame and find the metric  $\tilde{\eta}_{\mu\nu}$  of the rotating frame; it would then be possible to compute the geodesics in the rotating frame using Eq. (1.5.12).

In a similar way to the fictitious forces arising in rotating frames, the gravitational force can be described as a fictitious force. In the absense of rotation, the path of a particle moving without external force is seen to accelerate towards massive bodies. In other words, matter density deflects particle paths towards itself. This is a property also possessed by curved spaces; the path followed by a free particle on a non-flat spacetime can bend. MENTION MATTER IS SIMILAR TO CURVATURE THEN. The brilliant insight by Einstein was that upgrading the flat spacetime of special relativity to a curved spacetime would give a relativistic theory of gravity; this theory is general relativity. In the same way that fictitious forces arise from departing from an inertial frame with rotation, the gravitational force is a fictitious force arising from departing from an inertial frame; the difference is that an inertial frame now must follow a geodesic. This explains why an observer standing on earth experiences a reaction force, the frame of the observer is not following a geodesic, or not free falling, therefore to counteract the fictitious gravitational force generated the ground must push back with a reaction force.

Given that POSTULATE says the local laws of physics in a free falling frame are indistinguishable from special relativity, any equation of motions that we want to hold in general relativity must agree with special relativity in the low curvature limit. As a general rule, if there is a law of physics expressed as a differential equation on Minkowski space that we want to use in curved space, we must replace all partial derivatives of fields with co-variant derivatives of tensor fields; this process is called the minimal coupling approach MAYBE MAKE THIS MORE OBVIOUS WITH LAGRANGEANS?. An easy example is the wave equation from Eq. (1.4.7),

$$\eta^{\mu\nu} \partial_\mu \partial_\nu \phi = 0 \rightarrow g^{\mu\nu} \nabla_\mu \nabla_\nu \phi = 0 \quad (1.4.19)$$

where we had to replace  $\partial_\mu \rightarrow \nabla_\mu$  and replace the Minkowski metric  $\eta$  with the curved space metric  $g_{\mu\nu}$  like  $\eta \rightarrow g$ . Writing the laws of physics as tensor equations is extremely useful as they must hold for over all points in a curved spacetime in any coordinate system; the power of these equations is that they can be written without reference to an explicit coordinate system. If a coordinate system is then picked, assuming knowledge of  $g_{\mu\nu}$ , then the wave equation becomes

$$g^{\mu\nu} \nabla_\mu \nabla_\nu \phi = g^{\mu\nu} \nabla_\mu \partial_\nu \phi, \quad (1.4.20)$$

$$= g^{\mu\nu} \partial_\mu \partial_\nu \phi - g^{\mu\nu} \Gamma_{\mu\nu}^\rho \partial_\rho \phi, \quad (1.4.21)$$

in terms of partial derivatives. There is the small question of uniqueness here, what is to stop us adding arbitrary amounts and types of terms that vanish in the no curvature limit. For a simple example one is free to choose the wave equation to be

$$g^{\mu\nu} \nabla_\mu \nabla_\nu \phi + f(x^\mu) R^n = 0, \quad (1.4.22)$$

for constant  $n$ , function  $f$  and the Ricci scalar  $R$  discussed in REF. This equation certainly returns the regular wave equation in the low curvature limit where  $R \rightarrow 0$ . The general rule is to keep things simple and terms such as  $R$  which are proportional to second order derivatives of the metric are thought to be less

dominant that terms such as  $\Gamma^\mu_{\rho\sigma}$  which are proportional to first derivatives of the metric. Navigating this minefield of which terms to include in the laws of physics leads to the topic of modified gravity REF, the next simplest theories beyond general relativity.

As another quick example the Maxwell equations are very simple to extend to curved space

maybe principle of minimal coupling to gravity is easier to understand with lagrangeans?

do postulates of GR and SR better?

decide how to deal with geodesic / path in the early parts of this section

#### 1.4.4 The Stress-Energy-Momentum Tensor

At the heart of field theory in physics is the stress-energy-momentum tensor  $\mathbf{T}$ , also called the energy-momentum tensor or stress tensor for short. Roughly speaking, component  $T^{00}$  is energy density, components  $T^{0i} = T^{i0}$  contain energy flux or momentum density and components  $T^{ij} = T^{ji}$  contain momentum fluxes. The diagonal part of  $T^{ij}$  can also be thought of as containing pressure and the off-diagonal terms containing shear stress. In flat space, the conservation of energy and momentum can be written as

$$\partial_\mu T^{\mu\nu} = 0, \quad (1.4.23)$$

in the absence of external forces. Equation (1.4.23) is also called the continuity equation and can be split into two sets of familiar equations,

$$\partial_0 T^{00} = -\partial_i T^{i0}, \quad (1.4.24)$$

$$\partial_0 T^{0j} = -\partial_i T^{ij}, \quad (1.4.25)$$

where the first equation states *"The rate of change of energy density is equal and opposite to the divergence of energy flux density"* and the second equation states *"The rate of change of momentum density is equal and opposite to the divergence of momentum flux density"*.

The stress tensor is also very useful in curved space and the continuity equation becomes,

$$\nabla_\mu T^{\mu\nu} = \partial_\mu T^{\mu\nu} + \Gamma^\mu_{\mu\rho} T^{\rho\nu} + \Gamma^\nu_{\mu\rho} T^{\mu\rho} = 0, \quad (1.4.26)$$

which can be rewritten using Eq. (1.3.142) as

$$\partial_\mu(\sqrt{-g}T^{\mu\nu}) = -\sqrt{-g}\Gamma^\nu_{\mu\rho}T^{\mu\rho}, \quad (1.4.27)$$

$$\partial_\mu(\mathcal{T}^{\mu\nu}) = -\Gamma^\nu_{\mu\rho}\mathcal{T}^{\mu\rho}, \quad (1.4.28)$$

where the second equation writes the stress tensor as a tensor density  $\mathcal{T} = \sqrt{-g}\mathbf{T}$  making the equation resemble the flat space continuity equation more closely. The take away message is that traditional continuity of energy and momentum no longer hold for curved spaces. This point will be revisited in section REF where a different type of variable is defined to try recover traditional continuity.

#### 1.4.5 The Einstein Equation

Building on the vague notion of matter causing spacetime curvature it would be helpful to have a mathematical law saying how much curvature is caused by a matter distribution. The first guess that Einstein arrived at was to write  $R_{\mu\nu} = kT_{\mu\nu}$  for some constant  $k$ . The problem is that given  $\nabla_\mu T^{\mu\nu} = 0$  is the generic equation of continuity for matter, it would imply  $\nabla_\mu R^{\mu\nu}$  vanishes which is not generally true. As shown in Eq. (1.3.116), the Einstein tensor  $G_{\mu\nu}$  does satisfy  $\nabla_\mu G^{\mu\nu} = 0$ ; the next simplest guess at a physical law for spacetime curvature would be  $G_{\mu\nu} = kT_{\mu\nu}$ . Remarkably this turns out to be correct and has successfully described all gravitational physics to date.

SOME EARLY EXPERIMENTAL STUFF LIKE PRECESSION, GRAVITATIONAL TIME DILATION, LIGHT RAY DEFLECTION, RED SHIFT FOR ATOMIC SPECTRA.

At the core of General Relativity is the Einstein Equation

$$G_{\mu\nu} = \frac{8\pi G}{c^4} T_{\mu\nu}, \quad (1.4.29)$$

also called the Einstein Field Equations. This equation relates spacetime curvature, encoded in the Einstein tensor  $G_{\mu\nu}$ , to the matter distribution described by the stress tensor  $T_{\mu\nu}$ . To be able to solve this equation in the presence of matter a curvature dependant equation of motion to dictate how matter moves is required. This leads nicely to Wheeler's insightful one line summary of general relativity:

*"Spacetime tells matter how to move; matter tells spacetime how to curve."*

This desceptively simple equation can describe an infinite amount of vastly diverse spacetime geometries including regular flat Minkowski space, black holes, stars, planets, gravitational waves and even the entire universe; to properly describe the entire universe a small modification has to be made to this equation as shown in REF.

### General Relativity in Vacuum

In the case of a vacuum spacetime with  $T_{\mu\nu} = 0$ , or one where the matter distribution is supposed to be so small that it does not cause a spacetime curvature backreaction, the Einstein equation simplifies greatly to

$$G_{\mu\nu} = 0. \quad (1.4.30)$$

Taking the trace of the above equation and the definition of  $G_{\mu\nu}$  in Eq. (REF), we can see that

$$g^{\mu\nu} G_{\mu\nu} = 0 = g^{\mu\nu} (R_{\mu\nu} - \frac{1}{2} R g_{\mu\nu}) = R(1 - \frac{D}{2}), \quad (1.4.31)$$

where  $D$  is the number of spacetime dimensions. Clearly for  $D \neq 2$  a vanishing einstein implies a vanishing Ricci scalar  $R$ ; if the Ricci scalar vanishes then  $G_{\mu\nu} = R_{\mu\nu}$  and the Einstein equation in vacuum simplifies to

$$R_{\mu\nu} = 0. \quad (1.4.32)$$

In the special case of  $D = 2$  it can be shown that  $R_{\mu\nu} = R g_{\mu\nu}/2$  [MAYBE REF EARLIER SECTION ON RIEMANN TENSOR] and the Einstein tensor  $G_{\mu\nu} \equiv 0$  which renders Einstein's equation nonsensical.

#### 1.4.6 Black Holes

As it turns out, vacuum General Relativity can describe more than just Minkowski space. Arguably the most important family of solutions to Einstein's equations in vacuum are black holes. The first black hole solution was found by Karl Schwarzschild, whos surname fittingly means "*black shield*" in German. This solution, known as the Schwarzschild solution, was discovered in 1916 with the intention of computing the spacetime curvature in the vacuum about a spherically symmetric mass such as stars and planets. The solution for  $g_{\mu\nu}$  was assumed to take the following ansatz,

$$ds^2 = g_{\mu\nu} dx^\mu dx^\nu = -A(r) dt^2 + B(r) dr^2 + r^2 (d\theta + \sin^2(\theta) d\phi^2) \quad (1.4.33)$$

which is manifestly spherically symmetric and static; in the case  $A(r) = B(r) = 1$  the solution is exactly Minkowski space in spherical polar coordinates. Schwarzschild saught a solution of this form that at large radius as  $r \rightarrow \infty$  the functions  $A \rightarrow 1$  and  $B \rightarrow 1$ , this means at large radius the solution tends to flat space. By solving  $R_{\mu\nu} = 0$  from REF, Schwarzschild found a solution of the form

$$g_{\mu\nu} dx^\mu dx^\nu = - \left(1 - \frac{2Gm}{rc^2}\right) dt^2 + \left(1 - \frac{2Gm}{rc^2}\right)^{-1} dr^2 + r^2 (d\theta + \sin^2(\theta) d\phi^2), \quad (1.4.34)$$



known as the Schwarzschild solution. The constants  $G$  and  $c$  are included for completeness, but are equal to one in Planck units. The Schwarzschild solution describes the spacetime about a non-spinning sphere of mass  $m$  and as  $r \rightarrow \infty$  or  $m \rightarrow 0$  we do approach the vacuum Minkowski spacetime as desired.

### Polar-Areal Coordinates

The type of coordinates used in the Schwarzschild solution are called polar-areal coordinates; these are coordinates that satisfy  $g_{\theta\theta} = r^2$ ,  $g_{\phi\phi} = \sin^2(\theta)r^2$  and otherwise  $g_{\mu\phi} = g_{\mu\theta} = 0$  CHECK THIS. Polar areal coordinates return a length of  $2\pi r_0$  when integrating the length of a complete circle at fixed radius  $r_0$ . This can be calculated using Eq. (1.2.56) and integrating with respect to  $\phi$  around a circle while keeping  $t = t_0$ ,  $r = r_0$  and  $\theta = \pi/2$  constant,

$$\int_0^{2\pi} \sqrt{g_{\phi\phi}} \Big|_{t=t_0, r=r_0, \theta=\frac{\pi}{2}} d\phi = r_0 \sin\left(\frac{\pi}{2}\right) \int_0^{2\pi} d\phi = 2\pi r_0, \quad (1.4.35)$$

which is the same result as in regular flat space. Using Eq. (1.2.64) the surface area of a sphere with  $t = t_0$ ,  $r = r_0$  can be calculated like

$$\int_0^\pi \left[ \int_0^{2\pi} \sqrt{g_{\phi\phi}g_{\theta\theta}} \Big|_{t=t_0, r=r_0} d\phi \right] d\theta = r_0^2 \int_0^\pi \left[ \int_0^{2\pi} d\phi \right] \sin^2(\theta) d\theta = 4\pi r_0^2, \quad (1.4.36)$$

where  $\sqrt{g_{\phi\phi}g_{\theta\theta}}$  is the determinant of the metric on the two-dimensional surface defined by  $t = t_0$  and  $r = r_0$ . Both the circumference of a circle and the area of a sphere are the same as would be in flat space, this property comes from the metric ansatz in Eq. (1.4.33).

### Coordinate Singularities and Physical Singularities

There is obviously some kind of problem at  $r = 2mG/c^2$ , known as the Schwarzschild radius, as  $g_{rr}$  diverges here. For any planet or star observed, the radius of the object would be much larger than the Schwarzschild metric and so the solution should be seen as invalid inside the object as it has been derived in vacuum. For a valid solution to Einstein's equations inside a spherically symmetric star or planet a non-zero stress tensor must be assumed, this is explored in more detail in REF.

What Schwarzschild didn't realise before his unfortunately early death was that his solution could in fact be trusted down to radii well inside the Schwarzschild radius  $r_s = 2m$ . This solution describes the eternal, non-spinning black hole of mass  $m$  called the Schwarzschild black hole. The problem at radius  $r = 2m$  (where we have now set  $c = G = 1$ ) is due to the choice of coordinates and is not physically problematic. An easy way to show this is to compute a curvature scalar for the spacetime and show that it is smooth at  $r = 2m$ . The first choice of curvature scalar would be the Ricci scalar, but this was assumed to be zero in vacuum so is not useful here. Another curvature scalar is the Kretschmann scalar  $k$ , defined in Eq. (1.3.118), which does not generally vanish in vacuum. Vacuum general relativity asserts that  $R_{\mu\nu} = 0$ , while that guarantees that  $R = 0$  it does not guarantee that  $R_{\mu\nu\rho\sigma} = 0$ . Calculating the Kretschmann scalar for the Schwarzschild metric gives

$$k_{sc} = \frac{48m^2}{r^6}. \quad (1.4.37)$$

As can be seen,  $k$  is continuous and infinitely differentiable at  $r = 2m$  but as  $r \rightarrow 0$ ,  $k \rightarrow \infty$  and there is a real coordinate independent singularity called a physical singularity. Scalar curvature invariants are useful as if they diverge in one coordinate system then they must diverge in all coordinate systems as they do not transform under coordinate transformations. It should be noted that  $\sqrt{-g}$  is a scalar density and not a true scalar so cannot be used as a scalar curvature invariant.

To remove the coordinate singularity at  $r = 2m$ , new coordinate singularities can be introduced. One example is to use ingoing-Eddington-Finkelstein coordinates  $\{v, s, \theta, \phi\}$  defined by

$$\frac{ds}{dr} = \left(1 - \frac{2m}{r}\right), \quad (1.4.38)$$

$$v = t + s, \quad (1.4.39)$$

which transforms the line element to

$$g_{\mu\nu}x^\mu x^\nu = -\left(1 - \frac{2m}{r}\right)dv^2 + 2dvdr + r^2(d\theta + \sin^2(\theta)d\phi^2), \quad (1.4.40)$$

and as can be seen the metric no longer diverges at  $r = 2m$ . Being careful to notice that now the metric is not diagonal, the metric determinant can be calculated, giving  $\sqrt{-g} = r^2 \sin(\theta)$ . Given that the metric is finite at  $r = 2m$  and the metric determinant is non-zero, the metric inverse is guaranteed to be well behaved at  $r = 2m$  as well. Therefore it has been demonstrated that the singularity at  $r = 2m$  in Schwarzschild polar-areal coordinates is a coordinate singularity that vanishes when using ingoing-Eddington-Finkelstein coordinates; therefore there is no physical singularity.

Throughout this section we have ignored the fact that the inverse metric also diverges as  $\theta \rightarrow 0$  or  $\theta \rightarrow \pi$ , this is a coordinate singularity that is present in flat space (which is equivalent to the Schwarzschild spacetime with  $m = 0$ ). This coordinate singularity arises in flat space due to the azimuthal angle  $\phi$  being undefined at  $\theta = 0$  and  $\theta = \pi$ . There are no physical singularities in flat space, as you might expect, and this coordinate singularity vanishes when using cartesian coordinates.

### Isotropic Coordinates

A coordinate system that will be very useful later on in REF is the isotropic coordinate system. Isotropic coordinates have the line element,

$$g_{\mu\nu}dx^\mu dx^\nu = -\Omega(r)^2 dt^2 + \Psi^2(r) \underbrace{\left(dr^2 + r^2(d\theta^2 + \sin^2(\theta)d\phi^2)\right)}_{\text{flat space}} \quad (1.4.41)$$

where the flat space line element is multiplied by a scale factor  $\Psi^2(r)$ . The reason these coordinates are called isotropic coordinates is that each spatial direction is equivalent when using Cartesian coordinates, as can be seen by writing the line element,

$$g_{\mu\nu}dx^\mu dx^\nu = -\Omega(r)^2 dt^2 + \Psi^2(r) (dx^2 + dy^2 + dz^2), \quad (1.4.42)$$

where  $r^2 = x^2 + y^2 + z^2$ . The Schwarzschild black hole solution can be expressed in isotropic coordinates as well,

$$g_{\mu\nu}dx^\mu x^\nu = -\left(\frac{1 - \frac{m}{2r}}{1 + \frac{m}{2r}}\right)^2 dt^2 + \left(1 + \frac{m}{2r}\right)^4 (dr^2 + r^2(d\theta^2 + \sin^2(\theta)d\phi^2)) \quad (1.4.43)$$

$$= -\left(\frac{1 - \frac{m}{2r}}{1 + \frac{m}{2r}}\right)^2 dt^2 + \left(1 + \frac{m}{2r}\right)^4 ds_E^2, \quad (1.4.44)$$

where  $ds_E^2$  is the three-dimensional Euclidean space. As  $r \rightarrow \infty$  the line element reduces to the Minkowski space one. The radius  $r = m/2$  has the same coordinate singularity that was seen in polar areal coordinates and at first glance one might think that there is a physical singularity at  $r = 0$ . However, if a new radial coordinate  $\xi$  is used, where  $r = \frac{m^2}{4\xi}$  for some constant, the line element becomes

$$g_{\mu\nu}dx^\mu x^\nu = -\left(\frac{1 - \frac{m}{2\xi}}{1 + \frac{m}{2\xi}}\right)^2 dt^2 + \left(1 + \frac{m}{2\xi}\right)^4 (d\xi^2 + \xi^2(d\theta^2 + \sin^2(\theta)d\phi^2)). \quad (1.4.45)$$

This is a remarkable result, inverting the radial coordinate about  $r = 2/m$  has returned an exactly identical metric. Given that at  $r = \infty$  we have flat space this implies that at  $\xi = \infty$  (or  $r = 0$ ) there is another separate flat space, not a physical singularity might have been thought. This second flat space as  $\xi \rightarrow \infty$  is often called the alternate (PARALLEL MAYBE) universe and they are joined by the in-traversable Einstein-Rosen bridge at  $r = 2/m$ . The reason that the physical singularity at  $r = 0$  does not appear in isotropic coordinates is desceptively simple; in isotropic coordinates  $r = 0$  does not correspond to the same point on the manifold as  $r = 0$  does in the polar areal gauge for any value of  $t$ ,  $\theta$  or  $\phi$ . Infact, the physical singularity of the black hole is outside of the patch on the manifold covered by isotropic coordinates. The idea of pathes is covered later EXPAND THIS WITH PENROSE MAYBE/

As described in section REF, spherically symmetric non-vacuum solutions to Einstein's equations can be found using isotropic coordinates; these solutions represent stars, planets and exotic balls of matter. The isotropic gauge is used when superposing these solutions later on in sections REF. EXPAND THIS

## Penrose Diagrams and the Causal Structure of the Schwarzschild Black Hole



Figure 1.2: Diagram for proof of Penrose diagram of a Schwarzschild diagram.

## Spinning, Charged Black Holes and Higher Dimensions

do polar areal, then transform to isotropic for use later. then talk about other types of black holes. talk about the horizon maybe and causal disconnect

The subject of black holes in General Relativity is huge.

reference kerr don't bother writing it

grav time dilation - maybe put this in the general GR bit, along with precession mercuries orbit?

ref higher dimensions maybe

BIRKOFFS THEOREM

NEED A PROPER BH SOLUTION SECTION IN THE NR SECTION THAT HAS ALL THE NUMERICAL APPROACHES

### 1.4.7 The Cosmological Constant

A discussion of general relativity is incomplete without discussing the cosmological constant  $\Lambda$ . At a geometric level, the cosmological constant encodes the homogeneous spacetime curvature in the absence of matter, and indeed setting  $\Lambda \rightarrow 0$  (in vacuum) returns asymptotically flat vacuum general relativity. The cosmological constant is added into Einstein's equation, Eq. (1.4.29), with a term like  $\Lambda g_{\mu\nu}$ ,

$$R_{\mu\nu} - \frac{1}{2}Rg_{\mu\nu} + \Lambda g_{\mu\nu} = \frac{8\pi G}{c^4}T_{\mu\nu}. \quad (1.4.46)$$

Each term still has a zero-divergence as  $\nabla_\mu g_{\alpha\beta} = 0$  due to the Levi-Civita connection defined in section 1.3.3. The Einstein equation in vacuum becomes

$$R_{\mu\nu} - \frac{1}{2}Rg_{\mu\nu} + \Lambda g_{\mu\nu} = 0, \quad (1.4.47)$$

and the trace becomes

$$R = \frac{2D}{D-2}\Lambda \quad (1.4.48)$$

for  $D$  spacetime dimensions. This quite nicely shows us that in the limit  $\Lambda = 0$  the normal vacuum GR solution  $R = 0$  is returned. In the case  $\Lambda \neq 0$  it describes a homogeneous curved universe with constant non-zero  $R$ .

### Friedmann–Lemaître–Robertson–Walker Spacetime

To model the entire universe more realistically, an isotropic uniform fluid is added. A uniform matter distribution is often done with a perfect fluid with stress tensor

$$T_{\mu\nu} = (\rho + P)u_\mu u_\nu + Pg_{\mu\nu}, \quad (1.4.49)$$

where  $\rho$  and  $P$  are the rest frame density and pressure. The fluid is taken to be at rest with  $u^i = 0$  and  $g(\mathbf{u}, \mathbf{u}) = -1$ . The line element takes the following ansatz

$$ds^2 = -dt^2 + a^2(t)\gamma_{ij}dx^i dx^j, \quad (1.4.50)$$

where  $a(t)$  is the scale factor of the universe and the spacelike metric  $\gamma$  is given by

$$\gamma_{ij}dx^i dx^j = \begin{cases} dr^2 + \sin^2(r)(d\theta^2 + \sin^2(\theta)d\phi^2) & , \text{ (closed)} \\ dr^2 + r^2(d\theta^2 + \sin^2(\theta)d\phi^2) & , \text{ (flat)} \\ dr^2 + \sinh^2(r)(d\theta^2 + \sin^2(\theta)d\phi^2) & , \text{ (hyperbolic)} \end{cases} \quad (1.4.51)$$

for either uniformly curved hyperbolic space, uniformly curved closed space or flat space. This spacetime is called the Friedmann–Lemaître–Robertson–Walker spacetime and the trace of Einstein's equation in four dimensions becomes,

$$R = 4\Lambda - 8\pi T, \quad (1.4.52)$$

where planck units are used and  $T = T_{\mu\nu}g^{\mu\nu}$ . It should be noted that  $R$  and  $T$  are constant over the entire spatial domain of the spacetime for a moment of time. This form of Einstein's equation makes it abundantly clear that the cosmological constant has the same effect on curvature as a uniform matter distribution. In the case  $4\Lambda = 8\pi T$ , Einstein's equation is once again  $R = 0$  and can be solved with the flat metric of Minkowski (but now it is not in vacuum unless  $T = \Lambda = 0$ ). If  $8\pi T > 4\Lambda$ , then the spatial hypersurface of the universe is closed and finite sized. Finally, if  $4\Lambda > 8\pi T$  then the spatial hypersurface of the universe is open or hyperbolic; as a radial geodesics is followed, the amount of space grows faster than the  $r^2$  as expected in flat space.

Putting the ansatz for the metric and stress tensor into the Einstein equation returns an ODE for  $a(t)$ . Along with an equation of state,  $P(\rho)$ , the continuity equation  $\nabla_\mu T^{\mu\nu} = 0$  returns an ODE for  $\rho(t)$ . The two solutions  $\rho(t)$  and  $a(t)$ , along with knowledge of whether the spatial time-slices are flat, closed or hyperbolic, fully specify the spacetime. These solutions cover many topics such as the big bang, inflation, universe expansion, bouncing cosmologies (ending with a big crunch) and also minkowski space given the correct conditions.

### 1.4.8 The Lagrangean Formulation of General Relativity

A common procedure in theoretical physics is to encapsulate the solution space in an action functional  $S$ ,

$$S = \int \mathcal{L} \sqrt{-g} dx^4. \quad (1.4.53)$$

Using the calculus of variation on this action returns differential equations governing the system. As found by Hilbert [REF] the following lagrangean density  $\mathcal{L} = R$ , equal to the Ricci scalar, returns the vacuum Einstein equations under varying with respect to  $g^{\mu\nu}$ .

$$\delta S = \int [\sqrt{-g}(\delta R) + R(\delta\sqrt{-g})] dx^4 \quad (1.4.54)$$

$$= \int \left[ \sqrt{-g} \delta(g^{\mu\nu} R_{\mu\nu}) - \frac{1}{2} \sqrt{-g} g_{\mu\nu} R(\delta g^{\mu\nu}) \right] dx^4 \quad (1.4.55)$$

$$= \int \left[ \sqrt{-g} g^{\mu\nu} (\delta R_{\mu\nu}) + \sqrt{-g} \left( R_{\mu\nu} - \frac{1}{2} R g_{\mu\nu} \right) \delta g^{\mu\nu} \right] dx^4 \quad (1.4.56)$$

where we used Eq. (1.3.139) to vary  $\sqrt{-g}$ . Remembering that the difference of two christoffel symbols such as,

$$\delta \Gamma_{\mu\nu}^{\lambda} = \Gamma_{\mu\nu}^{\lambda} |_{g^{\mu\nu} + \delta g^{\mu\nu}} - \Gamma_{\mu\nu}^{\lambda} |_{g^{\mu\nu}} \quad (1.4.57)$$

is a tensor, and using normal coordinates [WRITE UP NORMAL COORDS] the left hand term of Eq. (1.4.56) becomes

$$g^{\mu\nu} \delta R_{\mu\nu} = g^{\mu\nu} \left( \partial_{\lambda} \delta \Gamma_{\mu\nu}^{\lambda} - \partial_{\nu} \delta \Gamma_{\mu\lambda}^{\lambda} \right), \quad (1.4.58)$$

$$= g^{\mu\nu} \left( \nabla_{\lambda} \delta \Gamma_{\mu\nu}^{\lambda} - \nabla_{\nu} \delta \Gamma_{\mu\lambda}^{\lambda} \right), \quad (1.4.59)$$

$$= \nabla_{\lambda} \left( g^{\mu\nu} \delta \Gamma_{\mu\nu}^{\lambda} - g^{\mu\lambda} \delta \Gamma_{\mu\nu}^{\nu} \right), \quad (1.4.60)$$

$$= \nabla_{\lambda} X^{\lambda}. \quad (1.4.61)$$

The ability to transform the partial derivatives into covariant derivatives comes from using normal coordinates. Putting everything together,  $\delta S$  becomes

$$\delta S = \int \left[ \nabla_{\mu} X^{\mu} + \left( R_{\mu\nu} - \frac{1}{2} R g_{\mu\nu} \right) \right] \sqrt{-g} dx^4, \quad (1.4.62)$$

$$= \int_B X^{\mu} \hat{s}_{\mu} \sqrt{|^{(3)}g|} dx^3 + \int \left[ R_{\mu\nu} - \frac{1}{2} R g_{\mu\nu} \right] \sqrt{-g} dx^4, \quad (1.4.63)$$

$$(1.4.64)$$

where the integral over  $B$  represents the surface integral over the boundary of our spacetime with metric  $^{(3)}g_{ij}$ ; on  $B$   $\delta g^{\mu\nu} \rightarrow 0$  and therefore  $X^{\mu} \rightarrow 0$ . Setting  $dS = 0$  implies

$$R_{\mu\nu} - \frac{1}{2} R g_{\mu\nu} = 0, \quad (1.4.65)$$

which is the vacuum Einstein equation.

### Non-Vacuum Spacetimes

Matter is often added into a spacetime at the level of the lagrangean with a term  $\frac{16\pi G}{c^4} \mathcal{L}_m$ . The cosmological constant can be added in exactly the same way with  $\mathcal{L}_{\Lambda}$ . The total lagrangean becomes,

$$S = \int \left( R + \frac{16\pi G}{c^4} \mathcal{L}_m + \mathcal{L}_{\Lambda} \right) \sqrt{-g} dx^4. \quad (1.4.66)$$

As we have already seen earlier in this section, the variation of  $R$  with respect to the inverse metric components  $g^{\mu\nu}$  returns the vacuum Einstein equation; adding the two new terms from  $\mathcal{L}_m$  and  $\mathcal{L}_\Lambda$ , setting  $\delta S = 0$  gives different equation

$$R_{\mu\nu} - \frac{1}{2}Rg_{\mu\nu} + \frac{16\pi G}{c^4} \frac{1}{\sqrt{-g}} \frac{\delta(\mathcal{L}_m\sqrt{-g})}{\delta g^{\mu\nu}} + \frac{1}{\sqrt{-g}} \frac{\delta(\mathcal{L}_\Lambda\sqrt{-g})}{\delta g^{\mu\nu}} = 0. \quad (1.4.67)$$

Comparing the  $\mathcal{L}_\Lambda$  term to the Einstein equation with cosmological constant in Eq. (1.4.46) we must have

$$g_{\mu\nu}\Lambda = \frac{1}{\sqrt{-g}} \frac{\delta(\mathcal{L}_\Lambda\sqrt{-g})}{\delta g^{\mu\nu}}, \quad (1.4.68)$$

$$= \mathcal{L}_\Lambda \frac{1}{\sqrt{-g}} \frac{\delta(\sqrt{-g})}{\delta g^{\mu\nu}} + \frac{\delta(\mathcal{L}_\Lambda)}{\delta g^{\mu\nu}}, \quad (1.4.69)$$

$$= -\frac{1}{2}g_{\mu\nu}\mathcal{L}_\Lambda + \frac{\delta(\mathcal{L}_\Lambda)}{\delta g^{\mu\nu}}, \quad (1.4.70)$$

$$(1.4.71)$$

which is solved by  $\mathcal{L}_\Lambda = -2\Lambda$ . Comparing the matter term instead returns another definition of the stress tensor,

$$T_{\mu\nu} := -\frac{2}{\sqrt{-g}} \frac{\delta(\mathcal{L}_m\sqrt{-g})}{\delta g^{\mu\nu}}, \quad (1.4.72)$$

$$= -2 \frac{\delta\mathcal{L}_m}{\delta g^{\mu\nu}} + g_{\mu\nu}\mathcal{L}_m. \quad (1.4.73)$$

Collecting these results, the full lagrangean is,

$$\mathcal{L} = R + \frac{16\pi G}{c^4} \mathcal{L}_m - 2\Lambda, \quad (1.4.74)$$

or in Planck units,

$$\mathcal{L} = R + 16\pi\mathcal{L}_m - 2\Lambda. \quad (1.4.75)$$

The form of  $\mathcal{L}_m$  is problem specific, depending on the type of matter. The equation of motion of the matter, described by a set of fields  $\phi_i$ , and their partial derivatives with respect to  $x^\mu$  is,

$$\sqrt{-g} \frac{\delta\mathcal{L}}{\delta\phi_i} - \partial_\mu \left( \sqrt{-g} \frac{\delta\mathcal{L}}{\delta\partial_\mu\phi_i} \right) = 0. \quad (1.4.76)$$

If the  $\phi_i$  are scalar fields then the equation of motion simplifies, using Eq. (1.3.142), to

$$\frac{\delta\mathcal{L}}{\delta\phi_i} - \nabla_\mu \left( \frac{\delta\mathcal{L}}{\delta\nabla_\mu\phi_i} \right) = 0. \quad (1.4.77)$$

## Modified Theories of Gravity

CAN HELP WITH MORE THEORETICAL THEORIES, NEXT EXPANSIONS OF R SUCH AS MODIFIED GRAV OR CHERNS SIEMANS OR HORNDENSKI.

[ADD SOME MOTIVATION OF WHY WE LIKE LAGRANGEANS, EASY TO QUNATIZE OR ADD MORE MATTER RO INTERACTIONS OF MATTER? note hilbert did einstein eq before einstein

## 1.5 Stuff

### 1.5.1 notes

maybe put the field theory bit straight into the curved space bit and don't bother with SR as much?

prove the diff of christoffels is a tensor?

NEwman penrose formalism?

GRChombo section?

einstein summation conventions? and upstairs/downstairs in conventions

check tensor vs tensor field

maybe work coordinate transformation into the text earlier with the introduction of vectors? maybe split the long diff geom section (functions, curves and tensors) into two sections, functions, curves, coords, trans, vectors part 1 then covectors, tensors and tensor transformation part 2, forms part 3 then differentiation then calculus?

mention SR and the fact that GR is based on the equivalence principles (weak and strong?) somewhere

maybe make SR as a solution to the Einstein equation a different section to just SR.

decide when to use SR and GR acronyms

connection/christoffel and capitalise or not?

talk about newman penrose scalars for GW extraction? nah

check capital letters

define trace

3+1 stress tensor is wrong for Klein Gordon

adm metric is wrong in 4th term report

add a section with intro reading such as books Alcubierre, Baumgarte, and GR stuff like Sean Carroll, Tong, Harvey ..

use invisible (with star) subsections to break up longer sections

### 1.5.2 Differential Forms

A differential  $p$ -form is an antisymmetric  $(0, p)$  tensor; the tensor components (e.g.  $A_{\alpha\beta\ldots\zeta}$ ) vanish if there is a repeating index, equal 1 for an even permutation of indices (like 1,2,3,...,N) and  $-1$  for an odd permutation (such as 2,1,3,4,...,N). Note that a 0-form is a function, a 1-form is a co-vector and for an  $N$ -dimensional manifold the  $N$ -form is unique and the  $p$ -forms with  $p > N$  vanish.

When considering differential forms, the conventional covector basis is often changed from  $\theta^\mu$  to  $dx^\mu$  which will lend itself nicely to integrating  $p$ -forms on manifolds later. This convention means we can write the metric as  $\mathbf{g} = g_{\mu\nu} dx^\mu \otimes dx^\nu$ ; the same can be done for any tensor. Note that the metric cannot be a 2-form as it is not an antisymmetric tensor, in fact the metric is a symmetric tensor.

Differential forms have their own unique differential operator called the exterior derivative, it acts on a  $p$ -form and returns a  $p + 1$ -form. For a  $p$ -form  $\mathbf{A} = A_\mu dx^\mu$ , the exterior derivative is given by

$$(dA)_{\mu_1\ldots\mu_{p+1}} = (p+1)\partial_{[\mu_1} A_{\mu_2\ldots\mu_{p+1}]}, \quad (1.5.1)$$

where the square brackets mean the antisymmetric [check as i might need epsilons here]. This derivative guarentees to return a tensor without the need for a connection or metric on the manifold, unlike the partial derivative that we will see next. One common example of an exterior derivative is of a 1-form, say  $\mathbf{A}$ , giving

$$(\mathrm{d}A)_{\mu\nu} = \partial_\mu A_\nu - \partial_\nu A_\mu, \quad (1.5.2)$$

which returns a 2-form. To be a 2-form the tensor must be antisymmetric under swapping indeces like  $(\mathrm{d}A)_{\mu\nu} = -(\mathrm{d}A)_{\nu\mu}$ , which is trivially true, and must transform like a tensor. Performing a coordinate transformation on  $(\mathrm{d}A)_{\mu\nu}$  we see it transforms like

$$\frac{\partial}{\partial \tilde{x}^\mu} \tilde{A}_\nu - \frac{\partial}{\partial \tilde{x}^\nu} \tilde{A}_\mu = \frac{\partial x^\rho}{\partial \tilde{x}^\mu} \frac{\partial}{\partial x^\rho} \left( \frac{\partial x^\sigma}{\partial \tilde{x}^\nu} A_\sigma \right) - \frac{\partial x^\sigma}{\partial \tilde{x}^\nu} \frac{\partial}{\partial x^\sigma} \left( \frac{\partial x^\rho}{\partial \tilde{x}^\mu} A_\rho \right), \quad (1.5.3)$$

$$= \frac{\partial x^\rho}{\partial \tilde{x}^\mu} \frac{\partial x^\sigma}{\partial \tilde{x}^\nu} \left( \frac{\partial}{\partial x^\rho} A_\sigma - \frac{\partial}{\partial x^\sigma} A_\rho \right) + \frac{\partial x^\rho}{\partial \tilde{x}^\mu} \frac{\partial}{\partial x^\rho} \left( \frac{\partial x^\sigma}{\partial \tilde{x}^\nu} \right) A_\sigma - \frac{\partial x^\sigma}{\partial \tilde{x}^\nu} \frac{\partial}{\partial x^\sigma} \left( \frac{\partial x^\rho}{\partial \tilde{x}^\mu} \right) A_\rho, \quad (1.5.4)$$

$$= \frac{\partial x^\rho}{\partial \tilde{x}^\mu} \frac{\partial x^\sigma}{\partial \tilde{x}^\nu} \left( \frac{\partial}{\partial x^\rho} A_\sigma - \frac{\partial}{\partial x^\sigma} A_\rho \right) + \left( \frac{\partial^2 x^\rho}{\partial \tilde{x}^\mu \partial \tilde{x}^\nu} - \frac{\partial^2 x^\rho}{\partial \tilde{x}^\nu \partial \tilde{x}^\mu} \right) A_\rho, \quad (1.5.5)$$

$$= \frac{\partial x^\rho}{\partial \tilde{x}^\mu} \frac{\partial x^\sigma}{\partial \tilde{x}^\nu} \left( \frac{\partial}{\partial x^\rho} A_\sigma - \frac{\partial}{\partial x^\sigma} A_\rho \right), \quad (1.5.6)$$

which is exactly the tensor transformation law.

COVER HER THAT DD GIVES ZERO? HODGE ? REWRITE DIFF EQNS WITH FORM NOTATION AND HODGE THEORY? PROVE

### 1.5.3 Parallel Transport

Parallel transport is the procedure of moving tensors along a smooth curve in a manifold. The curve  $\Gamma$  can be expressed parametrically as  $x^\mu(\tau)$  with respect to a parameter  $\tau$ , this automatically gives us the tangent vector  $\mathbf{X}$  to  $\Gamma$  like

$$X^\mu(\tau) = \frac{\partial x^\mu(\tau)}{\partial \tau} = \dot{x}^\mu. \quad (1.5.7)$$

Parallel transporting a tensor  $\mathbf{T}$  along  $\Gamma$  requires that  $\nabla_{\mathbf{X}} \mathbf{T}$  must be satisfied along  $\Gamma$  where  $\nabla_{\mathbf{X}} = x^\mu \nabla_\mu$ .

MAYBE DO THE FAMOUS VECTOR ON A SPHERE EXAMPLE

Having discussed parallel transport, we can re-derive geodesics. Take a vector field  $\mathbf{X}$  and parallel transport is along it's own integral curves, therefore  $\mathbf{X}$  must satisfy  $\nabla_{\mathbf{X}} \mathbf{X} = 0$ . With a little algebra we can show that this describes a geodesic,

$$x^\mu \nabla_\mu X^\nu = 0, \quad (1.5.8)$$

$$x^\mu \nabla_\mu X^\nu = X^\mu \partial_\mu X^\nu + X^\mu \Gamma^\nu_{\rho\mu} X^\rho, \quad (1.5.9)$$

$$= \frac{\partial x^\mu(\tau)}{\partial \tau} \frac{\partial}{\partial x^\mu} \frac{\partial x^\nu(\tau)}{\partial \tau} + \Gamma^\nu_{\rho\mu} \frac{\partial x^\mu(\tau)}{\partial \tau} \frac{\partial x^\rho(\tau)}{\partial \tau}, \quad (1.5.10)$$

$$= \frac{\partial}{\partial \tau} \frac{\partial x^\nu(\tau)}{\partial \tau} + \Gamma^\nu_{\rho\mu} \frac{\partial x^\mu(\tau)}{\partial \tau} \frac{\partial x^\rho(\tau)}{\partial \tau}, \quad (1.5.11)$$

$$= \ddot{x}^\nu + \Gamma^\nu_{\rho\mu} \dot{x}^\rho \dot{x}^\mu \quad (1.5.12)$$

and we have re-derived Eq. (1.2.71). Again this aligns with our intuition of a geodesic in flat space. We already remarked in Section 1.2.6 that  $\ddot{x}^\mu = 0$  describes a straight line in flat space (when using cartesian coordinates) and now we can add another interpretation; in flat space a geodesic (which is a straight line) can be created by transporting a vector along it's own direction.



### 1.5.4 Low Curvature Limit of General Relativity

An important use of General Relativity is it's use in the low curvature limit. The simplest example of this would be Special Relativity; if General Relativity i[DO] reproduce Special Relativity in the limit of vanishing curvature then it is. We work with the assumption of a vacuum spacetime with no Cosmological constant and seek solutions to the Einstein equation with metric  $g_{\mu\nu} = \eta_{\mu\nu}$  where

$$\eta_{\mu\nu} = \begin{pmatrix} -1 & 0 & 0 & 0 \\ 0 & 1 & 0 & 0 \\ 0 & 0 & 1 & 0 \\ 0 & 0 & 0 & 1 \end{pmatrix} \quad (1.5.13)$$

in Cartesian coordinates. As seen before, in Eq.[REF]REF the Einstein equation in vacuum simplfies to just a vanishing Ricci tensor,

$$R_{\mu\nu} = 0, \quad (1.5.14)$$

$$= \partial_\rho \Gamma^\rho_{\mu\nu} - \partial_\nu \Gamma^\rho_{\mu\rho} + \Gamma^\rho_{\rho\sigma} \Gamma^\sigma_{\mu\nu} - \Gamma^\rho_{\mu\sigma} \Gamma^\sigma_{\rho\nu}. \quad (1.5.15)$$

Given that the Connection symbols  $\Gamma^\mu_{\nu\rho}$  vanish everywhere for the metric components  $\eta_{\mu\nu}$  then Eq. (1.5.14) is trivially satisfied and we have proved that Special Relativity is the zero-curvature limit of GR.

Relaxing the condition  $g_{\mu\nu} = \eta_{\mu\nu}$  to  $g_{\mu\nu} = \eta_{\mu\nu} + h_{\mu\nu}$ , where the components  $h_{\mu\nu} \ll 1$ , we can create a vacuum spacetime consisting of small curvature fluctuations; this turns out to describe gravitational waves. Ignoring terms of order  $\mathcal{O}(h^2)$  we can see that

$$g^{\mu\nu} = \eta^{\mu\nu} - h^{\mu\nu}, \quad (1.5.16)$$

$$h^{\rho\sigma} = \eta^{\mu\rho} \eta^{\nu\sigma} h_{\mu\nu}, \quad (1.5.17)$$

$$g^{\mu\nu} g_{\nu\rho} = \delta^\mu_\rho = \eta^{\mu\nu} \eta_{\nu\rho} + \eta^{\mu\nu} h_{\nu\rho} - h^{\mu\nu} \eta_{\nu\rho} + \mathcal{O}(h^2), \quad (1.5.18)$$

$$= \delta^\mu_\rho + \eta^{\mu\nu} h_{\nu\rho} - \eta^{\mu\alpha} \eta^{\nu\beta} h_{\alpha\beta} \eta_{\nu\rho}, \quad (1.5.19)$$

$$= \delta^\mu_\rho + \underbrace{\eta^{\mu\nu} h_{\nu\rho} - \eta^{\mu\alpha} h_{\alpha\rho}}_{=0}. \quad (1.5.20)$$

Note that we raise/lower the indeces of  $h_{\mu\nu}/h^{\mu\nu}$  with  $\boldsymbol{\eta}$  and not  $\boldsymbol{g}$  THIS IS WRONG. Looking at the connection symbols and Ricci tensor while ignoring  $\mathcal{O}(h^2)$  terms we get

$$\Gamma^\rho_{\mu\nu} = \frac{1}{2} (\eta^{\rho\sigma} - h^{\rho\sigma}) (\partial_\mu (\eta_{\sigma\nu} + h_{\sigma\nu}) + \partial_\nu (\eta_{\mu\sigma} + h_{\mu\sigma}) - \partial_\sigma (\eta_{\mu\nu} + h_{\mu\nu})), \quad (1.5.21)$$

$$= \frac{1}{2} \eta^{\rho\sigma} (\partial_\mu h_{\sigma\nu} + \partial_\nu h_{\mu\sigma} - \partial_\sigma h_{\mu\nu}) + \mathcal{O}(h^2), \quad (1.5.22)$$

$$R_{\mu\nu} = \partial_\rho \Gamma^\rho_{\mu\nu} - \partial_\nu \Gamma^\rho_{\mu\rho} + \mathcal{O}(h^2), \quad (1.5.23)$$

$$= \frac{1}{2} \eta^{\rho\sigma} (\partial_\rho \partial_\mu h_{\sigma\nu} - \partial_\rho \partial_\sigma h_{\mu\nu} - \partial_\nu \partial_\mu h_{\sigma\rho} + \partial_\sigma \partial_\mu h_{\rho\mu}) + \mathcal{O}(h^2), \quad (1.5.24)$$

$$R = (\eta^{\mu\nu} - h^{\mu\nu}) R_{\mu\nu}, \quad (1.5.25)$$

$$= \eta^{\mu\nu} \eta^{\rho\sigma} (\partial_\mu \partial_\rho h_{\sigma\nu} - \partial_\sigma \partial_\rho h_{\mu\nu}) + \mathcal{O}(h^2). \quad (1.5.26)$$

To simplify the solving of Einsteins eqn [FIX THIS] we can consider coordinate transformation like  $x^\mu \rightarrow x^\mu + \zeta^\mu$  where  $\zeta^\mu \ll 1$ . It can easily be shown that to first order in  $\zeta^\mu$  and  $h_{\mu\nu}$  that  $h_{\mu\nu}$  transforms like

$$h_{\mu\nu} \rightarrow h_{\mu\nu} + \partial_\mu \zeta_\nu + \partial_\nu \zeta_\mu \quad (1.5.27)$$

where raising/lowering the indeces of  $\boldsymbol{\zeta}$  is done with  $\boldsymbol{\eta}$  as terms of order  $\mathcal{O}(h)\mathcal{O}(\zeta)$  are ignored.

Note [TALK ABOUT G PLUS H RATHER THAN ETA PLUS H FOR BH RINGDOWN AND MAYBE BS STABILITY? THIS IS MORE PERTURBATION THEORY THOUGH]

[MENTION : GW'S, PRECESSION, LIGHT DEFLECTION, TIME DILATION AROUND EARTH/-SUN, MAYBE MENTION INTERSTELLAR'S TIME DILATION? ARE THESE REALLY LOW ENERGY LIMIT? MENTION POST NEWTONIAN OTHER THINGS?]

## Chapter 2

# Numerical Relativity, Numerical Methods and Boson Stars

MAYBE PUT SOME STUFF HERE ABOUT NUMERICAL ALGORITHMS LIKE RK4 EULAR STEP LEAPFROG AND DO ERROR GROWTH RATES AND COURANT

## 2.1 Numerical Relativity

### 2.1.1 Spacetime Foliation

Einstein's equation is a classical field equation which governs the dynamics of physical objects and spacetime curvature.

$$R_{\mu\nu} - \frac{1}{2}Rg_{\mu\nu} = \frac{8\pi G}{c^4}T_{\mu\nu} \quad (2.1.1)$$

The above version is fully covariant, agnostic of the definition of time, and many solutions are known analytically, for instance Black Hole geometries. When the system of interest becomes more complicated, such as the case of orbiting objects which will be discussed later, finding an analytic expression becomes impossible. For low energy dynamics, Newtonian theory, Post-Newtonian theory and perturbation theory can make more progress; however this report will focus on the highly nonlinear regime where Numerical relativity is truly the only hope to solve Einstein's equations. To do this it is common to split spacetime into 3+1 dimensions, evolving a 3 dimensional manifold (maybe with matter) on a computer along the final 4th dimension. To do this we need to define a suitable hypersurface  $\Sigma \in \mathcal{M}$ . This is usually done by demanding the hypersurface  $\Sigma_t$  be the set of points  $p \in \mathcal{M}$  where some scalar function  $f : \mathcal{M} \mapsto \mathbb{R}$  satisfies  $f(p) = t$ . This hypersurface should be a Cauchy surface, intersecting all causal curves only once, or a partial Cauchy surface which intersects all causal curves at most once. Generally we will choose a partial Cauchy surface due to the finite memory of computers, however by picking certain compactified coordinates it is possible to use a Cauchy surface [REF]. A foliation  $\mathcal{F}$  is then the union of a set of  $\Sigma_t$  for some range of the parameter  $t$ ,

$$\mathcal{F} = \cup_t(\Sigma_t) \subseteq \mathcal{M}. \quad (2.1.2)$$

This means we should be careful to pick a parameter  $t$  such that the foliation is not self intersecting for the parameter range that covers the region of  $\mathcal{M}$  that we are interested in simulating. Fortunately the time coordinate in a suitable coordinate system works in all cases covered by this report; it also gives the physical interpretation of  $\Sigma_t$  being an instance of time. Now we should define unit normal vector  $n$  to  $\Sigma_t$ ,

$$n^\mu = -\frac{\nabla^\mu t}{\sqrt{|g_{\mu\nu}\nabla^\mu t\nabla^\nu t|}} \quad \& \quad n_\mu = -\frac{dt_\mu}{\sqrt{|g_{\mu\nu}\nabla^\mu t\nabla^\nu t|}}. \quad (2.1.3)$$

For simplicity we define the lapse function  $\alpha$  to be

$$\alpha := \frac{1}{\sqrt{|g_{\mu\nu}\nabla^\mu t\nabla^\nu t|}}. \quad (2.1.4)$$

giving us  $n_\mu = -\alpha dt_\mu$  as well as the normal evolution vector  $m_\mu = \alpha n_\mu$ . Defining two infinitesimally close points  $(p, q) \in (\Sigma_t, \Sigma_{t'})$  where  $q^\mu = p^\mu + m^\mu \delta t$  we see,

$$t(q) = t(p^\mu + m^\mu \delta t) = t(p) + \frac{dt}{dx^\mu} m^\mu \delta t = t(p) + dt_\mu m^\mu \delta t = t(p) + \delta t, \quad (2.1.5)$$

showing that  $m^\mu$  points between neighbouring hypersurfaces; therefore when creating evolution equations we should care about Lie derivatives along  $m^\mu$ ,  $\mathcal{L}_m$ , rather than  $\mathcal{L}_n$ .

### 2.1.2 The 3+1 Decomposition

With the notion of a spacetime foliation we should define how to project tensors onto  $\Sigma_t$ ; clearly scalars need no projecting. Splitting a vector  $X^\mu e_\mu = X_\parallel^\mu e_\mu + X_\perp^\mu e_\mu$  into components tangent or normal to  $\Sigma_t$

we define the orthogonal projector  $\perp_\nu^\mu$  and parallel projector  $-n^\mu n_\nu$ ,

$$X_\parallel^\mu = [\delta_\nu^\mu + n^\mu n_\nu] X^\nu = \perp_\nu^\mu X^\nu, \quad (2.1.6)$$

$$X_\perp^\mu = -n^\mu n_\nu X^\nu. \quad (2.1.7)$$

Considering scalars such as  $\phi = w_\mu X^\mu$  or  $\psi = T^{\mu\nu} w_\mu w_\nu$ , and remembering scalars don't vary under projection, it is simple to show that any tensor  $T$  can be projected by contracting a projection operator  $\perp$  on any free index,

$$T_\parallel^{ij\dots}_{kl\dots} = \mathcal{T}^{ij\dots}_{kl\dots} = \perp_\mu^i \perp_\nu^j \perp_k^\rho \perp_l^\sigma \dots T^{\mu\nu\dots}_{\rho\sigma\dots}. \quad (2.1.8)$$

We can find the 3-metric  $\gamma_{\mu\nu}$  of  $\Sigma_t$  by projecting  $g_{\mu\nu}$ ,

$$\gamma_{ij} = \perp_i^\mu \perp_j^\nu g_{\mu\nu} = g_{\mu\nu} + n_\mu n_\nu \rightarrow \gamma_j^i = \perp_j^i, \quad (2.1.9)$$

and we find it is equivalent to the projector  $\perp$ ; this had to be the case as  $\perp_{ij} dx^i dx^j$  gives the line element along  $\Sigma_t$ . With this machinery we can define the extrinsic curvature tensor  $\mathcal{K}_{ij}$  representing curvature due to the choice of spacetime foliation; it could be nonzero for certain foliations of Minkowski space. It is not the same as the 3-Ricci tensor  $\mathcal{R}_{ij}$  which is due to genuine spacetime curvature of  $\mathcal{M}$  regardless of foliation. The extrinsic curvature tensor is defined the following way,

$$\mathcal{K}_{ij} = \mathcal{K}_{ji} := -\perp_i^\mu \perp_j^\nu \nabla_\mu n_\nu = -\perp_i^\mu \nabla_\mu n_j = -\nabla_i n_j - n_i a_j, \quad (2.1.10)$$

$$\mathcal{K} = \mathcal{K}_i^i = -\nabla \cdot \mathbf{n}, \quad (2.1.11)$$

where  $a_i = \mathbf{n} \cdot \nabla n_i$  is called the Eulerian acceleration; it should be noted  $\mathcal{K}_{ij}$  is symmetric. It can also be shown to take the following form,

$$\mathcal{K}_{ij} = -\frac{1}{2} \mathcal{L}_n \gamma_{ij} = -\frac{1}{2\alpha} \mathcal{L}_m \gamma_{ij}, \quad (2.1.12)$$

which gives the intuitive explanation of  $\mathcal{K}_{ij}$  being the rate of change of the 3-metric  $\gamma_{ij}$  with respect to the foliation. The next object we should discuss is the projected covariant 3-derivative  $\mathcal{D}_i$ . This is the covariant derivative belonging to  $\Sigma_t$  and hence its arguments should be tensors belonging to  $\Sigma_t$ . This means we can define it as so,

$$\mathcal{T}^{ij\dots}_{kl\dots} = \perp_\mu^i \perp_\nu^j \perp_k^\rho \perp_l^\sigma \dots T^{\mu\nu\dots}_{\rho\sigma\dots}, \quad (2.1.13)$$

$$\mathcal{D}_m \mathcal{T}^{ij\dots}_{kl\dots} := \perp_m^\mu \perp_\mu^i \perp_\nu^j \perp_k^\rho \perp_l^\sigma \dots \nabla_\mu T^{\mu\nu\dots}_{\rho\sigma\dots}. \quad (2.1.14)$$

A simple example is the derivative of a vector  $X^i \mathbf{e}_i \in \mathcal{T}(\Sigma_t)$ ,

$$\mathcal{D}_i X^j = \partial_i X^j + \Upsilon_{jk}^i X^k, \quad (2.1.15)$$

$$\Upsilon_{jk}^i = \frac{1}{2} \gamma^{il} [\partial_j \gamma_{lk} + \partial_k \gamma_{jl} - \partial_l \gamma_{jk}], \quad (2.1.16)$$

where  $\Upsilon_{jk}^i$  is the Christoffel symbol of  $\Sigma_t$ . Another useful example is  $a^\mu$  which can be equated to,

$$a_\mu = \mathbf{n} \cdot \nabla n_\mu = \mathcal{D}_\mu \ln \alpha = \frac{1}{\alpha} \mathcal{D}_\mu \alpha, \quad (2.1.17)$$

and allows us to evaluate the Lie derivative of the projector  $\perp_j^i$ ,

$$\mathcal{L}_m \perp_j^i = \alpha n^k \nabla_k \perp_j^i + \perp_k^i \nabla_j \alpha n^k - \perp_j^k \nabla_k \alpha n^i, \quad (2.1.18)$$

$$= \alpha n^k \nabla_k [n^i n_j] + \alpha \nabla_j n^i - [\alpha K_j^i + n^i \mathcal{D}_j \alpha], \quad (2.1.19)$$

$$= 0. \quad (2.1.20)$$

The result  $\mathcal{L}_m \perp_j^i = 0$  is incredibly important, it tells us that the projector commutes with  $\mathcal{L}_m$  and as a result any tensor  $\mathbf{T}$  which when projected onto  $\Sigma_t$ , written  $\mathcal{T}$ , satisfies

$$\mathcal{L}_m \mathcal{T}^{ij\dots}_{kl\dots} = \perp_\mu^i \perp_\nu^j \perp_k^\rho \perp_l^\sigma \mathcal{L}_m T^{\mu\nu\dots}_{\rho\sigma\dots}. \quad (2.1.21)$$

In other words, evolving a projected tensor along integral curves of  $m$  leaves the tensor parallel to  $\Sigma_t$ .

### 2.1.3 Gauss, Codazzi and Ricci Equations

The projections of the 4-dimensional curvature tensors into a combination of 3-dimensional curvature tensors and  $\mathcal{K}$  is very useful as it captures all the degrees of freedom of the 4-dimensional Riemann tensor in terms of variables on  $\Sigma_t$ . This property is crucial when numerically simulating a single time slice  $\Sigma_t$  as we only have access to variables on  $\Sigma_t$ .

#### The Gauss Equations

From the definition of the Riemann tensor in section 1.3.4 we know,

$$[\mathcal{D}_i \mathcal{D}_j - \mathcal{D}_j \mathcal{D}_i]v^k = \mathcal{R}^k_{\phantom{k}mij} v^m, \quad (2.1.22)$$

$$[\nabla_\alpha \nabla_\beta - \nabla_\beta \nabla_\alpha]v^\gamma = R^\gamma_{\phantom{\gamma}\lambda\alpha\beta} v^\lambda, \quad (2.1.23)$$

where the vector  $v^m = \perp^\mu_\rho v^\rho$  is tangent to  $\Sigma_t$ . Expanding the  $\mathcal{D}$ 's in terms of  $\nabla$ 's gives,

$$\mathcal{D}_i \mathcal{D}_j v^k = \perp^\mu_i \perp^\sigma_j \perp^k_\xi \nabla_\mu (\perp^\nu_\sigma \perp^\xi_\rho \nabla_\nu v^\rho), \quad (2.1.24)$$

and using the following properties; impotence of projections  $\perp^\mu_i \perp^\mu_j = \perp^i_j$ , null projection of orthogonal vectors  $\perp(\mathbf{n}) = 0$ , metric compatibility  $\nabla_\mu \perp^i_j = n_j \nabla_\mu n^i + n^i \nabla_\mu n_j$  and Eq. (2.1.10) for  $\mathcal{K}_{ij}$  we obtain the Gauss relation,

$$\perp^\mu_i \perp^\nu_j \perp^\sigma_\rho R^\rho_{\phantom{\rho}\sigma\mu\nu} = \mathcal{R}^k_{\phantom{k}lij} + \mathcal{K}^k_i \mathcal{K}_{lj} - \mathcal{K}^k_j \mathcal{K}_{il}. \quad (2.1.25)$$

Contracting over  $i, k$  above and relabelling indices we get the contracted Gauss relation,

$$\perp^\mu_i \perp^\nu_j R_{\mu\nu} + \gamma_{i\mu} n^\nu \perp^\rho_j n^\sigma R^\mu_{\phantom{\mu}\nu\rho\sigma} = \mathcal{R}_{ij} + \mathcal{K} \mathcal{K}_{ij} - \mathcal{K}^k_j \mathcal{K}_{ik}. \quad (2.1.26)$$

Contracting again and realising  $R_{\mu\nu\rho\sigma} n^\mu n^\nu n^\rho n^\sigma = 0$  from antisymmetry in indices 0 and 1 or 2 and 3 in the Riemann tensor, gives the scalar Gauss equation,

$$R + 2R_{\mu\nu} n^\mu n^\nu = \mathcal{R} + \mathcal{K}^2 - \mathcal{K}_{ij} \mathcal{K}^{ij}. \quad (2.1.27)$$

#### The Codazzi Equations

The Codazzi relations are derived from a different start point. Instead of projecting the Riemann tensor fully onto  $\Sigma_t$  with projection operators  $\perp$  and a spacelike vector  $\mathbf{v}$ , it is now projected with a timelike vector  $\mathbf{n}$ ,

$$[\nabla_\alpha \nabla_\beta - \nabla_\beta \nabla_\alpha]n^\gamma = R^\gamma_{\phantom{\gamma}\lambda\alpha\beta} n^\lambda, \quad (2.1.28)$$

and again projecting to  $\Sigma_t$  with three projection operators. The following relations are used

$$\nabla_j n^k = -\mathcal{K}^k_j - a^k n_j, \quad (2.1.29)$$

$$\perp^i_\mu \perp^j_\nu \perp^\rho_k \nabla_i \nabla_j n^k = -\mathcal{D}_i \mathcal{K}^k_j + a^k \mathcal{K}_{ij}, \quad (2.1.30)$$

which lead immediately to the Codazzi relation,

$$\perp^\mu_i \perp^\nu_j \perp^k_\rho n^\sigma R^\rho_{\phantom{\rho}\sigma\mu\nu} = \mathcal{D}_j \mathcal{K}^k_i - \mathcal{D}_i \mathcal{K}^k_j, \quad (2.1.31)$$

and the contracted Codazzi relation,

$$\perp^\mu_i n^\nu R_{\mu\nu} = \mathcal{D}_i \mathcal{K} - \mathcal{D}_\mu \mathcal{K}^\mu_i. \quad (2.1.32)$$

## The Ricci Equation

Finally we turn our attention to the Ricci equation, the projection of the Riemann tensor twice onto  $\Sigma_t$  and twice contracting with  $\mathbf{n}$ . This is done by projecting Eq (2.1.28) with two projectors  $\perp$  and one timelike  $\mathbf{n}$ . If we contract with  $n^\gamma$  then the antisymmetry in the first two Riemann tensor indices would identically give to zero, therefore the unique choice (upto a minus sign) is to project with  $n^\beta$ ,

$$R_{\gamma\lambda\alpha\beta}n^\lambda n^\beta = n^\beta [\nabla_\alpha \nabla_\beta - \nabla_\beta \nabla_\alpha] n_\gamma, \quad (2.1.33)$$

and project the remaining free indices with  $\perp$  like,

$$\perp_i^\gamma \perp_j^\alpha R_{\gamma\lambda\alpha\beta} n^\lambda n^\beta = \perp_i^\gamma \perp_j^\alpha n^\beta [\nabla_\alpha \nabla_\beta - \nabla_\beta \nabla_\alpha] n_\gamma. \quad (2.1.34)$$

Rearranging Eqs. (2.1.10) and (2.1.17),

$$\nabla_\sigma n_\mu = -\mathcal{K}_{\mu\sigma} - n_\sigma \mathcal{D}_\mu \ln(\alpha), \quad (2.1.35)$$

which can be used to expand the right hand side of Eq. (2.1.36),

$$\perp_i^\gamma \perp_j^\alpha R_{\gamma\lambda\alpha\beta} n^\lambda n^\beta = \perp_i^\gamma \perp_j^\alpha n^\beta [-\nabla_\alpha \mathcal{K}_{\gamma\beta} + \nabla_\beta \mathcal{K}_{\gamma\alpha}] \quad (2.1.36)$$

$$+ \perp_i^\gamma \perp_j^\alpha n^\beta [-\nabla_\alpha (n_\beta \mathcal{D}_\gamma \ln(\alpha)) + \nabla_\beta (n_\alpha \mathcal{D}_\gamma \ln(\alpha))], \quad (2.1.37)$$

$$= \perp_i^\gamma \perp_j^\alpha n^\beta n^\sigma \nabla_\sigma \mathcal{K}_{\gamma\alpha} + \perp_i^\gamma \perp_j^\alpha \mathcal{K}_{\gamma\beta} \nabla_\alpha n^\beta \quad (2.1.38)$$

$$+ \perp_i^\gamma \perp_j^\alpha n^\beta [-n_\beta \nabla_\alpha (\mathcal{D}_\gamma \ln(\alpha)) + n_\alpha \nabla_\beta \mathcal{D}_\gamma \ln(\alpha) + (\mathcal{D}_\gamma \ln(\alpha)) \nabla_\beta n_\alpha], \quad (2.1.39)$$

$$= \perp_i^\gamma \perp_j^\alpha n^\beta n^\sigma \nabla_\sigma \mathcal{K}_{\gamma\alpha} - \mathcal{K}_{ik} \mathcal{K}_j^k \quad (2.1.38)$$

$$+ \mathcal{D}_j \mathcal{D}_i \ln(\alpha) + \mathcal{D}_i \ln(\alpha) \mathcal{D}_j \ln(\alpha), \quad (2.1.39)$$

$$= \perp_i^\gamma \perp_j^\alpha n^\beta n^\sigma \nabla_\sigma \mathcal{K}_{\gamma\alpha} - \mathcal{K}_{ik} \mathcal{K}_j^k + \frac{1}{\alpha} \mathcal{D}_j \mathcal{D}_i \alpha, \quad (2.1.39)$$

where  $\mathbf{n}^2 = -1$ ,  $\perp_i^\mu n_\mu = 0$ ,  $\mathcal{D}_\alpha \ln \alpha = n^\beta \nabla_\beta n_\alpha$  from Eq. (2.1.17) and  $n^\beta \nabla_\alpha n_\beta = 0$  were used. This expression can be simplified by calculating the Lie derivative of  $\mathcal{K}$ ,

$$\mathcal{L}_m \mathcal{K}_{ij} = \perp_i^\mu \perp_j^\nu \mathcal{L}_m \mathcal{K}_{\mu\nu}, \quad (2.1.40)$$

$$= \alpha \perp_i^\mu \perp_j^\nu \mathcal{L}_n \mathcal{K}_{\mu\nu}, \quad (2.1.41)$$

$$= \alpha \perp_i^\mu \perp_j^\nu [\alpha \mathbf{n} \cdot \nabla \mathcal{K}_{\mu\nu} + 2\mathcal{K}_{k(\nu} \nabla_{\mu)} n^k], \quad (2.1.42)$$

$$= \alpha \perp_i^\mu \perp_j^\nu n^\sigma \nabla_\sigma \mathcal{K}_{\mu\nu} - 2\alpha \mathcal{K}_{ik} \mathcal{K}_j^k, \quad (2.1.43)$$

where the results  $\mathcal{L}_m \mathcal{K} = \alpha \mathcal{L}_n \mathcal{K}$  from Eq. (2.1.12),  $\mathcal{L}_m \mathcal{K}_{\alpha\beta} \in \Sigma_t$  from Eq. (2.1.21) and Eq. (2.1.10) were used. Putting everything together we arrive at the Ricci equation,

$$\perp_i^\mu \perp_j^\nu n^\rho n^\sigma R_{\mu\rho\nu\sigma} = \frac{1}{\alpha} \mathcal{L}_m \mathcal{K}_{ij} + \frac{1}{\alpha} \mathcal{D}_j \mathcal{D}_i \alpha + \mathcal{K}_{ik} \mathcal{K}_j^k. \quad (2.1.44)$$

This is the final contraction of the Riemann tensor that can be made with  $\perp$  and  $\mathbf{n}$  as any projections with three or more contractions with  $\mathbf{n}$  would identically give zero due to the symmetries of the Riemann tensor.

### 2.1.4 Decomposition of Einstein's Equation

To evolve General Relativity numerically we must project the Einstein Equation into 3+1 dimensions. Relations between three and four dimensional geometric objects have been derived above and will be used to decompose the Einstein tensor  $G_{\mu\nu} = R_{\mu\nu} - g_{\mu\nu} R/2$  from the left hand side of Eq. (2.1.1). The second component, for simulating non-vacuum spacetimes, is the 3+1 decomposition of the Stress tensor

$T_{ab}$ . We contract twice with  $\mathbf{n}$ , then once with  $\mathbf{n}$  while projecting onto  $\Sigma_t$  and finally twice projecting onto  $\Sigma_t$  to get an energy, momentum and stress-like split,

$$\mathcal{E} = \mathbf{T}(\mathbf{n}, \mathbf{n}) = T_{\mu\nu} n^\mu n^\nu, \quad (2.1.45)$$

$$\mathcal{S}_i = -\mathbf{T}(\mathbf{n}, \cdot) = -\perp_i^\mu n^\nu T_{\mu\nu}, \quad (2.1.46)$$

$$\mathcal{S}_{ij} = \perp_i^\mu \perp_j^\nu T_{\mu\nu}, \quad (2.1.47)$$

and by construction,

$$T_{\mu\nu} = \mathcal{E} n_\mu n_\nu + \mathcal{S}_\mu n_\nu + \mathcal{S}_\nu n_\mu + \mathcal{S}_{\mu\nu}. \quad (2.1.48)$$

With this and the Gauss-Codazzi equations of section 2.1.3 we can project the Einstein equation. Lets first look at the scalar equation,

$$G_{\mu\nu} n^\mu n^\nu = R_{\mu\nu} n^\mu n^\nu + \frac{1}{2} R = 8\pi \mathcal{E}, \quad (2.1.49)$$

and equating the geometric terms to the scalar Gauss equation we get the Hamiltonian constraint,  $\mathcal{H} = 0$ ,

$$\mathcal{H} = \mathcal{K}_{\mu\nu} \mathcal{K}^{\mu\nu} - \mathcal{K}^2 - \mathcal{R} + 16\pi \mathcal{E}. \quad (2.1.50)$$

Now looking at the once projected part we see,

$$\perp_i^\mu n^\nu G_{\mu\nu} = \perp_i^\mu n^\nu R_{\mu\nu} = -8\pi \mathcal{S}_i, \quad (2.1.51)$$

and substituting the geometric terms for the contracted Codazzi relation we get the momentum constraint,  $\mathcal{P}_i = 0$ ,

$$\mathcal{P}_i = \mathcal{D}_i \mathcal{K} - \mathcal{D}_j \mathcal{K}_i^j + 8\pi \mathcal{S}_i. \quad (2.1.52)$$

Finally, the space-space projection gives the 6 evolution PDE's. This time start with the trace reversed Einstein Equation

$$R_{\mu\nu} = 8\pi \left[ T_{\mu\nu} - \frac{1}{2} T g_{\mu\nu} \right], \quad (2.1.53)$$

$$\perp_i^\mu \perp_j^\nu R_{\mu\nu} = 8\pi \left[ \mathcal{S}_{ij} - \frac{1}{2} (\mathcal{S} - \mathcal{E}) \gamma_{ij} \right], \quad (2.1.54)$$

where we used  $T = [\gamma^{\mu\nu} - n^\mu n^\nu] T_{\mu\nu} = \mathcal{S} - \mathcal{E}$ . Project the Ricci tensor, we use the contracted Gauss equation but replace the term with  $R^\mu_{\nu\rho\sigma}$  with the Ricci equation in Eq. (2.1.44). Rearranging gives a normal evolution for the extrinsic curvature,

$$\mathcal{L}_m \mathcal{K}_{ij} = -\mathcal{D}_j \mathcal{D}_i \alpha + \alpha \left[ \mathcal{R}_{ij} + \mathcal{K} \mathcal{K}_{ij} - 2\mathcal{K}_i^k \mathcal{K}_{kj} + 4\pi [\gamma_{ij} (\mathcal{S} - \mathcal{E}) - 2\mathcal{S}_{ij}] \right]. \quad (2.1.55)$$

Along with the definition of  $\mathcal{K}_{ij}$  in Eq. (2.1.12),

$$\mathcal{L}_m \gamma_{ij} = -2\alpha \mathcal{K}_{ij}, \quad (2.1.56)$$

this gives the normal evolution equations for  $\gamma_{ij}$  and  $\mathcal{K}_{ij}$ . In 4 or  $n$  spacetime dimensions the normal evolution equations contain 6 or  $\frac{n^2-n}{2}$  differential equations, the Hamiltonian constraint is a single differential equation, the momentum constraint contains 3 or  $n-1$  differential equations and the Einstein equation contains 10 or  $\frac{n^2+n}{2}$  differential equations. In four spacetime dimensions this corresponds to 6 evolution equations and 4 constraint equations over the surface  $\Sigma_t$ .



adm.png

### 2.1.5 Foliation Adapted Coordinates

Picking coordinates in GR introduces a large gauge freedom which allows us to use a level set of the time coordinate  $x^0 = t$  to define our foliation hypersurfaces  $\Sigma_t$ . The other three coordinates  $x^i$  for  $i \in [1, 2, 3]$  can be used to span each hypersurface  $\Sigma_t$  however we define. It is conventional to split the normal evolution vector  $m^\mu$  into time  $t^\mu$  and space parts  $\beta^\mu$ ,

$$m^\mu = t^\mu - \beta^\mu = (\partial_0)^\mu - \beta^i (\partial_i)^\mu, \quad (2.1.57)$$

$$m^\mu = (1, -\beta^1, -\beta^2, -\beta^3). \quad (2.1.58)$$

We can view  $t^\mu$  as the (not necessarily causal) worldline for a simulation gridpoint, hence we would like to evolve our PDE's along  $t^\mu$  on a computer. Equations (2.1.57) and (2.1.58) along with the definition of  $\mathbf{m}$ ,  $\mathbf{m} = \alpha \mathbf{n}$ , specify  $n^\mu$  and  $n_\mu$ ,

$$n^\mu = \frac{1}{\alpha} (1, -\beta^1, -\beta^2, -\beta^3), \quad (2.1.59)$$

$$n_\mu = -\alpha (1, 0, 0, 0). \quad (2.1.60)$$

The decomposed metric can be calculated, using the property that  $\beta$  is tangent to  $\Sigma_t$  and orthogonal to  $m$ ,

$$g_{00} = \mathbf{g}(\partial_0, \partial_0) = \mathbf{g}(\mathbf{m} + \beta^i \partial_i, \mathbf{m} + \beta^j \partial_j) = \mathbf{g}(\mathbf{m}, \mathbf{m}) + \beta^i \beta_j \langle \partial_i, \mathbf{d}\mathbf{x}^j \rangle = -\alpha^2 + \beta^i \beta_i, \quad (2.1.61)$$

$$g_{0i} = \mathbf{g}(\partial_0, \partial_i) = \mathbf{g}(\mathbf{m} + \beta^j \partial_j, \partial_i) = \beta^j \mathbf{g}(\partial_j, \partial_i) = \beta_i, \quad (2.1.62)$$

$$g_{ij} = \mathbf{g}(\partial_i, \partial_j) = \gamma(\partial_i, \partial_j) = \gamma_{ij}. \quad (2.1.63)$$

This is commonly called the 3+1 ADM metric [REF] and  $\alpha, \beta^i$  are referred to the lapse and shift vector in this context. The line element and metric are commonly written as,

$$ds^2 = -\alpha^2 dt^2 + \gamma_{ij} [dx^i + \beta^i dt] [dx^j + \beta^j dt], \quad (2.1.64)$$

$$g_{\mu\nu} = \begin{pmatrix} -\alpha^2 + \beta^i \beta_i & \beta_i \\ \beta_j & \gamma_{ij} \end{pmatrix}, \quad (2.1.65)$$

$$g^{\mu\nu} = \frac{1}{\alpha^2} \begin{pmatrix} -1 & \beta^i \\ \beta^j & \alpha^2 \gamma^{ij} - \beta^i \beta^j \end{pmatrix} \quad (2.1.66)$$

and using Cramers rule for metric determinant,

$$g^{00} = \frac{\det\{\gamma_{ij}\}}{\det\{g_{\mu\nu}\}}, \quad (2.1.67)$$

we get the important relationship,

$$\sqrt{-g} = \alpha \sqrt{\gamma}, \quad (2.1.68)$$

where  $g$  and  $\gamma$  are the determinants of  $g_{\mu\nu}$  and  $\gamma_{ij}$  respectively.

### 2.1.6 ADM Equations

Now that we have some coordinates suitable for the spacetime foliation we can find the Arnowitt-Deser-Misner (ADM) evolution equations for  $\mathcal{K}_{ij}$  and  $\gamma_{ij}$ . First expand the Lie derivative  $\mathcal{L}_m$  using

$$t^\mu = (1, 0, 0, 0) \rightarrow \mathcal{L}_t T^{\mu\nu\dots}_{\rho\sigma\dots} = \partial_t T^{\mu\nu\dots}_{\rho\sigma\dots} \quad (2.1.69)$$

$$\mathcal{L}_m = \mathcal{L}_t - \mathcal{L}_\beta = \partial_t - \mathcal{L}_\beta \quad (2.1.70)$$

and the ADM equations can be written by expanding the  $\mathcal{L}_m$  in the normal evolution equations in section 2.1.4 for  $\mathcal{K}$  and  $\gamma$ . The ADM equations are,

$$\partial_t \mathcal{K}_{ij} = \mathcal{L}_\beta \mathcal{K}_{ij} - \mathcal{D}_j \mathcal{D}_i \alpha + \alpha [\mathcal{R}_{ij} + \mathcal{K} \mathcal{K}_{ij} - 2\mathcal{K}_i^k \mathcal{K}_{kj} + 4\pi [\gamma_{ij} (\mathcal{S} - \mathcal{E}) - 2\mathcal{S}_{ij}]], \quad (2.1.71)$$

$$\partial_t \gamma_{ij} = \mathcal{L}_\beta \gamma_{ij} - 2\alpha \mathcal{K}_{ij}. \quad (2.1.72)$$

Unfortunately, these PDE's turn out to be ill-posed [REF]; this means that the time evolution of these equations does not depend smoothly on the initial data. The ill-posedness of the ADM equations is resolved in the next section.

### 2.1.7 BSSN

To tackle the ill-posedness of the ADM equations in section 2.1.6 the Baumgarte-Shapiro-Shibata-Nakamura (BSSN) formalism [REF] is introduced. The first step in BSSN is to decompose the 3-metric into the conformal metric  $\tilde{\gamma}_{ij}$  and the conformal factor  $\chi$ ,

$$\tilde{\gamma}_{ij} = \chi \gamma_{ij}, \quad (2.1.73)$$

$$\det\{\tilde{\gamma}_{ij}\} = \tilde{\gamma} = \chi^3 \gamma = 1, \quad (2.1.74)$$

with the above being the convention used in GRChombo described in [REF]. Other conventions include factors such as  $\tilde{\gamma}_{ij} = \psi^{-4} \gamma_{ij}$  or  $e^{-\phi} \gamma_{ij}$ . Along with this the extrinsic curvature  $\mathcal{K}_{ij}$  is modified to be trace free,

$$\tilde{A}_{ij} = \chi \left[ \mathcal{K}_{ij} - \frac{1}{3} \mathcal{K} \gamma_{ij} \right], \quad (2.1.75)$$

so that  $\tilde{A}_{ij} \gamma^{ij} = 0$ . During an evolution the conditions  $\text{tr} \tilde{A}_{ij} = 0$  and  $\tilde{\gamma} = 1$  are enforced which are observed to improve numerical stability; however it is unclear why beyond heuristic arguments. The

definition of  $\chi = \gamma^{-1/3}$  is good for black hole simulations where  $\gamma \rightarrow \infty$  but  $\chi \rightarrow 0$ ; for example the isotropic schwarzschild metric has

$$\gamma = \left[1 + \frac{M}{2r}\right]^{12}, \quad (2.1.76)$$

$$\chi = \left[\frac{r}{\frac{M}{2} + r}\right]^4. \quad (2.1.77)$$

The next step is to introduce the conformal connection functions as auxiliary variables,

$$\tilde{\Upsilon}^i = \tilde{\gamma}^{jk} \tilde{\Upsilon}_{jk}^i = -\partial_i \tilde{\gamma}^{ij}, \quad (2.1.78)$$

$$\tilde{\Upsilon}_{jk}^i = \frac{1}{2} \tilde{\gamma}^{il} [\partial_j \tilde{\gamma}_{kl} + \partial_k \tilde{\gamma}_{lj} - \partial_l \tilde{\gamma}_{jk}] = \Upsilon_{jk}^i + \left[ \delta_j^i \partial_k + \delta_k^i \partial_j - \gamma^{il} \gamma_{jk} \partial_l \right] \ln \sqrt{\chi}. \quad (2.1.79)$$

This reduces the set of vacuum evolution variables to  $\{\chi, \tilde{\gamma}_{ij}, \mathcal{K}, \tilde{\mathcal{A}}_{ij}, \tilde{\Upsilon}^i\}$ . It is conventional to use  $-\partial_i \tilde{\gamma}^{ij}$  to evaluate the conformal connection coefficients when they appear in the RHS of an equation, but  $\partial_j \tilde{\Upsilon}^i$  is calculated by differentiating the evolution variable  $\tilde{\Upsilon}^i$ . One final necessity, not included in the CCZ4 formulation discussed later, is to add multiples of the constraint equations (in section 2.1.4) to the evolution equations to change the characteristic matrix and improve stability.

The BSSN formalism is not the only way to find a well-posed set of evolution equations for general relativity. Another strongly hyperbolic formalism is the generalised harmonic gauge [?] with,

$$\square x^\mu = H^\mu, \quad (2.1.80)$$

for some functions  $H^\mu$ .

### 2.1.8 Z4 Formalism

The Z4 formalism [?] generalises the Einstein equation to include an unphysical field  $Z_\mu$ , along with damping terms parameterised by  $\kappa_1, \kappa_2$ ,

$$R_{\mu\nu} + \nabla_\mu Z_\nu + \nabla_\nu Z_\mu - \kappa_1 [n_\mu Z_\nu + n_\nu Z_\mu - [1 + \kappa_2] g_{\mu\nu} n^\alpha Z_\alpha] = 8\pi G \left[ T_{\mu\nu} - \frac{1}{2} T g_{\mu\nu} \right]. \quad (2.1.81)$$

Of course regular General Relativity is returned setting  $Z_\mu = 0$ . It is shown in [] that achieving  $Z_\mu = 0$  whilst dynamically evolving  $Z_\mu$  is equivalent to solving the constraints.  $Z_\mu$  is subjected to a wave equation, transporting constraint violation off the computational domain. It can be shown that the system is driven to  $Z_\mu = 0$  for  $k_1 > 0$  and  $k_2 < -1$ . It is much cheaper to evolve the variables  $Z_\mu$ , driven to zero, than do perform four elliptic solves for the constraints  $\{\mathcal{H}, \mathcal{M}^i\}$  on each timestep.

### 2.1.9 CCZ4

Joining BSSN with Z4 gives the CCZ4 formalism. The additional modifications,

$$\Theta = -n \cdot Z = -\alpha Z^0, \quad (2.1.82)$$

$$\hat{\Upsilon}^i = \tilde{\Upsilon}^i + \frac{2\gamma^{ij} Z_j}{\chi}, \quad (2.1.83)$$

are made, leaving us with the following set of vacuum evolution variables  $\{\chi, \tilde{\gamma}_{ij}, \mathcal{K}, \tilde{\mathcal{A}}_{ij}, \hat{\Upsilon}^i, \Theta\}$ . Notably the pair of variables  $\mathcal{R}_{ij} + \mathcal{D}_{(i} Z_{j)}$ , and traced version  $\mathcal{R} + \mathcal{D} \cdot \mathbf{Z}$ , always appear together; separately they ruin strong hyperbolicity but together they do not. The evolution equations can now be found in the CCZ4 scheme by doing a 3+1 decomposition of the Z4 modified Einstein equation in Eq. (2.1.81)

and following the BSSN formalism. To illustrate this, the equation of motion for  $\chi$  is derived. Using Eqs. (1.3.122) and (2.1.56) with  $\chi^{-3} = \gamma$ ,

$$\mathcal{L}_m \gamma = \gamma \gamma^{ij} \mathcal{L}_m \gamma_{ij} = -2\gamma \alpha \gamma^{ij} \mathcal{K}_{ij} = -2\gamma \alpha \mathcal{K}. \quad (2.1.84)$$

This can be used to simplify the Lie derivative of  $\chi$ ,

$$\mathcal{L}_m \chi = \mathcal{L}_{\partial_t} \chi - \mathcal{L}_\beta \chi, \quad (2.1.85)$$

$$= (\partial_t)^i \partial_i \chi + \omega \chi \partial_i (\partial_t)^i - \beta^i \partial_i \chi - \omega \chi \partial_i \beta^i, \quad (2.1.86)$$

$$= \partial_t \chi - \beta^i \partial_i \chi + \frac{2}{3} \chi \partial_i \beta^i, \quad (2.1.87)$$

$$\mathcal{L}_m \chi = \mathcal{L}_m \gamma^{-\frac{1}{3}}, \quad (2.1.88)$$

$$= -\frac{1}{3} \gamma^{-\frac{4}{3}} \mathcal{L}_m \gamma, \quad (2.1.89)$$

$$= \frac{2}{3} \gamma^{-\frac{1}{3}} \alpha \mathcal{K}, \quad (2.1.90)$$

$$= \frac{2}{3} \chi \gamma \alpha \mathcal{K}, \quad (2.1.91)$$

where  $\omega = -2/3$  is the weight of  $\chi$ . The equation for the lie derivative for a tensor density  $\mathcal{T}$  of weight  $w$ ,

$$\mathcal{L}_\xi \mathcal{T} = \tilde{\mathcal{L}}_\xi \mathcal{T} + w \mathcal{T} \partial_\mu \xi^\mu, \quad (2.1.92)$$

given in Eq. 1.3.31 was used where  $\tilde{\mathcal{L}}_\chi$  represents the differential operator that is equivalent to  $\mathcal{L}_\chi$  if it didn't act on a tensor density. Finally, rearranging gives the equation of motion for  $\chi$ ,

$$\partial_t \chi = \beta^k \partial_k \chi + \frac{2\chi}{3} [\alpha \mathcal{K} - \partial_k \beta^k]. \quad (2.1.93)$$

A similar process returns the CCZ4 equations but care should be taken to include the Z4 terms where they are needed. The complete list of CCZ4 equations used in simulations with GRChombo [REF] are given below.

$$\partial_t \chi = \beta^k \partial_k \chi + \frac{2\chi}{3} [\alpha \mathcal{K} - \partial_k \beta^k] \quad (2.1.94)$$

$$\partial_t \tilde{\gamma}_{ij} = \beta^k \partial_k \tilde{\gamma}_{ij} + \tilde{\gamma}_{kj} \partial_i \beta^k + \tilde{\gamma}_{ik} \partial_j \beta^k - \frac{2}{3} \tilde{\gamma}_{ij} \partial_k \beta^k - 2\alpha \tilde{\mathcal{A}}_{ij} \quad (2.1.95)$$

$$\begin{aligned} \partial_t \mathcal{K} = & \beta^k \partial_k \mathcal{K} + \alpha [\mathcal{R} + 2\mathcal{D} \cdot \mathbf{Z} + \mathcal{K} [\mathcal{K} - 2\Theta]] - 3\alpha \kappa_1 [1 + \kappa_2] \Theta \\ & - \chi \tilde{\gamma}^{kl} \mathcal{D}_k \mathcal{D}_l \alpha + 4\pi G \alpha [\mathcal{S} - 3\mathcal{E}] \end{aligned} \quad (2.1.96)$$

$$\begin{aligned} \partial_t \tilde{\mathcal{A}}_{ij} = & \beta^k \partial_k \tilde{\mathcal{A}}_{ij} + \chi \left[ \alpha [\mathcal{R}_{ij} + 2\mathcal{D}_{(i} Z_{j)} - 8\pi G \mathcal{S}_{ij}] - \mathcal{D}_i \mathcal{D}_j \alpha \right]^{TF} \\ & + \tilde{\mathcal{A}}_{ij} \left[ \alpha [\mathcal{K} - 2\Theta] - \frac{2}{3} \mathcal{K}^2 \right] + 2\tilde{\mathcal{A}}_{k(i} \partial_{j)} \beta^k - 2\alpha \tilde{\gamma}^{kl} \tilde{\mathcal{A}}_{ik} \tilde{\mathcal{A}}_{lj} \end{aligned} \quad (2.1.97)$$

$$\partial_t \Theta = \beta^k \partial_k \Theta + \frac{1}{2} \alpha \left[ \mathcal{R} + 2\mathcal{D} \cdot \mathbf{Z} - \tilde{\mathcal{A}}_{kl} \tilde{\mathcal{A}}^{kl} + \frac{2}{3} \mathcal{K}^2 - 2\Theta \mathcal{K} \right] - \kappa_1 \alpha \Theta [2 + \kappa_2] - Z^k \partial_k \alpha - 8\pi G \alpha \mathcal{E} \quad (2.1.98)$$

$$\begin{aligned} \partial_t \hat{\Upsilon}^i = & \beta^k \partial_k \hat{\Upsilon}^i + \frac{2}{3} \left[ \partial_k \beta^k \left[ \hat{\Upsilon}^i + 2\kappa_3 \frac{Z^i}{\chi} \right] - 2\alpha \mathcal{K} \frac{Z^i}{\chi} \right] - 2\alpha \kappa_1 \frac{Z^i}{\chi} \\ & + 2\tilde{\gamma}^{ij} [\alpha \partial_j \Theta - \Theta \partial_j \alpha] - 2\tilde{\mathcal{A}}^{ij} \partial_j \alpha - \alpha \left[ \frac{4}{3} \tilde{\gamma}^{ij} \partial_j \mathcal{K} + 3\tilde{\mathcal{A}}^{ij} \frac{\partial_j \chi}{\chi} \right] \\ & - \left[ \hat{\Upsilon}^j + 2\kappa_3 \frac{Z^j}{\chi} \right] \partial_j \beta^i + 2\alpha \hat{\Upsilon}^i_{jk} \tilde{\mathcal{A}}^{jk} + \tilde{\gamma}^{jk} \partial_j \partial_k \beta^i + \frac{1}{3} \tilde{\gamma}^{ij} \partial_k \partial_j \beta^k - 16\pi G \alpha \tilde{\gamma}^{ij} \mathcal{S}_j \end{aligned} \quad (2.1.99)$$

$$\partial_t \varphi = \beta^k \partial_k \varphi - \alpha \Pi \quad (2.1.100)$$

$$\partial_t \Pi = \beta^k \partial_k \Pi - \chi \tilde{\gamma}^{ij} \partial_i \varphi \partial_j \alpha + \alpha \left[ \chi \tilde{\Upsilon}^k \partial_k \varphi + \frac{1}{2} \tilde{\gamma}^{lk} \partial_k \chi \partial_l \varphi - \chi \tilde{\gamma}^{ij} \partial_i \partial_j \varphi + \mathcal{K} \Pi + V' \varphi \right] \quad (2.1.101)$$

Note that Eqs. (2.1.100) and (2.1.101) are for the 3+1 Klein-Gordon equation which will be derived later in section 2.2.3. Also to be noted, in the CCZ4 equations there is an additional parameter  $\kappa_3$  premultiplying terms in the evolution of  $\hat{\Upsilon}^i$  which experimentally were found to ruin numerical stability for black hole simulations []. Setting  $\kappa_3 < 1$  stabilises the simulation but at the cost of covariance. Later on it was realised that setting  $\kappa_3 = 1$  and  $\alpha\kappa_1 \rightarrow \kappa_1$  retains covariance as well as numerical stability [REF].

The CCZ4 scheme proves useful in my simulations for a few reason. Firstly, any initial data that does not satisfy the constraints will not do so along evolution either when using BSSN. Given that superposition of solutions in GR does not generally give a new solution, but does approximate one for separated compact objects, all the simulated binaries considered in the report will have non constraint satisfying initial data. The use of the CCZ4 scheme will also help simulations satisfy the constraints even if they initially satisfy them; one reason being that finite resolution imposes some small deviation from the continuum solution. More importantly, the use of adaptive mesh refinement AMR introduces large interpolation errors into the simulation at the boundary of the different grid resolution levels. Finally, the Sommerfeld boundary conditions used are inexact in GR and will introduce small errors at the boundary that ruin constraint satisfaction. In all above cases, the CCZ4 system forces the evolution towards constraint satisfaction, despite the numerical errors and approximations.

### 2.1.10 Gauge Conditions

In GR, the lapse  $\alpha$  and shift  $\beta^i$  are freely specifiable being gauge variables, however they must be chosen carefully along with a suitable initial Cauchy surface  $\Sigma_{t_0}$  for sensible foliations and numerical accuracy. Figure 2.1 (left) shows how a poor initial Cauchy surface could extend to the singularity for ingoing Eddington-Finkelstein coordinates; likely causing a simulation crash. In this work  $\Sigma_{t_0}$  is chosen to be in the isotropic gauge as in figure 2.1 (right); not only does this allow trivial swapping between spherical polar and Cartesian (used in the simulation) coordinates but also provides an initial Cauchy surface free of singularities and easy to compute. For a poor choice of lapse function, even a well chosen  $\Sigma_{t_0}$  can advance to the singularity in finite simulation time.

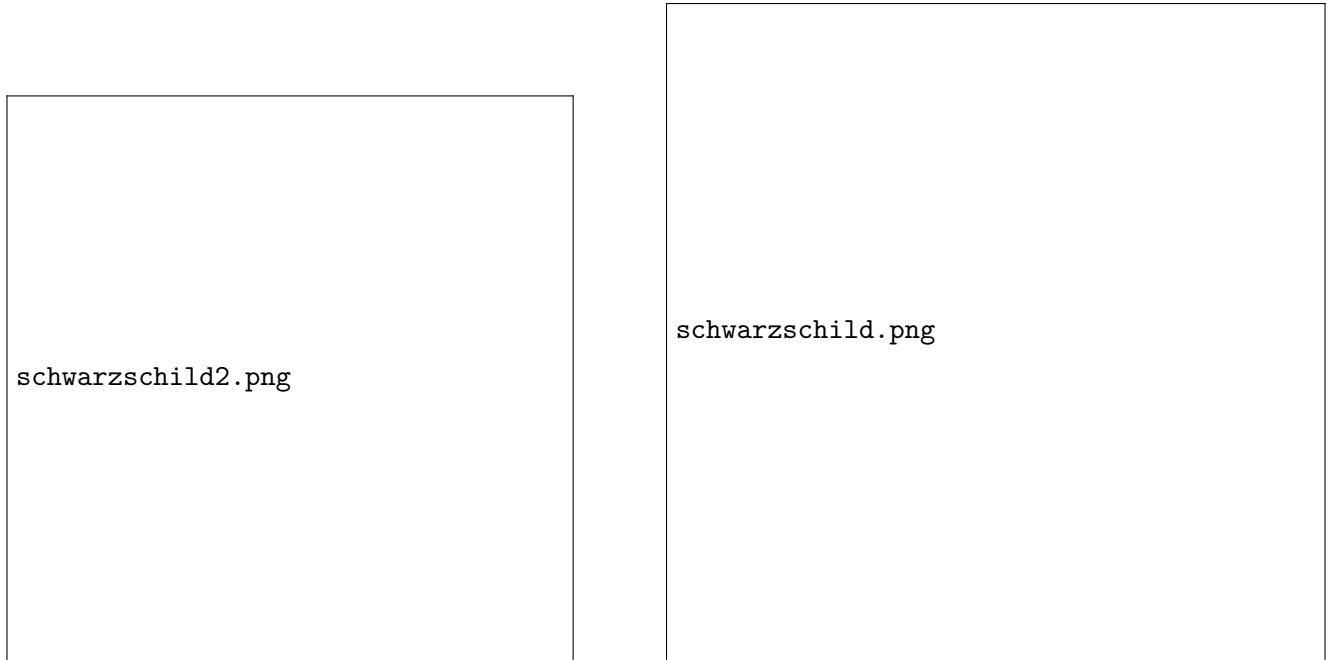


Figure 2.1: Penrose Diagrams,  $\Sigma_{t_0}$  dashed, Left: Ingoing Eddington-Finkelstein Coordinates, Right: Isotropic Coordinates.

## Lapse Gauge Conditions

The simplest lapse choice would be to enforce  $\alpha = 1$ , called geodesic slicing, with the hypersurface following integral curves of  $n^\mu$ ; given that geodesics can converge this can lead to hypersurface self-intersection which breaks the definition of a Cauchy surface and the simulation will likely fail. Another problem is that a black hole singularity can be reached in finite simulation time. Geodesic slicing can be modified to the maximal slicing condition which keeps the volume element  $\sqrt{-g}$  constant along geodesics. This means as  $\gamma \rightarrow \infty$  nearing a singularity  $\alpha \rightarrow 0$  from Eq. (2.1.68), causing the hypersurface to advance more slowly before a singularity is reached. This property is called singularity avoiding and is crucial for numerical stability (unless using excision?). Maximal slicing can be implemented by forcing  $\mathcal{K} = \partial_t \mathcal{K} = 0 \forall t$  which requires a slow elliptic solve for  $\alpha$  at each timestep. Instead  $\alpha$  is promoted to an evolution variable and is evolved along with every other simulation variable. To do this we can pick an algebraic slicing condition of the Bona-Masso type,

$$\mathcal{L}_m \alpha = \partial_t \alpha - \beta^i \partial_i \alpha = -\alpha^2 f(\alpha) \mathcal{K}. \quad (2.1.102)$$

This is used with  $f = 2\alpha^{-1}$  in GRChombo [REF] giving,

$$\mathcal{L}_m \alpha = -2\alpha \mathcal{K}, \quad (2.1.103)$$

and using gaussian normal coordinates  $\beta^i = 0$  it reduces to,

$$\alpha = 1 + \ln \gamma, \quad (2.1.104)$$

which is called 1+log slicing; this is very common in Numerical Relativity codes. In practice 1+log slicing is strongly singularity avoiding reaching  $\alpha = 0$  before the singularity. This is modified in the CCZ4 scheme to,

$$\partial_t \alpha = -2\alpha [\mathcal{K} - 2\Theta] + \beta^i \partial_i \alpha, \quad (2.1.105)$$

which is very similar to before; it should be noted that the advection term is important for black hole simulations.

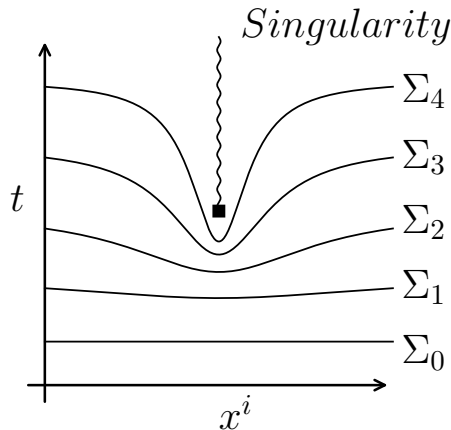


Figure 2.2: Diagram showing the time evolution of a hypersurface using a singularity avoiding lapse gauge condition. The vertical squiggled line represents a physical singularity that is formed at some point in spacetime, potentially from the collapse of matter to a black hole.

## Shift Gauge Conditions

So far the shift vector  $\beta^i$  has been ignored, the simplest choice for it would be  $\beta^i = 0$  as in 1+log slicing. Using 1+log slicing causes great stretching and shearing of  $\Sigma_t$  in the neighbourhood of a singularity as in Fig. (2.2); the effect of this is that neighbouring gridpoints have large differences in field values leading to inaccurate and unstable evolutions. Another negative side effect is that the computational domain can fall inside an event horizon in black hole simulations. To counteract this we want to pick a shift vector that minimises hypersurface shear  $\sigma_{ij}$  which can be defined as [REF] [ref 1977 smarr and york],

$$\sigma_{ij} := \perp_i^\mu \perp_j^\nu \left[ \nabla_{(\mu} n_{\nu)} - \frac{1}{3} \gamma^{ab} \nabla_{(a} n_{b)} \gamma_{\mu\nu} \right], \quad (2.1.106)$$

where  $\sigma_{ij}$  is tracefree corresponding to shearing rather than inflation or expansion. Minimising the total shear  $\Sigma$ ,

$$\Sigma = \int \sigma_{ij} \sigma^{ij} \sqrt{\gamma} dx^3, \quad (2.1.107)$$

with respect to  $\beta^i$  leads to an elliptic PDE to be solved for each  $\beta^i$  at each time step that minimises shear,

$$\delta \Sigma = 0 \rightarrow \mathcal{D}_i \sigma^{ij} = 0. \quad (2.1.108)$$

This is known as the minimal shift condition. As before, promoting  $\beta^i$  to be evolution variables is computationally cheaper than solving a set of PDE's at each time step. A very common choice is to promote the elliptic PDE for  $\beta^i$  into a hyperbolic equation via introducing a  $\partial_t^2 \beta^i$  term and an artificial damping term parameterised by  $\eta$ . This becomes a damped wave equation and is supposed to transport away any part of  $\beta^i$  which does not satisfy  $\mathcal{D}_i \sigma^{ij} = 0$ . This requires Sommerfeld (outgoing wave) boundary conditions as in [REF]. In GRChombo the standard gamma driver shift condition is used,

$$\partial_t \beta^i = F B^i, \quad (2.1.109)$$

$$\partial_t B^i = \partial_t \tilde{\Gamma}^i - \eta B^i, \quad (2.1.110)$$

where  $F = 3/4$  and  $\eta = 1$  are used.

### 2.1.11 stuff

FIX THE FUCKING HAND REFERNECES!

## 2.2 Mathematical Modelling of Boson Stars

### 2.2.1 Action

The Boson Stars considered are a complex Klein Gordon Scalar field,  $\varphi$ , minimally coupled to gravity. The action is the Einstein-Hilbert vacuum action plus the matter action for curved space,

$$S = \int_{\mathcal{M}} [\mathcal{L}_{EH} + \mathcal{L}_M] \sqrt{-g} dx^4, \quad (2.2.1)$$

$$\mathcal{L}_{EH} = \frac{1}{16\pi G} R, \quad (2.2.2)$$

$$\mathcal{L}_M = -\frac{1}{2} g^{\mu\nu} \nabla_\mu \varphi^* \nabla_\nu \varphi - \frac{1}{2} V(|\varphi|^2), \quad (2.2.3)$$

Here  $V$  is the Klein-Gordon potential and it's effect on boson stars is discussed in [1]. Some common choices of potentials are,

$$V = \frac{m^2 c^2}{\hbar^2} |\varphi|^2, \quad (2.2.4)$$

$$V = \frac{m^2 c^2}{\hbar^2} |\varphi|^2 + \frac{1}{2} \Lambda_4 |\varphi|^4, \quad (2.2.5)$$

$$V = \frac{m^2 c^2}{\hbar^2} |\varphi|^2 \left( 1 - \frac{|\varphi|^2}{2\sigma^2} \right)^2, \quad (2.2.6)$$

where  $\hbar$  and  $c$  are given for completeness but will be set to unity from now on. Considering only the  $m^2$  term, which corresponds to the squared mass of the particle in the quantum theory, we get a massive wave equation linear in  $\varphi$ , leading to so called mini Boson stars. Having  $\Lambda_4 \neq 0$  gives self-interacting stars which have a nonlinear wave equation corresponding to particle creation and annihilation at the quantum level; self interacting potentials can include higher order terms in  $\varphi$  such as  $|\varphi|^6$ ,  $|\varphi|^8$  and more. These self interacting potentials tend to have star solutions with a higher density. Finally, Eq. (2.2.6) describes the solitonic potential, giving rise to boson stars with compactnesses comparable to neutron stars.

Varying the action with respect to the metric and scalar field return the Einstein Field equations and the Klein Gordon equation of curved space respectively,

$$R_{\mu\nu} - \frac{1}{2} R g_{\mu\nu} = \frac{8\pi G}{c^4} T_{\mu\nu}, \quad (2.2.7)$$

$$g^{\mu\nu} \nabla_\mu \nabla_\nu \varphi = \frac{\partial V}{\partial |\varphi|^2} \varphi. \quad (2.2.8)$$

Collectively these are known as the Einstein-Klein-Gordon (EKG) equations. From Eq. (1.4.73), the boson-specific stress energy tensors are,

$$T_{\mu\nu} := -2 \frac{\delta \mathcal{L}_M}{\delta g^{\mu\nu}} + g_{\mu\nu} \mathcal{L}_M, \quad (2.2.9)$$

$$T_{\mu\nu} = \frac{1}{2} \nabla_\mu \varphi^* \nabla_\nu \varphi + \frac{1}{2} \nabla_\nu \varphi^* \nabla_\mu \varphi - \frac{1}{2} g_{\mu\nu} \left[ g^{\alpha\beta} \nabla_\alpha \varphi^* \nabla_\beta \varphi + V \right]. \quad (2.2.10)$$

Studying neutron stars requires the fermionic, or ordinary fluid, stress tensor  $\mathbf{T}_F$ ;

$$T_F^{\mu\nu} = \left[ \rho c^2 + P \right] \frac{u^\mu u^\nu}{c^2} + P g^{\mu\nu} + 2u^{(\mu} q^{\nu)} + \pi^{\mu\nu} + \dots \quad (2.2.11)$$

The continuity equation from Eq. (1.4.26),  $\nabla_\nu T^{\mu\nu} = 0$ , returns the highly nonlinear relativistic Navier-Stokes equations of curved space. The viscosity term  $\pi^{\mu\nu}$  and heat flux  $q^\mu$  are often omitted for simplicity. The remaining variables  $\rho$ ,  $P$  and  $u^\mu$  are the fluid density, pressure and worldline tangent. Just as in flat space, the Navier-Stokes equations can develop shockwaves and the use of sophisticated shock capturing schemes is required, unlike the linear Klein-Gordon equation which is linear in the principal part.



### 2.2.2 Solitons

A soliton is a wave that exhibits particle-like behaviour. More precisely, in classical field theory, a soliton is a field or set of fields in a localised configuration that can travel at constant speed but not disperse. For our purposes, we look for solitons in the Einstein-Klein-Gordon (EKG) system which are self gravitating localised scalar field and metric configurations. In the case of the real scalar field it was shown by [REF] that there are no long lived stars; however promoting the field to a complex scalar we can find a spherically symmetric stationary soliton with the following scalar field,

$$\varphi = \Phi(r)e^{i\omega t}, \quad (2.2.12)$$

in spherical polar coordinates  $x^\mu \in \{t, r, \theta, \phi\}$ . Traditionally, the polar areal gauge has been used for the metric's ansatz,

$$g_{\mu\nu}dx^\mu dx^\nu = -a^2(r)dt^2 + b^2(r)dr^2 + r^2 [d\theta^2 + \sin^2\theta d\phi^2], \quad (2.2.13)$$

where the boundary condition  $b^2(0) = 1$  is demanded to avoid a conical singularity at the origin. However an isotropic gauge is more useful for simulations due to easier conversion to cartesian space-coordinates, for more information on isotropic coordinates see section 1.4.6. The polar areal solution must then be transformed into an isotropic solution. Alternatively, the approach taken in this report, is to start with an isotropic ansatz,

$$g_{\mu\nu}dx^\mu dx^\nu = -\Omega^2(r)dt^2 + \Psi^2(r)d\mathbf{x}^2, \quad (2.2.14)$$

where  $d\mathbf{x}^2$  denotes the euclidean 3D line element; this changes between spherical polar or cartesian coordinates trivially. This ends up being slightly harder to solve for numerically, but no conversion to isotropic coordinates is needed afterwards.

To get a set of ODE's to solve for the functions  $\{\Omega(r), \Psi(r), \Phi(r)\}$  we must turn to the Einstein Equation and Klein Gordon Equation. The Einstein Equations for  $\{\mu, \nu\} = \{0, 0\}, \{1, 1\}, \{2, 2\}$  are the only components that give unique non-zero equations in spherical symmetry; they are,

$$\frac{\Omega^2 [r\Psi'^2 - 2\Psi [r\Psi'' + 2\Psi']]}{r\Psi^4} = 4\pi G \left[ \Omega^2 \left[ \frac{P'^2}{\Psi^2} + V \right] + \omega^2 P^2 \right], \quad (2.2.15)$$

$$\frac{2\Psi\Psi' [r\Omega' + \Omega] + r\Omega\Psi'^2 + 2\Psi^2\Omega'}{r\Psi^2\Omega} = 4\pi G \left[ P'^2 - \Psi^2 V + \frac{\omega^2 P^2 \Psi^2}{\Omega^2} \right], \quad (2.2.16)$$

$$r \left[ -\frac{r\Psi'^2}{\Psi^2} + \frac{r\Psi'' + \Psi'}{\Psi} + \frac{r\Omega'' + \Omega'}{\Omega} \right] = -4\pi G r^2 \Psi^2 \left[ \frac{P'^2}{\Psi^2} + V - \frac{\omega^2 P^2}{\Omega^2} \right]. \quad (2.2.17)$$

The Einstein tensor  $G_{\mu\nu} = R_{\mu\nu} - \frac{1}{2}Rg_{\mu\nu}$  (left above) and the stress tensor  $T_{\mu\nu}$  (right above) were obtained with a private, self written Mathematica notebook. Substituting the metric ansatz Eq. (2.2.14) and the field ansatz Eq. (2.2.12) into Eq. (2.2.8), the Klein Gordon equation becomes,

$$g^{\mu\nu}\nabla_\mu\nabla_\nu\varphi = \frac{\partial V}{\partial|\varphi|^2}\varphi, \quad (2.2.18)$$

$$\frac{1}{\sqrt{-g}}\partial_\mu \left[ \sqrt{-g}g^{\mu\nu}\partial_\nu\Phi(r)e^{i\omega t} \right] = \frac{\partial V}{\partial|\varphi|^2}\Phi(r)e^{i\omega t}, \quad (2.2.19)$$

$$\Phi'' = \Phi\Psi^2 \left[ V' - \frac{\omega^2}{\Omega^2} \right] - \Phi' \left[ \frac{\Omega'}{\Omega} + \frac{\Psi'}{\Psi} + \frac{2}{r} \right]. \quad (2.2.20)$$

Simplifying the Einstein Equations and combining with the Klein Gordon equation we get three ODE's

to solve; the EKG system has been reduced to two second order ODE's and a first order ODE,

$$\Omega' = \frac{\Omega}{r\Psi' + \Psi} \left[ 2\pi Gr\Psi \left[ \Phi'^2 - \Psi^2 V + \frac{\omega^2 \Phi^2 \Psi^2}{\Omega^2} \right] - \Psi' - \frac{r\Psi'^2}{2\Psi} \right], \quad (2.2.21)$$

$$\Psi'' = \frac{\Psi'^2}{2\Psi} - \frac{2\Psi'}{r} - 2\pi G \left[ V\Psi^3 + \Phi'^2\Psi + \frac{\omega^2 \Phi^2 \Psi^3}{\Omega^2} \right], \quad (2.2.22)$$

$$\Phi'' = \Phi\Psi^2 \left[ V' - \frac{\omega^2}{\Omega^2} \right] - \Phi' \left[ \frac{\Omega'}{\Omega} + \frac{\Psi'}{\Psi} + \frac{2}{r} \right]. \quad (2.2.23)$$

This is turned into a set of five first order ODE's to numerically integrate from  $r = 0$  out to large radius. Note that if we had used the polar areal ansatz in Eq. (2.2.13) the equation for  $\Phi$  would also be first order; reducing the EKG system to four first order ODE's.

### 2.2.3 3+1 Klein Gordon System

Now let's project the Klein Gordon equation in a 3+1 split to get the evolution equations. The first step is to turn the second order Klein-Gordon equation into two first order ones

$$\mathcal{L}_m \varphi = \dots, \quad (2.2.24)$$

$$\mathcal{L}_m \Pi = \dots, \quad (2.2.25)$$

where  $\Pi$  is the foliation dependant definition of conjugate momentum to the complex scalar field,

$$\Pi := -\mathcal{L}_n \varphi. \quad (2.2.26)$$

Decomposing the Klein Gordon Equation,

$$\nabla^\mu \nabla_\mu \varphi = V' \varphi = \frac{1}{\sqrt{-g}} \partial_\mu [\sqrt{-g} [\gamma^{\mu\nu} - n^\mu n^\nu] \partial_\nu \varphi] = \frac{1}{\sqrt{-g}} \partial_\mu [\sqrt{-g} [\mathcal{D}^\mu \varphi - n^\mu \mathcal{L}_n \varphi]]. \quad (2.2.27)$$

The term with  $\mathcal{D}^\mu$  simplifies like,

$$\frac{1}{\sqrt{-g}} \partial_\mu [\sqrt{-g} \mathcal{D}^\mu \varphi] = \frac{1}{\alpha \sqrt{\gamma}} \partial_\mu [\alpha \sqrt{\gamma} \mathcal{D}^\mu \varphi] = \mathcal{D}_\mu \mathcal{D}^\mu \varphi + \mathcal{D}^\mu \varphi \partial_\mu \ln \alpha, \quad (2.2.28)$$

and the remainder becomes,

$$-\frac{1}{\sqrt{-g}} \partial_\mu [\sqrt{-g} n^\mu \mathcal{L}_n \varphi] = -[\nabla \cdot n + n \cdot \partial] \mathcal{L}_n \varphi = -\mathcal{K} \Pi + \mathcal{L}_n \Pi. \quad (2.2.29)$$

Combining these results, the full Klein Gordon system is constructed,

$$\mathcal{L}_m \Pi = -\mathcal{D}^\mu \varphi \partial_\mu \alpha + \alpha [\mathcal{K} \Pi - \mathcal{D}_\mu \mathcal{D}^\mu \varphi + V' \varphi], \quad (2.2.30)$$

$$\mathcal{L}_m \varphi = -\alpha \Pi. \quad (2.2.31)$$

The final matter term we must decompose is the Klein-Gordon stress tensor in Eq. (2.2.10) with Eqs. (2.1.45), (2.1.46) and (2.1.47).

$$\rho = n^\mu n^\nu T_{\mu\nu} = \frac{1}{2} |\Pi|^2 + \frac{1}{2} \gamma^{ij} \mathcal{D}_i \varphi^* \mathcal{D}_j \varphi + \frac{1}{2} V(|\varphi|^2), \quad (2.2.32)$$

$$S_i = -\perp_i^\mu n^\nu T_{\mu\nu} = \frac{1}{2} [\Pi^* \mathcal{D}_i \varphi + \Pi \mathcal{D}_i \varphi^*], \quad (2.2.33)$$

$$S_{ij} = \perp_i^\mu \perp_j^\nu T_{\mu\nu} = \mathcal{D}_{(i} \varphi \mathcal{D}_{j)} \varphi^* - \frac{1}{2} [\gamma^{ij} \mathcal{D}_i \varphi \mathcal{D}_j \varphi^* - |\Pi|^2 + V(|\varphi|^2)]. \quad (2.2.34)$$

### 2.2.4 Klein Gordon's Noether Charge

For the complex scalar field, we have the U(1) symmetry,

$$\varphi \rightarrow \varphi e^{i\epsilon} \approx \varphi + i\epsilon\varphi, \quad (2.2.35)$$

$$\varphi^* \rightarrow \varphi^* e^{-i\epsilon} \approx \varphi^* - i\epsilon\varphi^*, \quad (2.2.36)$$

which leaves the Lagrangian unchanged and therefore the total action. The associated conserved current  $j$  and current density  $\mathcal{J}$  are then,

$$j^\mu = \frac{\delta\mathcal{L}}{\delta\nabla_\mu\varphi}\delta\varphi + \frac{\delta\mathcal{L}}{\delta\nabla_\mu\varphi^*}\delta\varphi^*, \quad (2.2.37)$$

$$j^\mu = ig^{\mu\nu} [\varphi\nabla_\nu\varphi^* - \varphi^*\nabla_\nu\varphi], \quad (2.2.38)$$

where the current satisfies the continuity equation,

$$\nabla_\mu j^\mu = 0. \quad (2.2.39)$$

Using Eq. (1.3.142), the continuity equation can be re-written as,

$$\nabla_\mu j^\mu = \frac{1}{\sqrt{-g}}\partial_\mu(\sqrt{-g}j^\mu) = \frac{1}{\sqrt{-g}}\partial_\mu\mathcal{J}^\mu = 0, \quad (2.2.40)$$

where  $\mathcal{J}^\mu = \sqrt{-g}j^\mu$  is the current expressed as a tensor density. Therefore,

$$\partial_\mu\mathcal{J}^\mu = 0, \quad (2.2.41)$$

is also true and even in curved space the current  $\mathcal{J}$  obeys a conservation equation; this means there must be some conserved charge  $\mathcal{Q}$  associated with the current. Integrating Eq. (2.2.41) over a manifold  $\mathcal{M}$  gives,

$$\int_{\mathcal{M}} \nabla_\mu j^\mu \sqrt{-g} \, dx^4 = 0, \quad (2.2.42)$$

$$\int_{\mathcal{M}} \partial_\mu [\sqrt{-g}j^\mu] \, dx^4 = 0, \quad (2.2.43)$$

$$\int_{\mathcal{M}} \partial_\mu \mathcal{J}^\mu \, dx^4 = 0, \quad (2.2.44)$$

$$\int_{t_0}^{t_1} \left[ \int_{\Sigma_t} \partial_0 \mathcal{J}^0 \, dx^3 \right] dt = - \int_{t_0}^{t_1} \left[ \int_{\Sigma_t} \partial_i \mathcal{J}^i \, dx^3 \right] dt, \quad (2.2.45)$$

$$\int_{t_0}^{t_1} \left[ \int_{\Sigma_t} \partial_0 \mathcal{J}^0 \, dx^3 \right] dt = - \int_{t_0}^{t_1} \left[ \int_{\partial\Sigma_t} \hat{s}_i \mathcal{J}^i \, dx^2 \right] dt, \quad (2.2.46)$$

$$\int_{t_0}^{t_1} \left[ \int_{\Sigma_t} \partial_0 \mathcal{J}^0 \, dx^3 \right] dt = 0, \quad (2.2.47)$$

where the flat space divergence theorem was used and  $\hat{s}$  is the flat space normal to  $\partial\Sigma_t$ , the boundary of  $\Sigma_t$ . The term containing  $\hat{s}_i \mathcal{J}^i$  integrates to zero over  $\partial\Sigma_t$  due to  $\mathcal{J}$  vanishing on  $\partial\Sigma_t$ . The  $\mathcal{J}^0$  term can be simplified by permuting the time derivative using,

$$\partial_0 \int_{\Sigma_t} \mathcal{J}^0 \, dx^3 = \int_{\Sigma_t} \partial_0 \mathcal{J}^0 \, dx^3 + \lim_{\Delta x^0 \rightarrow 0} \left[ \frac{1}{\Delta x^0} \int_{\Delta\Sigma_t} [\mathcal{J}^0 + \Delta x^0 \partial_0 \mathcal{J}^0] \, dx^3 \right], \quad (2.2.48)$$

where the last term vanishes as  $\mathcal{J}$  vanishes near  $\partial\Sigma$ , and Eq. (2.2.47) becomes,

$$\int_{t_0}^{t_1} \left[ \partial_0 \int_{\Sigma_t} \mathcal{J}^0 \, dx^3 \right] dt = 0, \quad (2.2.49)$$

and the formula for the conserved charge  $Q$  can be read off as,

$$\partial_0 Q = 0, \quad (2.2.50)$$

$$Q = \int_{\Sigma_t} \mathcal{J}^0 dx^3. \quad (2.2.51)$$

The charge density  $\mathcal{Q}$  is defined as,

$$Q := \int_{\Sigma_t} \mathcal{Q} \sqrt{\gamma} dx^3, \quad (2.2.52)$$

$$\mathcal{Q} = \frac{\mathcal{J}^0}{\sqrt{\gamma}} = \frac{\sqrt{-g} j^0}{\sqrt{\gamma}} = \alpha j^0, \quad (2.2.53)$$

where Eq. (2.1.68), saying  $\sqrt{-g} = \alpha\sqrt{\gamma}$ , was used. Finally we get an expression for the total Noether charge  $N = Q$ ,

$$N = i \int_{\Sigma_t} \sqrt{-g} [\varphi \nabla^0 \varphi^* - \varphi^* \nabla^0 \varphi] dx^3. \quad (2.2.54)$$

Using  $\sqrt{-g} = \alpha\sqrt{\gamma}$  again and  $\alpha \nabla^0 \varphi = -n_\mu \nabla^\mu \varphi = \Pi$  from Eq. (2.2.26) we get the following neat formula,

$$N = i \int_{\Sigma_t} [\varphi \Pi^* - \varphi^* \Pi] \sqrt{\gamma} dx^3. \quad (2.2.55)$$

Equivalently, the Noether charge density  $\mathcal{N}$  is ,

$$\mathcal{N} = i (\varphi \Pi^* - \varphi^* \Pi). \quad (2.2.56)$$

MAYBE POINT THIS SECTION AT THE CONTINUITY PAPER, OR JSUT SAY WE GENERALISE IT IN THERE?

THE IDEAS OF THIS SECTION ARE FURTHER EXPLORED FOR ENERGY, MOMENTUM, ANGULAR MOMENTUM AND PROCA FIELDS IN SECTION REFFF

### 2.2.5 Boosted Boson Stars and Black Holes

Let us now consider a moving star, this corresponds to boosting a stationary soliton solution. There is no unique way of doing this as any coordinate transformation that reduces to a Minkowski spacetime boost at large radius will do the job. All the degrees of freedom we have can be absorbed into a coordinate gauge choice, so it makes sense to choose the trivial, constant valued boost, with rapidity  $\chi = \text{arctanh}(v)$  for a velocity  $v$ , from Special Relativity. Using Cartesian coordinates, boost matrix  $\Lambda$  for a boost in the  $x$  direction is,

$$\Lambda_\nu^\mu = \exp \begin{pmatrix} 0 & -\chi & 0 & 0 \\ -\chi & 0 & 0 & 0 \\ 0 & 0 & 1 & 0 \\ 0 & 0 & 0 & 1 \end{pmatrix} = \begin{pmatrix} \cosh(\chi) & -\sinh(\chi) & 0 & 0 \\ -\sinh(\chi) & \cosh(\chi) & 0 & 0 \\ 0 & 0 & 1 & 0 \\ 0 & 0 & 0 & 1 \end{pmatrix}. \quad (2.2.57)$$

Declaring the boosted and rest frame to have coordinates  $x^\mu$  and  $\tilde{x}^\mu$ ,

$$\tilde{x}^\mu = [\Lambda^{-1}]^\mu_\nu x^\nu, \quad (2.2.58)$$

and the metric transforms via the tensor transformation law like,

$$\tilde{g}_{\mu\nu}(\tilde{x}^\sigma) = \frac{\partial x^\alpha}{\partial \tilde{x}^\mu} \frac{\partial x^\beta}{\partial \tilde{x}^\nu} g_{\alpha\beta}(\tilde{x}^\sigma) = \Lambda^\alpha_\mu \Lambda^\beta_\nu g_{\alpha\beta}(\tilde{x}^\sigma), \quad (2.2.59)$$

where the inverse boost matrix  $\Lambda^{-1}$  can be found simply by  $\Lambda^{-1}(\chi) = \Lambda(-\chi)$ . We choose the boosted soliton's initial Cauchy surface to be the level set of  $\tilde{t} = 0$ ; this corresponds to the star begin stationary in the boosted frame. The coordinates and metric transform as,

$$x^\mu = \{t, x, y, z\} = \{\tilde{t} \cosh(\chi) + \tilde{x} \sinh(\chi), \tilde{x} \cosh(\chi) + \tilde{t} \sinh(\chi), \tilde{y}, \tilde{z}\}, \quad (2.2.60)$$

$$g_{\mu\nu} = \text{diag}\{-\Omega^2, \Psi^2, \Psi^2, \Psi^2\}, \quad (2.2.61)$$

$$\tilde{g}_{\mu\nu} = \begin{pmatrix} -\Omega^2 \cosh^2(\chi) + \Psi^2 \sinh^2(\chi) & \sinh(\chi) \cosh(\chi) [\Omega^2 - \Psi^2] & 0 & 0 \\ \sinh(\chi) \cosh(\chi) [\Omega^2 - \Psi^2] & \Psi^2 \cosh^2(\chi) - \Omega^2 \sinh^2(\chi) & 0 & 0 \\ 0 & 0 & \Psi^2 & 0 \\ 0 & 0 & 0 & \Psi^2 \end{pmatrix}, \quad (2.2.62)$$

as the star is at rest using coordinates  $x^\mu$  rather than  $\tilde{x}^\mu$ . Comparing this boosted metric to the  $3+1$  decomposed metric in Eq. (2.1.65) we can read off the shift vector  $\tilde{\beta}_i$ , the 3 metric  $\tilde{\gamma}_{ij}$  and obtain the lapse and metric determinant,

$$\tilde{\alpha}^2 = \frac{\Psi^2 \Omega^2}{\Psi^2 \cosh^2(\chi) - \Omega^2 \sinh^2(\chi)}, \quad (2.2.63)$$

$$\tilde{\gamma} = \det \tilde{\gamma}_{ij} = \Psi^4 [\Psi^2 \cosh^2(\chi) - \Omega^2 \sinh^2(\chi)]. \quad (2.2.64)$$

Finally, the conformal 3-metric with unit determinant is,

$$\bar{\gamma}_{ij} = \tilde{\gamma}^{-\frac{1}{3}} \begin{pmatrix} \Psi^2 \cosh^2(\chi) - \Omega^2 \sinh^2(\chi) & 0 & 0 \\ 0 & \Psi^2 & 0 \\ 0 & 0 & \Psi^2 \end{pmatrix}, \quad (2.2.65)$$

where normally  $\tilde{\gamma}_{ij}$  is the conformal 3-metric, but to avoid confusion it is denoted  $\bar{\gamma}_{ij}$  in this section. Turning our attention to the matter fields now we only need to change the coordinate dependance, like  $\varphi(x) \rightarrow \varphi(\tilde{x})$ , given that  $\varphi$  and  $\Pi$  are (complex) scalar fields. Given that  $\tilde{t} = 0$  describes a time slice in the rest frame (where the star has non-zero velocity),  $t = \tilde{x} \sinh(\chi)$  in the rest frame and we get the following boosted complex scalar field,

$$\varphi = \Phi(r) e^{i\omega \tilde{x} \sinh(\chi)}, \quad (2.2.66)$$

where  $r$  is the radius in the boosted frame;  $r = \sqrt{\tilde{x}^2 \cosh^2(\chi) + \tilde{y}^2 + \tilde{z}^2}$ . Note the field is modulated by an oscillatory phase now with wavenumber  $k = \omega \tilde{x} \sinh(\chi)$ ; nodal planes in  $\text{Re}(\varphi)$  appear perpendicular to velocity. The conjugate momentum  $\tilde{\Pi}$ , defined in Eq. (2.2.26), in the rest frame it becomes,

$$\tilde{\Pi}(\tilde{x}^\mu) = -\mathcal{L}_{\tilde{n}} \varphi(\tilde{x}^\mu) = -\frac{1}{\tilde{\alpha}} \tilde{m} \cdot \tilde{\partial} \varphi = -\frac{1}{\tilde{\alpha}} [\tilde{\partial}_0 - \tilde{\beta}^i \tilde{\partial}_i] \Phi(r) e^{i\omega t}. \quad (2.2.67)$$

Inconveniently we cannot simply evaluate  $\tilde{\Pi}$  in the boosted frame as this has a different spacetime foliation and the normal vector  $\mathbf{n} \neq \tilde{\mathbf{n}}$  is genuinely changed; not just transforming components under coordinate transformation. Explicitly writing the contravariant components of the shift vector,

$$\tilde{\beta}^i = \left( \frac{\sinh(\chi) \cosh(\chi) [\Omega^2 - \Psi^2]}{\Psi^2 \cosh^2(\chi) - \Omega^2 \sinh^2(\chi)}, 0, 0 \right), \quad (2.2.68)$$

and using the following derivative formulae,

$$\partial_{\tilde{t}} = \cosh(\chi) \partial_t + \sinh(\chi) \partial_x, \quad (2.2.69)$$

$$\partial_{\tilde{x}} = \cosh(\chi) \partial_x + \sinh(\chi) \partial_t, \quad (2.2.70)$$

$$\partial_t \varphi = \Phi \partial_t e^{i\omega t} = i\omega \Phi e^{i\omega t}, \quad (2.2.71)$$

$$\partial_x \varphi = \frac{\partial r}{\partial x} \Phi' e^{i\omega t} = \frac{x}{r} \Phi' e^{i\omega t}, \quad (2.2.72)$$

we get an expression for the conjugate momentum of a boosted star. Again, setting  $\tilde{t} = 0$  gives the conjugate momentum on the surface  $\tilde{t} = 0$  to be used as initial conditions,

$$\tilde{\Pi} = -\frac{1}{\tilde{\alpha}} \left[ \left[ \sinh(\chi) - \tilde{\beta}^1 \cosh(\chi) \right] \frac{\tilde{x} \cosh(\chi)}{r} \Phi' + i\omega \left[ \cosh(\chi) - \tilde{\beta}^1 \sinh(\chi) \right] \Phi \right] e^{i\omega \tilde{x} \sinh(\chi)}. \quad (2.2.73)$$

The penultimate ingredient is the intrinsic curvature  $\tilde{\mathbf{K}}$ , defined in Eq. (2.1.10). Similarly to the conjugate momentum, the definition of  $\tilde{\mathbf{K}}$  depends on the spacetime foliation so using  $K_{ij} = 0$  in the stars rest frame and using the tensor transformation to conclude that  $\tilde{K}_{ij} = 0$  in the rest frame (where the star moves) is incorrect. Instead the components  $\tilde{K}_{ij}$  must be calculated from scratch with the correct normal vector  $\mathbf{n}$  like,

$$\tilde{\mathcal{K}}_{\mu\nu} := -\frac{1}{2} \mathcal{L}_{\tilde{\mathbf{n}}} \tilde{\gamma}_{\mu\nu} = -\frac{1}{2\tilde{\alpha}} \mathcal{L}_{\tilde{\mathbf{m}}} \tilde{\gamma}_{\mu\nu} = -\frac{1}{2\tilde{\alpha}} \left[ \tilde{m} \cdot \tilde{\partial} \tilde{\gamma}_{ij} + \tilde{\gamma}_{ik} \tilde{\partial}_j \tilde{m}^k + \tilde{\gamma}_{jk} \tilde{\partial}_i \tilde{m}^k \right]. \quad (2.2.74)$$

A private, self written mathematica script gives the following explicit form for the components of  $\tilde{K}_{ij}$ ,

$$\alpha^{-1} \tilde{\mathcal{K}}_{xx} = \cosh^2(\chi) \sinh(\chi) \frac{x}{r} \frac{[v^2 \Omega^2 \Omega' + \Psi \Omega \Psi' - 2\Psi^2 \Omega']}{\Psi^2 \Omega}, \quad (2.2.75)$$

$$\alpha^{-1} \tilde{\mathcal{K}}_{xy} = \cosh(\chi) \sinh(\chi) \frac{y}{r} \frac{[\Omega \Psi' - \Psi \Omega']}{\Psi \Omega}, \quad (2.2.76)$$

$$\alpha^{-1} \tilde{\mathcal{K}}_{xz} = \cosh(\chi) \sinh(\chi) \frac{z}{r} \frac{[\Omega \Psi' - \Psi \Omega']}{\Psi \Omega}, \quad (2.2.77)$$

$$\alpha^{-1} \tilde{\mathcal{K}}_{yy} = -\sinh(\chi) \frac{x}{r} \frac{\Psi'}{\Psi}, \quad (2.2.78)$$

$$\tilde{\mathcal{K}}_{zz} = \tilde{\mathcal{K}}_{yy}, \quad (2.2.79)$$

where the  $\{x, y, z\}$  need to be expanded in terms of  $\{\tilde{x}, \tilde{y}, \tilde{z}\}$  and  $r = \sqrt{x^2 + y^2 + z^2}$ .

The final object needed is the three-dimensional connection symbols  $\Upsilon^i_{jk}$ , these are calculated numerically after the initial data is loaded in using the definition from Eq. (1.3.77),

$$\Upsilon^i_{jk} = \frac{1}{2} \gamma^{im} (\partial_k g_{jm} + \partial_j g_{mk} - \partial_m g_{jk}). \quad (2.2.80)$$

The boost formalism described here can apply this to the Black Hole spacetime by an identical procedure setting

$$\varphi = 0, \quad (2.2.81)$$

$$\Pi = 0, \quad (2.2.82)$$

$$\Omega = \frac{1 - \frac{M}{2r}}{1 + \frac{M}{2r}}, \quad (2.2.83)$$

$$\Psi = \left[ 1 + \frac{M}{2r} \right]^2, \quad (2.2.84)$$

corresponding to the isotropic Schwarzschild black hole given in section 1.4.6.

## 2.2.6 Spherical Harmonics in Curved Space DO I KEEP THIS SECTION? MAYBE JUST FOR INTERPITING SOME SIMS

Spherical harmonics are an orthonormal function basis for the surface of a sphere. They arise when looking for solutions to the 3D spherical polar laplacian

$$\nabla^2 \varphi = \frac{1}{\sqrt{|g|}} \partial_\mu \left( \sqrt{|g|} g^{\mu\nu} \partial_\nu \varphi \right), \quad \mu, \nu \in \{1, 2, 3\}. \quad (2.2.85)$$

On the hypersurface  $r = 1$  we get the following metric

$$g_{\mu\nu} = \begin{pmatrix} 1 & 0 \\ 0 & \sin^2 \theta \end{pmatrix}, \quad (2.2.86)$$

and on this surface the spherical harmonics  $Y_{lm}(\theta, \phi)$  satisfy the following condition.

$$\mathcal{D}_\mu \mathcal{D}^\mu Y_{lm}(\theta, \phi) = -l(l+1)Y_{lm}(\theta, \phi), \quad x^\mu \in \{\theta, \phi\} \quad (2.2.87)$$

This means we can take any spherically symmetric and static metric with  $g_{\phi\phi} = \sin^2 \theta g_{\theta\theta}$  and replace the angular part of the wave equation with  $l(l+1)$ . For a spherically symmetric spacetime this gives the Klein Gordon equation for scalar hair.

$$\nabla_\mu \nabla^\mu \varphi = V' \varphi, \quad \varphi = T(t)R(r)Y_{lm}(\theta, \phi) \quad (2.2.88)$$

$$\varphi^{-1} \nabla_\mu \nabla^\mu \varphi = g^{tt} \frac{\ddot{T}}{T} + \frac{1}{R\sqrt{|g|}} \partial_r \left( \sqrt{|g|} g^{rr} \partial_r R \right) - l(l+1)g^{\theta\theta} \quad (2.2.89)$$

This is a second order ODE for the radial profile  $R$  and is an eigenvalue problem for  $\omega$  if we assume  $T = e^{i\omega t}$ . Assuming  $T = e^{-kt}$  can be done on-top of the black hole metric () and requires the assumption of no back reaction of the scalar field on the metric; this gives an eigenvalue problem in  $k$  instead. This leads to the following ODE for the radial profile.

$$\frac{1}{R\sqrt{|g|}} \partial_r \left( \sqrt{|g|} \Psi^{-4} \partial_r R \right) = k^2 \frac{\Omega^2}{\Psi^2} + \frac{l(l+1)}{r^2 \Psi^4} + V' \quad (2.2.90)$$

Simulations shown later involve boson stars of mass  $M$  and black holes of mass  $M \rightarrow 10M$ ; these simulations often produce scalar hair about these black holes that is orders of magnitude less massive than the boson stars. In this regime the above equation is assumed relevant.

MAYBE JUST USE THIS SECTION TO TALK ABOUT THE COLLISIONS THAT MAYBE SEEM TO FOLLOW THIS RULE ... SAY HOW EVEN THOUGHT ITS NOT REALLY SPHERICALLY SYMMETRIC MAYBE IT CAN BE APPROXIMATES BY THIS? AND WE CAN'T USE SUPERPOSITION OF SOLUTIONS REALLY

## 2.3 GRChombo

### 2.3.1 Numerical Discretisation of Spacetime

euler step not stable, in comes runge kutta, mention there are other schemes but we don't use it

#### Runge-Kutta Integration

#### Method of Lines

### 2.3.2 Boundary Conditions

### 2.3.3 Overview of GRChombo

GRChombo [] is a recently developed Numerical Relativity code built on top of Chombo [], a PDE solver with fully adaptive mesh refinement (AMR). The advantage of AMR is that regridding, and subsequently sub-volumes of high resolution, is calculated during runtime. This is especially useful for simulating fluids in GR as they can develop features requiring higher resolution in places a human may not expect making pre-specified mesh refinement hard to use. GRChombo uses the CCZ4 system with 1+log slicing and the Gamma driver shift condition, discussed in sections (). GRChombo also supports vectorisation and parallelisation with OpenMP and MPI making it suitable for use on supercomputer clusters.

So far I have implemented initial data for a single or binary system of compact objects which can be either a Schwarzschild black hole or a boson star. The initial data uses isotropic coordinates and can be boosted along coordinate axes, but not yet general directions, giving the possibility of single boosted objects, accelerated head on collisions, grazing collisions and inspirals/quasi-orbits. It should be noted that my implementation was built on top of the pre-existing complex scalar field class (written by Miren). The remainder of this section will cover the numerical aspects of my work.

TALK MORE ABOUT GRCHOMBO AND MAYBE REF THE NEW PAPER

### 2.3.4 Simulation Units

MAKE THIS WORK WITH THE CONVENTIONS SECTION ASND THEN DESCRIBE WHAT IS NEW FOR ONLY THE SIMULATIONS

GRChombo defaults to geometric units, as described in section (1.2). The scalar field  $\varphi$  appears in the action as

$$S = \int_{\mathcal{M}} [g^{\mu\nu} \partial_\mu \varphi \partial_\nu \varphi^* + \dots] dx^4 \quad (2.3.1)$$

and given  $S$  and the metric are dimensionless, dimensional analysis tells us  $\varphi$  has units of inverse length in natural units, or units of energy. The Klein-Gordon mass  $m$

$$\square \varphi = m^2 \varphi \quad (2.3.2)$$

can be absorbed into new dimensionless spatial coordinates  $\tilde{x}^i = x^i m$  changing the KG equation to the scale invariant form.

$$\square \varphi = \varphi \quad (2.3.3)$$

### 2.3.5 Boson Star Initial Data

Following on from the EKG ODE's in Eqs. (2.2.21), (2.2.22) and (2.2.23) we now seek to solve them numerically to obtain initial data for a single static boson star. The system can be reduced to a set of five first order ODE's with five boundary conditions. For a physical star we would like to impose  $\Phi(0) = \Phi_c$ ,  $\Phi'(0) = 0$ ,  $\Phi(r \rightarrow \infty) \rightarrow 0$ ,  $\Omega'(0) = 0$ ,  $\Omega(r \rightarrow \infty) \rightarrow 1$ ,  $\Psi'(0) = 0$  and  $\Psi(r \rightarrow \infty) \rightarrow 1$  to be regular at the origin and match the Schwarzschild vacuum solution at large radius; however this is seven boundary conditions and we can only impose five. The condition  $\Omega(0)' = 0$  cannot be specified as Eq. (2.2.21) is



first order in derivatives of  $\Omega$  but given that  $r$  and  $\Psi'$  both vanish at the origin then  $\Omega'$  must also vanish at the origin automatically. One more boundary condition can be removed by asking for the boson star solution to match the isotropic Schwarzschild solution in Eq. (1.4.43) and therefore,

$$\Omega = \left( \frac{1 - \frac{m}{2r}}{1 + \frac{m}{2r}} \right) \quad \& \quad \Psi = \left( 1 + \frac{m}{2r} \right)^2 \quad (2.3.4)$$

where  $m$  can be interpreted as the mass of the boson star; this mass will not enter the boundary condition so can be safely ignored. Combining the two equations above gives

$$\sqrt{\Psi}(1 + \Omega) = 2 \quad (2.3.5)$$

for a vacuum spacetime. Imposing the single condition  $\sqrt{\Psi(\infty)}(1 + \Omega(\infty)) = 2$ , rather than both  $\Omega(\infty) = 1$  and  $\Psi(\infty) = 1$ , then gives asymptotic flatness in just one boundary condition. One final point of importance is the frequency  $\omega$  turns the Klein-Gordon ODE into an eigenvalue problem, admitting only discrete values of  $\omega$ .

The problem has now been reduced to five ODE's with the following five boundary conditions,

$$\{\Phi(0), \Phi'(0), \Psi'(0), \Omega(0), \sqrt{\Psi(\infty)}(1 + \Omega(\infty)); \omega\} = \{\Phi_c, 0, 0, \omega_0, 2; \omega_0\}, \quad (2.3.6)$$

subjected to the condition of an eigenvalue  $\omega = \omega_0$ . The first attempt to find the radial profile  $\{\Phi(r), \Omega(r), \Psi(r)\}$  of the boson star was to use a relaxation method [REF] as it trivially incorporates the above two-point boundary conditions. In practice this method did not work well with the eigenvalue problem in  $\omega$ . Unlike with a shooting method, there was no obvious way of telling whether the guess  $\omega$  was larger or smaller than the correct value. Even if this problem were overcome, a numerical solution with relaxation is computationally slow, even with Successive Over-Relaxation [REF] [20]; perhaps a multigrid method could work here but a simpler method was used.

### Shooting Method

To find the initial data for a single Boson star, a private c++ script was written using RK4 [REF] to integrate the EKG system taking five initial conditions, and eigenvalue guess  $\omega_0$ ,

$$\{\Phi(0), \Phi'(0), \Psi(0), \Psi'(0), \Omega(0); \omega\} = \{\Phi_c, 0, \Psi_c, 0, \omega_0; \omega_0\}. \quad (2.3.7)$$

Unfortunately  $\omega_0$  and  $\Psi_c$  are unknown apriori, but guessing any values reasonably close to unity, such as  $\omega_0 = 0.5$  and  $\Psi_c = 2$ , still give a boson star. This will generally result in the following asymptotic metric,

$$g_{\mu\nu}(r \rightarrow \infty) \rightarrow \text{diag}(-A^2, B^2, B^2, B^2), \quad (2.3.8)$$

for constant  $A$  and  $B$ .

Before we discuss how to find the correct value of  $\omega$ , there is a subtle numerical problem to adress. Using spherical polar coordinates in flat space, the Klein-Gordon equation (2.2.8) with  $V = m^2|\varphi|^2$  and ansatz  $\varphi = \Phi_{flat}(r)e^{i\omega t}$  reduces to,

$$\frac{1}{\sqrt{-g}}\partial_\mu(\sqrt{-g}g^{\mu\nu}\partial_\nu)\varphi = \frac{\partial V}{\partial|\varphi|^2}\varphi, \quad (2.3.9)$$

$$\partial_t(g^{tt}\partial_t)\Phi_{flat}(r)e^{i\omega t} + \frac{1}{r^2}\partial_r(r^2g^{rr}\partial_r)\Phi_{flat}(r)e^{i\omega t} = m^2\Phi_{flat}(r)e^{i\omega t}, \quad (2.3.10)$$

$$\omega^2\Phi_{flat}(r) + \frac{1}{r^2}\partial_r(r^2\partial_r)\Phi_{flat}(r) = m^2\Phi_{flat}(r), \quad (2.3.11)$$

$$(2.3.12)$$

where  $\sqrt{-g} = r^2 \sin(\theta)$ ,  $g^{tt} = -1$  and  $g^{rr} = 1$ . This has general solution,

$$\Phi_{flat}(r) = \frac{1}{r} \left( C_1 e^{-r\sqrt{m^2 - \omega^2}} + C_2 e^{r\sqrt{m^2 - \omega^2}} \right), \quad (2.3.13)$$

for  $\Phi_{flat}(r)$  and two constants  $C_1$  and  $C_2$ . Due to finite resolution during numerical integration, at large radius  $C_2$  will never be exactly zero and will eventually grow (along increasing radius) and spoil the numerical integration; even though this behaviour was derived in flat space it is still present in curved space with spherical symmetry - especially at such large radius that space is approximately flat. In practice, the scalar field  $\Phi$  will decay to some value roughly twenty orders of magnitude smaller than the central density  $\Phi(0)$  and is effectively zero within numerical noise. At this point the coefficient  $C_2$  is excited by noise and starts to grow exponentially. At a radius  $r_*$  when the growing mode is deemed to be dominating, usually detected by an axis crossing ( $\Phi(r_*) = 0$  or a turning point  $\Phi'(r_*) = 0$ ) the conditions  $\Phi(r > r_*) = \Phi'(r > r_*) = 0$  are enforced during integration. This creates a vacuum for  $r > r_*$  and the spacetime is pure Schwarzschild. After this point, an exponentially growing stepsize was used to reach radii of order  $10^8$  to  $10^{10}$  times larger than desired for evolutions and the values  $A = \Omega_\infty = \sqrt{-g_{00}}$  and  $B = \Psi_\infty = \sqrt{g_{ii}}$  can be read off.

Interval bisection was used to find the best value of  $\omega$ ,  $\omega_0$ , to machine precision; for the ground state we can tell that  $\omega > \omega_0$  if  $\Phi(r)$  develops a turning point before an axis crossing and  $\omega < \omega_0$  if  $\Phi(r)$  develops an axis crossing before a turning point. To find the  $n$ 'th excited state, which has  $n$  axis crossing for  $\Phi(r)$  and  $\Phi(r \rightarrow \infty) \rightarrow 0$  a similar scheme is followed to find the eigenvalue  $\omega_n$ . If  $\Phi(r)$  has  $n + 1$  axis crossings then  $\omega > \omega_n$  and if  $\Phi(r)$  has  $n$  axis crossings followed by a turning point then  $\omega < \omega_n$ . This method of doing a numerical integration and iteratively restarting to get closer to the target solution is known as a shooting method.

Putting everything together, a boson star solution with eigen value  $\omega_0$  (or  $\omega_n$  for excited stars) and asymptotic metric Eq. (2.3.8) can be obtained. To find a star with asymptotic metric  $\eta_{\mu\nu}$  of flat space, the initial conditions are iteratively improved like  $\Omega_c \rightarrow \Omega_c/\Omega_\infty$  and  $\Psi_c \rightarrow \Psi_c/\Psi_\infty$ ; the interval bisection for  $\omega$  is then restarted. This is iterated three to five times which leaves  $A = \Omega_\infty = 1$  and  $B = \Psi_\infty = 1$  to extreme precision and the isotropic boson star is created. This whole process requires a few seconds runtime for a high resolution 200,000 grid-point simulation on a regular laptop.

Figures 2.5 and 2.6 show the numerical result for the radial profile of a mini boson star ( $\Lambda = 0$ ) and an excited mini boson star. Note two mass definitions are plotted; the ADM mass (calculated as a function of finite  $r$ ) and the aspect mass  $M_A(r)$  which corresponds to assuming the metric's solution is Schwarzschild with  $M_A(r)$  rather than  $M$ . Polytropic fluid stars were also simulated as a preliminary test of the code; they are much easier to create not needing to solve an eigenvalue problem and don't have an asymptotically growing mode. Figures () show how the ADM mass of boson stars varies with central amplitude  $\Phi(0)$  and  $r_{99}$ , the radius which  $\Phi(r_{99}) = \Phi(0)/100$ . It should be noted that the  $\Lambda = 0$  case agrees with the known maximum mass, the Kaup limit [ ]  $M_{max} \approx 0.633 M_{PL}^2 m^{-1}$  with the highest measured mass being  $M_{max} = 0.63299(3) M_{PL}^2 m^{-1}$  corresponding to a central amplitude of  $\sqrt{4\pi G} \Phi(0)_{max} = 0.271(0)$ .

While many different boson stars have been made to test the initial data code, all the following evolutions use the same boson star with parameters  $\Lambda = 0$ ,  $\sqrt{4\pi G} \Phi(0) = 0.1 \rightarrow \Phi(0) \approx 0.0282$  and ADM mass  $M = 0.532(7)$ . This is as the stars are heavy enough to form black holes under collisions and large deformations, but stable enough to not collapse to a black hole for moderate perturbations.

EXPLAIN EIGENVALUES AND GROUND STATES BETTER.

### 2.3.6 Single Star Evolutions

The first simulation done was of the  $\Phi(0) = 0.02820$  mini boson star; as mentioned before all simulations are done with this star. The star is supposed to remain in the centre of the grid and not change as it

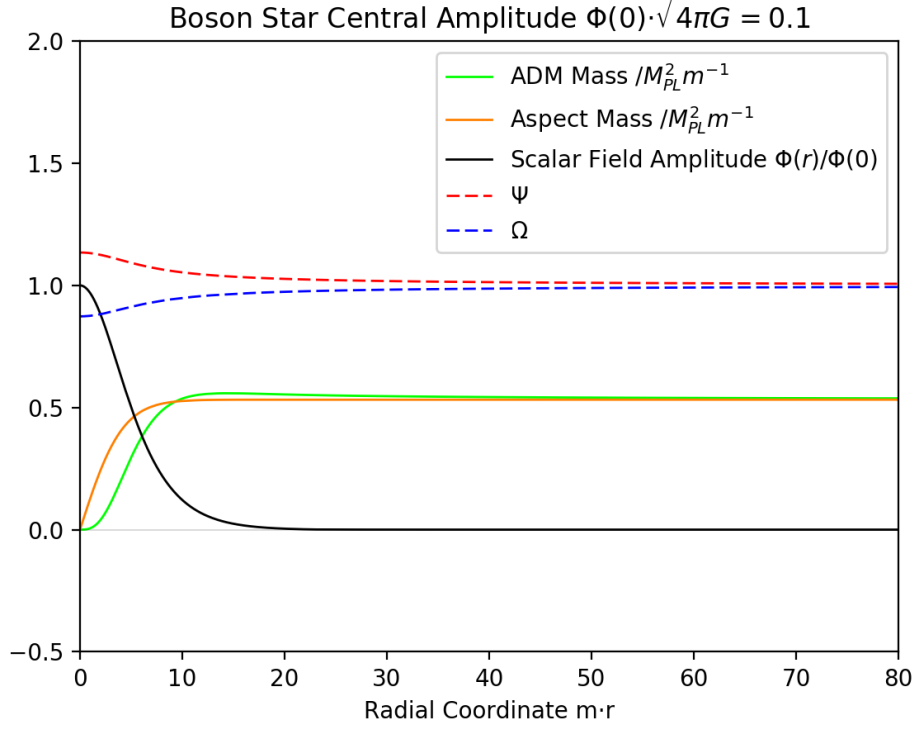


Figure 2.3: Boson star radial profile for the ground state

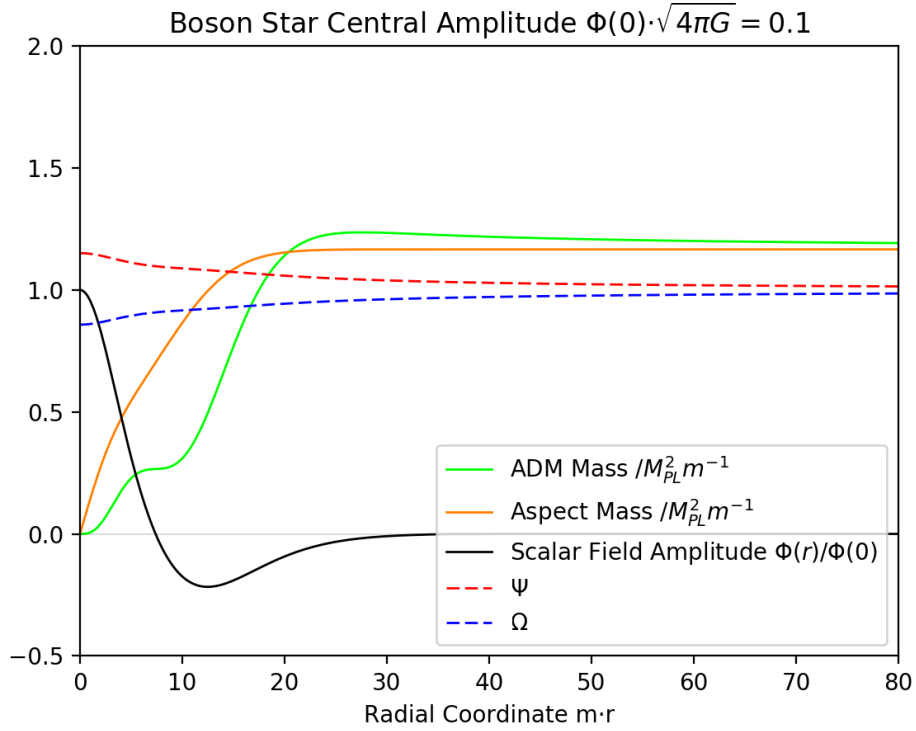


Figure 2.4: Boson Star radial profile : 1st Excited state

is a rest frame soliton; this is observed through evolution with GRChombo. Figure () shows a rough initial phase in  $|\varphi|$  which changes significantly upon changing the AMR regridding, hence it is likely only

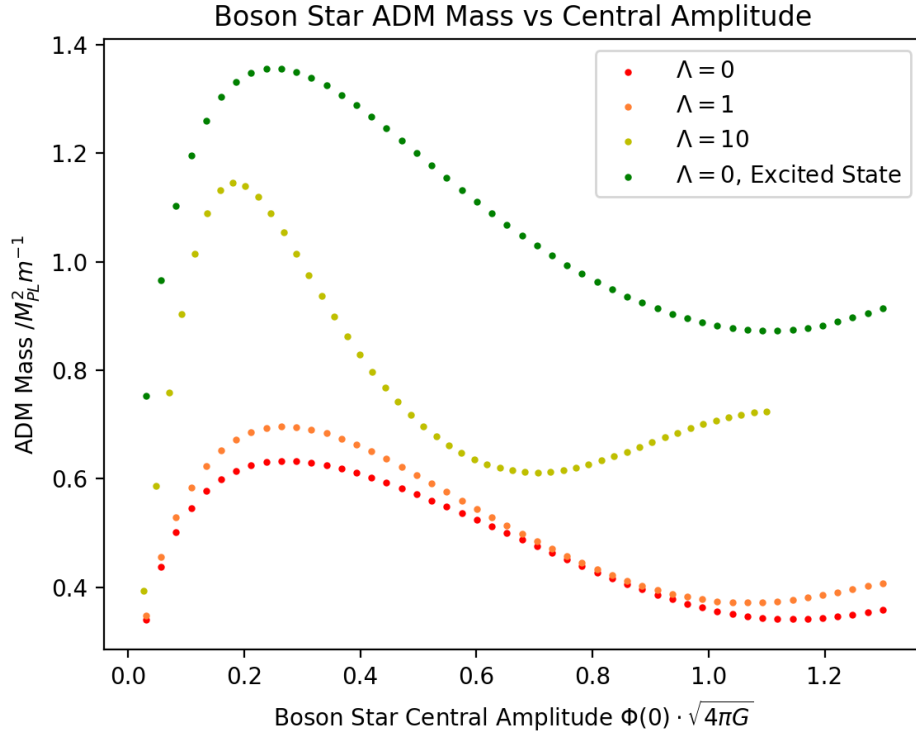


Figure 2.5: ADM mass vs  $\Phi(0)$

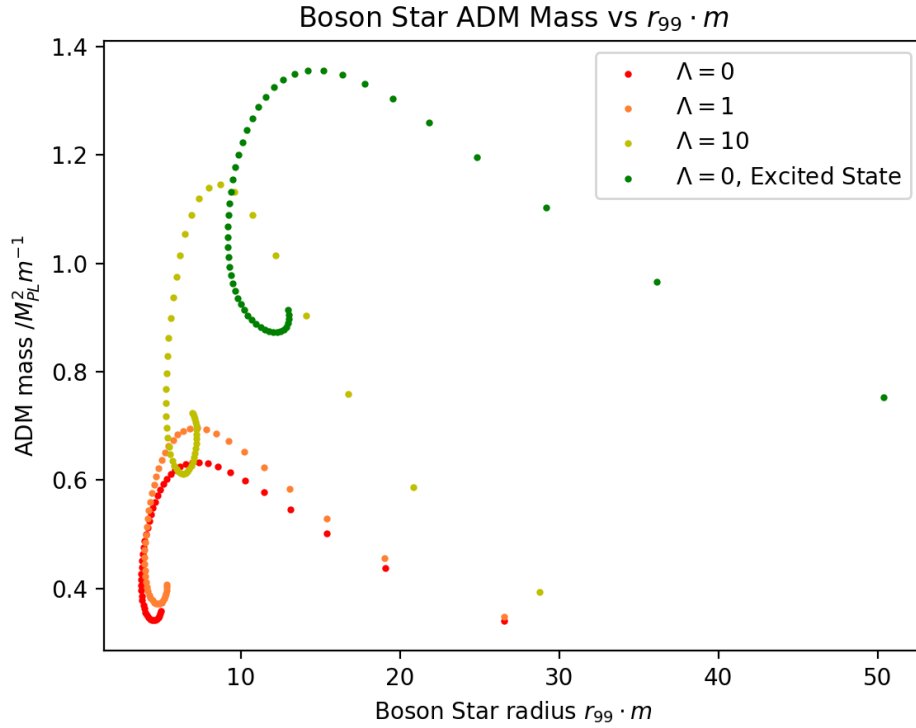


Figure 2.6: ADM mass vs  $r_{99}$

a side effect of the interpolation errors at the boundary of AMR regions. Figure () shows that the star conserves  $\mathcal{N}$  upto 4 figures and the constraint  $\mathcal{H}$  is driven towards zero as desired.

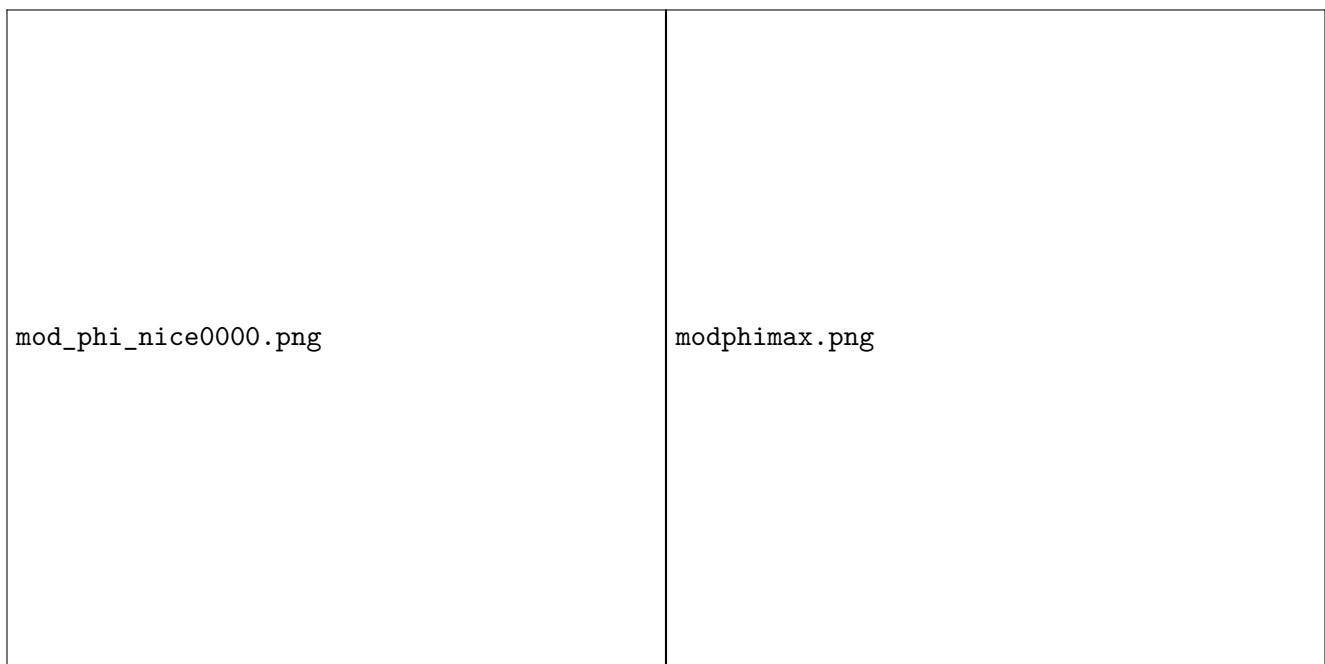


Figure 2.7: Left: 2D slice of initial  $|\varphi|$ , Right: Maximum of  $|\varphi|$  during evolution.

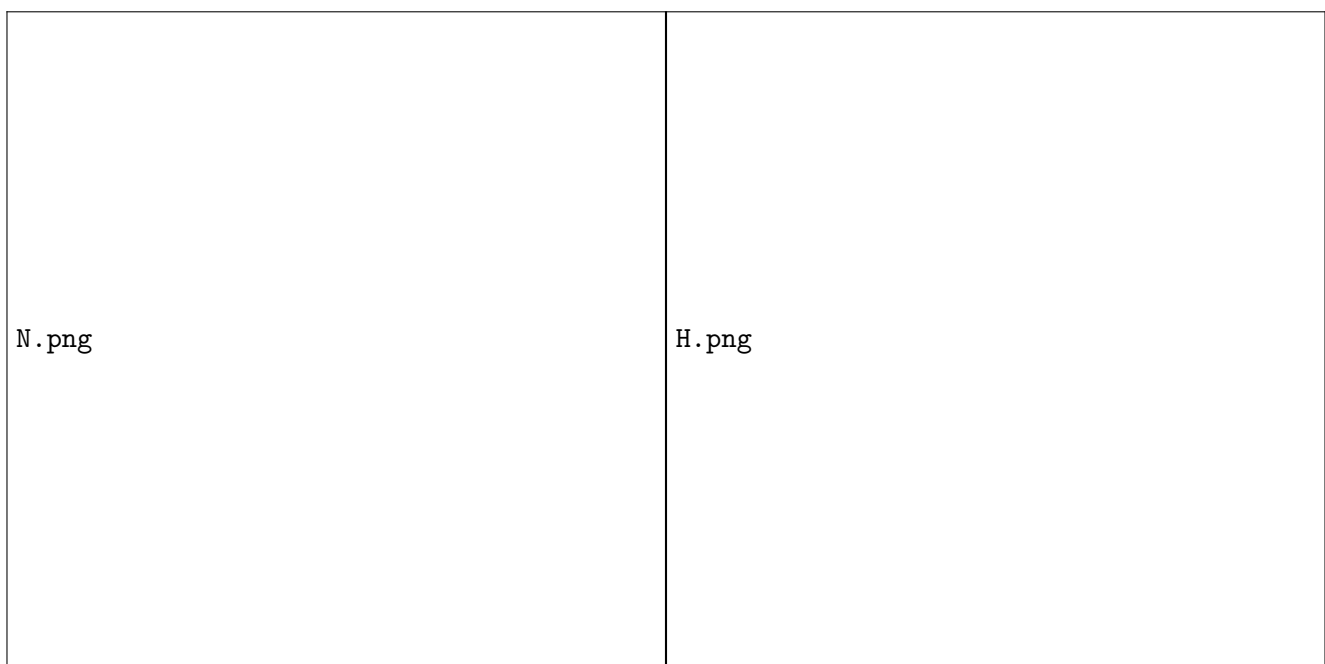


Figure 2.8: Left: Total Noether charge  $\mathcal{N}$  during evolution, Right:  $\|\mathcal{H}\|_2$  during evolution.

### 2.3.7 Superposition of Initial Data

Suppose we have two compact objects with fields  $\varphi$ ,  $\Pi$ ,  $\gamma_{ij}$ ,  $\mathcal{K}_{ij}$ ,  $\alpha$  and  $\beta^i$ . The chosen scheme to superpose solutions is below.

$$\begin{aligned}\varphi &= \varphi^{(1)} + \varphi^{(2)} \\ \Pi &= \Pi^{(1)} + \Pi^{(2)} \\ \mathcal{K}_j^i &= \mathcal{K}_j^{(1)i} + \mathcal{K}_j^{(2)i} \\ \gamma_{\mu\nu} &= \gamma_{\mu\nu}^{(1)} + \gamma_{\mu\nu}^{(2)} \\ \beta_i &= \beta_i^{(1)} + \beta_i^{(2)} \\ \alpha &= \sqrt{\alpha_{(1)}^2 + \alpha_{(2)}^2 - 1} \quad \text{or} \quad \left[ \alpha_{(1)}^{-1} + \alpha_{(2)}^{-1} - 1 \right]^{-1} \\ \chi &= \det \left\{ \gamma_{\mu\nu}^{(1)} + \gamma_{\mu\nu}^{(2)} \right\}^{-1/3}\end{aligned}$$

When a black hole is involved  $\Omega(r = \frac{2}{M}) = 0$  so the event horizon causes the lapse to cross through zero; this is circumvented by setting

$$\alpha = \sqrt{\chi} \tag{2.3.14}$$

and the lapse is real, non-negative for a spacelike hypersurface  $\Sigma$ . Superposing the scalar field  $\varphi$  is exact for the mini boson star (); for every other variable and type of star case superposition is inexact. Luckily, for sufficiently separated compact objects, superposition gives a very close approximation to the exact numerical solution. The use of CCZ4 also forces the evolution towards a constraint satisfying one.

### 2.3.8 Head-on Collisions

All the cases studied here are for stationary initial data  $\tilde{\mathcal{A}}_{ij} = 0, \mathcal{K} = 0$  in-falling from an initial separation of  $d \cdot m = 32$  due to gravitational attraction. Firstly we consider the equal mass Boson star binary, initial data in figure (). At first they slowly infall creating a short lived object with three maxima, shown in figure (,left), then collapse to a black hole with a decaying spherical harmonic cloud (figures ) outside. As with all the simulations from now on we assume a black hole forms if  $\chi \ll 16^{-1}$  where  $\chi = 16^{-1}$  is the value taken on the horizon for the isotropic Schwarzschild metric.

The second case considered is the same Boson star outside a black hole parameterised by  $M = 10M_{BS}$  where  $M_{BS}$  is the ADM mass of the Boson star. The scalar field tidally deforms into an ellipsoid with high central density, well beyond Kaup limit of  $\varphi(0) \sim 0.0764$ , and spontaneous collapse to a smaller external black hole is observed. After collapse, figure (), there is an elongated cloud about the new small black hole; there are many nodal lines in  $\text{Re}(\varphi)$  which focus on the large black hole showing the cloud is in-falling.

Final case consists of an equal mass Black Hole and Boson Star, initial configuration in Figure 11. As can be seen from the plot of  $\text{Re}(\phi)$  and  $|\phi|$ , in Figure 12, most of the star falls into the black hole, however some scalar field manages to excite an intricate spherical harmonic cloud pattern.

In all three cases, the Noether charge drops rapidly upon the formation of a black hole; this will be explained in the next section. However some scalar field lingers after collapse, in each case the hair takes the form of spherical harmonics discussed in (). Also observed is the decay of the spherical harmonics to zero amplitude in these simulations with no angular momentum.

### 2.3.9 Binary Inspiral

The only considered case here is the Quasi-circular orbit and inspiral of two equal mass boson stars. The initial boosts were determined by a newtonian calculation yielding

$$v^2 = \frac{M}{2d} \tag{2.3.15}$$



Figure 2.9: Initial Data, Left:  $\chi$ , Right:  $|\varphi|$ .



Figure 2.10: Scalar field amplitude before and after black hole formation, Left: Time  $t \cdot m = 150$ , Right: Time  $t \cdot m = 200$ .

where  $M = 0.53(29)$  is the ADM mass of the Boson Star and  $d$  is the initial separation. For a relatively low separation of  $d \cdot m = 32$  code units, shown in Figures 13,14 (Left), we get  $v \sim 0.0915$ . The boson stars are observed to complete roughly half an orbit before merging and collapse, forming a black hole. Here a Kerr black hole is assumed to have formed as the spacetime has a significant angular momentum which should partially infall with the scalar field.

Figure 15 shows the total Noether charge, which is no longer conserved. When the black hole forms,

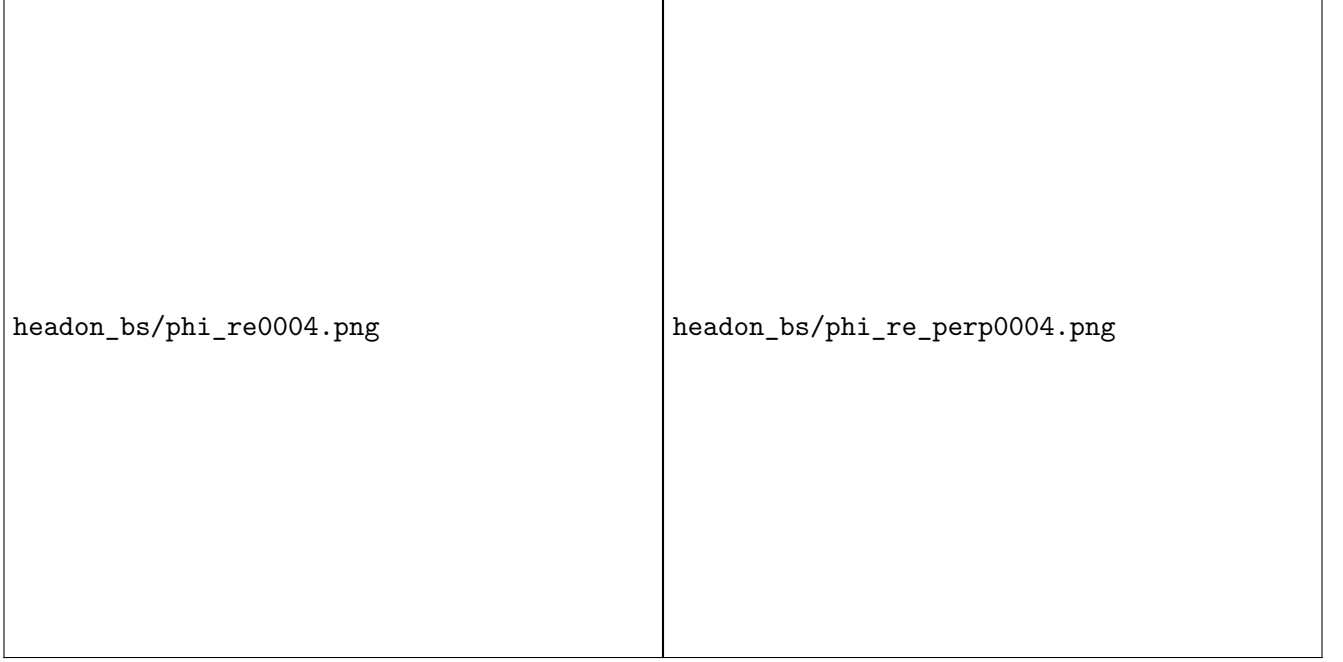


Figure 2.11: Real part of scalar field after black hole formation, Left: xy plane, Right: yz plane, perpendicular to initial star separation.

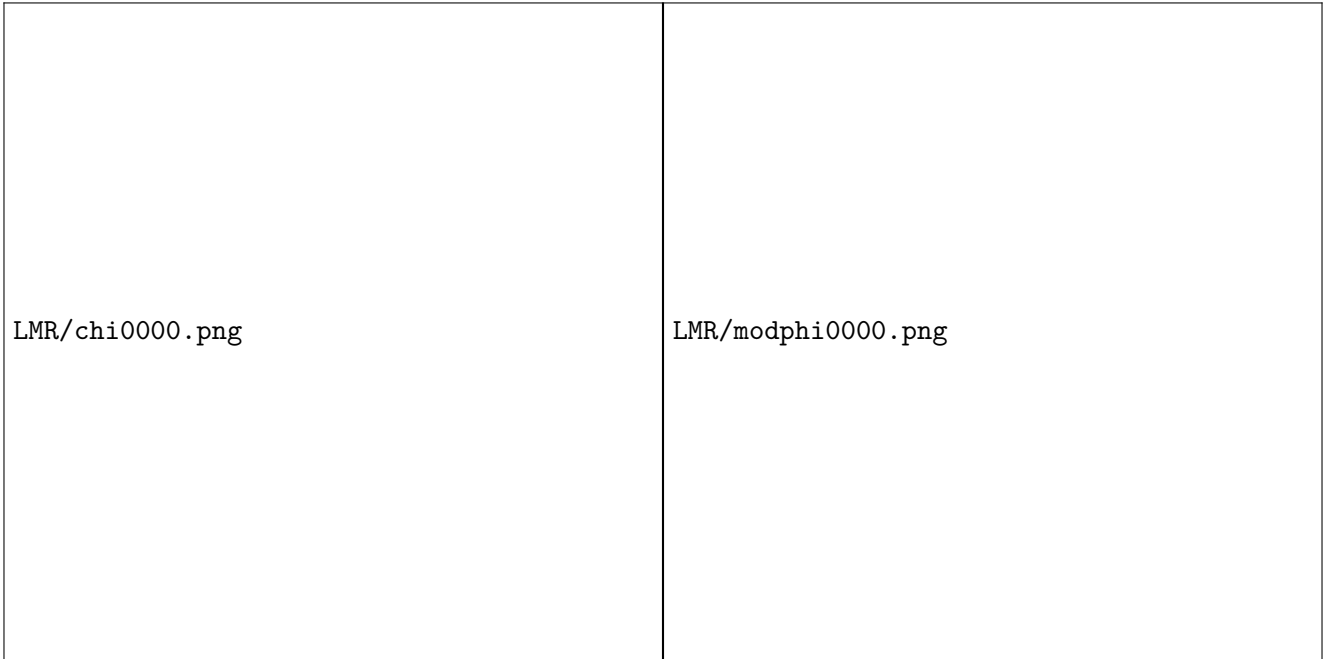


Figure 2.12: Initial Data, Left:  $\chi$ , Right:  $|\varphi|$ .

the in-falling scalar field moves towards zero radius and gets hugely compressed. The huge compression causes extreme field gradients which induces continuous regridding in the AMR, but this is capped at 7 layers in this simulation to make runtime feasible. When the 8th AMR level is needed it is simply not added and resolution becomes low enough that any Noether charge near the centre is so under-resolved that it seems to fall between the gridpoints. Interestingly, Figures 13,14 (Right) show a scalar field configuration lingering around the black hole, mostly outside the contour  $\chi = 0.7$ , looking like scalar



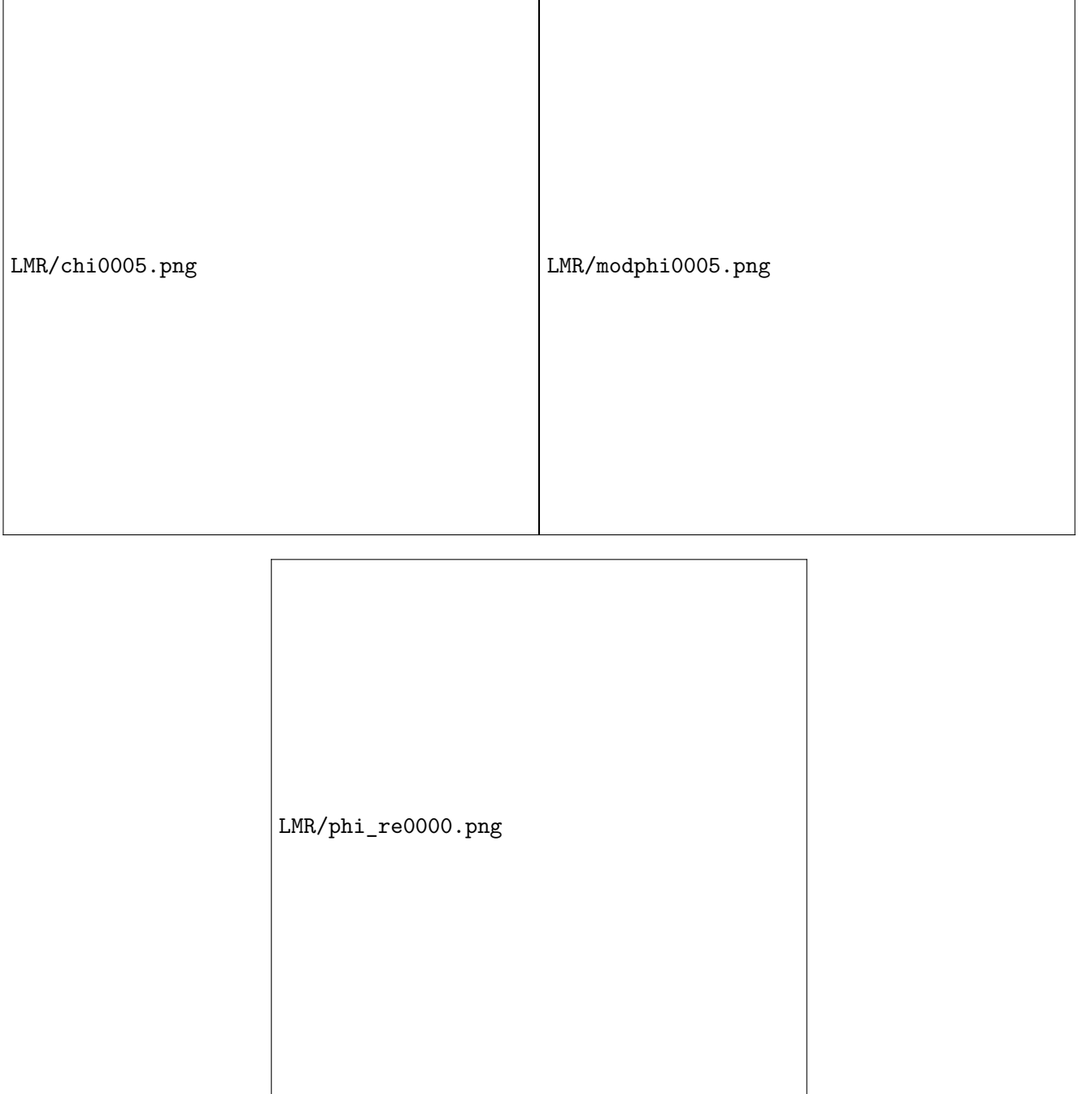


Figure 2.13: Final Data at time  $t \cdot m = 125$ , Left: Conformal factor  $\chi$ , Right: Scalar field modulus  $|\varphi|$ , Bottom: Real part of scalarfield  $\text{Re}(\varphi)$ .

hair. Also Figure 15 (Left) of the Noether charge appears to take significantly longer to decay than in the linear collision simulations. It can be seen in Figure 14 in the plot of  $\text{Re}(\varphi)$  that the cloud has angular nodes corresponding to angular momentum similarly to boosted stars picking up nodal planes perpendicular to momentum and Figure 10 (Bottom) of the infalling cloud.

The gravitational wave (GW) signal can be seen in Figure 15 (Right), extracted at a radius  $r \cdot m = 90$ . At the time  $t \cdot m \approx 700$  the gravitational wave signal due to the merger appears; in order to record a longer inspiral simulations with larger initial separations need to be simulated. Currently there appears to be some small problem with the initial data, also observed in the collisions with no angular momentum, that

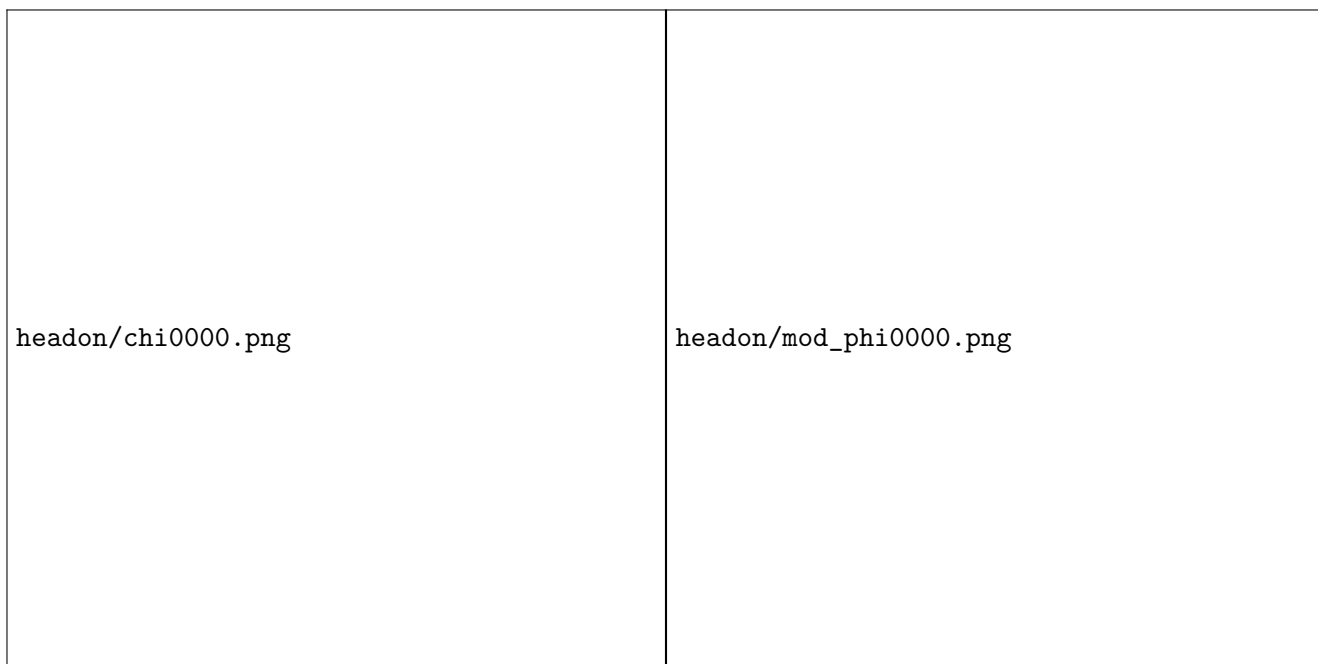


Figure 2.14: Initial data for equal mass Boson Star and Black Hole, Left:  $\chi$ , Right:  $|\varphi|$



Figure 2.15: Time  $t \cdot m = 905$  for equal mass Boson Star and Black Hole, Left:  $\text{Re}(\varphi)$ , Right:  $|\varphi|$

manifests itself in noisy GW extraction and the Hamiltonian constraint initially sharply rising.

### 2.3.10 STUFF

I think I want a stationary star headon collision maybe collision with angular momentum collision of bs with bh

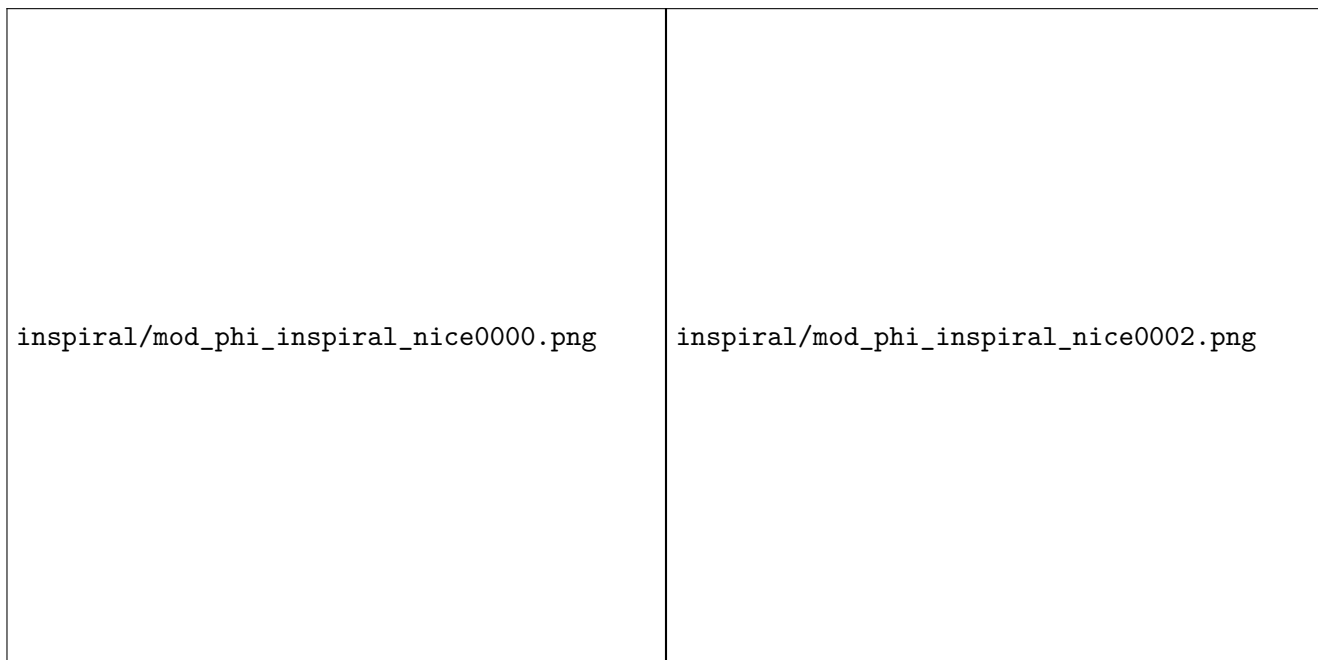


Figure 2.16: Boson Star  $|\varphi|$ . Left: initial data, Right: later time  $t \cdot m = 700$



Figure 2.17: Boson Star  $\text{Re}(\varphi)$ . Left: initial data, Right: later time  $t \cdot m = 700$

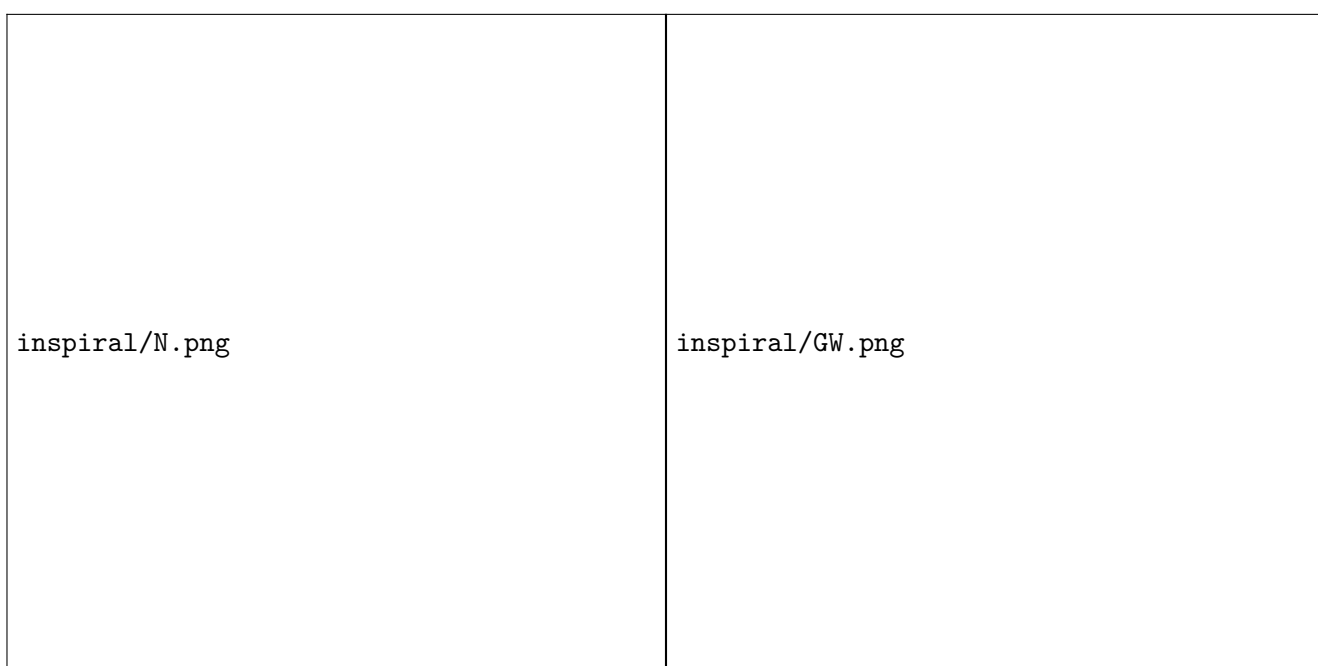


Figure 2.18: Left: Total Noether charge  $\mathcal{N}$  during evolution, Right:  $\Psi_4$  over 22 harmonic during evolution.

## Chapter 3

# MALAISE PAPER

Through numerical simulations of boson-star head-on collisions, we explore the quality of binary initial data obtained from the superposition of single-star spacetimes. Our results demonstrate that evolutions starting from a plain superposition of individual boosted boson-star spacetimes are vulnerable to significant unphysical artefacts. These difficulties can be overcome with a simple modification of the initial data suggested in [?] for collisions of oscillatons. While we specifically consider massive complex scalar field boson star models up to a 6th-order-polynomial potential, we argue that this vulnerability is universal and present in other kinds of exotic compact systems and hence needs to be addressed.

### 3.1 Introduction

The rise of gravitational-wave (GW) physics as an observational field, marked by the detection of GW150914 [?] and followed by about 50 further compact binary events [?, ?] over the past years, has opened up unprecedented opportunities to explore gravitational phenomena. From tests of general relativity [?, ?, ?, ?, ?, ?] to the exploration of BH populations [?, ?, ?, ?, ?] or charting the universe with independent new methods [?, ?], GW astronomy offers potential for revolutionary insight into long-standing open questions; for a review see [?]. Some answers, such as the association of a soft gamma-ray burst with the neutron star merger GW170817 [?, ?] have already raised our understanding to new levels. GW physics furthermore establishes new concrete links to other fields of research, most notably to particle and high-energy physics and the exploration of the dark sector of the universe [?, ?]. Two important ingredients of this remarkable connection are the characteristic interaction of fundamental fields with compact objects through superradiance [?] and their capacity to form compact objects through an elaborate balance between the intrinsically dispersive character of the fields and their self-gravitation. The latter feature has given rise to the hypothesis of a distinct class of compact objects as early as the 1950s [?]. In contrast to their well known fermionic counterparts – stars, white dwarfs or neutron stars – these compact objects are composed of bosonic particles or fields and, hence, commonly referred to as *Boson Stars* (BS). GW observations provide the first systematic approach to search for populations of these objects or to constrain their abundance. As with all other GW explorations, the success of this exploration is heavily reliant on the availability of accurate theoretical predictions for the anticipated GW signals. This type of calculation, using numerical relativity techniques [?], is the topic of this work.

The idea of bosonic stars dates back to Wheeler’s 1955 study of gravitational-electromagnetic entities or *geons* [?]. By generalising from real to complex-valued fundamental fields, it is even possible to obtain genuinely stationary solutions to the Einstein-matter equations. First established for spin 0 or scalar fields [?, ?, ?], this idea has more recently been extended to spin 1 or vector (aka *Proca*<sup>1</sup>) fields [?] as well as wider classes of scalar BSs [?, ?]. In the wake of the dramatic progress of numerical relativity in the simulations of black holes (BHs) [?, ?, ?] (see [?] for a review), the modelling of BSs and binary systems involving BSs has rapidly gathered pace.

The first BS models computed in the 1960s consisted of a massive but non-interacting complex scalar field  $\varphi$ . This class of stationary BSs, commonly referred to as *mini boson stars*, consists of a one parameter family of ground-state solutions characterised by the central scalar-field amplitude that reveals a stability structure analogous to that of Tolman-Oppenheimer-Volkoff [?, ?] stars: a stable and an unstable branch of ground-state solutions are separated by the configuration with maximal mass [?, ?, ?]. For each ground-state model, there furthermore exists a countable hierarchy of excited states with  $n > 0$  nodes in the scalar profile [?, ?, ?]. Numerical evolutions of these excited BSs demonstrate their unstable character, but also reveal significant variation in the instability time scales [?].

Whereas mini BS models are limited in terms of their maximum compactness, self-interacting scalar fields can result in significantly more compact stars, even denser than neutron stars [?, ?, ?, ?]. This raises

---

<sup>1</sup>Even though the term “boson star” generally applies to compact objects formed of any bosonic fields, it is often used to specifically denote stars made up of a *scalar* field. Stars composed of vector fields, in contrast, are most commonly referred to as *Proca* stars. Unless specified otherwise, we shall accordingly assume the term boson star to imply scalar-field matter.

the intriguing question whether compact BS binaries may reveal themselves through characteristic GW emission analogous to that from BHs or NSs [?]. Recent studies conclude that this may well be within the grasp of next-generation GW detectors and, in the case of favourable events, even with advanced LIGO [?, ?, ?].

One of the characteristic properties of BSs is the quantised nature of their spin. The linearised Einstein equations in the slow-rotation limit lead to a two-dimensional Poisson equation that does not admit everywhere regular solutions except for trivial constants; in consequence BSs cannot rotate perturbatively [?]. By relaxing the slow-rotation approximation, Schunck and Mielke [?] computed the first (differentially) rotating BSs and found that these solutions have an integer ratio of angular momentum to particle number. The structure of spinning BS models has been studied extensively over the years [?, ?, ?, ?, ?, ?, ?, ?]. The quantised nature of the angular momentum also applies to Proca and *Dirac* (spin  $\frac{1}{2}$ ) stars [?], but numerical studies of the formation of rotating stars have revealed a striking difference between the scalar and vector case: while collapsing scalar fields shed all their angular momentum through an axisymmetric instability, the collapse of vector fields results in spinning Proca stars with no indication of an instability [?, ?]. This observation is supported by analytic calculations [?], but the instability may be quenched by self-interaction terms in the potential function or in the Newtonian limit [?]. For further reviews of the structure and dynamics of single BSs, we note the reviews [?, ?, ?, ?].

The first simulations of BS binaries have considered the head-on collision of configurations with phase differences between the constituent stars or opposite frequencies [?]; see also [?, ?]. The phase or frequency differences manifest themselves most pronouncedly in the dynamics and GW emission at late times around merger. These collisions result in either a BH, a non-rotating BS or a near-annihilation of the scalar field in the case of opposite frequencies. BS binaries with orbital angular momentum generate a GW signal qualitatively similar to that of BH binaries during the inspiral phase, but exhibit a much more complex structure around merger [?, ?]. In agreement with the above mentioned BS formation studies, the BS inspirals also seem to avoid the formation of spinning BSs, although they may settle down into single nonrotating BSs.

In spite of the rapid progress of this field, the computation of GW templates for BSs still lags considerably behind that of BH binaries, both in terms of precision and coverage of the parameter space. Clearly, the presence of the matter fields adds complexity to this challenge, but also alleviates some of the difficulties through the non-singular character of the BS spacetimes. The first main goal of our study is to highlight the substantial risk of obtaining spurious physical results due to the use of overly simplistic initial data constructed by plain superposition of single-BS spacetimes. Our second main goal is to demonstrate how an astonishingly simple modification of the superposition procedure, first identified by Helfer *et al.* [?] for oscillatons, overcomes most of the problems encountered with plain superposition. We summarise our main findings as follows.

- (0) An adjustment of the superposition procedure, given by Eq. (3.3.3), results in a significant reduction of the constraint violations inherent to the initial data; see Fig. 3.3.
- (0) In the head-on collision of mini BS binaries with rather low compactness, we observe a significant drop of the radiated GW energy with increasing distance  $d$  if we use plain superposition. This physically unexpected dependence on the initial separation levels off only for rather large  $d \gtrsim 150 M$ , where  $M$  denotes the Arnowitt-Deser-Misner (ADM) mass [?]. In contrast, the total radiated energy computed from the evolution of our adjusted initial data displays the expected behaviour over the entire studied range  $75.5 M \leq d \leq 176 M$ : a very mild increase in the radiated energy with  $d$ . In the limit of large  $d \gtrsim 150 M$ , both types of simulations agree within numerical uncertainties; see upper panel in Fig. 3.6.
- (0) In collisions of highly compact BSs with solitonic potentials, the radiated energy is largely independent of the initial separations for both initial data types, but for plain superposition we consistently obtain  $\sim 10\%$  more radiation than for the adjusted initial data; see bottom panel in Fig. 3.6. Furthermore, we find plain superposition to result in a slightly faster infall. The most

dramatic difference, however, is the collapse into individual BHs of both BSs well before merger if we use plain superposition. No such collapse occurs if we use adjusted initial data. Rather, these lead to the expected near-constancy of the central scalar-field amplitude of the BSs throughout most of the infall; see Fig. 3.9.

- (0) We have verified through evolutions of single boosted BSs that the premature collapse into a BH is closely related to the spurious metric perturbation (3.3.2) that arises in the plain superposition procedure. Artificially adding the same perturbation to a single BS spacetime induces an unphysical collapse of the BS that is in qualitative and quantitative agreement with that observed in the binary evolution starting with plain superposition; see Fig. 3.9.

The detailed derivation of these results begins in Sec. 3.2 with a review of the formalism and the computational framework of our BS simulations. We discuss in more detail in Sec. 3.3 the construction of initial data through plain superposition and our modification of this method. In Sec. 3.4, we compare the dynamics of head-on collisions of mini BSs and highly compact solitonic BS binaries starting from both types of initial data. We note the substantial differences in the results thus obtained and argue why we regard the results obtained with our modification to be correct within numerical uncertainties. We summarise our findings and discuss future extensions of this work in Sec. 3.5.

Throughout this work, we use units where the speed of light and Planck's constant are set to unity,  $c = \hbar = 1$ . We denote spacetime indices by Greek letters running from 0 to 3 and spatial indices by Latin indices running from 1 to 3.

## 3.2 Formalism

### 3.2.1 Action and covariant field equations

The action for a complex scalar field  $\varphi$  minimally coupled to gravity is given by

$$S = \int \sqrt{-g} \left\{ \frac{1}{16\pi G} R - \frac{1}{2} [g^{\mu\nu} \nabla_\mu \bar{\varphi} \nabla_\nu \varphi + V(\varphi)] \right\} x, \quad (3.2.1)$$

where  $g_{\alpha\beta}$  denotes the spacetime metric and  $R$  the Ricci scalar associated with this metric. The characteristics of the resulting BS models depend on the scalar potential  $V(\varphi)$ ; in this work, we consider *mini boson stars* and *solitonic boson stars*, obtained respectively for the potential functions

$$V_{\min} = \mu^2 |\varphi|^2, \quad V_{\text{sol}} = \mu^2 |\varphi|^2 \left( 1 - 2 \frac{|\varphi|^2}{\sigma_0^2} \right)^2. \quad (3.2.2)$$

Here,  $\mu$  denotes the mass of the scalar field and  $\sigma_0$  describes the self-interaction in the solitonic potential which can result in highly compact stars [?]. Note that  $V_{\text{sol}} \rightarrow V_{\min}$  in the limit  $\sigma_0 \rightarrow \infty$ .

Variation of the action (3.2.1) with respect to the metric and the scalar field yield the Einstein and matter evolution equations

$$G_{\alpha\beta} = 8\pi G T_{\alpha\beta} = 8\pi G \left[ \partial_{(\alpha} \bar{\varphi} \partial_{\beta)} \varphi - \frac{1}{2} g_{\alpha\beta} (g^{\mu\nu} \partial_\mu \bar{\varphi} \partial_\nu \varphi + V(\varphi)) \right], \quad (3.2.3)$$

$$\nabla^\mu \nabla_\mu \varphi = \varphi V'(\varphi) \overline{|\varphi|^2} V. \quad (3.2.4)$$

Readers who are mainly interested in the results of our work and/or are familiar with the equations governing BS spacetimes may proceed directly to Sec. 3.3.

### 3.2.2 3+1 formulation

For all simulations performed in this work, we employ the 3+1 spacetime split of ADM [?] and York [?]; see also [?]. Here, the spacetime metric is decomposed into the physical 3-metric  $\gamma_{ij}$ , the shift vector  $\beta^i$



and the lapse function  $\alpha$  according to

$$s^2 = g_{\alpha\beta} x^\alpha x^\beta = -\alpha^2 t^2 + \gamma_{mn}(x^m + \beta^m t)(x^n + \beta^n t), \quad (3.2.5)$$

where the level sets  $x^0 = t = \text{const}$  represent three-dimensional spatial hypersurfaces with timelike unit normal  $n_\mu$ . Defining the extrinsic curvature

$$K_{ij} = -\frac{1}{2\alpha}(\partial_t \gamma_{ij} - \beta^m \partial_m \gamma_{ij} - \gamma_{im} \partial_j \beta^m - \gamma_{mj} \partial_i \beta^m), \quad (3.2.6)$$

the Einstein equations result in a first-order-in-time set of differential equations for  $\gamma_{ij}$  and  $K_{ij}$  that is readily converted into the conformal Baumgarte-Shapiro-Shibata-Nakamura-Oohara-Kojima (BSSNOK) formulation [?, ?, ?]. More specifically, we define

$$\begin{aligned} \chi &= \gamma^{-1/3}, \quad K = \gamma^{mn} K_{mn}, \quad \tilde{\gamma}_{ij} = \chi \gamma_{ij}, \\ \tilde{A}_{ij} &= \chi \left( K_{ij} - \frac{1}{3} \gamma_{ij} K \right), \quad \tilde{\Gamma}^i = \tilde{\gamma}^{mn} \tilde{\Gamma}_{mn}^i, \end{aligned} \quad (3.2.7)$$

where  $\gamma = \det \gamma_{ij}$ , and  $\tilde{\Gamma}_{mn}^i$  are the Christoffel symbols associated with  $\tilde{\gamma}_{ij}$ . The Einstein equations are then given by (see for example Sec. 6 in [?] for more details)

$$\partial_t \chi = \beta^m \partial_m \chi + \frac{2}{3} \chi (\alpha K - \partial_m \beta^m), \quad (3.2.8)$$

$$\partial_t \tilde{\gamma}_{ij} = \beta^m \partial_m \tilde{\gamma}_{ij} + 2 \tilde{\gamma}_{m(i} \partial_{j)} \beta^m - \frac{2}{3} \tilde{\gamma}_{ij} \partial_m \beta^m - 2\alpha \tilde{A}_{ij}, \quad (3.2.9)$$

$$\partial_t K = \beta^m \partial_m K - \chi \tilde{\gamma}^{mn} D_m D_n \alpha + \alpha \tilde{A}^{mn} \tilde{A}_{mn} + \frac{1}{3} \alpha K^2 + 4\pi G \alpha (S + \rho), \quad (3.2.10)$$

$$\begin{aligned} \partial_t \tilde{A}_{ij} &= \beta^m \partial_m \tilde{A}_{ij} + 2 \tilde{A}_{m(i} \partial_{j)} \beta^m - \frac{2}{3} \tilde{A}_{ij} \partial_m \beta^m + \alpha K \tilde{A}_{ij} - 2\alpha \tilde{A}_{im} \tilde{A}^m_j \\ &\quad + \chi (\alpha \mathcal{R}_{ij} - D_i D_j \alpha - 8\pi G \alpha S_{ij})^{\text{TF}}, \end{aligned} \quad (3.2.11)$$

$$\begin{aligned} \partial_t \tilde{\Gamma}^i &= \beta^m \partial_m \tilde{\Gamma}^i + \frac{2}{3} \tilde{\Gamma}^i \partial_m \beta^m - \tilde{\Gamma}^m \partial_m \beta^i + \tilde{\gamma}^{mn} \partial_m \partial_n \beta^i + \frac{1}{3} \tilde{\gamma}^{im} \partial_m \partial_n \beta^n \\ &\quad - \tilde{A}^{im} \left( 3\alpha \frac{\partial_m \chi}{\chi} + 2\partial_m \alpha \right) + 2\alpha \tilde{\Gamma}_{mn}^i \tilde{A}^{mn} - \frac{4}{3} \alpha \tilde{\gamma}^{im} \partial_m K - 16\pi G \frac{\alpha}{\chi} j^i, \end{aligned} \quad (3.2.12)$$

where ‘TF’ denotes the trace-free part and auxiliary expressions are given by

$$\begin{aligned} \Gamma_{jk}^i &= \tilde{\Gamma}_{jk}^i - \frac{1}{2\chi} (\delta^i_k \partial_j \chi + \delta^i_j \partial_k \chi - \tilde{\gamma}_{jk} \tilde{\gamma}^{im} \partial_m \chi), \\ \mathcal{R}_{ij} &= \tilde{\mathcal{R}}_{ij} + \mathcal{R}_{ij}^\chi, \\ \mathcal{R}_{ij}^\chi &= \frac{\tilde{\gamma}_{ij}}{2\chi} \left[ \tilde{\gamma}^{mn} \tilde{D}_m \tilde{D}_n \chi - \frac{3}{2\chi} \tilde{\gamma}^{mn} \partial_m \chi \partial_n \chi \right] + \frac{1}{2\chi} \left( \tilde{D}_i \tilde{D}_j \chi - \frac{1}{2\chi} \partial_i \chi \partial_j \chi \right), \\ \tilde{\mathcal{R}}_{ij} &= -\frac{1}{2} \tilde{\gamma}^{mn} \partial_m \partial_n \tilde{\gamma}_{ij} + \tilde{\gamma}_{m(i} \partial_{j)} \tilde{\Gamma}^m + \tilde{\Gamma}^m \tilde{\Gamma}_{(ij)m} + \tilde{\gamma}^{mn} \left[ 2\tilde{\Gamma}_{m(i}^k \tilde{\Gamma}_{j)kn} + \tilde{\Gamma}_{im}^k \tilde{\Gamma}_{k j n} \right], \\ D_i D_j \alpha &= \tilde{D}_i \tilde{D}_j \alpha + \frac{1}{\chi} \partial_{(i} \chi \partial_{j)} \alpha - \frac{1}{2\chi} \tilde{\gamma}_{ij} \tilde{\gamma}^{mn} \partial_m \chi \partial_n \alpha. \end{aligned} \quad (3.2.13)$$

Here,  $\tilde{D}$  and  $\tilde{\mathcal{R}}$  denote the covariant derivative and the Ricci tensor of the conformal metric  $\tilde{\gamma}_{ij}$ , respectively.

The matter terms in Eqs. (3.2.8)-(3.2.12) are defined by

$$\rho = T_{\mu\nu} n^\mu n^\nu, \quad j_\alpha = -\perp^\nu_\alpha T_{\mu\nu} n^\mu, \quad S_{\alpha\beta} = \perp^\mu_\alpha \perp^\nu_\beta T_{\mu\nu}, \quad \perp^\mu_\alpha = \delta^\mu_\alpha + n^\mu n_\alpha. \quad (3.2.14)$$

In adapted coordinates, we only need  $\rho$  and the spatial components  $j^i$ ,  $S_{ij}$  which are determined by the scalar field through Eq. (3.2.3). Defining, in analogy to the extrinsic curvature (3.2.6),

$$\Pi = -\frac{1}{2\alpha} (\partial_t \varphi - \beta^m \partial_m \varphi) \quad \Leftrightarrow \quad \partial_t \varphi = \beta^m \partial_m \varphi - 2\alpha \Pi, \quad (3.2.15)$$

we obtain

$$\begin{aligned}\rho &= 2\Pi\bar{\Pi} + \frac{1}{2}\partial^m\bar{\varphi}\partial_m\varphi + \frac{1}{2}V, & S + \rho &= 8\bar{\Pi}\Pi - V, \\ j_i &= \bar{\Pi}\partial_i\varphi + \Pi\partial_i\bar{\varphi}, \\ S_{ij} &= \partial_{(i}\bar{\varphi}\partial_{j)}\varphi - \frac{1}{2}\gamma_{ij}\left(\gamma^{mn}\partial_m\bar{\varphi}\partial_n\varphi - 4\bar{\Pi}\Pi + V\right).\end{aligned}\quad (3.2.16)$$

The evolution of the scalar field according to Eq. (3.2.4) in terms of our 3+1 variables is given by Eq. (3.2.15) and

$$\partial_t\Pi = \beta^m\partial_m\Pi + \alpha\left[\Pi K + \frac{1}{2}V'\varphi + \frac{1}{4}\tilde{\gamma}^{mn}\left(\partial_m\varphi\partial_n\chi - 2\chi\tilde{D}_m\tilde{D}_n\varphi\right)\right] - \frac{1}{2}\chi\tilde{\gamma}^{mn}\partial_m\varphi\partial_n\alpha, \quad (3.2.17)$$

where  $V' = V/(|\varphi|^2)$

Finally, we evolve the gauge variables  $\alpha$  and  $\beta^i$  with 1+log slicing and the  $\Gamma$ -driver condition (the so-called moving puncture conditions [?, ?]),

$$\partial_t\alpha = \beta^m\partial_m\alpha - 2\alpha K, \quad \partial_t\beta^i = \beta^m\partial_m\beta^i + \frac{3}{4}B^i, \quad \partial_tB^i = \beta^m\partial_mB^i + \partial_t\tilde{\Gamma}^i - \eta B^i, \quad (3.2.18)$$

where  $\eta$  is a constant we typically set to  $M\eta \approx 1$  in units of the ADM mass  $M$ .

Additionally to the evolution equations (3.2.8)-(3.2.12), the Einstein equations also imply four equations that do not contain time derivatives, the Hamiltonian and momentum constraints

$$\mathcal{H}\mathcal{R} + K^2 - K^{mn}K_{mn} - 16\pi\rho = 0, \quad (3.2.19)$$

$$\mathcal{M}_iD_iK - D_mK^m_i + 8\pi j_i = 0. \quad (3.2.20)$$

While the constraints are preserved under time evolution in the continuum limit, some level of violations is inevitable due to numerical noise or imperfections of the initial data. We will return to this point in more detail in Sec. 3.3 below.

For the time evolutions discussed in Sec. 3.4, we have implemented the equations of this section in the LEAN code [?] which is based on the CACTUS computational toolkit [?]. The equations are integrated in time with the method of lines using the fourth-order Runge-Kutta scheme with a Courant factor 1/4 and fourth-order spatial discretisation. Mesh refinement is provided by CARPET [?] in the form of “moving boxes” and we compute apparent horizons with AHFINDERDIRECT [?, ?].

### 3.2.3 Stationary boson stars and initial data

The initial data for our time evolution are based on single stationary BS solutions in spherical symmetry. Using spherical polar coordinates, areal radius and polar slicing, the line element can be written as

$$s^2 = -e^{2\Phi}t^2 + \left(1 - \frac{2m}{r}\right)^{-1}r^2 + r^2(\theta^2 + \sin^2\theta\phi^2). \quad (3.2.21)$$

where  $\Phi$  and  $m$  are functions of  $r$  only. It turns out convenient to express the complex scalar field in terms of amplitude and frequency,

$$\varphi(t, r) = A(r)e^{\omega t}, \quad \omega = \text{const} \in \mathbb{R}. \quad (3.2.22)$$

At this point, our configurations are characterised by two scales, the scalar mass  $\mu$  and the gravitational constant<sup>2</sup>  $G$ . In the following, we absorb  $\mu$  and  $G$  by rescaling all dimensional variables according to

$$\hat{t} = \mu t, \quad \hat{r} = \mu r, \quad \hat{m} = \mu m, \quad \hat{A} = \sqrt{G}A, \quad \hat{\omega} = \omega/\mu; \quad (3.2.23)$$

---

<sup>2</sup>Or, equivalently, the Planck mass  $M_{\text{Pl}} = \sqrt{\hbar c/G} = 1/\sqrt{G}$  for  $\hbar = c = 1$ .

note that  $\mu$  has the dimension of a frequency or wave number and  $\sqrt{G}$  is an inverse mass. Using the Planck mass  $M_{\text{Pl}} = 1/\sqrt{G} = 1.221 \times 10^{19}$  GeV, we can restore SI units from the dimensionless numerical variables according to

$$r = \hat{r} \times \left( \frac{\mu}{1.937 \times 10^{-10} \text{ eV}} \right)^{-1} \text{ km}, \quad \omega = \hat{\omega} \times \frac{\mu}{6.582 \times 10^{-16} \text{ eV}} \text{ Hz}, \quad A = \hat{A} M_{\text{Pl}},$$

and likewise for other variables. The rescaled version of the potential (3.2.2) is given by

$$\hat{V}_{\text{min}} = \hat{A}^2, \quad \hat{V}_{\text{sol}} = \hat{A}^2 \left( 1 - 2 \frac{\hat{A}^2}{\hat{\sigma}_0^2} \right)^2 \quad \text{with} \quad \hat{\sigma}_0 = \sqrt{G} \sigma_0. \quad (3.2.24)$$

In terms of the rescaled variables, the Einstein-Klein-Gordon equations in spherical symmetry become

$$\partial_{\hat{r}} \Phi = \frac{\hat{m}}{\hat{r}(\hat{r} - 2\hat{m})} + 2\pi\hat{r} \left( \hat{\eta}^2 + \hat{\omega}^2 e^{-2\Phi} \hat{A}^2 - \hat{V} \right), \quad (3.2.25)$$

$$\partial_{\hat{r}} \hat{m} = 2\pi\hat{r}^2 \left( \hat{\eta}^2 + \hat{\omega}^2 e^{-2\Phi} \hat{A}^2 + \hat{V} \right), \quad (3.2.26)$$

$$\partial_{\hat{r}} \hat{A} = \left( 1 - \frac{2\hat{m}}{\hat{r}} \right)^{-1/2} \hat{\eta}, \quad (3.2.27)$$

$$\partial_{\hat{r}} \hat{\eta} = -2 \frac{\hat{\eta}}{\hat{r}} - \hat{\eta} \partial_{\hat{r}} \Phi + \left( 1 - \frac{2\hat{m}}{\hat{r}} \right)^{-1/2} (\hat{V}' - \hat{\omega}^2 e^{-2\Phi}) \hat{A} \quad \text{with} \quad \hat{V}' = \frac{\hat{V}}{(\hat{A})^2}. \quad (3.2.28)$$

By regularity, we have the following boundary conditions at the origin  $\hat{r} = 0$  and at infinity,

$$\hat{A}(0) = \hat{A}_{\text{ctr}} \in \mathbb{R}^+, \quad \hat{m}(0) = 0, \quad \hat{\eta}(0) = 0, \quad \Phi(\infty) = 0, \quad \hat{A}(\infty) = 0. \quad (3.2.29)$$

This two-point-boundary-value problem has two free parameters, the central amplitude  $\hat{A}_{\text{ctr}}$  and the frequency  $\hat{\omega}$ . For a given value  $\hat{A}_{\text{ctr}}$ , however, only a discrete (albeit infinite) number of frequency values  $\hat{\omega}$  will result in models with  $\hat{A}(\infty) = 0$ ; all other frequencies lead to an exponentially divergent scalar field as  $r \rightarrow \infty$ . The “correct” frequencies are furthermore ordered by  $\hat{\omega}_n < \hat{\omega}_{n+1}$ , where  $n \geq 0$  is the number of zero crossings of the scalar profile  $\hat{A}(\hat{r})$ ;  $n = 0$  corresponds to the ground state and  $n > 0$  to the  $n^{\text{th}}$  excited state [?]. Finding the frequency for a regular star for user-specified  $\hat{A}_{\text{ctr}}$  and  $n$  is the key challenge in computing BS models. We obtain these solutions through a shooting algorithm, starting with the integration of Eqs. (3.2.25)-(3.2.28) outwards for  $\hat{A}(0) = \hat{A}_{\text{ctr}}$  specified,  $\Phi(0) = 1$ , and our “initial guess”  $\hat{\omega} = 1$ . Depending on the number of zero crossings in this initial-guess model, we repeat the calculation by increasing or decreasing  $\hat{\omega}$  by one order of magnitude until we have obtained an upper and a lower limit for  $\hat{\omega}$ . Through iterative bisection, we then rapidly converge to the correct frequency. Because we can only determine  $\hat{\omega}$  to double precision, we often find it necessary to capture the scalar field behaviour at large radius by matching to its asymptotic behaviour

$$\varphi \sim \frac{1}{\hat{r}} \exp \left( -\sqrt{1 - \hat{\omega}^2 e^{-2\Phi}} \right), \quad (3.2.30)$$

outside a user-specified radius  $\hat{r}_{\text{match}}$ . Finally, we can use an additive constant to shift the function  $\Phi(\hat{r})$  to match its outer boundary condition. In practice, we impose this condition in the form of the Schwarzschild relation  $e^{2\Phi} = (1 - 2\hat{m}/\hat{r})$  at the outer edge of our grid; in vacuum this is exact even at finite radius, and we can safely ignore the scalar field at this point thanks to its exponential falloff.

For a given potential, the solutions computed with this method form a one-parameter family characterised by the central scalar field amplitude  $\hat{A}_0$ . In Fig. 3.1 we display two such families for the potentials (3.2.24) with  $\hat{\sigma}_0 = 0.2$  in the mass-radius diagram using the areal radius  $\hat{r}_{99}$  containing 99% of the BS’s total mass. In that figure, we have also marked by circles two specific models, one mini BS and one solitonic

Model	$\sqrt{G}A_{\text{ctr}}$	$\sqrt{G}\sigma_0$	$\mu M_{\text{BS}}$	$\omega/\mu$	$\mu r_{99}$	$\max \frac{m(r)}{r}$
mini	0.0124	$\infty$	0.395	0.971	22.31	0.0249
sol	0.17	0.2	0.713	0.439	3.98	0.222

Table 3.1: Parameters of the two single, spherically symmetric ground state BS models employed for our simulations of head-on collisions. Up to the rescaling with the scalar mass  $\mu$ , each BS is determined by the central amplitude  $A_{\text{ctr}}$  of the scalar field and the potential parameter  $\sigma_0$  of Eq. (3.2.2). The mass  $M_{\text{BS}}$  of the boson star, the scalar field frequency  $\omega$ , the areal radius  $r_{99}$  containing 99 % of the total mass  $M_{\text{BS}}$  and the compactness, defined here as the maximal ratio of the mass function to radius, represent the main features of the stellar model.

BS, which we use in the head-on collisions in Sec. 3.4 below. We have chosen these two models to represent one highly compact and one rather squishy BS; note that both models are located to the right of the maximal  $\hat{M}(\hat{r})$  and, hence, stable stars. Their parameters and properties are summarised in Table 3.1.

The formalism discussed so far provides us with BS solutions in radial gauge and polar slicing. In order to reduce the degree of gauge adjustment in our moving puncture time evolutions, however, we prefer using conformally flat BS models in isotropic gauge. In isotropic coordinates, the line element of a spherically symmetric spacetime has the form

$$\mu^2 s^2 = -e^{2\Phi} \hat{t}^2 + \psi^4 (\hat{R}^2 + \hat{R}^2 \Omega^2), \quad (3.2.31)$$

where  $\Omega^2 = \theta^2 + \sin^2 \theta \phi^2$ . Comparing this with the polar-areal line element (3.2.21), we obtain two conditions,

$$\psi^4 \hat{R}^2 = \hat{r}^2, \quad \psi^4 \hat{R}^2 = X^2 \hat{r}^2 \quad \text{with} \quad X = \left(1 - \frac{2\hat{m}}{\hat{r}}\right)^{-1/2}. \quad (3.2.32)$$

In terms of the new variable  $f(\hat{r}) = \hat{R}/\hat{r}$ , we obtain the differential equation

$$\frac{f}{\hat{r}} = \frac{f}{\hat{r}} (X - 1), \quad (3.2.33)$$

which we integrate outwards by assuming  $\hat{R} \propto \hat{r}$  near  $\hat{r} = 0$ . The integrated solution can be rescaled by a constant factor to ensure that at large radii – where the scalar field has dropped to a negligible level – we recover the Schwarzschild value  $\psi = 1 + \frac{\hat{m}}{2\hat{R}}$ , in accordance with Birkhoff’s theorem. Bearing in mind that  $\psi^4 \hat{R}^2 = \hat{r}^2$ , this directly leads to the outer boundary condition

$$\hat{R}_{\text{ob}} = \frac{\hat{r}_{\text{ob}} - \hat{m}_{\text{ob}}}{2} \left[ 1 + \sqrt{1 - \frac{\hat{m}_{\text{ob}}^2}{(\hat{r}_{\text{ob}} - \hat{m}_{\text{ob}})^2}} \right], \quad (3.2.34)$$

end, hence, the overall scaling factor applied to the function  $\hat{R}(\hat{r})$ .

In isotropic coordinates, the resulting spacetime metric is trivially converted from spherical to Cartesian coordinates  $\hat{x}^i = (\hat{x}, \hat{y}, \hat{z})$  using  $\hat{R}^2 + \hat{R}^2 \Omega^2 = \hat{x}^2 + \hat{y}^2 + \hat{z}^2$ , so that

$$\mu^2 s^2 = -e^{2\Phi} \hat{t}^2 + \psi^4 \delta_{ij} \hat{x}^i \hat{x}^j. \quad (3.2.35)$$

For convenience, will drop the caret on the rescaled coordinates and variables from now on and implicitly assume that they represent dimensionless quantities to be converted into dimensional form according to Eq. (3.2.23).

### 3.2.4 Boosted boson stars

The single BS solutions can be converted into boosted stars through a straightforward Lorentz transformation. For this purpose, we denote the star's rest frame by  $\mathcal{O}$  with Cartesian 3+1 coordinates  $x^\alpha = (t, x^k)$  and consider a second frame  $\tilde{\mathcal{O}}$  with Cartesian 3+1 coordinates  $\tilde{x}^{\tilde{\alpha}} = (\tilde{t}, \tilde{x}^{\tilde{k}})$  that moves relative to  $\mathcal{O}$  with constant velocity  $v^i$ . These two frames are related by the transformation

$$\Lambda^{\tilde{\alpha}}_{\mu} = \left( \frac{\gamma}{-\gamma v^i} \middle| \frac{-\gamma v_j}{\delta^i_j + (\gamma - 1) \frac{v^i v_j}{|v|^2}} \right) \Leftrightarrow \Lambda^{\mu}_{\tilde{\alpha}} = \left( \frac{\gamma}{\gamma v^i} \middle| \frac{\gamma v_j}{\delta^i_j + (\gamma - 1) \frac{v^i v_j}{|v|^2}} \right).$$

Starting with the isotropic rest-frame metric (3.2.31) and the complex scalar field  $\varphi(t, R) = A(R)e^{\omega t + \vartheta_0}$  with  $R = \sqrt{\delta_{mn}x^m x^n}$ , we obtain a general boosted model in terms of the 3+1 variables in Cartesian coordinates  $\tilde{x}^{\tilde{k}}$  as follows.

- (0) A straightforward calculation leads to the first derivatives of the metric, its inverse and the scalar field in Cartesian coordinates  $x^i$  in the rest frame,

$$\begin{aligned} \partial_t g_{\mu\nu} &= \partial_t g^{\mu\nu} = 0, & \partial_t \varphi_R &= -\omega \varphi_I, & \partial_t \varphi_I &= \omega \varphi_R, \\ \partial_i g_{00} &= -2e^{2\Phi} \frac{\Phi}{R} \frac{x^i}{R}, & \partial_i g^{00} &= 2e^{-2\Phi} \frac{\Phi}{R} \frac{x^i}{R}, \\ \partial_i g_{kk} &= 4\psi^3 \frac{\psi}{R} \frac{x^i}{R}, & \partial_i g^{kk} &= -4\psi^{-5} \frac{\psi}{R} \frac{x^i}{R}, \\ \partial_i \varphi_R &= \frac{\eta}{f} \cos(\omega t + \phi_0) \frac{x^i}{R}, & \partial_i \varphi_I &= \frac{\eta}{f} \sin(\omega t + \phi_0) \frac{x^i}{R}, \end{aligned} \quad (3.2.36)$$

where  $\varphi_R$  and  $\varphi_I$  are the real and imaginary part of the scalar field, and

$$\frac{\psi}{R} = -\frac{1}{2} \frac{X-1}{X} \frac{\psi}{R}, \quad \frac{\Phi}{R} = \frac{X^2-1}{2XR} + \frac{2\pi R}{f^2} X(\eta^2 + \omega^2 e^{-2\Phi} A^2 - V). \quad (3.2.37)$$

- (0) We Lorentz transform the spacetime metric, the scalar field and their derivatives to the boosted frame  $\tilde{\mathcal{O}}$  according to

$$\begin{aligned} \tilde{g}_{\tilde{\alpha}\tilde{\beta}} &= \Lambda^{\mu}_{\tilde{\alpha}} \Lambda^{\nu}_{\tilde{\beta}} g_{\mu\nu}, & \tilde{g}^{\tilde{\alpha}\tilde{\beta}} &= \Lambda^{\tilde{\alpha}}_{\mu} \Lambda^{\tilde{\beta}}_{\nu} g^{\mu\nu}, & \partial_{\tilde{\gamma}} \tilde{g}_{\tilde{\alpha}\tilde{\beta}} &= \Lambda^{\lambda}_{\tilde{\gamma}} \Lambda^{\mu}_{\tilde{\alpha}} \Lambda^{\nu}_{\tilde{\beta}} \partial_{\lambda} g_{\mu\nu}, \\ \tilde{\varphi}(\tilde{x}^{\alpha}) &= \varphi(x^{\mu}), & \partial_{\tilde{\alpha}} \tilde{\varphi} &= \Lambda^{\mu}_{\tilde{\alpha}} \partial_{\mu} \varphi. \end{aligned} \quad (3.2.38)$$

- (0) We construct the 3+1 variables in the boosted frame from these quantities according to

$$\tilde{\alpha} = \left( -\tilde{g}^{\tilde{0}\tilde{0}} \right)^{-1/2}, \quad \tilde{\beta}_{\tilde{k}} = \tilde{g}_{\tilde{0}\tilde{k}}, \quad \tilde{\gamma}_{\tilde{k}\tilde{l}} = \tilde{g}_{\tilde{k}\tilde{l}}, \quad \tilde{\beta}^{\tilde{k}} = \tilde{\gamma}^{\tilde{k}\tilde{m}} \tilde{\beta}_{\tilde{m}}, \quad (3.2.39)$$

$$\begin{aligned} \tilde{K}_{\tilde{k}\tilde{l}} &= -\frac{1}{2\tilde{\alpha}} \left( \partial_{\tilde{t}} \tilde{\gamma}_{\tilde{k}\tilde{l}} - \tilde{\beta}^{\tilde{m}} \partial_{\tilde{m}} \tilde{\gamma}_{\tilde{k}\tilde{l}} - \tilde{\gamma}_{\tilde{m}\tilde{l}} \partial_{\tilde{k}} \tilde{\beta}^{\tilde{m}} - \tilde{\gamma}_{\tilde{k}\tilde{m}} \partial_{\tilde{l}} \tilde{\beta}^{\tilde{m}} \right), \\ \tilde{\Pi} &= -\frac{1}{2\tilde{\alpha}} \left( \partial_{\tilde{t}} \tilde{\varphi} - \tilde{\beta}^{\tilde{m}} \partial_{\tilde{m}} \tilde{\varphi} \right), \end{aligned} \quad (3.2.40)$$

with

$$\partial_{\tilde{t}} \tilde{\gamma}_{\tilde{k}\tilde{l}} = \partial_{\tilde{0}} \tilde{g}_{\tilde{k}\tilde{l}}, \quad \tilde{\gamma}_{\tilde{k}\tilde{m}} \partial_{\tilde{l}} \tilde{\beta}^{\tilde{m}} = \partial_{\tilde{l}} \tilde{g}_{\tilde{0}\tilde{k}} - \tilde{\beta}^{\tilde{m}} \partial_{\tilde{l}} \tilde{g}_{\tilde{k}\tilde{m}}. \quad (3.2.41)$$

- (0) In addition to these expressions, we need to bear in mind the coordinate transformation. The computational domain of our time evolution corresponds to the boosted frame  $\tilde{\mathcal{O}}$ . A point  $\tilde{x}^{\tilde{\alpha}} = (\tilde{t}, \tilde{x}^{\tilde{k}})$  in that domain therefore has rest-frame coordinates

$$(t, x^k) = x^{\mu} = \Lambda^{\mu}_{\tilde{\alpha}} \tilde{x}^{\tilde{\alpha}}. \quad (3.2.42)$$

It is at  $(t, x^k)$ , where we need to evaluate the rest frame variables  $\Phi(R)$ ,  $X(R)$ , the scalar field  $\varphi(t, R)$  and their derivatives. In particular, different points on our initial hypersurface  $\tilde{t} = 0$  will in general correspond to different times  $t$  in the rest frame.

### 3.3 Boson-star binary initial data

The single BS models constructed according to the procedure of the previous section are exact solutions of the Einstein equations, affected only by a numerical error that we can control by increasing the resolution, the size of the computational domain and the degree of precision of the floating point variable type employed. The construction of binary initial data is conceptually more challenging due to the non-linear character of the Einstein equations; the superposition of two individual solutions will, in general, not constitute a new solution. Instead, such a superposition incurs some violation of the constraint equations (3.2.19), (3.2.20). The purpose of this section is to illustrate how we can substantially reduce the degree of constraint violation with a relatively simple adjustment in the superposition. Before introducing this “trick”, we first summarise the superposition as it is commonly used in numerical simulations.

#### 3.3.1 Simple superposition of boson stars

The most common configuration involving more than one BS is a binary system, and this is the scenario we will describe here. We note, however, that the method generalises straightforwardly to any number of stars. Let us then consider two individual BS solutions with their centres located at  $x_A^i$  and  $x_B^i$ , velocities  $v_A^i$  and  $v_B^i$ . The two BS spacetimes are described by the 3+1 (ADM) variables  $\gamma_{ij}^A$ ,  $\alpha_A$ ,  $\beta_A^i$  and  $K_{ij}^A$ , the scalar field variables  $\varphi_A$  and  $\Pi_A$ , and likewise for star B. We can construct from these individual solutions an approximation for a binary BS system via the pointwise superposition

$$\begin{aligned}\gamma_{ij} &= \gamma_{ij}^A + \gamma_{ij}^B - \delta_{ij}, & K_{ij} &= \gamma_{m(i} \left[ K_{j)n}^A \gamma_A^{nm} + K_{j)n}^B \gamma_B^{nm} \right], \\ \varphi &= \varphi_A + \varphi_B, & \Pi &= \Pi_A + \Pi_B.\end{aligned}\tag{3.3.1}$$

One could similarly construct a superposition for the lapse  $\alpha$  and shift vector  $\beta^i$ , but their values do not affect the physical content of the initial hypersurface. In our simulations we instead initialise them by  $\alpha = \sqrt{\chi}$  and  $\beta^i = 0$ .

A simple superposition approach along the lines of Eq. (3.3.1) has been used in numerous studies of BS as well as BH binaries including higher-dimensional BHs [?, ?, ?, ?, ?, ?]. For BHs and higher-dimensional spacetimes in particular, this leading-order approximation has proved remarkably successful and in some limits a simple superposition is exact, such as infinite initial separation, in Brill-Lindquist initial data for non-boosted BHs<sup>7</sup> [?] or in the superposition of Aichelburg-Sexl shockwaves [?] for head-on collisions of BHs at the speed of light. It has been noted in Helfer *et al.* [?], however, that this simple construction can result in spurious low-frequency amplitude modulations in the time evolution of binary oscillatons (real-scalar-field cousins of BSs); cf. their Fig. 7. Furthermore, they have proposed a straightforward remedy that essentially eliminates this spurious modulation. As we will see in the next section, the repercussions of the *simple superposition* according to Eqs. (3.3.1) can be even more dramatic for BS binaries, but they can be cured in the same way as in the oscillaton case. We note in this context that BSs may be more vulnerable to superposition artefacts near their centres due to the lack of a horizon and its potentially protective character in the superposition of BHs.

The key problem of the construction (3.3.1) is the equation for the spatial metric  $\gamma_{ij}$ . This is best illustrated by considering the centre  $x_A^i$  of star A. In the limit of infinite separation, the metric field of its companion star B becomes  $\gamma_{ij}^B \rightarrow \delta_{ij}$ . This is, of course, precisely the contribution we subtract in the third term on the right-hand-side and all would be well. In practice, however, the BSs start from initial positions  $x_A^i$  and  $x_B^i$  with finite separation  $d = ||x_A^i - x_B^i||$  and we consequently perturb the metric at star A’s centre by

$$\delta\gamma_{ij} = \gamma_{ij}^B(x_A^i) - \delta_{ij}\tag{3.3.2}$$

away from its equilibrium value  $\gamma_{ij}^A(x_A^i)$ . This metric perturbation can be interpreted as a distortion of the volume element  $\sqrt{\gamma}$  at the centre of star A. More specifically, the volume element at star A’s

<sup>7</sup>Note that for Brill-Lindquist one superposes the conformal factor  $\psi$  rather than  $\psi^4$  as in the method discussed here.

centre is enhanced by  $\mathcal{O}(1)\%$  for initial separations  $\mathcal{O}(100)M$  and likewise for the centre of star B (by symmetry); see appendix A of Ref. [?] for more details.<sup>8</sup> The energy density  $\rho$ , on the other hand, is barely altered by the presence of the other star, because of the exponential fall-off of the scalar field. The leading-order error therefore consists in a small excess mass that has been added to each BS’s central region. We graphically illustrate this effect in the upper half of Fig. 3.2 together with some of the possible consequences. As we will see, this qualitative interpretation is fully borne out by the phenomenology we observe in the binaries’ time evolutions.

Finally, we would like to emphasise that, while evaluating the constraint violations is in general a good rule of thumb to check whether the field configuration is a solution of the system, it does *not* inform one whether it is *the intended* solution; a system with some constraint violation may have drifted closer to a different, unintended solution. In the present case, in addition to the increased constraint violation, the constructed BS solutions possess significant excitations. Thus, while applying a constraint damping system like conformal Z4 [?, ?] may eventually drive the system to a solution, it may no longer be what was originally intended to be the initial condition of an unexcited BS star.

### 3.3.2 Improved superposition

The problem of the simple superposition is encapsulated by Eq. (3.3.2) and the resulting deviation of the volume elements at the stars’ centres away from their equilibrium values. At the same time, the equation presents us with a concrete recipe to mitigate this error: we merely need to replace in the simple superposition (3.3.1) the first relation  $\gamma_{ij} = \gamma_{ij}^A + \gamma_{ij}^B - \delta_{ij}$  by

$$\gamma_{ij} = \gamma_{ij}^A + \gamma_{ij}^B - \gamma_{ij}^B(x_A^i) = \gamma_{ij}^A + \gamma_{ij}^B - \gamma_{ij}^A(x_B^i). \quad (3.3.3)$$

The two expressions on the right-hand side are indeed equal thanks to the symmetry of our binary: its constituents have equal mass, no spin and their velocity components satisfy  $v_A^i v_A^j = v_B^i v_B^j$  for all  $i, j = 1, 2, 3$  in the centre-of-mass frame. Equation (3.3.3) manifestly ensures that at positions  $x_A^i$  and  $x_B^i$  we now recover the respective star’s equilibrium metric and, hence, volume element. We graphically illustrate this improvement in the bottom panel of Fig. 3.2.

A minor complication arises from the fact that the resulting spatial metric does not asymptote towards  $\delta_{ij}$  as  $R \rightarrow \infty$ . We accordingly impose outgoing Sommerfeld boundary conditions on the asymptotic background metric  $2\delta_{ij} - \gamma_{ij}^A(x_B^i)$ ; in a set of test runs, however, we find this correction to result in very small changes well below the simulation’s discretisation errors.

Finally, we note that the leading-order correction to the superposition as written in Eq. (3.3.3) does not work for asymmetric configurations with unequal masses or spins. Generalising the method to arbitrary binaries requires the subtraction of a spatially varying term rather than a constant  $\gamma_{ij}^B(x_A^i) = \gamma_{ij}^A(x_B^i)$  or  $\delta_{ij}$ . Such a generalisation may consist, for example, of a weighted sum of the terms  $\gamma_{ij}^A(x_B^i)$  and  $\gamma_{ij}^B(x_A^i)$ . Leaving this generalisation for future work, we will focus on equal-mass systems in the remainder of this study and explore the degree of improvement achieved with Eq. (3.3.3).

## 3.4 Models and results

For our analysis of the two types of superposed initial data, we will now discuss time evolutions of binary BS head-on collisions. A head-on collision is characterised by the two individual BS models and three further parameters, the initial separation in units of the ADM mass,  $d/M$ , and the initial velocities  $v_A$  and  $v_B$  of the BSs. We perform all our simulations in the centre-of-mass frame, so that for equal-mass binaries,  $v_A = -v_B v$ . One additional parameter arises from the type of superposition used for the initial data construction: we either use the “plain” superposition of Eq. (3.3.1) or the “adjusted” method (3.3.3).

<sup>8</sup>Due to the slow decay of this effect  $\propto 1/\sqrt{d}$  [?], a simple cure in terms of using larger  $d$  is often not practical.

Label	star A	star B	$v$	initial data	$d/M$
<b>mini</b>	mini	mini	0.1	plain	75.5, 101, 126, 151, 176
<b>+mini</b>	mini	mini	0.1	adjusted	75.5, 101, 126, 151, 176
<b>sol</b>	sol	sol	0.1	plain	16.7, 22.3, 27.9, 33.5, 39.1
<b>+sol</b>	sol	sol	0.1	adjusted	16.7, 22.3, 27.9, 33.5, 39.1

Table 3.2: The four types of BS binary head-on collisions simulated in this study. The individual BSs A and B are given either by the mini or solitonic model of Table 3.1, and start with initial velocity  $v$  directed towards each other. The initial data is constructed either by plain superposition (3.3.1) or by adjusting the superposed data according to Eq. (3.3.3). For each type of binary, we perform five collisions with initial separations  $d$  listed in the final column.

For all our simulations, we set  $v = 0.1$ ; this value allows us to cover a wide range of initial separations without the simulations becoming prohibitively long. The BS binary configurations summarised in Table 3.2 then result in four sequences of head-on collisions labelled **mini**, **+mini**, **sol** and **+sol**, depending in the nature of the constituent BSs and the superposition method. For each sequence, we vary the BSs initial separation  $d$  to estimate the dependence of the outcome on  $d$ . First, however, we test our interpretation of the improved superposition (3.3.3) by computing the level of constraint violations in the initial data.

### 3.4.1 Initial constraint violations

As discussed in Sec. 3.3.1 and in Appendix A of Ref. [?], the main shortcoming of the plain superposition procedure consists in the distortion of the volume element near the individual BSs' centres and the resulting perturbation of the mass-energy inside the stars away from their equilibrium values. If this interpretation is correct, we would expect this effect to manifest itself in an elevated level of violation of the Hamiltonian constraint (3.2.19) which relates the energy density to the spacetime curvature. Put the other way round, we would expect our improved method (3.3.3) to reduce the Hamiltonian constraint violation. This is indeed the case as demonstrated in the upper panels of Fig. 3.3 where we plot the Hamiltonian constraint violation of the initial data along the collision axis for the configurations **mini** and **+mini** with  $d = 101 M$  and the configurations **sol** and **+sol** with  $d = 22.3 M$ .

In the limit of zero boost velocity  $v = 0$ , this effect is even tractable through an analytic calculation which confirms that the improved superposition (3.3.3) ensures  $\mathcal{H} = 0$  at the BS's centres in isotropic coordinate; see 3.6 for more details.

Our adjustment (3.3.3) also leads to a reduction of the momentum constraint violations of the initial data, although the effect is less dramatic here. The bottom panels of Fig. 3.3 display the momentum constraint  $\mathcal{M}_x$  of Eq. (3.2.20) along the collision axis normalised by the momentum density  $8\pi j_x$ ; we see a reduction by a factor of a few over large parts of the BS interior for the modified data **+mini** and **+sol**.

The overall degree of initial constraint violations is rather small in all cases, well below 0.1% for our adjusted data. These data should therefore also provide a significantly improved initial guess for a full constraint solving procedure. We leave such an analysis for future work and in the remainder of the work explore the impact of the adjustment (3.3.3) on the physical results obtained from the initial data's time evolutions.

### 3.4.2 Convergence and numerical uncertainties

In order to put any differences in the time evolutions into context, we need to understand the uncertainties inherent to our numerical simulations. For this purpose, we have studied the convergence of the GW radiation generated by the head-on collisions of mini and solitonic BSs.



Figure 3.4 displays the convergence of the radiated energy  $E_{\text{rad}}$  as a function of time for the **+mini** configuration with  $d = 101 M$  of Table 3.1 obtained for grid resolutions  $h_1 = M/6.35$ ,  $h_2 = M/9.53$  and  $h_3 = M/12.70$  on the innermost refinement level and corresponding grid spacings on the other levels. The functions  $E_{\text{rad}}(t)$  and their differences are shown in the bottom and top panel, respectively, of Fig. 3.4 together with an amplification of the high-resolution differences by the factor  $Q_2 = 2.86$  for second-order convergence. The observation of second-order convergence is compatible with the second-order ingredients of the LEAN code, prolongation in time and the outgoing radiation boundary conditions. We believe that this dominance is mainly due to the smooth behaviour of the BS centre as compared with the case of black holes [?]. By using the second-order Richardson extrapolated result, we determine the discretisation error of our energy estimates as 0.9% for  $h_3$  which is the resolution employed for all remaining mini BS collisions. We have performed the same convergence analysis for the plain-superposition counterpart **mini** and for the dominant  $(\ell, m) = (2, 0)$  multipole of the Newman-Penrose scalar of both configurations and obtained the same convergence and very similar relative errors.

In Fig. 3.5, we show the same convergence analysis for the solitonic collision **+sol**i with  $d = 22.3 M$  and resolutions  $h_1 = M/22.9$ ,  $h_2 = M/45.9$ ,  $h_3 = M/68.8$ . We observe second-order convergence during merger and ringdown and slightly higher convergence in the earlier infall phase. For the uncertainty estimate we conservatively use the second-order Richardson extrapolated result and obtain a discretisation error of about 0.07% for our medium resolution  $h_2$  which is the value we employ in our solitonic production runs. Again, we have repeated this analysis for the plain **sol**i counterpart and the  $(2, 0)$  GW multipole observing the same order of convergence and similar uncertainties. Our error estimate for the solitonic configurations is rather small in comparison to the mini BS collisions and we cannot entirely rule out a fortuitous cancellation of errors in our simulations. From this point on, we therefore use a conservative discretisation error estimate of 1% for all our BS simulations.

A second source of uncertainty in our results is due to the extraction of the GW signal at finite radii rather than  $\mathcal{I}^+$ . We determine this error by extracting the signal at multiple radii, fitting the resulting data by the series expansion  $f = f_0 + f_1/r$ , and comparing the result at our outermost extraction radius with the limit  $f_0$ . This procedure results in errors in  $E_{\text{rad}}$  ranging between 0.5% and 3%. With the upper range, we arrive at a conservative total error budget for discretisation and extraction of about 4%. As a final test, we have repeated the **mini** and **+mini** collisions for  $d = 101 M$  with the independent GRCHOMBO code [?, ?] using the CCZ4 formulation [?] and obtain the same results within  $\approx 1.5\%$ . Bearing in mind these tests and a 4% error budget, we next study the dynamics of the BS head-on collisions with and without our adjustment of the initial data.

### 3.4.3 Radiated gravitational-wave energy

For our first test, we compute the total radiated GW energy for all our head-on collisions focusing in particular on its dependence on the initial separation  $d$  of the BS centres. In this estimate we exclude any spurious or “junk” radiation content of the initial data by starting the integration at  $t = R_{\text{ex}} + 40 M$ . Unless specified otherwise, all our results are extracted at  $R_{\text{ex}} = 300 M$  for mini BS collisions and  $R_{\text{ex}} = 84 M$  for the solitonic binaries.

The main effect of increasing the initial separation is a reduction of the (negative) binding energy of the binary and a corresponding increase of the collision velocity around merger. In the large  $d$  limit, however, this effect becomes negligible. For the comparatively large initial separations chosen in our collisions, we would therefore expect the function  $E_{\text{rad}}$  to be approximately constant, possibly showing a mild increase with  $d$ . The mini BS collisions shown as black  $\times$  symbols in the upper panel of Fig. 3.6 exhibit a rather different behaviour: the radiated energy rapidly decreases with  $d$  and only levels off for  $d \gtrsim 150 M$ . We have verified that the excess energy for smaller  $d$  is not due to an elevated level of junk radiation which consistently contribute well below 0.1% of  $E_{\text{rad}}$  in all our mini BS collisions and has been excluded from the results of Fig. 3.6 anyway. The **+mini** BS collisions, in contrast, results in an approximately constant  $E_{\text{rad}}$  with a total variation approximately at the level of the numerical uncertainties. For  $d \gtrsim 150 M$ ,

both types of initial data yield compatible results, as is expected. The key benefit of our adjusted initial data is that they provide reliable results even for smaller initial separations suitable for starting BS inspirals.

The discrepancy is less pronounced for the head-on collisions of solitonic BS collisions; both types of initial data result in approximately constant  $E_{\text{rad}}$ . They differ, however, in the predicted amount of radiation at a level that is significant compared to the numerical uncertainties. As we will see below, this difference is accompanied by drastic differences in the BS's dynamics during the long infall period. We furthermore note that the mild but steady increase obtained for the adjusted **+sol**i agrees better with the physical expectations.

The differences in the total radiated GW energy also manifest themselves in different amplitudes of the  $(2, 0)$  multipole of the Newman-Penrose scalar  $\Psi_4$ . This is displayed in Figs. 3.7 and 3.8 where we show the GW modes for the mini and solitonic collisions, respectively. The most prominent difference between the results for plain and adjusted initial data is the significant variation of the amplitude of the  $(2, 0)$  mode in the plain mini BS collisions in the upper panel of Fig. 3.7. In contrast, the differences in the amplitudes in Fig. 3.8 for the solitonic collisions are very small. In fact, the differences in the radiated energy of the **sol**i and **+sol**i collisions mostly arise from a minor stretching of the signal for the **sol**i case; this effect is barely perceptible in Fig. 3.8 but is amplified by the integration in time when we calculate the energy. Finally, we note the different times of arrival of the main pulses in Fig. 3.8; especially for larger initial separation, the merger occurs earlier for the **sol**i configurations than for their adjusted counterparts **+sol**i. We will discuss this effect together with the evolution of the scalar field amplitude in the next subsection.

#### 3.4.4 Evolution of the scalar amplitude and gravitational collapse

The adjustment (3.3.3) in the superposition of oscillatons was originally developed in Ref. [?] to reduce spurious modulations in the scalar field amplitude; cf. their Fig. 7. In our simulations, this effect manifests itself most dramatically in the collisions of our solitonic BS configurations **sol**i and **+sol**i. From Fig. 3.1, we recall that the single-BS constituents of these binaries are stable, but highly compact stars, located fairly close to the instability threshold. We would therefore expect them to be more sensitive to spurious modulations in their central energy density. This is exactly what we observe in all time evolutions of the **sol**i configurations starting with plain-superposition initial data. As one example, we show in Fig. 3.9 the scalar amplitude at the individual BS centres and the BS trajectories as functions of time for the **sol**i and **+sol**i configurations starting with initial separation  $d = 22.3 M$ . Let us first consider the **sol**i configuration using plain superposition displayed by the solid (black) curves. In the upper panel of Fig. 3.9, we clearly see that the scalar amplitude steadily increases, reaching a maximum around  $t \approx 30 M$  and then rapidly drops to a near-zero level. Our interpretation of this behaviour as a collapse to a BH is confirmed by the horizon finder which reports an apparent horizon of irreducible mass  $m_{\text{irr}} = 0.5 M$  just before the scalar field amplitude collapses; the time of the first identification of an apparent horizon is marked by the vertical dotted black line at  $t \approx 30 M$ . For reference we plot in the bottom panel the trajectory of the BS centres along their collision (here the  $x$ ) axis. In agreement with the horizon mass  $m_{\text{irr}} = 0.5 M$ , the trajectory clearly indicates that around  $t \approx 30 M$ , the BSs are still far away from merging into a single BH; in units of the ADM mass, the individual BS radius is  $r_{99} = 2.78 M$ . We interpret this early BH collapse as a spurious feature due to the use of plain superposition in the initial data construction. This behaviour is also seen in the case of the real scalar field oscillatons in [?].

We have tested this hypothesis with the evolution of the adjusted initial data. These exhibit a drastically different behaviour in the collision **+sol**i displayed by the dashed (red) curves in Fig. 3.9. Throughout most of the infall, the central scalar amplitude is constant, it increases mildly when the BS trajectories meet near  $x = 0$ , and then rapidly drops to zero. Just as the maximum amplitude is reached, the horizon finder first computes an apparent horizon, now with  $m_{\text{irr}} = 0.99 M$ , as expected for a BH resulting from the merger; see the vertical red line in the figure.

As a final test of our interpretation, we compare the behaviour of the binary constituents with that of single BSs boosted with the same velocity  $v = 0.1$ . As expected, the scalar field amplitude at the centre of such a single BS remains constant within high precision, about  $\mathcal{O}(10^{-5})$ , on the timescale of our collisions. We have then repeated the single BS evolution by poisoning the initial data with the very same term (3.3.2) that is also added near a single BS's centre by the plain-superposition procedure. The resulting scalar amplitude at the centre of this poisoned BS is shown as the dash-dotted (blue) curve in Fig. 3.9 and nearly overlaps with the corresponding curve of the `sol`i binary. Furthermore, the poisoned single BS collapses into a BH after nearly the same amount of time as indicated by the vertical blue dotted curve in the figure<sup>5</sup>. Clearly this behaviour of the single boosted BS is unphysical, and strongly indicates that the plain superposition of initial data introduces the same unphysical behaviour to our `sol`i binary constituents. We have repeated this analysis for our entire sequence of `sol`i binaries with very similar results: the individual BSs always collapse to distinct BHs about  $\Delta t \approx 50 M$  before the binary merger.

Finally, the trajectories in the bottom panel of Fig. 3.9 indicate that the BS merger occurs a bit later for the `+sol`i case than its plain-superposition counterpart `sol`i. This is indeed a systematic effect we see for all initial separations  $d$  and which agrees with the different arrival times of the peak GW signals that we have already noticed in Fig. 3.8. We do not have a rigorous explanation of this effect, but note that the two trajectories in Fig. 3.9 start diverging right at the time of spurious BH formation in the `sol`i binary. Perhaps some of the binding energy in BS collisions is converted into deformation energy rather than simply kinetic energy of the stars' centres of mass, slowing down the infall compared to the BH case<sup>6</sup>. Another explanation may consider the generally repulsive character of the scalar field which endows it with support against gravitational collapse. When the infalling BSs collapse to BHs, the scalar field essentially disappears as a potentially repulsive ingredient and the ensuing collision is sped up. Whatever ultimately generates this effect, the key observation of our study is that even rather mild imperfections in the initial data can drastically affect the physical outcome of the time evolution.

### 3.5 Conclusions

We have simulated head-on collisions of equal-mass, non-spinning boson stars and the GW radiation generated in the process. The main focus of our study is the construction of BS binary initial data and the ensuing impact of systematic errors on the physical results of the simulations. In particular, we have contrasted the relatively common method of plain superposition according to Eq. (3.3.1) with the adjusted procedure (3.3.3) first identified in Ref. [?] for oscillatons.

Our results demonstrate that the adjustment (3.3.3) in the construction of initial data leads to major improvements in the initial constraint violations and the time evolutions of binary BS collisions. In contrast, we find that the use of plain superposition for BS binary initial data may not only result in quantitatively wrong physical diagnostics but can even result in completely spurious physical behaviour such as premature gravitational collapse. In spite of the great simplicity of the adjustment (3.3.3) and its success in overcoming the most severe errors in the ensuing evolution, it is not free of shortcomings. (i) In its present form, the adjustment only works for a restricted class of binaries, namely equal-mass systems with no spin and velocity vectors satisfying  $v_A^i v_A^j = v_B^i v_B^j$ . (ii) Even with the adjustment, the initial data contain some residual constraint violations; it should therefore primarily be regarded as an improved initial guess for a constraint solving procedure rather than the “real deal” in its own right. These shortcomings clearly point towards the most urgent generalisations of our work, overcoming the symmetry restrictions and adding a numerical constraint solver.

<sup>5</sup>Recall that this BS model is stable but fairly close to the stability threshold in Fig. 3.1 and therefore does not require a large perturbation to be toppled over the edge.

<sup>6</sup>We note that the relativistic Love numbers (which measure the tidal deformability) of non-rotating BHs are zero [?].

## Acknowledgments

We thank Andrew Tolley, Serguei Ossokine and Richard Brito for fruitful discussions. This work is supported by STFC Consolidator Grant Nos. ST/V005669/1 and ST/P000673/1, NSF-XSEDE Grant No. PHY-090003, STFC Capital Grant Nos. ST/P002307/1, ST/R002452/1, STFC Operations Grant No. ST/R00689X/1 (project ACTP 186), PRACE Grant No. 2020225359, and DIRAC RAC13 Grant No. ACTP238. Computations were performed on the San Diego Supercomputing Center’s clusters Comet and Expanse, the Texas Advanced Supercomputing Center’s Stampede2, the Cambridge Service for Data Driven Discovery (CSD3) system, Durham COSMA7 system and the Jewels cluster at GCS@FZJ, Germany. T.H. is supported by NSF Grants No. PHY-1912550 and AST-2006538, NASA ATP Grants No. 17-ATP17-0225 and 19-ATP19-0051, NSF-XSEDE Grant No. PHY-090003, and NSF Grant PHY-20043. This work has received funding from the European Union’s Horizon 2020 research and innovation programme under the Marie Skłodowska-Curie grant agreement No. 690904. This research project was conducted using computational resources at the Maryland Advanced Research Computing Center (MARCC). The authors acknowledge the Texas Advanced Computing Center (TACC) at The University of Texas at Austin for providing HPC resources that have contributed to the research results reported within this paper. URL: <http://www.tacc.utexas.edu> [?]

## 3.6 Analytic treatment of the Hamiltonian constraint

For the case of two non-boosted BSs, we can analytically compute the Hamiltonian constraint violation at the stars’ centres. Let us consider for this purpose the metric ansatz (3.2.31). From this line element, we directly extract the spatial metric

$$\gamma_{ij}^A = \psi_A^4 \delta_{ij}. \quad (3.6.1)$$

for a non-boosted BS at position  $x_A^i$ . This metric is time-independent, so that for zero shift vector the extrinsic curvature vanishes,  $K_{ij}^A = 0$ . For the second binary member, we likewise obtain a metric  $\gamma_{ij}^B$  and extrinsic curvature  $K_{ij}^B = 0$ , now centred at position  $x_B^i$ .

For sufficiently large initial separation  $d = \|x_B^i - x_A^i\|$ , the exponential falloff of the scalar field implies

$$\begin{aligned} \phi_A(x_B) &= \phi_B(x_A) \approx 0, \\ \Pi_A(x_B) &= \Pi_B(x_A) \approx 0. \end{aligned} \quad (3.6.2)$$

The superposition of the two stars’ scalar fields results in

$$\varphi = \varphi_A + \varphi_B, \quad \Pi = \Pi_A + \Pi_B, \quad (3.6.3)$$

and, combined with Eqs. (3.6.2),

$$\begin{aligned} \rho(x_A) &= \rho_A(x_A), \\ \rho(x_B) &= \rho_B(x_B). \end{aligned} \quad (3.6.4)$$

The single BS spacetimes are solutions to the Einstein equations; by using Eq. (3.6.1), their individual Hamiltonian constraints (3.2.19) simplify to

$$\mathcal{H}_A = 8\delta^{ij}\partial_i\partial_j\psi_A + 16\pi\psi_A^5\rho_A = 0, \quad (3.6.5)$$

and likewise for star B.

Next, we construct a binary spacetime by superposing the metric which leads to

$$\psi^4 = \psi_A^4 + \psi_B^4 - c^4, \quad (3.6.6)$$

where  $c$  is a constant which we keep arbitrary for the moment. For the Hamiltonian constraint of the superposed spacetime at the centre of star A, we find

$$\begin{aligned}\mathcal{H}(x_A^i) &= 8\delta^{ij}\partial_i\partial_j\psi_A(x_A^i) + 8\delta^{ij}\partial_i\partial_j\psi_B(x_A^i) \\ &\quad + 16\pi \left[ \psi_A(x_A^i)^4 + \psi_B(x_A^i)^4 - c^4 \right]^{5/4} \rho(x_A^i).\end{aligned}\tag{3.6.7}$$

We can now choose the constant  $c$  in accordance with the “trick” in Eq. (3.3.3), namely

$$c = \psi_B(x_A^i),\tag{3.6.8}$$

and the constraint simplifies to

$$\begin{aligned}\mathcal{H}(x_A^i) &= 8\delta^{ij}\partial_i\partial_j\psi_A(x_A^i) + 8\delta^{ij}\partial_i\partial_j\psi_B(x_A^i) \\ &\quad + 16\pi\psi_A(x_A^i)^4\rho(x_A^i).\end{aligned}\tag{3.6.9}$$

By Eq. (3.6.5), the derivative of the conformal factor  $\psi_A$  cancels out the density  $\rho_A$ , so that

$$\mathcal{H}(x_A^i) = 8\delta^{ij}\partial_i\partial_j\psi_B(x_A^i).\tag{3.6.10}$$

Using the analogue of Eq. (3.6.5) for star B, we trade the right-hand side for the energy density,

$$\mathcal{H}(x_A^i) = -16\pi\psi_B(x_A^i)^4\rho_B(x_A^i).\tag{3.6.11}$$

For sufficiently large separation  $d$  of the stars, however, this vanishes by Eq. (3.6.2) which is the result we wished to compute. By symmetry, we likewise obtain  $\mathcal{H}(x_B^i) = 0$ , which concludes our calculation.

malaise\_source/statBS-eps-converted-to.pdf

Figure 3.1: One parameter families of mini BSs (black solid) with a non-interacting potential  $\hat{V}_{\min}$  and solitonic BSs (red dashed) with potential  $\hat{V}_{\text{sol}}$  and  $\hat{\sigma}_0 = 0.2$  as given in Eq. (3.2.24). In Sec. 3.4 we simulate head-on collisions of two specific models marked by the circles and with parameters listed in Table 3.1.

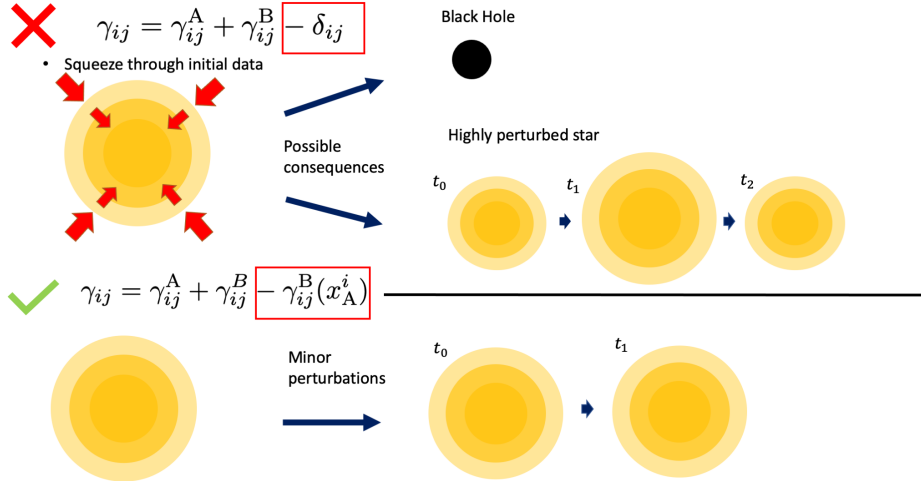


Figure 3.2: Graphical illustration of the spurious dynamics that may be introduced by the simple superposition procedure (3.3.1). *Upper panel:* The spurious increase in the volume element mimics a squeezing of the stellar core that effects a pulsation of the star or may even trigger gravitational collapse to a BH. *Lower panel:* No such squeezing occurs with the adjusted superposition (3.3.3), and the binary evolution starts with approximately unperturbed stars.



Figure 3.3: Upper row: The Hamiltonian constraint violation  $\mathcal{H}$  – Eq. (3.2.19) – normalised by the respective BS’s central energy density  $16\pi\rho_{\text{ctr}}$  is plotted along the collision axis of the binary configurations **mini**, **+mini** with  $d = 101 M$  (left) and **sol**i, **+sol**i with  $d = 22.3 M$  (right). The degree of violations is substantially reduced in the BS interior by using the improved superposition (3.3.3) for **+mini** and **+sol**i relative to their plain counterparts; the maxima of  $\mathcal{H}$  have dropped by over an order of magnitude in both cases. Bottom row: The same analysis for the momentum constraint  $\mathcal{M}_x$  normalised by the central BS’s momentum density  $8\pi j_x$ . Here the improvement is less dramatic, but still yields a reduction by a factor of a few in the BS core.

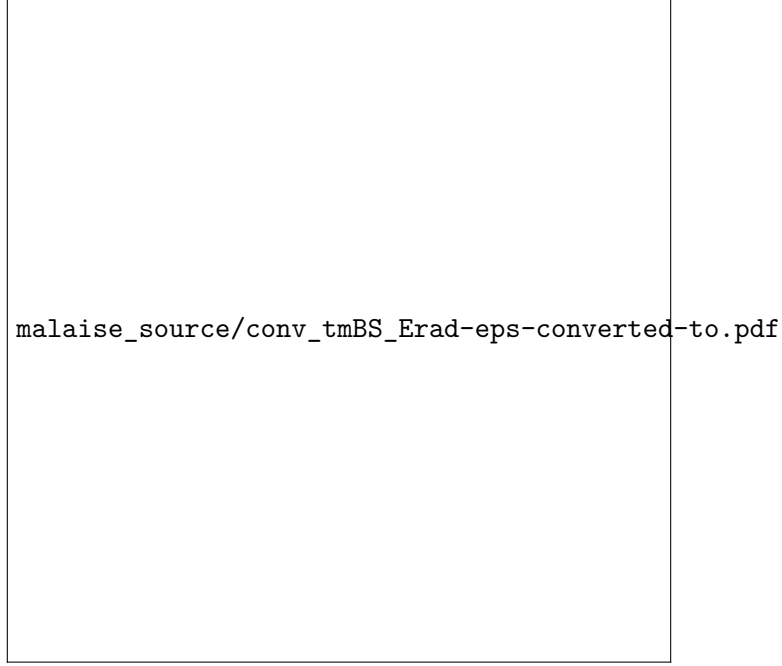


Figure 3.4: Convergence analysis for the GW energy extracted at  $R_{\text{ex}} = 252 M$  from the head-on collision **+mini** of Table 3.1 with  $d = 101 M$ . For the resolutions  $h_1 = M/6.35$ ,  $h_2 = M/9.53$  and  $h_3 = 12.70$  (on the innermost refinement level), we obtain convergence close to second order (upper panel). The numerical error, obtained by comparing our results with the second-order Richardson extrapolated values (bottom panel), is 0.9 % (1.6 %, 3.6 %) for our high (medium, coarse) resolutions.

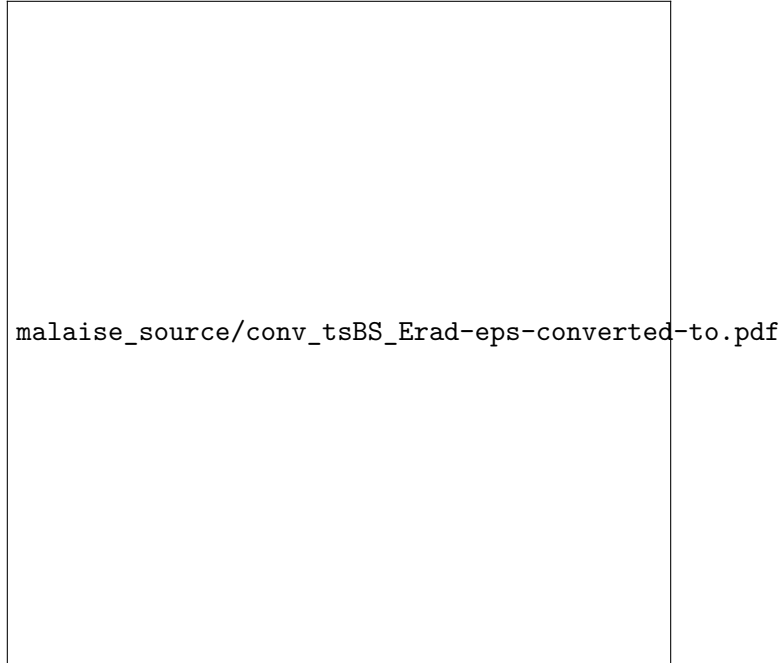


Figure 3.5: Convergence analysis as in Fig. 3.4 but for the configuration **+soli** of Table 3.1 with  $d = 22.3 M$  and resolutions  $h_1 = M/22.9$ ,  $h_2 = M/45.9$  and  $h_3 = M/68.8$ . The numerical error, obtained by comparing our results with the second-order Richardson extrapolated values (bottom panel), is 0.03 % (0.07 %, 0.6 %) for our high (medium, coarse) resolutions.





Figure 3.6: The GW energy  $E_{\text{rad}}$  generated in the head-on collision of mini (upper panel) and solitonic (lower panel) BS binaries starting with initial separation  $d$  and velocity  $v = 0.1$  towards each other. For comparison, a non-spinning, equal-mass BH binary colliding head-on with the same boost velocity  $v = 0.1$  radiates  $E_{\text{rad}} = 6.0 \times 10^{-4} M$  [?].



Figure 3.7: The  $(2, 0)$  mode of the Newman-Penrose scalar for the mini boson star collisions of Table 3.1.



Figure 3.8: The  $(2, 0)$  mode of the Newman-Penrose scalar for the solitonic boson star collisions of Table 3.1.



Figure 3.9: The central scalar-field amplitude  $|\varphi_{\text{ctr}}|$  as a function of time for one BS in the head-on collisions of solitonic BSs with distance  $d = 22.3 M$  (black solid and red long-dashed) as well as a single BS spacetime with the same parameters (green dashed) and the same single BS spacetime “poisoned” with the metric perturbation (3.3.2) that would arise in a simple superposition (see text for details). The dotted vertical lines mark the first location of an apparent horizon in the simulation of the same colour; as expected, no horizon ever forms in the evolution of the unpoisoned single BS. In the bottom panel, we show for reference the coordinate trajectories of the BS centres as obtained from locally Gauss-fitting the scalar profile. Around merger this procedure becomes inaccurate, so that the values around  $t \approx 70 M$  should be regarded as qualitative measures, only.

## Chapter 4

# Local Continuity of Angular Momentum and Noether Charge for Matter in General Relativity

Conservation laws have many applications in numerical relativity. However, it is not straightforward to define local conservation laws for general dynamic spacetimes due the lack of coordinate translation symmetries. In flat space, the rate of change of energy-momentum within a finite spacelike volume is equivalent to the flux integrated over the surface of this volume; for general spacetimes it is necessary to include a volume integral of a source term arising from spacetime curvature. In this work a study of continuity of matter in general relativity is extended to include angular momentum of matter and Noether currents associated with gauge symmetries. Expressions for the Noether charge and flux of complex scalar fields and complex Proca fields are found using this formalism. Expressions for the angular momentum density, flux and source are also derived which are then applied to a numerical relativity collision of boson stars in 3D with non-zero impact parameter as an illustration of the methods.

## 4.1 Local Continuity of Angular Momentum and Noether Charge for Matter in General Relativity

### 4.1.1 Introduction

Conservation laws play an important role in many areas of physics. For a general Lagrangian density  $\mathcal{L}$ , dependant on fields  $\phi_i$  and derivatives  $\partial_k \phi_i$  for  $i \in \{1, 2, \dots, m\}$  and  $k \in \{1, 2, \dots, n\}$ , if a field transformation  $\phi_i \rightarrow \phi_i + \delta \phi_i$  leaves the Lagrangian constant the Euler-Lagrange equations imply there is a conserved current  $\mathbf{J}$ , with zero divergence, given by

$$J^k = \sum_i \frac{\partial \mathcal{L}}{\partial (\partial_k \phi_i)} \delta \phi_i. \quad (4.1.1)$$

In curved space a conserved current  $\mathbf{J}$  satisfies  $\nabla_\mu J^\mu = 0$ . A charge  $Q$  within 3-volume  $V$  and a flux  $F$  though  $\partial V$ , the boundary of  $V$ , can be associated with  $\mathbf{J}$  as described later in Eqs. (4.1.19) and (4.1.20). If  $\mathbf{J}$  is conserved then  $Q$  is a conserved charge satisfying

$$\partial_t Q = F. \quad (4.1.2)$$

This says the rate of change of a charge in a volume  $V$  is equal to the flux across the boundary  $\partial V$  of  $V$ . In the case that  $\mathbf{J}$  has a non-zero divergence,  $\nabla_\mu J^\mu \neq 0$ , Eq. (4.1.2) generalises to the continuity equation

$$\partial_t Q = F - S, \quad (4.1.3)$$

where  $S$  is defined in Eq. (4.1.21);  $S$  is the source of  $\mathbf{J}$  in  $V$  which can be understood as the destruction or creation of charge  $Q$ . Eq. (4.1.3) is a simplified version of Eq. (4.1.15), later referred to as the QFS system.

Evaluation of the continuity equations above, and their corresponding charges  $Q$ , have many uses in the study of fundamental fields in Numerical Relativity. One such use is the measurement of the Noether current  $\mathbf{J}$  of a complex scalar/vector field which arises from a  $U(1)$  gauge symmetry of the matter fields  $\psi_j$  of the form  $\psi_j \rightarrow \psi_j e^{ia} \sim \psi_j + ia\psi_j$  for some small constant  $a$  and  $j \in \{1, 2, \dots, n\}$ . The total charge  $Q$ , also called Noether charge in this case, is useful to track during numerical simulations as it gives insight into the numerical quality of a simulation. A violation of Noether charge conservation can arise from insufficient resolution in some region of the simulation or due to boundary conditions in a finite volume simulation. In the case of Sommerfeld (outgoing wave) boundary conditions [1] we might expect charge to be transported out of a finite computational domain and the total charge  $Q$  in the simulation should decrease. Monitoring only  $Q$  within some volume  $V$ , it is impossible to tell whether Noether charge violation is due to a flux  $F$  through the surface  $\partial V$  or undesirable numerical inaccuracies such as dissipation. It is more useful to check whether the continuity Eq. (4.1.2) (or equivalently Eq. (4.1.3) if there were a non-zero source term) is obeyed for a finite domain  $V$ ; if this fails there is likely a problem as the continuity equations should be exactly observed for general spacetimes.

Another use of the continuity equations is to measure the amount of energy-momentum belonging to matter fields within a volume  $V$ . This has many possible applications such as calculating the total energy or momentum of compact objects such as boson stars and neutron stars. The energy-momentum of matter obeys a conservation law in General Relativity as given by Penrose [2] where the considered spacetime is assumed to admit a Killing vector. In the case a Killing vector exists then a conserved current  $\mathbf{J}$  associated with the energy-momentum tensor  $\mathbf{T}$  can be identified. The current is  $J^\mu = T^\mu_\nu \xi^\nu$  for some Killing vector  $\xi$  and satisfies  $\nabla_\mu J^\mu = 0$ . If  $\xi$  is a Killing vector then Eq. (4.1.2) is the correct continuity equation and the charge  $Q$  is conserved. In General Relativity the existence of Killing vectors is rare, reserved for spacetimes with special symmetries. Generic dynamic spacetimes with no symmetries, such as inspirals and grazing collisions of compact objects, have no easily identifiable Killing vector fields. If there is no Killing vector the divergence of  $\mathbf{J}$  becomes  $\nabla_\mu J^\mu = T^{\mu\nu} \nabla_\mu \xi_\nu$  and the source term  $S$  is non-zero. Now Eq. (4.1.3) is the correct continuity equation and the charge  $Q$  is no longer conserved. In section 4.1.5 we will show how the choice of  $\xi$  affects the type of current  $\mathbf{J}$ , and therefore charge  $Q$ , obtained. While measures of energy or momentum are interesting in their own right, the measure of Eq. (4.1.3) within some volume  $V$  can be a good measure of numerical quality of a simulation in a similar fashion to the measure of Noether charge mentioned already.

When dealing with black hole spacetimes resolution requirements typically become very strict towards the singularity and lead to a local violation of Eqs. (4.1.2) and (4.1.3). This might not doom a simulation as for most physical applications in GR singularities are contained by an event horizon and are therefore causally disconnected from the rest of the simulation; a resolution problem in the vicinity of a singularity therefore may not propagate to the exterior. It could be helpful instead to consider a volume  $\tilde{V}$  equal to  $V$  but removing a set of finite volumes  $\tilde{V}_i$  which surround any singularities. Testing Eqs. (4.1.2) and (4.1.3) in volume  $\tilde{V}$  would then give a measure of the simulation resolution untainted by the resolution issues at a singularity.

Currently in Numerical Relativity it is common to measure energy-momentum in a localised region with with Eq. (4.1.19) for the charge  $Q$  where the charge density  $\mathcal{Q}$  is given in section 4.1.5. Examples of this can be seen in [3], [4], [5] and [6]. While this is a good measure it neglects any radiation and the transfer of energy-momentum between matter and spacetime curvature; if the spacetime does not contain the corresponding Killing vector the charge cannot be treated as a conserved quantity. Instead the combination of variables  $Q - S$ , where  $S$  is defined in Eq. (4.1.21) and  $\mathcal{S}$  in section 4.1.5, should be treated as a conserved quantity. Other popular methods to obtain the energy-momentum of a system include integrating asymptotic quantities such as the ADM mass and momentum, however these can not be used locally as they are defined in the limit of large radii only.

Recent work by Clough [7] evaluates  $Q$ ,  $F$  and  $S$  for energy and linear momentum with the assumption that the approximate Killing vector  $\xi$  is a coordinate basis vector satisfying  $\partial_i \xi^j = 0$ . Successful numerical tests of Eq. (4.1.3) are given for fixed and dynamic background simulations.

This paper builds on the work of [7] and generalises the system to measure angular momentum conservation and the conservation of Noether charges of complex scalar fields and spin-1 complex Proca fields. The assumption that the approximate Killing vector  $\xi$  is a basis vector satisfying  $\partial_i \xi^j = 0$  is dropped and leads to a more general source term  $\mathcal{S}$ . The QFS system for angular momentum is also tested using fully non-linear numerical Relativity simulations of a spacetime consisting of two boson stars colliding in a grazing fashion.

This paper is organised as follows. In section 4.1.2 the QFS system for a general non-conserved current is derived and section 4.1.3 explicitly expands the results for use with a spherical extraction surface. Even though no other extraction surfaces are considered, the results of 4.1.3 are easily adaptable to other shapes. Section 4.1.4 is a standalone derivation of the well known Noether charge density from the QFS perspective and goes on to find the flux variable; results for complex scalar fields and complex Proca fields are given. The application of the QFS system to energy momentum currents, angular momentum and energy are given in section 4.1.5. A fully non-linear test of the QFS system for angular momentum,

using [8, 9] to perform Numerical Relativity simulations, is presented in section 4.1.6 along with a convergence analysis.

### 4.1.2 Derivation of the QFS System

For a spacetime  $(\mathcal{M}, g)$  we start by defining a vector field  $\mathbf{J}$  and subjecting it to the following continuity equation,

$$\nabla_\mu J^\mu = S, \quad (4.1.4)$$

where  $S$  is a source term and describes the non-conservation of  $\mathbf{J}$ . In the case  $S = 0$  the current is conserved. We are interested in the charge density  $\mathcal{Q}$  and source density  $\mathcal{S}$  associated with  $\mathbf{J}$  in a spatial 3-volume  $V \in \Sigma$ . Here  $\Sigma$  is the usual 3-dimensional spacelike manifold  $\Sigma$  consisting of the set of all points with constant time coordinate  $t$ , equipped with metric  $\gamma$ . We are also interested in the flux density  $\mathcal{F}$  through  $\partial V$ , the boundary of  $V$  with metric  $\sigma$ .  $\Sigma$  is spanned by spatial coordinates  $x^i$  related to the full spacetime coordinates  $x^\mu$  by  $x^\mu = \{t, x^i\}$ . The normal to  $\Sigma$  is the unit co-vector  $\mathbf{n}$  defined as,

$$n_\mu := \frac{\nabla_\mu t}{\sqrt{g^{\rho\sigma} \nabla_\rho t \nabla_\sigma t}} = -(\alpha, 0, 0, 0), \quad (4.1.5)$$

$$n^\mu = \frac{1}{\alpha} (t^\mu - \beta^\mu) = \frac{1}{\alpha} (1, -\beta^i), \quad (4.1.6)$$

where  $(\alpha, \beta^i)$  are the usual lapse and shift from the ADM 3+1 spacetime decomposition [10]. The reader is directed to section 2.1 or [11] for a comprehensive introduction to the 3 + 1 decomposition. In Eq. (4.1.6),  $t^\mu = (1, 0, 0, 0)$  is the future directed vector and is distinct from  $n^\mu$ . Time vector  $\mathbf{t}$  is useful as its integral curves form lines of constant spatial coordinates. With this knowledge we can define the 4-volume  $M$ , the spatial 3-volume  $V$  evolved along integral curves of  $\mathbf{t}$  between times  $t_0 \leq t \leq t_0 + \delta t$  in the limit  $\delta t \rightarrow 0$ . Finally we define the 3-dimensional volume  $H$ , with metric  $\mathbf{h}$ .  $H$  is the evolution of  $\partial V$  along integral curves of  $\mathbf{t}$  between times  $t_0 \leq t \leq t_0 + \delta t$  and is the 3-volume the flux crosses; clearly our definition of  $H$  will affect our definition of flux density. There is no reason to choose the timelike vector  $\mathbf{t}$ , rather than  $\mathbf{n}$ , to evolve  $V$  and  $\partial V$  in time and both will result in a different definition of flux density. However, it is shown in section 4.1.9 that these two choices result in the same total integrated flux. A diagram summarising the relevant geometry can be found in Fig. 4.1.

With the relevant geometry discussed we can derive the QFS system, Eq. (4.1.3), by integrating Eq. (4.1.4) over  $M$ ;

$$\int_M \nabla \cdot \mathbf{J} \sqrt{-g} \, dx^4 = \int_M S \sqrt{-g} \, dx^4. \quad (4.1.7)$$

Let us start by using Gauss' theorem for curved space, discussed in section 1.3.5 or [12], on the left hand side,

$$\int_M \nabla \cdot \mathbf{J} \sqrt{-g} \, dx^4 = \int_{\partial M} \hat{\mathbf{s}} \cdot \mathbf{J} \sqrt{{}^{(3)}g} \, dx^3, \quad (4.1.8)$$

with  $\sqrt{{}^{(3)}g}$  being the volume element of a generic 3-surface and  $\hat{\mathbf{s}}$  being the corresponding unit normal. Note that  $\hat{\mathbf{s}}$  is outward directed when spacelike and inward directed when timelike. The integral of  $\nabla \cdot \mathbf{J}$  over  $M$  is now transformed to a surface integral of  $\mathbf{J}$  over the compound 3-volume  $\partial M$ . This surface is split into an integral over  $H$  and two integrals over  $V$  at times  $t_0$  and  $t_0 + \delta t$ . The integrals over  $V$  give,

$$\begin{aligned} & \left( \int_V^{(t=t_0)} - \int_V^{(t=t_0+\delta t)} \right) \mathbf{n} \cdot \mathbf{J} \sqrt{\gamma} \, d^3x, \\ &= - \int_V \left[ (\mathbf{n} \cdot \mathbf{J} \sqrt{\gamma})_{t+\delta t} - (\mathbf{n} \cdot \mathbf{J} \sqrt{\gamma})_t \right] d^3x, \end{aligned} \quad (4.1.9)$$

$$= -\delta t \partial_t \int_V \mathbf{n} \cdot \mathbf{J} \sqrt{\gamma} \, d^3x, \quad (4.1.10)$$

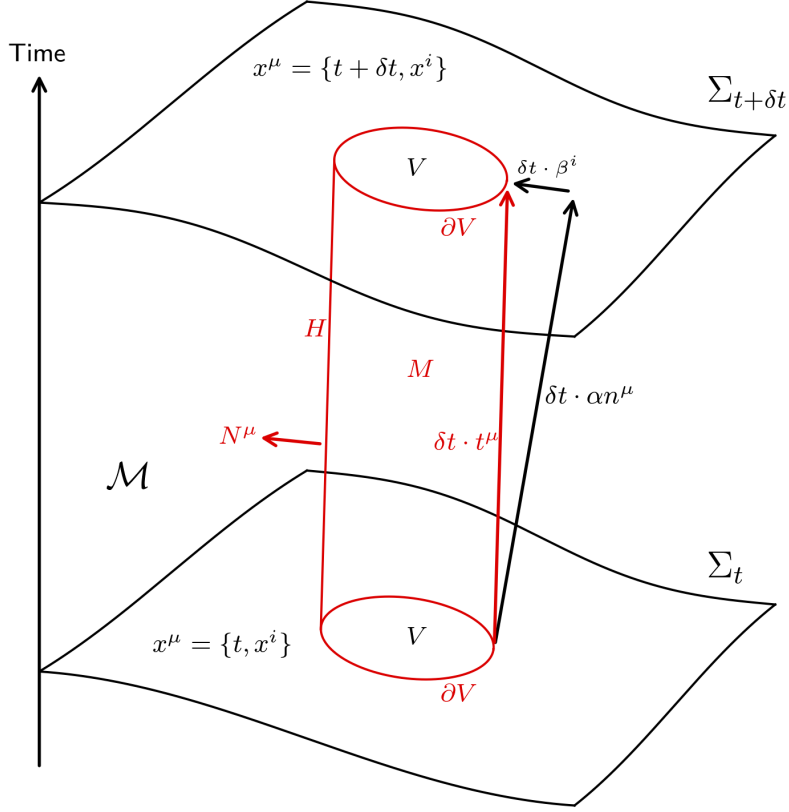


Figure 4.1: Diagram of relevant geometry for derivation of QFS system in section 4.1.2 on manifold  $\mathcal{M}$ .  $\Sigma_t$  is the spatial hypersurface at time  $t$  and  $\Sigma_{t+\delta t}$  is the spatial hypersurface at a later time  $t + \delta t$ .  $V$  is the coordinate volume, with surface  $\partial V$ , that we wish to use as an extraction volume on  $\Sigma_t$ . The sides of the red cylinder are  $H$ , defined by  $\partial V$  evolved along integral curves of  $\mathbf{t} = \partial_t$ . The interior of  $H$  between times  $t$  and  $t + \delta t$  is  $M$ . Evolving  $\partial V$  forward in time with  $\mathbf{n}$ , as demonstrated with the long black arrow, gives a different coordinate volume on  $\Sigma_{t+\delta t}$  than on  $\Sigma_t$ .

where we made use of the fact that the coordinate volume  $V$  is constant for all times due to it evolving in time with  $t^\mu$ . Here  $\sqrt{\gamma}$  is the volume element on the spacelike manifold  $\Sigma$ . Now let us evaluate the integral over  $H$ , with metric  $\mathbf{h}$  of signature  $\{-, +, +\}$ ,

$$\begin{aligned} & \int_H \mathbf{N} \cdot \mathbf{J} \sqrt{-h} d^2x dt, \\ &= \int_{\partial V} \mathbf{N} \cdot \mathbf{J} \sqrt{-h} d^2x \int_t^{t+\delta t} dt, \end{aligned} \tag{4.1.11}$$

$$= \delta_t \int_{\partial V} \mathbf{N} \cdot \mathbf{J} \sqrt{-h} d^2x, \tag{4.1.12}$$

where  $\mathbf{N}$  is the unit normal to  $H$  as shown in Fig. 4.1. Given that  $\mathbf{n}$  is not tangent to  $H$  (but the time vector  $\mathbf{t}$  is) we have  $\mathbf{N} \cdot \mathbf{n} \neq 0$  and  $\mathbf{N} \cdot \mathbf{t} = 0$ . This means we must normalise  $\mathbf{N}$  with metric  $\mathbf{g}$  and not  $\gamma$  as  $\mathbf{N}$  is not tangent to  $\Sigma$  and  $\mathbf{g}(\mathbf{N}, \mathbf{N}) \neq \gamma(\mathbf{N}, \mathbf{N})$ . In other words,  $\mathbf{N}$  is a 4-vector in the case we time evolve  $V$  with time vector  $\mathbf{t}$  but  $\mathbf{N}$  is a 3-vector if we time evolve with  $\mathbf{n}$ . Finally the right hand

side source integral from (4.1.7) becomes,

$$\begin{aligned} & \int_M S \sqrt{-g} \, dx^4, \\ &= \int_V S \sqrt{-g} \, dx^3 \int_t^{t+\delta t} dt, \end{aligned} \quad (4.1.13)$$

$$= \delta t \int_V S \alpha \sqrt{\gamma} \, dx^3. \quad (4.1.14)$$

Combining Eqs. (4.1.10), (4.1.12) and (4.1.14) transforms Eq. (4.1.7) into,

$$\partial_t \int_V \mathcal{Q} \sqrt{\gamma} \, d^3x = \int_{\partial V} \mathcal{F} \sqrt{\sigma} \, d^2x - \int_V \mathcal{S} \sqrt{\gamma} \, d^3x, \quad (4.1.15)$$

where the density, flux density and source density ( $\mathcal{Q}, \mathcal{F}, \mathcal{S}$ ) of angular momentum are defined as,

$$\mathcal{Q} := J^\mu n_\mu, \quad (4.1.16)$$

$$\mathcal{F} := \frac{\sqrt{-h}}{\sqrt{\sigma}} J^\mu N_\mu, \quad (4.1.17)$$

$$\mathcal{S} := \alpha S. \quad (4.1.18)$$

The integrated version of these quantities can be written as

$$Q := \int_V \mathcal{Q} \sqrt{\gamma} \, d^3x, \quad (4.1.19)$$

$$F := \int_{\partial V} \mathcal{F} \sqrt{\sigma} \, d^2x, \quad (4.1.20)$$

$$S := \int_V \mathcal{S} \sqrt{\gamma} \, d^3x. \quad (4.1.21)$$

For later sections it is useful to split the normal vector  $\mathbf{N}$  into its spacelike and timelike parts,

$$N_\mu = \perp N_\mu - \mathbf{n} \cdot \mathbf{N} n_\mu, \quad (4.1.22)$$

where  $\perp N_\mu = \perp_\mu^\nu N_\nu$  is the projected part of  $\mathbf{N}$  onto  $\Sigma$  with  $\mathbf{n} \cdot \perp \mathbf{N} = 0$  and  $\perp$  is the projection operator onto  $\Sigma$ ,

$$\perp_\mu^\nu = \delta_\mu^\nu + n^\mu n_\nu. \quad (4.1.23)$$

Using Eqs. (4.1.22) and (4.1.23) the flux term becomes,

$$\mathcal{F} = \frac{\sqrt{-h}}{\sqrt{\sigma}} J^\mu (\perp N_\mu - \mathbf{n} \cdot \mathbf{N} n_\mu), \quad (4.1.24)$$

$$= \frac{\sqrt{-h}}{\sqrt{\sigma}} (\gamma^{\mu\nu} J_\mu N_\nu - \mathbf{n} \cdot \mathbf{N} \mathcal{Q}). \quad (4.1.25)$$

The term on the left arises from flux through the surface  $\partial V$  and the term on the right is a consequence of the coordinate volume  $V$  moving with respect to a normal observer with worldline traced by  $\mathbf{n}$ . Writing the flux term as above makes it obvious how the definition of flux depends on the 3-volume  $H$  which determines  $\sqrt{-h}$ ,  $\sqrt{\sigma}$  and  $\mathbf{N}$ . Equivalently it can be seen that the density (4.1.16) and source (4.1.18) terms do not depend on the extraction surface.



### 4.1.3 Application to Spherical extraction

The numerical application of the QFS system in section 4.1.6 chooses a spherical volume  $V$  to extract the angular momentum flux. Using standard Cartesian and spherical polar coordinates,  $x_{\text{cart}}^i = \{x, y, z\}$  and  $x_{\text{polar}}^i = \{r, \theta, \phi\}$  respectively, we can define  $H$  as the coordinate volume  $r = r_0$ ,  $t_0 \leq t \leq t + \delta t$ . Thus, the normal  $\mathbf{N}$  to  $H$  is proportional to  $\nabla(r - r_0) = \nabla(\sqrt{x^2 + y^2 + z^2} - r_0)$ . Explicitly calculating the components  $N_\mu$ , and normalising to unity, with spherical polar spacelike coordinates gives,

$$N_\mu = \frac{\nabla_\mu r}{\sqrt{g^{\rho\sigma} \nabla_\rho r \nabla_\sigma r}}, \quad (4.1.26)$$

$$= \frac{1}{\sqrt{g^{rr}}}(0, 1, 0, 0). \quad (4.1.27)$$

Note that if we had chosen  $H$ , the future evolution of  $\partial V$ , to be evolved along the unit vector  $\mathbf{n}$  rather than time vector  $\mathbf{t}$  then we would have obtained a different definition of  $\mathbf{N}$  perpendicular to  $\mathbf{n}$  rather than  $\mathbf{t}$ . The consequences of the alternate choice of  $H$  are explored in section 4.1.9.

The density and source terms  $\mathcal{Q}$  and  $\mathcal{S}$  do not depend on the integration domain  $V$ , but the flux term  $\mathcal{F}$  does. The calculation of the Flux term requires the evaluation of the volume element  $\sqrt{-h}$  of  $H$ . Due to the choice that  $H$  is the surface of constant radial coordinate, finding the metric of this surface is straightforward. Here we define spherical polar coordinates  $x^\mu = \{t, r, \theta, \phi\}$  on  $\mathcal{M}$  and  $X^m = \{t, \theta, \phi\}$  spanning  $H$ . Projecting the 4-metric  $\mathbf{g}$  onto  $H$  we can write

$$^{(4)}h_{\mu\nu} = g_{\mu\nu} - N_\mu N_\nu, \quad (4.1.28)$$

where  $^{(4)}\mathbf{h}$  belongs to  $\mathcal{M}$ . The line element of a curve residing in  $H$  can be equivalently evaluated in  $\mathcal{M}$  or  $H$ ; the pullback of  $^{(4)}\mathbf{h}$  from  $\mathcal{M}|_{r=r_0}$  to  $H$  gives the 3-metric  $\mathbf{h}$  belonging to  $H$ ,

$$h_{mn} = ^{(4)}h_{\mu\nu} \frac{\partial x^\mu}{\partial X^m} \frac{\partial x^\nu}{\partial X^n}, \quad (4.1.29)$$

$$= \begin{pmatrix} g_{tt} & g_{t\theta} & g_{t\phi} \\ g_{\theta t} & g_{\theta\theta} & g_{\theta\phi} \\ g_{\phi t} & g_{\phi\theta} & g_{\phi\phi} \end{pmatrix}. \quad (4.1.30)$$

A similar argument can be made for  $\partial V$ , the set of all points satisfying  $r = r_0$  and  $t = t_0$ , with metric  $\sigma$ . The metric components and volume element are

$$\sigma_{ab} = \begin{pmatrix} g_{\theta\theta} & g_{\theta\phi} \\ g_{\phi\theta} & g_{\phi\phi} \end{pmatrix}, \quad (4.1.31)$$

$$\sqrt{\sigma} = \sqrt{g_{\theta\theta}g_{\phi\phi} - g_{\phi\theta}g_{\theta\phi}}. \quad (4.1.32)$$

Using Cramer's rule for the inverse of a matrix with Eqs. (4.1.30) and (4.1.31) we get

$$h^{tt} = \frac{\sigma}{h}, \quad (4.1.33)$$

and reading from Eq. (4.1.28) gives

$$^{(4)}h^{tt} = g^{tt} - N^t N^t, \quad (4.1.34)$$

$$= -\frac{1}{\alpha^2} \left( \frac{\gamma^{rr}}{g^{rr}} \right). \quad (4.1.35)$$

Similarly to Eq. (4.1.29), the pushforward of  $\mathbf{h}$  on  $H$  to  $^{(4)}\mathbf{h}$  on  $\mathcal{M}|_{r=r_0}$  gives

$$^{(4)}h^{\mu\nu} = h^{mn} \frac{\partial x^\mu}{\partial X^m} \frac{\partial x^\nu}{\partial X^n}, \quad (4.1.36)$$

$$= \begin{pmatrix} h^{tt} & 0 & h^{t\theta} & h^{t\phi} \\ 0 & 0 & 0 & 0 \\ h^{\theta t} & 0 & h^{\theta\theta} & h^{\theta\phi} \\ h^{\phi t} & 0 & h^{\phi\theta} & h^{\phi\phi} \end{pmatrix}, \quad (4.1.37)$$

which shows that  $h^{tt} = {}^{(4)}h^{tt}$ . Combining Eqs. (4.1.33) and (4.1.35) it can be shown that

$$\sqrt{-h} = \alpha \sqrt{\sigma} \sqrt{\frac{g^{rr}}{\gamma^{rr}}}. \quad (4.1.38)$$

Using this with Eq. (4.1.27) we can expand Eq. (4.1.17) for the flux term  $\mathcal{F}$ ,

$$\mathcal{F} = \frac{\sqrt{-h}}{\sqrt{\sigma}} J^\mu N_\mu = \frac{\alpha}{\sqrt{\gamma^{rr}}} J^r, \quad (4.1.39)$$

but for practical purposes it is helpful to decompose this in terms of 3+1 variables as in Eq. (4.1.25),

$$\mathcal{F} = \alpha \frac{\sqrt{g^{rr}}}{\sqrt{\gamma^{rr}}} (\gamma^{\mu\nu} J_\nu N_\mu - \mathbf{n} \cdot \mathbf{N} \mathcal{Q}), \quad (4.1.40)$$

$$= \alpha \frac{\sqrt{g^{rr}}}{\sqrt{\gamma^{rr}}} \left( \gamma^{r\nu} J_\nu \frac{1}{\sqrt{g^{rr}}} + \alpha^{-1} \beta^r \frac{1}{\sqrt{g^{rr}}} \mathcal{Q} \right), \quad (4.1.41)$$

$$= \frac{1}{\sqrt{\gamma^{rr}}} (\alpha \gamma^{r\nu} J_\nu + \beta^r \mathcal{Q}). \quad (4.1.42)$$

It is straightforward to re-derive the results of this section for other extraction volume shapes, such as cylinders or cubes/rectangles, with a redefinition of spacelike volume  $V$  giving rise to different  $\mathbf{N}$ ,  $H$  and  $\partial V$ . It is wise to pick suitable coordinates adapted to the symmetry of the problem.

#### 4.1.4 Noether Currents

In this section we apply the previous results of the QFS system Eq. (4.1.15) to the continuity of Noether charge for both a complex scalar and the Proca field. The charge  $\mathcal{Q}$  represents the number density of particles. Since the total particle number minus antiparticle number is always conserved the conservation law is exact and the source term  $\mathcal{S}$  vanishes.

Globally the total Noether charge should be conserved, however in numerical simulation this might not always be the case. Two common ways for non-conservation to occur are for the matter to interact with the simulation boundary conditions (often unproblematic) or some region of the simulation being insufficiently resolved (often problematic). Without knowledge of the Noether flux it is difficult to know what a change in Noether charge should be attributed to. If a large extraction volume containing the relevant physics shows a violation of Eq. (4.1.15) then the change in total Noether charge being due to boundary conditions can be ruled out and resolution is likely the culprit.

When considering black hole spacetimes it is common for Noether charge to be dissipated as matter approaches the singularity; this is due to resolution requirements typically becoming very high in this region. The violation of Eq. (4.1.15) inside a black hole horizon might not cause any resolution problems for the black hole exterior however due to causal disconnection. If the extraction volume is modified to exclude finite regions containing any black hole singularities then Eq. (4.1.15) could be used to monitor the conservation of Noether charge away from troublesome singularities. This would be a good way of checking the resolution of a matter field in situations such as boson/Proca stars colliding with black holes or scalar/vector accretion onto a black hole.

#### Complex Scalar Fields

In this section we consider the conserved Noether current associated with a complex scalar field  $\varphi$  with Lagrangian

$$\mathcal{L} = \left( \frac{1}{16\pi} R - \frac{1}{2} g^{\mu\nu} \nabla_\mu \bar{\varphi} \nabla_\nu \varphi - \frac{1}{2} V(\varphi \bar{\varphi}) \right) \sqrt{-g}, \quad (4.1.43)$$

where  $V$  is some real potential function. There is a  $U(1)$  symmetry where a complex rotation of the scalar field  $\varphi \rightarrow \varphi e^{ia}$ , for constant  $a$ , leaves the action unchanged. The associated Noether current  $\mathbf{J}$  can be found in [13],

$$J^\mu = ig^{\mu\nu}(\varphi\partial_\nu\bar{\varphi} - \bar{\varphi}\partial_\nu\varphi), \quad (4.1.44)$$

and satisfies  $\nabla \cdot \mathbf{J} = 0$ . The conservation is exact here which tells us the source term vanishes. In this case the Noether charge density (4.1.16) and flux density (4.1.25) are,

$$\mathcal{Q} = n_\mu J^\mu, \quad (4.1.45)$$

$$= i(\varphi n^\mu \partial_\mu \bar{\varphi} - \bar{\varphi} n^\mu \partial_\mu \varphi), \quad (4.1.46)$$

$$= i(\bar{\varphi}\Pi - \bar{\Pi}\varphi), \quad (4.1.47)$$

$$\mathcal{F} = \frac{\sqrt{-h}}{\sqrt{\sigma}}(i\gamma^{\nu\mu}N_\mu(\varphi\partial_\nu\bar{\varphi} - \bar{\varphi}\partial_\nu\varphi) - \mathbf{n} \cdot \mathbf{N}\mathcal{Q}), \quad (4.1.48)$$

where  $\Pi = -\mathbf{n} \cdot \nabla\varphi$  is the conjugate momentum of the scalar field. Using Eq. (4.1.42) for a spherical extraction surface, and spherical polar spacelike coordinates  $\{r, \theta, \phi\}$ , this explicitly becomes

$$\mathcal{F} = \frac{1}{\sqrt{\gamma^{rr}}}(\alpha\gamma^{\nu r}(\varphi\partial_\nu\bar{\varphi} - \bar{\varphi}\partial_\nu\varphi) + \beta^r\mathcal{Q}). \quad (4.1.49)$$

### Complex Vector Fields

The Complex vector field  $\mathbf{A}$ , also called a Proca field, has Lagrangian

$$\mathcal{L} = \left( \frac{1}{16\pi}R - \frac{1}{4}F^{\mu\nu}\bar{F}_{\mu\nu} - \frac{1}{2}V(A^\mu\bar{A}_\mu) \right) \sqrt{-g}, \quad (4.1.50)$$

where  $F_{\mu\nu} = \nabla_\mu A_\nu - \nabla_\nu A_\mu$ . Again  $V$  is some real potential function. The action is invariant under a similar  $U(1)$  complex rotation of the vector field  $A^\mu \rightarrow A^\mu e^{ia}$  for constant  $a$ . Following [14] this leads to the following Noether current  $\mathbf{J}$ ,

$$J_\mu = i \left( \bar{A}^\nu F_{\mu\nu} - A^\nu \bar{F}_{\mu\nu} \right), \quad (4.1.51)$$

which again satisfies  $\nabla \cdot \mathbf{J} = 0$  and the source term vanishes. Defining a  $3+1$  decomposition compatible with [15] gives,

$$A_\mu := n_\mu \Phi + a_\mu, \quad (4.1.52)$$

$$\Phi = -A_\mu n^\mu, \quad (4.1.53)$$

$$a_\mu = \perp_\mu^\nu A_\nu, \quad (4.1.54)$$

$$F_{\mu\nu} := n_\mu E_\nu - n_\nu E_\mu + B_{\mu\nu}, \quad (4.1.55)$$

$$E_\mu = \perp_\mu^\nu F_{\nu\alpha} n^\alpha, \quad (4.1.56)$$

$$B_{\mu\nu} = \perp_\mu^\alpha \perp_\nu^\beta F_{\alpha\beta} = D_\mu a_\nu - D_\nu a_\mu, \quad (4.1.57)$$

where  $\phi$ ,  $\mathbf{E}$ ,  $\mathbf{a}$  and  $\mathbf{B}$  all belong to  $\Sigma$ . Additionally  $\mathbf{D}$  is the covariant 3-derivative of  $\Sigma$ . Note that  $\mathbf{F}$  has no time-time component as  $n_\mu n_\nu F^{\mu\nu} = 0$  from the anti-symmetry of  $\mathbf{F}$ . Using these, the Noether charge (4.1.16) becomes,

$$\mathcal{Q} = n_\mu J^\mu, \quad (4.1.58)$$

$$= i \left( n^\mu \bar{A}^\nu F_{\mu\nu} - n^\mu A^\nu \bar{F}_{\mu\nu} \right), \quad (4.1.59)$$

$$= i \left( n^\mu \bar{a}^\nu n_\mu E_\nu - n^\mu a^\nu n_\mu \bar{E}_\nu \right), \quad (4.1.60)$$

$$= i \left( a^\nu \bar{E}_\nu - \bar{a}^\nu E_\nu \right). \quad (4.1.61)$$

Using Eq. (4.1.25), the Noether flux is,

$$\mathcal{F} = \frac{\sqrt{-h}}{\sqrt{\sigma}} (\vec{N}^\mu j_\mu - \mathbf{n} \cdot \mathbf{N} \mathcal{Q}), \quad (4.1.62)$$

$$= \frac{\sqrt{-h}}{\sqrt{\sigma}} (\vec{N}^\mu (\bar{A}^\nu F_{\mu\nu} - A^\nu \bar{F}_{\mu\nu}) - \mathbf{n} \cdot \mathbf{N} \mathcal{Q}). \quad (4.1.63)$$

Expanding  $\vec{N}^\mu \bar{A}^\nu F_{\mu\nu}$  using the 3+1 split,

$$\vec{N}^\mu \bar{A}^\nu F_{\mu\nu} = \vec{N}^\mu \bar{a}^\nu B_{\mu\nu} - \vec{N}^\mu \bar{\Phi} n^\nu n_\nu E_\mu, \quad (4.1.64)$$

$$= \gamma^{\mu\rho} N_\rho (\bar{a}^\nu B_{\mu\nu} + \bar{\Phi} E_\mu), \quad (4.1.65)$$

$$= \gamma^{\mu\rho} N_\rho (\bar{a}^\nu (\partial_\mu a_\nu - \partial_\nu a_\mu) + \bar{\Phi} E_\mu), \quad (4.1.66)$$

where the Christoffel symbols from  $D_\mu$  in  $B_{\mu\nu}$  cancel out. Putting this into the expression for the Proca Noether flux we get,

$$\begin{aligned} \mathcal{F} = \frac{\sqrt{-h}}{\sqrt{\sigma}} \{ & i\gamma^{\mu\rho} N_\rho [\bar{\Phi} E_\mu - \Phi \bar{E}_\mu + \bar{a}^\nu (\partial_\mu a_\nu - \partial_\nu a_\mu) \\ & - a^\nu (\partial_\mu \bar{a}_\nu - \partial_\nu \bar{a}_\mu)] - \mathbf{n} \cdot \mathbf{N} \mathcal{Q} \}, \end{aligned} \quad (4.1.67)$$

and equation (4.1.42) gives the flux term for a spherical extraction surface,

$$\begin{aligned} \mathcal{F} = \frac{1}{\sqrt{\gamma^{rr}}} ( & i\alpha \gamma^{\mu r} (\bar{\Phi} E_\mu - \Phi \bar{E}_\mu + \bar{a}^\nu (\partial_\mu a_\nu - \partial_\nu a_\mu) \\ & - a^\nu (\partial_\mu \bar{a}_\nu - \partial_\nu \bar{a}_\mu)) + \beta^r \mathcal{Q} ), \end{aligned} \quad (4.1.68)$$

where spherical polar spacelike coordinates  $\{r, \theta, \phi\}$  used.

#### 4.1.5 Energy-Momentum Currents

To find the current associated with energy-momentum we consider a vector field  $\mathbf{J}$  defined with respect to a second vector field  $\boldsymbol{\xi}$  and the stress tensor  $\mathbf{T}$  by

$$J^\mu := T^\mu_\nu \xi^\nu. \quad (4.1.69)$$

Calculating the divergence of this vector leads to the following continuity equation,

$$\nabla_\mu J^\mu = \underbrace{(\nabla_\mu T^\mu_\nu)}_{=0} \xi^\nu + T^\mu_\nu \nabla_\mu \xi^\nu, \quad (4.1.70)$$

$$\nabla_\mu J^\mu = T^{\mu\nu} \nabla_{(\mu} \xi_{\nu)}, \quad (4.1.71)$$

where (4.1.71) shows the divergence vanishes if  $\boldsymbol{\xi}$  is a Killing vector of the spacetime; a vanishing divergence corresponds to a conserved current with a zero source term. For more general spacetimes where  $\boldsymbol{\xi}$  is not Killing, the right hand side of (4.1.71) leads to a non-zero source term accounting for the transfer of energy-momentum between matter and spacetime curvature [7]. The choice of  $\boldsymbol{\xi}$  dictates the type of energy-momentum current retrieved; for instance  $\boldsymbol{\xi} = \partial_t$  will correspond to an energy current  $J^\mu = T^\mu_\nu (\partial_t)^\nu = T^\mu_t$  and the spacelike choice  $\boldsymbol{\xi} = \partial_i$  gives a momentum current  $J^\mu = T^\mu_\nu (\partial_i)^\nu = T^\mu_i$  corresponding to the coordinate  $x^i$ . For an account of energy and linear momentum continuity see [7].

## Angular Momentum

The numerical test of the QFS system (4.1.15) in section 4.1.6 measures the conservation of angular momentum. To do this we choose  $\xi = \partial_\phi$ , used in Eq. (4.1.69), which is the coordinate basis vector of some azimuthal coordinate  $\phi$ . The angular momentum current is

$$J^\mu = T_\nu^\mu (\partial_\phi)^\nu = T_\phi^\mu. \quad (4.1.72)$$

Any spacetime with azimuthal symmetry (e.g. the Kerr spacetime) will have a vanishing source term as  $\partial_\phi$  is a Killing vector. This includes numerical simulations of matter in a fixed background. The example simulation in section 4.1.6 is the fully nonlinear grazing collision of two boson stars and  $\xi$  is not a Killing vector for finite distances from the collision centre. In this case the source term is non-zero. Using the standard 3+1 decomposition of the stress tensor [11], [16] and explicitly expanding the density term from Eq. (4.1.16) gives,

$$\mathcal{Q} = T_\nu^\mu n_\mu (\partial_\phi)^\nu, \quad (4.1.73)$$

$$= (S_\nu^\mu + S^\mu n_\nu + S_\nu n^\mu + n_\nu n^\mu) n_\mu (\partial_\phi)^\nu, \quad (4.1.74)$$

$$= S_\nu n^\mu n_\mu (\partial_\phi)^\nu, \quad (4.1.75)$$

$$= -S_\phi, \quad (4.1.76)$$

$$= yS_x - xS_y, \quad (4.1.77)$$

where  $x$  and  $y$  are Cartesian coordinates related to spherical polar coordinates in the usual way. Combining Eqs. (4.1.25), (4.1.72) and (4.1.76) we can get the angular momentum flux through a spherical extraction surface,

$$\mathcal{F} = \frac{\sqrt{-h}}{\sqrt{\sigma}} (\gamma^{\mu\nu} T_{\rho\mu} (\partial_\phi)^\rho N_\nu + \mathbf{n} \cdot \mathbf{N} S_\phi), \quad (4.1.78)$$

$$= \frac{\sqrt{-h}}{\sqrt{\sigma}} (\gamma^{\mu\nu} S_{\phi\mu} N_\nu + \mathbf{n} \cdot \mathbf{N} S_\phi). \quad (4.1.79)$$

Using Eq. (4.1.42), for a spherical extraction surface, the flux term becomes,

$$\mathcal{F} = \alpha \frac{\sqrt{g^{rr}}}{\sqrt{\gamma^{rr}}} (\gamma^{\mu r} S_{\phi\mu} N_r - \frac{\beta^r}{\alpha} N_r S_\phi), \quad (4.1.80)$$

$$= \alpha \frac{\sqrt{g^{rr}}}{\sqrt{\gamma^{rr}}} (\gamma^{\mu r} S_{\phi\mu} N_r - \frac{\beta^r}{\alpha} N_r S_\phi), \quad (4.1.81)$$

$$= \frac{1}{\sqrt{\gamma^{rr}}} (\alpha \gamma^{\mu r} S_{\phi\mu} - \beta^r S_\phi) \quad (4.1.82)$$

in spherical polar coordinates. The explicit expansion of the source term  $\mathcal{S}$  is left for the section 4.1.8, but the result is given here,

$$\begin{aligned} \mathcal{S} &= \alpha S_\nu^{\mu(3)} \partial_\mu \xi^\nu + \alpha S_\nu^{\mu(3)} \Gamma_{\mu\sigma}^\nu \xi^\sigma \\ &\quad - S_\nu \beta^i \partial_i \xi^\nu + S_\nu \xi^\mu \partial_\mu \beta^\nu - \rho \xi^\mu \partial_\mu \alpha. \end{aligned} \quad (4.1.83)$$

As noted in section 4.1.8, when choosing a coordinate system to evaluate  $\mathcal{S}$ , if  $\xi$  is a coordinate basis vector then the  $\partial_i \xi^j$  terms vanish.

It would be simple to re-derive these results for linear momentum, by using  $\xi = \partial_i$  for momentum in the  $x^i$  direction for example, where  $x^i$  is some Cartesian spatial coordinate. Results for linear momentum can be found in [7].

## Energy

A local conservation system can also be applied to energy with the choice of an approximate Killing vector  $\xi$ ,  $\xi^\mu = (\partial_t)^\mu = t^\mu = (1, 0, 0, 0)$ , and energy current

$$J^\mu = T^\mu_\nu t^\nu = T^\mu_t. \quad (4.1.84)$$

Using the standard 3+1 decomposition of the stress-energy tensor from [11] or [16] the energy density  $\mathcal{Q}$  is,

$$\mathcal{Q} = T^\mu_\nu n_\mu \xi^\nu, \quad (4.1.85)$$

$$= T^\mu_\nu n_\mu (\alpha n^\nu + \beta^\nu), \quad (4.1.86)$$

$$= \alpha \rho - S_\mu \beta^\mu, \quad (4.1.87)$$

from Eq. (4.1.16). Similarly, combining Eqs. (4.1.17) and (4.1.22), the energy flux is,

$$\mathcal{F} = \frac{\sqrt{-h}}{\sqrt{\sigma}} T^\mu_\nu N_\mu \xi^\nu, \quad (4.1.88)$$

$$= \frac{\sqrt{-h}}{\sqrt{\sigma}} T^\mu_\nu (\perp N_\mu - \mathbf{n} \cdot \mathbf{N} n_\mu) (\alpha n^\nu + \beta^\nu), \quad (4.1.89)$$

$$= \frac{\sqrt{-h}}{\sqrt{\sigma}} (-\mathbf{n} \cdot \mathbf{N} \alpha \rho - \perp N_\mu S^\mu \alpha + \mathbf{n} \cdot \mathbf{N} S_\mu \beta^\mu + \perp N^\mu \beta^\nu S_{\mu\nu}), \quad (4.1.90)$$

and Eqs. (4.1.27) and (4.1.38) can be used for a spherical extraction surface,

$$\mathcal{F} = \frac{1}{\sqrt{\gamma^{rr}}} (\alpha \rho \beta^r - \alpha^2 S^r + \alpha S_\mu^r \beta^\mu - \beta^\mu S_\mu \beta^r). \quad (4.1.91)$$

The source term is omitted here as the expression derived in section 4.1.8 assumes that  $\xi$  is spacelike. For energy continuity a timelike approximate Killing vector  $\xi$  is used and leads to a different expression for the source term that can be found in [7] along with the above density  $\mathcal{Q}$  and flux term  $\mathcal{F}$ .

### 4.1.6 Numerical Application

To numerically test the QFS system, given in Eq. (4.1.15), for angular momentum an example spacetime consisting of colliding boson stars is simulated in 3D using [8, 9]. is a modern, open source, Numerical Relativity code with fully Adaptive Mesh Refinement (AMR) using the Berger-Rigoutsos block-structured adaptive mesh algorithm [17]. The CCZ4 constraint damping formulation [17, 18] is used with the moving puncture gauge [19, 20]. Time integration is done with 4th order Runge-Kutta method of lines.

### Numerical Setup of Simulations

The boson stars are composed of a complex scalar field  $\varphi$ , minimally coupled to gravity with the Lagrangian given in Eq. (4.1.43). Boson stars are stable self-gravitating spherically symmetric solutions of the Einstein-Klein-Gordon system in curved space; for a detailed review see [13]. In this work, the Klein-Gordon potential is chosen to be  $V = m^2 \varphi \bar{\varphi}$ , where  $m$  is the mass of a bosonic particle, leading to so called *mini boson stars*. The Kaup limit for the maximum mass of a mini boson star can be found numerically as approximately

$$M_{\text{Kaup}} \sim 0.633 \frac{\hbar c}{Gm} = 0.633 M_{\text{pl}}^2 m^{-1}, \quad (4.1.92)$$

where the physical constants are included for completeness, but have numerical value 1 in Planck units. Notably, the maximum mass of a mini boson star scales inversely with the boson particle mass  $m$ .

The Lagrangian in Eq. (4.1.43) with potential  $V = m^2 \varphi \bar{\varphi}$  is unchanged up to an overall constant under a rescaling of the boson mass like  $m \rightarrow bm$ , for some dimensionless constant  $b$ , while simultaneously rescaling  $x^\mu \rightarrow b^{-1}x^\mu$  for coordinates with dimension length/time. Consequently a mini boson star solution, categorised by the central scalar field amplitude  $\varphi_c$ , represents a one parameter family of solutions with ADM mass and radius inversely proportional to  $m$ . To keep the choice of  $m$  arbitrary the coordinates used in the simulation are  $mx^\mu$ , which are exactly Planck units in the case  $m = 1$  (i.e. the Planck mass).

To measure the charge associated with angular momentum, the following angular momentum measures are considered,

$$Q := \int_V \mathcal{Q} \sqrt{\gamma} d^3x, \quad (4.1.93)$$

$$F := \int_{\partial V} \mathcal{F} \sqrt{\gamma} d^2x, \quad (4.1.94)$$

$$S := \int_V \mathcal{S} \sqrt{\gamma} d^3x, \quad (4.1.95)$$

$$\tilde{Q} := Q(t=0) + \int_0^t F dt, \quad (4.1.96)$$

$$\delta Q_S := \int_0^t S dt, \quad (4.1.97)$$

$$\hat{Q} := Q + \delta Q_S, \quad (4.1.98)$$

$$\bar{Q} := \tilde{Q} - \delta Q_S, \quad (4.1.99)$$

where  $\mathcal{Q}$ ,  $\mathcal{F}$  and  $\mathcal{S}$  are defined in Eqs. (4.1.73), (4.1.82) and (4.1.83) respectively.  $\hat{Q}$  is the angular momentum modified by  $\delta Q_S$ ; this is equivalent to absorbing the source term into  $Q$ .  $\tilde{Q}$  is the initial angular momentum modified by the time integrated total flux. Equation (4.1.15) implies  $\hat{Q} = \tilde{Q}$  exactly, and we define the relative numerical error measure  $e_1$  by

$$e_1 := \frac{\hat{Q} - \tilde{Q}}{\hat{Q}}, \quad (4.1.100)$$

which converges to zero in the continuum limit. We can alternatively define a different relative error

$$e_2 := \frac{Q - \bar{Q}}{Q}, \quad (4.1.101)$$

where the source term is not absorbed into  $Q$ . Again, Eq. (4.1.15) implies that  $Q = \bar{Q}$ , or  $e_2 = 0$ , in the continuum limit.

The initial data of the numerical simulations consists of two boson stars, each with mass  $M = 0.395(0) m^{-1}$ , boosted towards each other in a grazing configuration. The data for two single boosted stars are superposed as in Ref. [21] to minimise errors in the Hamiltonian and momentum constraints and spurious oscillations in the scalar field amplitudes of the stars. The physical domain is a cube of size  $L = 1024 m^{-1}$ , the centre of this domain locates the origin of the Cartesian coordinates  $x$ ,  $y$  and  $z$ . The stars are placed at  $x_0^i = \pm(40, 4, 0) m^{-1}$  with respect to the centre of the physical domain, giving an initial impact parameter  $d = 8 m^{-1}$ , and the boost velocity is  $v^i = \mp(0.1, 0, 0)$  along the  $x$  axis. The stars travel towards each other and undergo a grazing collision to form a short lived dense object at time  $t \sim 375 m^{-1}$ . Afterwards, much of the scalar field (and angular momentum) leaves the extraction radii as it is ejected to spatial infinity. Figures. 4.2, 4.3 and 4.4 show the angular momentum within radii  $r = \{20, 40, 60\} m^{-1}$ . The Newtonian angular momentum for this configuration is

$$Mdv = 0.316(0)m^{-2} \quad (4.1.102)$$

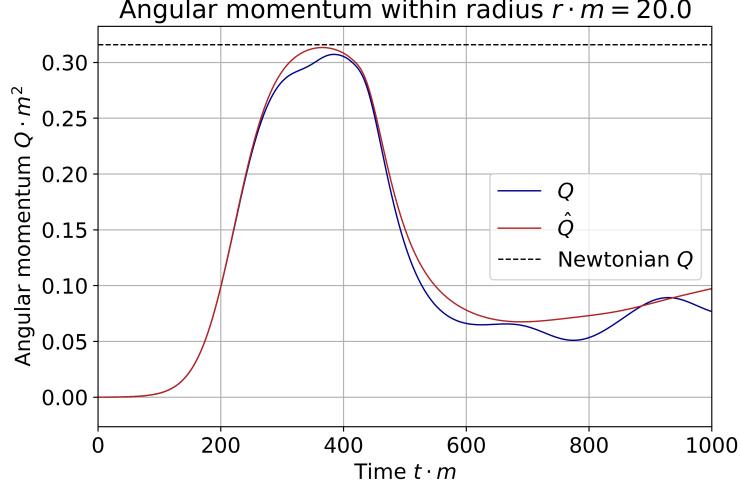


Figure 4.2: Integrated angular momentum within radius  $r < 20 \, m^{-1}$ .  $Q$  is the angular momentum integral in Eq. (4.1.93) and  $\hat{Q}$  includes the source term as in Eq. (4.1.98). The black dashed line indicates the Newtonian calculation for the angular momentum given in Eq. (4.1.102). The boson stars initially start outside the extraction radius.

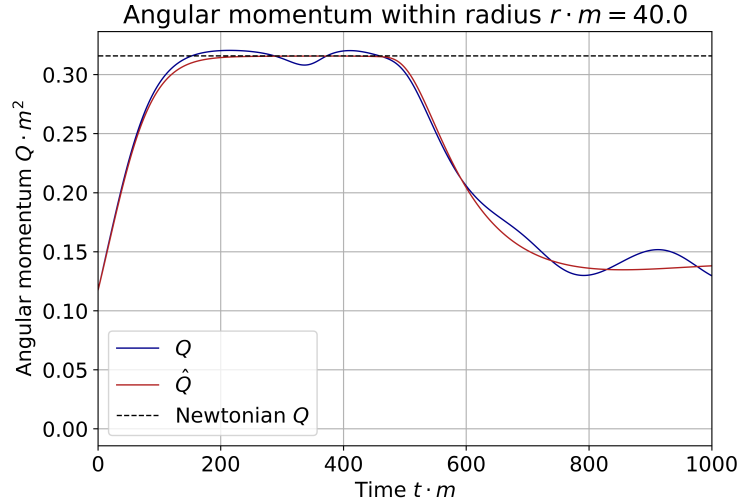


Figure 4.3: Integrated angular momentum within radius  $r < 40 \, m^{-1}$ . Quantities plotted are identical to Fig. 4.2. The boson stars initially start intersecting the extraction radius.

which is in close agreement with  $Q$  and  $\hat{Q}$  in Figs. 4.2, 4.3 and 4.4 while the matter is contained by the extraction radii. Given that we are dealing with a fully non-linear spacetime in general relativity there is no reason why the naive Newtonian angular momentum should agree so well with the numerically integrated values  $Q$  or  $\hat{Q}$ ; this could be due to the mass of the stars being  $M = 0.395(0) \, m^{-1}$ , well below the Kaup limit  $M_{\text{Kaup}} \sim 0.633 \, m^{-1}$  and the mild boost velocities  $v = 0.1$ . In the case that the star masses/densities and velocities tend to zero we expect general relativity to approach the Newtonian limit; conversely for large masses/densities and boost velocities the Newtonian estimate likely becomes less accurate.

Finally we note in Figs. 4.2, 4.3 and 4.4 that the source-corrected density variable  $\hat{Q}$  is less prone to oscillations than  $Q$  and is closer to being constant at early times when no angular momentum flux is radiated.  $\hat{Q}$  has another advantage over  $Q$ ; at extraction radii sufficiently far from any matter  $\hat{Q}$  will remain constant due to the flux  $\mathcal{F}$  vanishing.  $Q$  will only remain constant if the source term integral  $\delta Q_S$



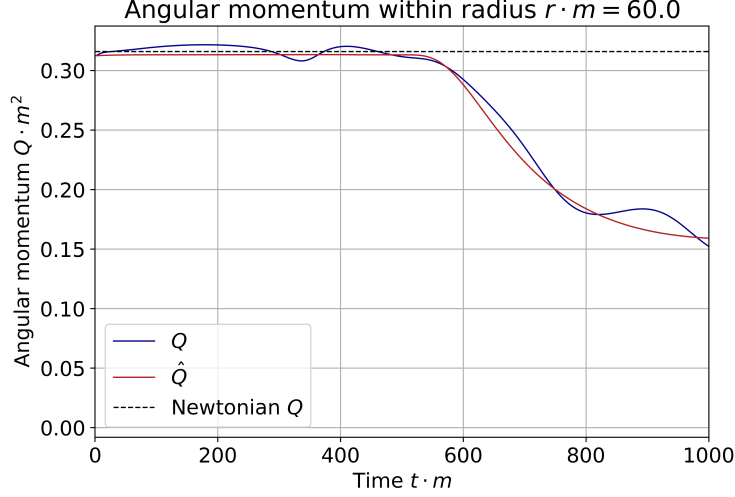


Figure 4.4: Integrated angular momentum within radius  $r < 60 \text{ m}^{-1}$ . Quantities plotted are identical to Figs. 4.2 and 4.3. The boson stars initially start inside the extraction radius.

also remains constant which does not happen in general dynamic spacetimes, even for large extraction radii.

### Convergence Analysis

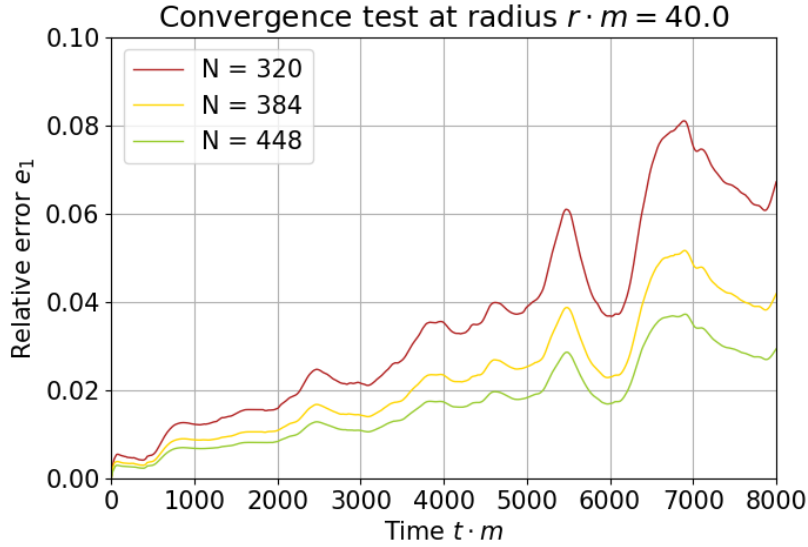


Figure 4.5: Relative error  $e_1$ , from Eq. (4.1.100), for the modified total angular momentum at extraction radius  $r = 40 \text{ m}^{-1}$ ; the modified total angular momentum  $\hat{Q}$  includes the source term. Figure includes four convergence simulations with  $N \in \{320, 384, 448\}$  gridpoints along the coarse grid.

Three numerical simulations are used to test the convergence of the angular momentum measures as the continuum limit is approached. They have  $N \in \{320, 384, 448\}$  gridpoints on the coarsest level, named level 0 with grid spacing  $\Delta x_0 = L/N$ . Each finer level, named level  $n$ , has grid spacing  $\Delta x_n = 2^{-n} \Delta x_0$ . Any gridpoints that fall inside radius  $r = 200 \text{ m}^{-1}$  are forced to be resolved by at least AMR level 1. Similarly, any points within radius  $r < 60 \text{ m}^{-1}$  are resolved by at least AMR level 3; this modification quadruples the default resolution for  $r < 60 \text{ m}^{-1}$  compared to level 1. These two radii have a 20% extra buffer zone to ensure that AMR boundaries are outside and away from the desired radii. On top of

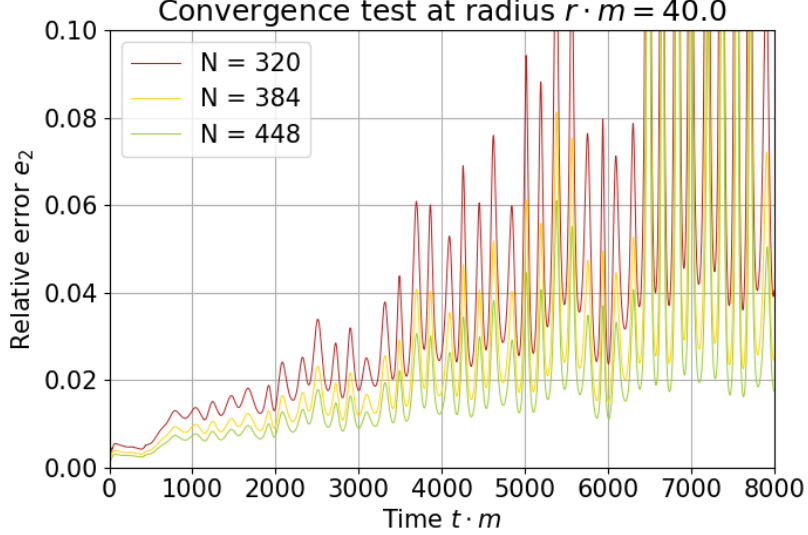


Figure 4.6: Relative error  $e_2$ , from Eq. (4.1.101), for the total angular momentum at extraction radius  $r = 40 \text{ m}^{-1}$ ; the total angular momentum  $Q$  excludes the source term. Figure includes four convergence simulations with  $N \in \{320, 384, 448\}$  gridpoints along the coarse grid.

this the AMR is triggered to regrid when a tagging criterion is exceeded; a description of the algorithm can be found in section 2.2.2 of [22]. The tagging criteria used in this paper involve gradients of the scalar field and spatial metric determinant; this loosely means as a region of spacetime becomes more curved, or matter becomes denser, the region is resolved with higher resolution. Figs. 4.5 and 4.6 show the relative errors  $e_1$  and  $e_2$  for the convergence sequence; it can be seen that  $e_1$ , the relative error of  $\hat{Q}$ , is less prone to oscillations than  $e_2$ , the relative error of  $Q$ . The choice of enforcing AMR regridding to level 3 within  $r < 60 \text{ m}^{-1}$  is very problem specific and the grid structure has been chosen carefully for the particular physical scenario to give higher resolution around the late time scalar field configuration at the origin; this enables accurate simulation of the extended object after merger. Simulations prior to this modification showed approximately five times higher relative error  $e_1$  and much worse Noether charge conservation. The highest resolution simulation, with  $N = 448$ , shows that the relative error  $e_1$  is 3% after  $8000 \text{ m}^{-1}$  time units.

We now obtain the order of convergence  $\omega$  of  $e_1$ . It is convenient to express  $e_1$  as three functions  $\{f_1, f_2, f_3\}$  corresponding to the three different resolution simulations with  $N = \{320, 384, 448\}$  and  $f_\infty$  to denote the continuum limit solution. A traditional convergence analysis, as in [23], assumes that the numerical error of a function (i.e. difference from  $f_\infty$ ) is dominated by a term proportional to  $\Delta x_i^\omega$  for an order of convergence  $\omega$ ; thus we can write

$$f_i + E(\Delta x_i)^\omega = f_\infty \quad (4.1.103)$$

for some constant coefficient  $E$  for all resolutions  $i$ . Equation (4.1.103) with  $i = \{1, 2, 3\}$  can be used to eliminate both  $E$  and  $f_\infty$  giving the well known result

$$\frac{f_3 - f_2}{f_2 - f_1} = \frac{\Delta x_3^\omega - \Delta x_2^\omega}{\Delta x_2^\omega - \Delta x_1^\omega} \quad (4.1.104)$$

for ideal convergence. Figure 4.7 shows  $f_3 - f_2$  and  $(f_2 - f_1)(\Delta x_3^\omega - \Delta x_2^\omega)/(\Delta x_2^\omega - \Delta x_1^\omega)$  for three orders of convergence  $\omega = \{2, 3, 4\}$ ; the two expressions should be equal for an ideal order of convergence  $\omega$ . It can be seen by eye that  $\omega = 3$  is the best estimate.

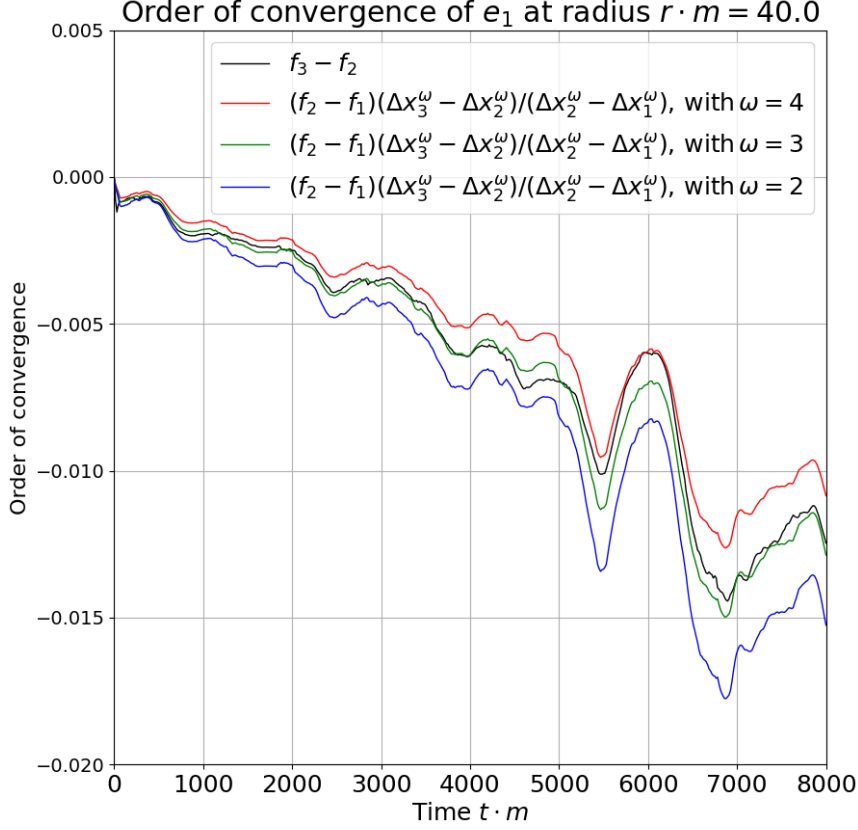


Figure 4.7: Estimating the order of convergence  $\omega$  of the angular momentum error  $e_1$  in Fig. 4.5 at extraction radius  $r = 40 \text{ m}^{-1}$ . The black curve shows the difference between  $f_3$  and  $f_2$ ; the relative error  $e_1$  of the two highest resolution simulations in Section 4.1.6. The three coloured curves show the difference between the two lowest resolution simulations  $f_2$  and  $f_1$ , but modified by  $(\Delta x_3^\omega - \Delta x_2^\omega)/(\Delta x_2^\omega - \Delta x_1^\omega)$  in accordance with Eq. (4.1.104), for three idealised orders of convergence  $\omega = \{2, 3, 4\}$ . The black curve is in best agreement with the green curve giving an estimate of  $\omega = 3$  for the order of convergence.

To quantify the order of convergence, rather than guessing, we define the deviation factor  $\mathcal{D}$  as

$$\mathcal{D}(\omega) = \int_{t_0}^{t_1} \left( \frac{f_3 - f_2}{f_2 - f_1} - \frac{\Delta x_3^\omega - \Delta x_2^\omega}{\Delta x_2^\omega - \Delta x_1^\omega} \right)^2 dt, \quad (4.1.105)$$

which averages the violation of Eq. (4.1.104) between times  $t_0 \leq t \leq t_1$ . Figure 4.8 plots  $\mathcal{D}$  versus  $\omega$  with a red curve and the order of convergence can be estimated by minimising  $\mathcal{D}(\omega)$  with respect to  $\omega$ . As can be seen in Fig. 4.8, the traditional order of convergence is approximately 3.2.

Given that  $e_1$  vanishes in the continuum limit we can set  $f_\infty = 0$  to find the order of convergence to zero. Using Eq. (4.1.103) with the two highest resolutions  $i = \{2, 3\}$ , and setting  $f_\infty = 0$ ,  $E$  can be eliminated to give

$$\frac{f_3}{f_2} = \frac{\Delta x_3^\omega}{\Delta x_2^\omega}. \quad (4.1.106)$$

Similarly to before, we can define a deviation factor  $\tilde{\mathcal{D}}$ ,

$$\tilde{\mathcal{D}}(\omega) = \int_{t_0}^{t_1} \left( \frac{f_3}{f_2} - \frac{\Delta x_3^\omega}{\Delta x_2^\omega} \right)^2 dt, \quad (4.1.107)$$

which time averages the violation of Eq. (4.1.106). The black curve in Fig. 4.8 plots Eq. (4.1.107) versus  $\omega$  and the order of convergence to zero can be estimated by minimising  $\tilde{\mathcal{D}}(\omega)$  with respect to  $\omega$ . As can be seen in Fig. 4.8, the order of convergence convergence to zero is approximately 1.9.

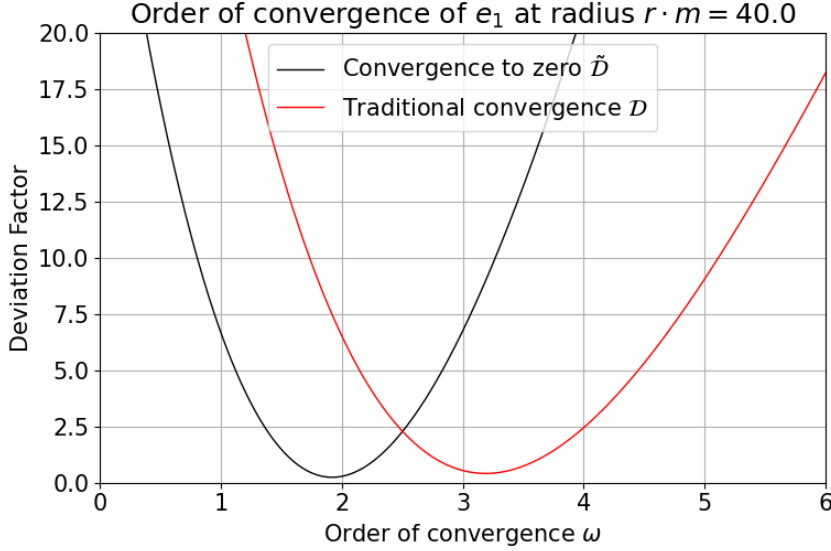


Figure 4.8: Estimating the order of convergence  $\omega$  of the angular momentum error  $e_1$  in Fig. 4.5 at extraction radius  $r = 40 \text{ m}^{-1}$ . The red curve gives the deviation from ideal traditional convergence  $\mathcal{D}$ , defined by Eq. (4.1.105), as a function of  $\omega$ . The black curve shows the deviation from ideal convergence to zero  $\tilde{\mathcal{D}}$ , using the definition given in Eq. (4.1.107), as a function of  $\omega$ . For both curves the estimated order of convergence is found by minimisation with respect to  $\omega$ ; this gives  $\omega = 3.2$  for traditional convergence and  $\omega = 1.9$  for convergence to zero.

#### 4.1.7 Conclusion

A derivation of the QFS system (4.1.15) for continuity equations, valid locally for general spacetimes, is derived and applied to spherical integration surfaces. Although spherical extraction surfaces are used, the methods of section 4.1.3 can be applied to general extraction surfaces with minor adjustments. The QFS system is used to calculate the well known Noether charge densities for complex scalar and complex vector (Proca) fields along with novel expressions for the flux variable  $\mathcal{F}$  in section 4.1.4. Next the QFS system for energy momentum currents associated with matter are found and the main result of this paper is the explicit derivation of the angular momentum QFS variables  $\mathcal{Q}$ ,  $\mathcal{F}$  and  $\mathcal{S}$ . The three variables can be used to measure the angular momentum of matter within a region, the flux of angular momentum of matter through the boundary of that region and the transfer of angular momentum between matter and curvature; they can also be used with Eq. (4.1.15) to determine the numerical quality of a simulation as the QFS system is exactly satisfied in the continuum limit. In section 4.1.6 the combination of variables  $\mathcal{Q}$  and  $\mathcal{S}$  is shown to be a superior measure of angular momentum than integrals of only the charge density  $\mathcal{Q}$  in two ways; firstly its measurement is less prone to oscillations and secondly it is conserved in the large radius limit.

The QFS system for angular momentum is numerically tested on a dynamic non-linear spacetime consisting of two colliding boson stars; the collision has a small impact parameter giving rise to a non-zero total angular momentum. The stars promptly collide and form a highly perturbed, localised scalar field configuration partially retaining angular momentum. The total angular momentum of the spacetime is measured using the QFS variables (Eqs. (4.1.76), (4.1.82) and (4.1.83)) and is shown to agree well with the Newtonian approximation. This is a good check on the normalisation of the QFS variables as they should return the Newtonian calculation in the low energy limit; even though we simulate a fully non-linear spacetime the density and boost velocity of the stars are mild. The final numerical result is the convergence test of the QFS system which measures the relative error described in 4.1.6. The relative error converges to zero with order  $\omega \approx 1.9$  in the continuum limit and the highest resolution simulation gives a fractional error of approximately 3% in the total angular momentum after 8000 time units.

The QFS system is straightforward to implement and it is hoped these results will be useful to the Numerical Relativity community for better measurement of local energy-momentum of matter and Noether charge as well as powerful check on simulation resolution.

## Acknowledgements

I would like to thank Katy Clough, Bo-Xuan Ge, Thomas Helfer, Eugene Lim, Miren Radia and Ulrich Sperhake for many helpful conversations. This work is supported by STFC-CDT PhD funding, PRACE Grant No. 2020225359 and DIRAC RAC13 Grant No. ACTP238. Computations were performed on the Cambridge Service for Data Driven Discovery (CSD3) system, the Data Intensive at Leicester (DIAL3) and the Juwels cluster at GCS@FZJ, Germany.

### 4.1.8 Source Term Calculation

Here we expand the source term  $\mathcal{S}$  from section 4.1.2,

$$\mathcal{S} = \alpha T_{\mu\nu} \nabla^\mu \xi^\nu. \quad (4.1.108)$$

Note that  $\xi$  is assumed spacelike,  $\xi^\mu n_\mu = 0 \rightarrow \xi^0 = 0$ . If the reader is interested in a timelike  $\xi$ , for calculating the source term of energy, it can be found in [7]. Expanding the stress tensor with the usual 3+1 components [11], [16] ( $S_{\mu\nu}, S_\mu, \rho$ ), gives

$$\frac{1}{\alpha} \mathcal{S} = S_{\mu\nu} \nabla^\mu \xi^\nu + S_\mu n_\nu \nabla^\mu \xi^\nu + S_\nu n_\mu \nabla^\mu \xi^\nu + \rho n_\mu n_\nu \nabla^\mu \xi^\nu. \quad (4.1.109)$$

Let us decompose each piece separately. Starting with the spacelike tensor  $S_{\mu\nu}$  term,

$$S_{\mu\nu} \nabla^\mu \xi^\nu = (S_{\rho\sigma} \perp_\mu^\rho \perp_\nu^\sigma) \nabla^\mu (\perp_n^\nu \xi^n), \quad (4.1.110)$$

$$= S_{\rho\sigma} (\perp_\mu^\rho \perp_\nu^\sigma \nabla^\mu (\perp_n^\nu \xi^n)), \quad (4.1.111)$$

$$= S_{\mu\nu} D^\mu \xi^\nu, \quad (4.1.112)$$

$$= S_j^i \partial_i \xi^j + S_j^{(3)} \Gamma_{ik}^j \xi^k, \quad (4.1.113)$$

where we used the idempotence of the projector  $\perp$  on components  $S_{\mu\nu}$  and  $\xi^\mu$  which are already projected onto  $\Sigma$ . Here  $D$  and  $^{(3)}\Gamma_{ik}^j$  are the covariant derivative and Christoffel symbol components of  $\Sigma$ . Some algebra shows that the terms containing  $S_\mu$  become

$$S_\nu n^\mu \nabla_\mu \xi^\nu + S^\mu n_\nu \nabla_\mu \xi^\nu = S_\nu \mathcal{L}_n \xi^\nu, \quad (4.1.114)$$

where we used the fact that  $S^0 = 0$ ,  $n_{i \neq 0} = 0$  and that we are free to swap between  $\partial_\mu \leftrightarrow \nabla_\mu$  derivatives in a Lie derivative. Finally the  $\rho$  term simplifies, using  $\nabla_\mu (n^\nu n_\nu) = 0$ , to

$$\rho n_\mu n_\nu \nabla^\mu \xi^\nu = \rho n_\nu \mathcal{L}_n \xi^\nu. \quad (4.1.115)$$

Combining Eqs. (4.1.113), (4.1.114) and (4.1.115) we can write the source term as,

$$\frac{1}{\alpha} \mathcal{S} = S_j^i \partial_i \xi^j + S_j^{(3)} \Gamma_{ik}^j \xi^k + S_\nu \mathcal{L}_n \xi^\nu + \rho n_\nu \mathcal{L}_n \xi^\nu, \quad (4.1.116)$$

We can expand the Lie derivatives to partial derivatives, for ease of numerical implementation, with the following assumptions  $n_\mu S^\mu = 0$ ,  $\xi^0 = 0$ ,  $n_{i \neq 0} = 0$  and  $\partial \xi^0 = 0$ .

$$S_\nu \mathcal{L}_n \xi^\nu = -\frac{1}{\alpha} S_\nu \beta^i \partial_i \xi^\nu + \frac{1}{\alpha} S_\nu \xi^\mu \partial_\mu \beta^\nu \quad (4.1.117)$$

$$\rho n_\nu \mathcal{L}_n \xi^\nu = -\frac{1}{\alpha} \rho \xi^\mu \partial_\mu \alpha \quad (4.1.118)$$

This gives us our final form for the angular momentum source density,

$$\begin{aligned} \mathcal{S} = & \alpha S_\nu^{\mu(3)} \partial_\mu \xi^\nu + \alpha S_\nu^{\mu(3)} \Gamma_{\mu\sigma}^\nu \xi^\sigma \\ & - S_\nu \beta^i \partial_i \xi^\nu + S_\nu \xi^\mu \partial_\mu \beta^\nu - \rho \xi^\mu \partial_\mu \alpha. \end{aligned} \quad (4.1.119)$$

If we pick a coordinate basis vector as our approximate Killing vector, for example with components  $\xi^\mu = (\partial_\phi)^\mu = (0, 0, 0, 1)^\mu$  in polar coordinates, then the  $\partial_\mu \xi^\nu$  terms will vanish. However if we wish to work in Cartesian coordinates, which is very common for numerical codes, then the vector components  $\tilde{\xi}^\mu$  become,

$$\tilde{\xi}^\mu = (\partial_\phi)^\nu \frac{\partial \tilde{x}^\mu}{\partial x^\nu} = (0, -y, x, 0), \quad (4.1.120)$$

where  $\tilde{x}^\mu$  are Cartesian coordinates and  $x^\mu$  are spherical polar coordinates.

#### 4.1.9 Generality of Result

Here we demonstrate that the choice of 4-volume  $M$  integrated in Eq. (4.1.7) does not change the resulting QFS system (4.1.3). We start by defining the extraction 3-volume  $V_1 \in \Sigma$  at time  $t = t_0$ . The boundary of  $V_1$  is the 2-volume  $\partial V_1$  with metric  $\sigma$ . As in section 4.1.2,  $\Sigma$  is the 3-manifold defined by the set of all points with constant time coordinate  $t$ , equipped with metric  $\gamma$  and unit normal  $\mathbf{n}$  like Eq. (4.1.5). We now choose to define a 4-volume  $\tilde{M}$ , different to  $M$ , as the evolution of  $V_1$  along integral curves of  $\mathbf{n}$  between times  $t_0 \leq t \leq t_0 + \delta t$  in the limit  $\delta t \rightarrow 0$ . The boundary of  $\tilde{M}$ ,  $\partial \tilde{M}$ , is composed of three coordinate 3-volumes,  $V_1 \in \Sigma_{t_0}$ ,  $V_2 \in \Sigma_{t_0 + \delta t}$  and  $\tilde{H}$ . Here  $V_2 = V_1 + \delta V$  and is the future of  $V_1$ , at time  $t = t_0 + \delta t$ , found by following integral curves of  $\mathbf{n}$ .  $\tilde{H}$  is the 3-volume defined by the time evolution of 2-volume  $\partial V_1$  with  $\mathbf{n}$ . A diagram showing the differences between the choices of time evolution vectors  $\mathbf{n}$  and  $\mathbf{t}$  is given in Fig. 4.9.

We start again by using Gauss' theorem like in Eq. (4.1.8) which results in three surface integrals over  $V_1 \in \Sigma_{t_0}$ ,  $V_2 \in \Sigma_{t_0 + \delta t}$ , and  $\tilde{H}$ ,

$$\begin{aligned} \int_{\tilde{M}} \nabla \cdot \mathbf{J} \sqrt{-g} d^4 x = & - \int_{V_2}^{t=t_0 + \delta t} \mathbf{n} \cdot \mathbf{J} \sqrt{\gamma} d^3 x \\ & + \int_{V_1}^{t=t_0} \mathbf{n} \cdot \mathbf{J} \sqrt{\gamma} d^3 x \\ & + \int_{\tilde{H}} \tilde{\mathbf{N}} \cdot \mathbf{J} \sqrt{-\tilde{h}} dx^2 dt, \end{aligned} \quad (4.1.121)$$

where  $\tilde{\mathbf{N}}$  is the unit normal to  $\tilde{H}$ . Starting with the integrals over  $V_1$  and  $V_2 = V_1 + \delta V$  we get,

$$- \int_{V_2}^{t=t_0 + \delta t} \mathbf{n} \cdot \mathbf{J} \sqrt{\gamma} d^3 x + \int_{V_1}^{t=t_0} \mathbf{n} \cdot \mathbf{J} \sqrt{\gamma} d^3 x, \quad (4.1.122)$$

$$= -\delta t \partial_t \int_{V_1} \mathbf{n} \cdot \mathbf{J} \sqrt{\gamma} d^3 x - \int_{\delta V} \mathbf{n} \cdot \mathbf{J} \sqrt{\gamma} d^3 x, \quad (4.1.123)$$

with the new integral over  $\delta V$  appearing because  $V_1 \neq V_2$  as  $V_1$  is evolved along integral curves of  $\mathbf{n}$  rather than time basis vector  $\mathbf{t} = \partial_t$ ; this is demonstrated in Fig. 4.9. In the limit that  $\delta t \rightarrow 0$  it can be seen that,

$$\int_{\delta V} \mathbf{n} \cdot \mathbf{J} \sqrt{\gamma} d^3 x = -\delta t \int_{\partial V_1} \beta^i s_i \mathbf{n} \cdot \mathbf{J} \sqrt{\gamma} d^2 x, \quad (4.1.124)$$

where  $s_i$  are the components of the unit normal to the coordinate surface  $\partial V_1$  in  $\mathbb{R}^3$  rather than  $\Sigma_{t_0}$ . The overall negative sign in Eq. (4.1.124) comes from the defined direction of the shift vector  $\beta$  as seen

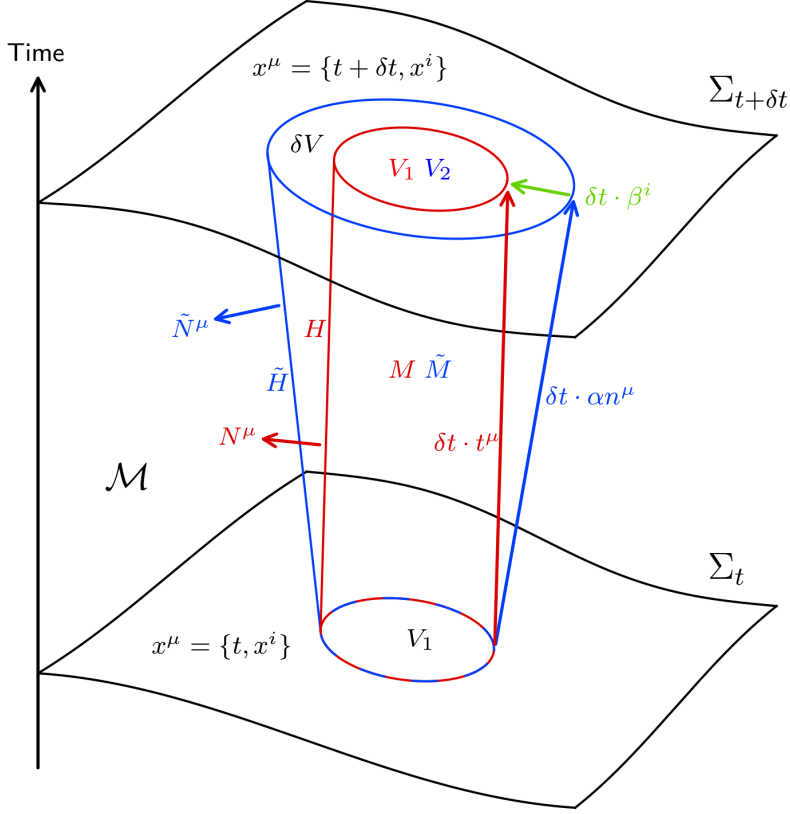


Figure 4.9: Comparison of two possible geometries for derivation of QFS system in section 4.1.2 on manifold  $\mathcal{M}$ .  $\Sigma_t$  is the spatial hypersurface at time  $t$  and  $\Sigma_{t+\delta t}$  is the spatial hypersurface at a later time  $t + \delta t$ .  $V_1$  is the coordinate volume, with surface  $\partial V_1$  (not labelled), that we wish to use as an extraction volume on  $\Sigma_t$ . The red cylinder, defined by  $\partial V_1$  evolved along integral curves of  $\mathbf{t} = \partial_t$ , is the same as in Fig. 4.1. Evolving  $\partial V_1$  forward in time with  $\mathbf{n}$ , as demonstrated with the blue cylinder, gives a different coordinate volume  $\partial V_2$  (not labelled) on  $\Sigma_{t+\delta t}$ . Similarly to the red cylinder, the blue cylinder has sides labelled by  $\tilde{H}$  and an interior  $\tilde{M}$ . The difference in the volumes  $V_1$  and  $V_2$  on  $\Sigma_{t+\delta t}$  is denoted by  $\delta V$ .

Fig. 4.9. Addressing the integral over  $\tilde{H}$  gives,

$$\begin{aligned} & \int_{\partial V_1} \int_{t_0}^{t_0+\delta t} \tilde{\mathbf{N}} \cdot \mathbf{J} \sqrt{-\tilde{h}} \, dx^2 dt, \\ & = \delta t \int_{\partial V_1} \tilde{\mathbf{N}} \cdot \mathbf{J} \sqrt{-\tilde{h}} \, dx^2. \end{aligned} \quad (4.1.125)$$

Combining Eqs. (4.1.123), (4.1.124) and (4.1.125) and a source term like in (4.1.7) we get,

$$\begin{aligned} \partial_t \int_{V_1} \mathbf{n} \cdot \mathbf{J} \sqrt{\gamma} \, d^3x = & \\ & \int_{\partial V_1} \left( \beta^i s_i \mathbf{n} \cdot \mathbf{J} \sqrt{\gamma} + \tilde{\mathbf{N}} \cdot \mathbf{J} \sqrt{-\tilde{h}} \right) dx^2 \\ & - \int_{V_1} S \alpha \sqrt{\gamma} \, d^3x, \end{aligned} \quad (4.1.126)$$

which is in the same form as Eq. (4.1.15) with definitions,

$$\mathcal{Q} := J^\mu n_\mu, \quad (4.1.127)$$

$$\mathcal{F} := \frac{\sqrt{-\tilde{h}}}{\sqrt{\sigma}} J^\mu \tilde{N}_\mu + \frac{\sqrt{\gamma}}{\sqrt{\sigma}} \beta^i s_i \mathcal{Q}, \quad (4.1.128)$$

$$\mathcal{S} := \alpha S, \quad (4.1.129)$$

where we used  $\mathbf{n} \cdot \mathbf{J} = \mathcal{Q}$  for the flux term. The density term  $\mathcal{Q}$  and source term  $\mathcal{S}$  are agnostic to our choice of extraction surface and its time evolution so have turned out the same as Eqs. (4.1.16) and (4.1.18). At first glance the flux term  $\mathcal{F}$  seems different to Eq. (4.1.25) but evaluating this term in a coordinate basis will show otherwise.

Choosing a spherical extraction surface as in Section 4.1.3 and using spherical polar coordinates,  $x^\mu = \{t, r, \theta, \phi\}$ ,  $V_1$  becomes the coordinate 3-volume  $r \leq r_0$ ,  $t = t_0$ . The unit normal  $\tilde{\mathbf{N}}$  satisfies  $\tilde{\mathbf{N}} \cdot \mathbf{n} = 0$  so  $\tilde{N}^\mu = (0, \tilde{N}^i)$  where,

$$\tilde{N}_i = \frac{\nabla_i(r - r_0)}{\sqrt{\gamma^{jk} \nabla_j(r - r_0) \nabla_k(r - r_0)}}, \quad (4.1.130)$$

$$= \left( \frac{1}{\sqrt{\gamma^{rr}}}, 0, 0 \right), \quad (4.1.131)$$

and the flat space normal has components  $s^i = s_i = (1, 0, 0)$  with respect to spherical polar coordinates over a different flat manifold. Using Eqs. (4.1.31) and (4.1.32) with Cramer's rule for matrix inverse, it can be shown that,

$$\gamma^{rr} = \frac{\det \sigma_{ab}}{\det \gamma_{ij}} = \frac{\sqrt{\sigma^2}}{\sqrt{\gamma^2}}, \quad (4.1.132)$$

$$\tilde{h}^{tt} = \frac{\det \sigma_{ab}}{\det \tilde{h}_{ij}} = -\frac{\sqrt{\sigma^2}}{\sqrt{-\tilde{h}}^2}, \quad (4.1.133)$$

where it should be noted that  $\tilde{h} < 0$  and  $\sigma > 0$ . Deriving Eq. (4.1.133) uses the fact that  $\tilde{H}$  intersects  $\Sigma$  on  $\partial V_1$  and therefore must have the same line element for variations in angular coordinates; hence  $g_{\theta\theta} = \tilde{h}_{\theta\theta}$ ,  $g_{\theta\phi} = \tilde{h}_{\theta\phi}$  and  $g_{\phi\phi} = \tilde{h}_{\phi\phi}$ . The final component we need is to calculate  $\tilde{h}^{tt}$  which can be done by projecting the 4-metric  $\mathbf{g}$  onto  $\tilde{H}$  as,

$${}^{(4)}\tilde{h}^{\mu\nu} = g^{\mu\nu} - \tilde{N}^\mu \tilde{N}^\nu, \quad (4.1.134)$$

$${}^{(4)}\tilde{h}^{tt} = g^{tt} - \tilde{N}^t \tilde{N}^t, \quad (4.1.135)$$

$$= -\alpha^{-2}, \quad (4.1.136)$$

where  ${}^{(4)}\tilde{\mathbf{h}}$  is a 4-tensor belonging to  $\mathcal{M}$  and  $\tilde{N}^t = 0$ . Using the pushforward of  $\tilde{\mathbf{h}}$  on  $\tilde{H}$  to  ${}^{(4)}\tilde{\mathbf{h}}$  on  $\mathcal{M}|_{p \in \tilde{H}}$ , similarly to Sec. 4.1.3, it can be shown that  ${}^{(4)}\tilde{h}^{tt} = h^{tt}$ . Equations (4.1.133) and (4.1.136) combine to give,

$$\sqrt{-\tilde{h}} = \alpha \sqrt{\sigma}, \quad (4.1.137)$$

again noting  $\tilde{h} < 0$ . Now we can re-write the flux (4.1.128) term as,

$$\mathcal{F} = \alpha J_\mu \tilde{N}^\mu + \frac{1}{\sqrt{\gamma^{rr}}} \beta^i s_i \mathcal{Q}, \quad (4.1.138)$$

$$\mathcal{F} = \alpha \gamma^{r\nu} J_\nu \tilde{N}_r + \frac{1}{\sqrt{\gamma^{rr}}} \beta^r \mathcal{Q}, \quad (4.1.139)$$

$$= \frac{1}{\sqrt{\gamma^{rr}}} (\alpha \gamma^{r\nu} J_\nu + \beta^r \mathcal{Q}), \quad (4.1.140)$$

and this is identical to Eq. (4.1.42) found earlier.



## 4.2 STUFF

MAYBE REMOVE THANKS AND PUT IT ONE BIG SECTION

MAYBE DELETE TEH CONVENTIONS

## Chapter 5

# STUFF TO DO

PUT A NICE FIGURE ON EACH CHAPTER PAGE?

CODE DEV? LIKE INITIAL DATA AND RANDOM SIMS IVE DONE ESPECIALLY WITH BLACK HOLES, MAYBE AN INITIAL DATA SECTION THEN FOLOWED BY MALAISE?

rename the sections maybe, or maybe not. is NUmerical relativity the best name for section that has no numerics and just does a 3+1 spacetime split?

ADD TO CONVENTIONS THAT LATE LATIN INDECES (I,J,K,...) SYMBOLISE 3D OBJECTS IN 4D SPACE ASWELL AS 3D OBJECST IN 3D SPACE

BOX IMPORTANT EQS? MAYBE NOT.

CHECK THE 3+1 SPLIT STRESS TENSOR AGREES WITH PAPERS ...

CHECK CURLY VS SMOOTH BRACKETS FOR SETS AND VECTORS ALL OVER

REF THE ADM METRIC?

make a note of the dx form notation but don't go into depth, maybe hint at intergating over a mfold?

maybe put BSSN and onwards in the GRCHOMBO SECTION? OR A CODE SECTION? and keep the first half as the adm decomposiiton section?

MAYBE ADD Z4 LAGRANGEAN OR UNDERSTAND IT BETTER? LOOK AT MARKUS THESIS? OR KATY?

CHECK CONVENTIONS ARE OBEYED IN INTRO NR BOSON Q MALAISE OTHER SECTRI-ONS...

MAKE SOME UNIFORM CONVENTION FOR STRESS TENSOR, MAYBE RHO FOR ENERGY DENSITY MAYBE EPSILON? SIMILAR FOR THE MOMENTA AND THE PROJECTED TENSOR? its in the ccz4 equations too ...

fig or Fig in figure referneceing?

DECIDE ON A FACTOR OF 16PI IN TEH MATTER LAGRANGEAN OF GR BETWEEN THE INTRO SECTION AND THE LATER SECTION. PROBABLY USE  $R/16\pi$  RATHER THAN  $16\pi \text{MATTER}$  ...

standardise complex phi, bar or star for conjugate? or dagger??

# Bibliography

# Bibliography

- [1] M. Alcubierre, B. Brügmann, P. Diener, M. Koppitz, D. Pollney, E. Seidel, and R. Takahashi, “Gauge conditions for long-term numerical black hole evolutions without excision,” *Phys. Rev. D*, vol. 67, p. 084023, 2003. gr-qc/0206072.
- [2] R. Penrose, “Quasi-local mass and angular momentum in general relativity,” *Proceedings of the Royal Society of London. Series A, Mathematical and Physical Sciences*, vol. 381, no. 1780, pp. 53–63, 1982.
- [3] N. Sanchis-Gual, C. Herdeiro, J. A. Font, E. Radu, and F. Di Giovanni, “Head-on collisions and orbital mergers of proca stars,” *Physical Review D*, vol. 99, Jan 2019.
- [4] F. Di Giovanni, N. Sanchis-Gual, P. Cerdá-Durán, M. Zilhão, C. Herdeiro, J. A. Font, and E. Radu, “Dynamical bar-mode instability in spinning bosonic stars,” *Physical Review D*, vol. 102, Dec 2020.
- [5] J. Bamber, K. Clough, P. G. Ferreira, L. Hui, and M. Lagos, “Growth of accretion driven scalar hair around kerr black holes,” *Phys. Rev. D*, vol. 103, p. 044059, Feb 2021.
- [6] W. E. East, “Superradiant instability of massive vector fields around spinning black holes in the relativistic regime,” *Phys. Rev. D*, vol. 96, p. 024004, Jul 2017.
- [7] K. Clough, “Continuity equations for general matter: applications in numerical relativity,” *Classical and Quantum Gravity*, vol. 38, p. 167001, jul 2021.
- [8] K. Clough, P. Figueras, H. Finkel, M. Kunesch, E. A. Lim, and S. Tunyasuvunakool, “Grchombo: numerical relativity with adaptive mesh refinement,” *Classical and Quantum Gravity*, vol. 32, no. 24, p. 245011, 2015.
- [9] T. Andrade, L. A. Salo, J. C. Aurrekoetxea, J. Bamber, K. Clough, R. Croft, E. de Jong, A. Drew, A. Duran, P. G. Ferreira, P. Figueras, H. Finkel, T. França, B.-X. Ge, C. Gu, T. Helfer, J. Jäykkä, C. Joana, M. Kunesch, K. Kornet, E. A. Lim, F. Muia, Z. Nazari, M. Radia, J. Ripley, P. Shellard, U. Sperhake, D. Traykova, S. Tunyasuvunakool, Z. Wang, J. Y. Widdicombe, and K. Wong, “Grchombo: An adaptable numerical relativity code for fundamental physics,” *Journal of Open Source Software*, vol. 6, no. 68, p. 3703, 2021.
- [10] R. Arnowitt, S. Deser, and C. W. Misner, “Republication of: The dynamics of general relativity,” *General Relativity and Gravitation*, vol. 40, p. 1997–2027, Aug 2008.
- [11] E.ourgoulhon, “3+ 1 formalism and bases of numerical relativity,” *arXiv preprint gr-qc/0703035*, 2007.
- [12] T. W. Baumgarte and S. L. Shapiro, *Numerical Relativity: Solving Einstein’s Equations on the Computer*. Cambridge University Press, 2010.
- [13] S. L. Liebling and C. Palenzuela, “Dynamical boson stars,” *Living Reviews in Relativity*, vol. 20, no. 1, p. 5, 2017.

- [14] M. Minamitsuji, “Vector boson star solutions with a quartic order self-interaction,” *Physical Review D*, vol. 97, May 2018.
- [15] M. Zilhão, H. Witek, and V. Cardoso, “Nonlinear interactions between black holes and proca fields,” *Classical and Quantum Gravity*, vol. 32, p. 234003, Nov 2015.
- [16] M. Alcubierre, *Introduction to 3+1 numerical relativity*, vol. 140. Oxford University Press, 2008.
- [17] C. Bona, T. Ledvinka, C. Palenzuela, and M. Žáček, “General-covariant evolution formalism for numerical relativity,” *Phys. Rev. D*, vol. 67, p. 104005, May 2003.
- [18] D. Alic, C. Bona-Casas, C. Bona, L. Rezzolla, and C. Palenzuela, “Conformal and covariant formulation of the z4 system with constraint-violation damping,” *Phys. Rev. D*, vol. 85, p. 064040, Mar 2012.
- [19] M. Campanelli, C. O. Lousto, P. Marronetti, and Y. Zlochower, “Accurate evolutions of orbiting black-hole binaries without excision,” *Phys. Rev. Lett.*, vol. 96, p. 111101, Mar 2006.
- [20] J. G. Baker, J. Centrella, D.-I. Choi, M. Koppitz, and J. van Meter, “Gravitational-wave extraction from an inspiraling configuration of merging black holes,” *Phys. Rev. Lett.*, vol. 96, p. 111102, Mar 2006.
- [21] T. Helfer, U. Sperhake, R. Croft, M. Radia, B.-X. Ge, and E. A. Lim, “Malaise and remedy of binary boson-star initial data,” 2021.
- [22] K. Clough, P. Figueras, H. Finkel, M. Kunesch, E. A. Lim, and S. Tunyasuvunakool, “GRChombo : Numerical relativity with adaptive mesh refinement,” *Classical and Quantum Gravity*, vol. 32, p. 245011, dec 2015.
- [23] W. H. Press, S. A. Teukolsky, W. T. Vetterling, and B. P. Flannery, *Numerical Recipes in C*. Cambridge, USA: Cambridge University Press, second ed., 1992.
- [24] blank